The Role of Gαq-Mediated Stress Granules in Neuron Function

by

Lela Jackson

A Dissertation Submitted to the Faculty of

WORCESTER POLYTECHNIC INSTITUTE

In Partial Fulfillment of the Requirements for the Degree of

DOCTOR OF PHILOSOPHY

in Biochemistry

June 9, 2022

Approved by:

Suzanne Scarlata, PhD Dissertation Advisor Professor Chemistry & Biochemistry Worcester Polytechnic Institute	Alonzo Ross, PhD Chairperson of Defense Professor Emeritus Biochemistry & Molecular Biotechnology University of Massachusetts Medical School
Amity Manning, PhD Professor Biology & Biotechnology Worcester Polytechnic Institute	Mary Munson, PhD Professor Biochemistry & Molecular Biotechnology University of Massachusetts Medical School

Acknowledgements

The completion of this dissertation would not be possible without the support I received from advisors, colleagues, friends and family during my time as a graduate student. Above all, thank you to my thesis advisor Dr. Suzanne Scarlata, who has been a tremendous source of encouragement and inspiration over the last five years. Thank you for accepting me into the group as a naïve first year student and providing mentorship through times of both success and failure. I would also like to extend gratitude to my thesis committee members Dr. Alonzo Ross, Dr. Mary Munson and Dr. Amity Manning for their valuable insight and perspectives regarding all aspects of my projects over the years.

Thank you to the past and present members of the Scarlata group as well as my fellow CBC graduate students who have not only been valuable mentors in the lab but have become amazing friends. Enormous thanks to Dr. Osama Garwain, who was my first mentor and provided me with the foundation necessary to successfully complete these projects. Thanks to Dr. Sid Yerramilli, who shared his insightful scientific feedback every step of the way. Thank you to Dr. Androniqi Qifti who has been by my side through this journey since the very beginning and always pushed me to step outside of my comfort zone. I am grateful to have had such hard working colleagues who helped keep me on track during the ups and downs of grad school.

Thanks to the many undergraduates that contributed to this work and provided me with opportunities to become a mentor myself, as well as Madison Rennie and Guanyu Lin, the graduate students who will continue investigating many aspects of this work in their own dissertations. Lastly, thank you to my friends and family, who have shown their undeniable love, support and patience during the last nine years I've spent in higher education.

Table of contents

List of figures

List of tables

List of abbreviations

AD	Alzheimer’s disease
Ago2	Argonaute 2
ALS	Amyotrophic lateral sclerosis
APP	Amyloid precursor protein
ASD	Autism spectrum disorder
ATP5f1b	ATP synthase F1 subunit beta
C3PO	Component 3 promoter of RISC
CHGb	Chromogranin B or secretogranin-1
DAG	Diacylglycerol
dsRNA	Double stranded RNA
eIF	Eukaryotic translation initiation factor proteins
FXR1/2	Fragile X mental retardation protein 1 and 2
G3BP1	Ras GTPase activating binding protein 1
GDP	Guanosine diphosphate
GPCR	G protein coupled receptor
GTP	Guanosine triphosphate
Gαq	Gαq protein alpha subunit
IDR	Intrinsically disordered region
IP_3	Inositol trisphosphate
miRNA/miR	Micro RNA
NGF	Nerve growth factor
PABPC1	Polyadenylate binding protein 1
PIP_2	Phosphatidylinositol 4,5-bisphosphate
PLCβ1	Phospholipase C β1

RISC	RNA induced silencing complex
RNAi	RNA interference
SG	Stress granule
siRNA	Small interfering RNA
TRAX	Translin-associated factor X

Abstract

Phospholipase Cβ1 (PLCβ1) is a multifunctional protein that both localizes to the plasma membrane and binds to cytosolic proteins. PLCβ1's traditional role takes place on the plasma membrane after being activated by G proteins in response to hormones and neurotransmitters, leading to an increase in intracellular calcium. Surprisingly, we discovered a population of PLCβ1 that binds to cytosolic proteins, and ~1/3 of these binding partners are stress granule (SG) proteins. SGs are dynamic membraneless organelles that shift untranslated mRNA and proteins into cytosolic aggregates when mammalian cells experience environmental stress. This is an advantageous process done to temporarily conserve energy until stress is relieved, but premature or irreversible SG formation has potential to become detrimental to gene regulation and therefore induce onset of disease. In the cytosol, PLCβ1 binds to SG proteins such as eukaryotic translation initiation factor 5a (eIF5a), polyadenylate binding protein 1 (PABPC1) and Ras GTPase activating binding protein 1 (G3BP1) in addition to a member of the RNA induced silencing complex (RISC) component 3 promoter of RISC (C3PO), as well as the multifunctional protein Argonaut 2 (Ago2). We found that PLCβ1 regulates the formation of SGs as it shuttles from the cytosol to the plasma membrane during G protein activation. The release of these binding partners due to loss of cytosolic PLCβ1 leads to the initiation of SG complexes and the promotion of RNA-induced silencing. It is also known that C3PO-PLCβ1 complexes are necessary to maintain a differentiated phenotype in neuronal cells. However, the interactions between PLCβ1, C3PO and Ago2, the role this ternary protein complex play in RNAi, and its contribution to neuronal differentiation had not been well studied. Additionally, the nature of SG formed by PLCβ1, and in turn consequence of Gαq stimulation were unknown. This thesis seeks to understand how re-localization of cytosolic PLCβ1 in response to Gαq stimulation by neurotransmitters and environmental stress influences neuronal stress response, RNA transcription and gene silencing, and may influence changes in cytosolic protein interactions, specifically involving PLCβ1, Ago2 and C3PO.

1 Chapter 1 – Introduction

1.1 Phospholipase Cβ1 signaling pathway

The Gαq and phospholipase Cβ1 (PLCβ1) pathway transduces signals from hormones and neurotransmitters. Gαq is part of one of three main classes of heterotrimeric guanine nucleotide binding proteins (G proteins) including α, β and γ subunits. G proteins are the largest known family of cell surface receptors, and are a very popular drug targets, accounting for >30% of all approved drugs.[1] G proteins are responsible for hundreds of physiological processes and are widely distributed throughout the human body. In its inactive state, Gαq binds to guanosine diphosphate (GDP) in a complex with the β and γ subunits. When Gαq is activated by neurotransmitters including acetylcholine, dopamine, serotonin and histamine, it disassociates from Gβ/γ, and GDP is exchanged for guanosine triphosphate (GTP).[1-2] This activation in turn causes PLCβ1 to become activated.[3]

PLC is divided into four subfamilies (β, γ, δ, and ε), with a total of eleven isoforms. These include four PLCβ, two PLCγ, four PLCδ and one PLCε proteins.[4] G protein α subunit is also divided into four subfamilies, Gαs, Gαi, Gαq, and Gα12, and these subunits bind to only β isoforms of PLC.[4] While on the membrane, PLCβ1 plays a key role in mediating calcium signals upon activation of Gαq by hormones and neurotransmitters. PLCβ1's main role in cells is on the plasma membrane where it hydrolyzes phosphatidylinositol 4,5-bisphosphate (PIP_2) to create diacylglycerol (DAG) and inositol trisphosphate (IP_3), two important second messengers that release intracellular calcium and regulate protein kinase C.[5] In neurons, PLCβ1 is the most abundant of the four, and has the highest affinity to bind with Gαq.[4] Activation of PLCβ1 by Gαq is vital to gene expression, cell proliferation and death.[6]

1.2 PLCβ1 interacts with RISC

C3PO may interact with PLCβ1 to reverse RNA interference (RNAi). It is known that PLCβ1 binds to stress granule maker proteins, so is it important to further understand how it is incorporated into RNAi activity. Component 3 Promoter of RNA induced silencing complex

(C3PO) is an octamer composed of two TRAX and six translin subunits.[7] The effects of C3PO are similar to that of PLCβ1, as it impacts learning, synaptic plasticity and memory by acting as the catalytic subunit of the RNA-induced silencing complex (RISC).[7-9] RISC is a ribonucleoprotein complex that promotes post-transcriptional gene silencing by cleaving and degrading mRNA. RISC activity is initiated in the nucleus by the RNase III enzyme dicer to process dsRNA into ~22 nucleotide microRNA's (miRNA or miR).[7-8] For degradation to happen, a guide strand of miRNA acts as a template for a complimentary mRNA passenger strand to bind. With perfect paring, Argonaut 2 (Ago2) will nick the miRNA passenger strand, allowing complementary mRNA access to hybridize to the guide strand. Once this happens, Ago2 will nick the mRNA between the 10^{th} and 11^{th} nucleotide, causing it to also become degraded.[10-11] If the base pairings between the guide strand and mRNA do not match perfectly, the Ago2-mRNA complex will stall and form aggregates such as stress granules.

1.3 Stress granule formation

Stress granules regulate miR transcription through PLCβ1's interactions with C3PO, and are driven by liquid-liquid phase separation. Stress granules are membraneless aggregates of stalled mRNA that form to save cells energy by prioritizing protein synthesis until stress is relieved.[12] Cells try to alleviate environmental stressors such as a change in osmotic pressure, heat or oxidative stress by localizing untranscribed mRNAs into compact granules.[12-13] These granules have no encapsulating membrane or envelope, and are effective in partitioning themselves from the cytosol and other organelles due to the high viscosity of their liquid like state. Stress granules give the cell an opportunity to sort mRNA's and decide whether it is appropriate to degrade, store or translate them.[14-15] It is important to note that assembly and disassembly of stress granules are vital to healthy neuronal function and plasticity, and premature or irreversible formation is associated with a broad range of diseases.[16]

The regulation of stress granule assembly and disassembly is not well understood, but proteins with poorly defined peptide segments, or intrinsically disordered domains (IDR's), with low complexity sequences drive the process of liquid-liquid phase separation (LLPS) away from the cytosol.[16] Cells have arranged themselves to organize chemical reactions into compartments or

organelles. To maintain order, membranes are usually used to separate these compartments from each other while allowing for some degree of diffusion. However, there are cellular structures, like nucleoli, centrosomes, P bodies and stress granules that are not bound by membranes.[17] These compartments have been described as dynamic liquid droplets within the cytoplasm, and can change their shape in response to stimuli.[18] This liquid state allows rapid mixing through random collision, providing a suitable medium for biochemical reactions to take place.[17] LLPS is possible through liquid-liquid de-mixing driven by hydrophobic effects or a difference in viscosity or surface tension (like oil and water).[17] In the case of stress granules, the mixture of components that make up the granules have higher affinity of attraction to each other over the surrounding environment that makes up the cytosol, allowing these separate structures to coexist.[17] Interestingly, these two phases have an equal chemical potential while having different concentrations of components, making it so that things can diffuse into and out of the phases in equal proportions, but there is no equilibration across the phase boundary.[17]

Stress granules are mostly composed of untranslated mRNA, but also include proteins such as Ago2, translation initiation factors (eIF), fragile X mental retardation protein 1 and 2 (FXR1/2), and polyadenylate binding protein (PABPC1).[16, 19-20] FXR1 is an RNA binding protein involved in mRNA regulation and is highly expressed in neurons.[18] Because of this, it is involved in synaptic plasticity and learning, and is highly associated with autism.[21] Chronic stress granules are linked to other diseases that affect memory and learning like Alzheimer's disease and frontotemporal lobar degeneration (dementia).[22] Mass spectrometry showed that the aforementioned proteins were all identified to be binding partners to cytosolic PLCβ1. Furthermore, stress granules are independent of processing bodies (P bodies), which are similar membraneless aggregates that traditionally do not contain translation initiation factors and only store degraded mRNA.[22] It is likely that stress granules only interact with P bodies to pass along decaying mRNA when it does not need to be stored or translated.[23] It has been seen that stress granules assemble and disassemble in two steps, a tightly packed core and a peripheral shell.[16] The formation of these two separate phases may also be important for miR diffusion and localization within neurons.

PLCβ1 helps prevents the formation of stalled transcription complexes by binding to stress granules proteins.[24] When PLCβ1 is bound to C3PO, small interfering RNA (siRNA) may fail to down regulate protein expression. The C terminus of C3PO competes with Gαq for binding to PLCβ1,[24] so it is believed that the role of PLCβ1 in neurons is split between the plasma membrane, when binding with Gαq, or the cytosol when interacting with C3PO and other cytosolic partners. Gene silencing events and calcium signaling is driven by the binding of PLCβ1 to either C3PO or Gαq respectively.[24] The need to shuttle PLCβ1 between the cytosol and plasma membrane depends on concentration of these proteins within the cell. This process is especially important to understand because the interaction of PLCβ1 with C3PO causes PC12 cells to differentiate.

1.4 PLCβ1 controls proliferation, neurite growth and synapse retraction

When PC12 cells proliferate, levels of PLCβ1 and Gαq are low and differentiation is not possible.[24] When treated with nerve growth factor (NGF), cells begin growing neurites and levels of PLCβ1 rise, peaking at ~24 hours.[24] Levels of Gαq remain low for ~48 hours until it becomes abundant enough to shift PLCβ1from the cytosol detaching from C3PO.[24] In this initial phase, down regulating either C3PO and PLCβ1 results in loss of neurite growth, while knockdown of Gαq shows no change in neurite growth or function.[24] When PLCβ1 interacts with C3PO, RISC activity is not promoted and some genes are not silenced, resulting in increased differentiation and synapse formation. This was tested by studying whether PLCβ1 and/or C3PO will change the population of miR's during the process of differentiation.

When neuronal cells differentiate, they go from a round, proliferative phenotype to sprouting multiple neurites that span 2-3 times that of the cell body.[25] When cells mature into a differentiated state, they no longer divide, proving it critical that stress granule disassembly in disease be better understood in terminally differentiated cells, such as neurons and cardiac cells. In the differentiated state, neurons can connect to each other via synapses and exchange information through neurotransmitters and electrical pulses.[26] This process is critical in memory storage and ability to learn. Differentiation is seen to be reversed with knockdown of PLCβ1 as well as over-stimulation of Gαq. In either case, C3PO is free from cytosolic PLCβ1, miR's are hydrolyzed by RISC and neurite growth is no longer possible.[24] With this, it needs to be understood how PLCβ1

impacts neurite growth and synapses development and retraction through regulation of miRNA populations.

1.5 Significance

G protein coupled receptors (GPCRs) are currently one of the most widely studied drug targets. As of 2017, there were 475 drugs (34% of all FDA approved drugs) on the market that act on GPCRs.[27] These drugs treat a wide variety of diseases including cancer, diabetes, metabolic and inflammatory diseases.[27] However, since loss of PLCβ1 is associated with neurodegenerative diseases including epileptic encephalopathy, schizophrenia and bipolar disorder it is vital to understand the mechanism of PLCβ1 in these conditions specifically. Alzheimer's disease, Parkinson's disease and amyotrophic lateral sclerosis (ALS) are also associated with PLCβ1 through its binding to α-synucleins.[28-29] PLCβ1 is highly expressed in many parts of the brain, and regulates synaptic plasticity and brain development specifically in the hippocampus through acetylcholine signaling.[30] Furthermore, patients with schizophrenia and bipolar disorder show loss of function of PLCβ1 in the frontal cortex.[7, 31] PLCβ1 was first discovered to be linked to these diseases through its mediation of calcium signaling, but it is believed that the function of PLCβ1 is more diverse. It was first believed that cytosolic PLCβ1 could regulate PIP_2 on the membranes of organelles, but recent data proves it may play a more significant role.[32]

It is known that interactions between Gαq and PLCβ1 lead to a change in calcium release, which regulates neurological gene expression. PLCβ1's role in RNAi needed to be explored to understand the mechanics behind stress granule formation and disassembly, protein production and changes in mRNA populations. By studying PLCβ1's general function in the cytosol and its association with RISC, we could better understand neurodegeneration, learning and memory. Reducing the level of cytosolic PLCβ1 as a result of environmental stresses including osmotic pressure, heat shock, and overexpression of Gαq changes mRNA populations within stress granules. Cells may prioritize protein production differently as a result of different environmental conditions, and because of this, we can study and identify miR populations specific to each type of stress.

Stress granule formation is necessary for normal cell survival, but a cell's inability to appropriately form or disassemble stress granules will impact neurological functions. Since PLCβ1 is abundant in neuronal cells, and these cell types do not regenerate rapidly, stress granules may accumulate and lead to detrimental outcomes more frequently in neurons compared to other cell types. Because of the risk factors associated with neuronal aging, it is vital that we understand what conditions promote stress granule assembly and disassembly in neurons, how persistent non-soluble protein/mRNA aggregates occur and the ways in which they impact neuronal diseases. Many neuronal diseases have no cure and affect millions of Americans every year. For example, Alzheimer's disease is the sixth leading cause of death in the United States and affects 1 in 3 elderly people.[33] ALS was responsible for the death of over 24,000 Americans between the years 2011-2014 and accounts for ~70% of all motor neuron disease diagnoses.[34] Autism is also a highly prevalent disorder, affecting 1 in 59 births equaling more than 3.5 million cases nationwide.[35]

1.6 Innovation

There are many multifunctional proteins that respond to environmental stimuli through diverse pathways. This thesis intends to further discover the multifunctional role of PLCβ1 in mammalian cells, and how environmental stimuli can affect the activity of this protein and its binding partners. It is known that the majority of PLCβ1 is localized to the plasma membrane, but the behavior of the remaining cytosolic fraction is not well understood. PLCβ1's role in calcium signaling is in addition to RNA silencing, stress sensing and prevention of stalled aggregates under basal conditions, so learning about these additional processes is crucial for understanding the significance of G protein signaling and the potential for creating drug therapeutics for neurodegenerative diseases specifically. We also want to understand the role of PLCβ1 in dictating the inclusion of mRNA populations into stress granules and know if localization of stress granules within neurons affects cell health by causing incomplete synapse formation.

1.7 References

1. Li, J.; Ge, Y.; Huang, J. X.; Stromgaard, K.; Zhang, X.; Xiong, X. F., Heterotrimeric G Proteins as Therapeutic Targets in Drug Discovery. *J Med Chem* **2020,** *63* (10), 5013-5030.
2. Li, J.; Ning, Y.; Hedley, W.; Saunders, B.; Chen, Y.; Tindill, N.; Hannay, T.; Subramaniam, S., The Molecule Pages database. *Nature* **2002,** *420* (6916), 716-7.
3. Sternweis, P. C.; Smrcka, A. V.; Gutowski, S., Hormone signalling via G-protein: regulation of phosphatidylinositol 4,5-bisphosphate hydrolysis by Gq. *Philos Trans R Soc Lond B Biol Sci* **1992,** *336* (1276), 35-41; discussion 41-2.
4. Rhee, S. G., Regulation of phosphoinositide-specific phospholipase C. *Annu Rev Biochem* **2001,** *70*, 281-312.
5. Putney, J. W.; Tomita, T., Phospholipase C Signaling and Calcium Influx. *Adv Biol Regul* **2012,** *52* (1), 152-164.
6. Dhanasekaran, N.; Tsim, S.-T.; Dermott, J. M.; Onesime, D., Regulation of cell proliferation by G proteins. *Oncogene* **1998,** *17* (11), 1383-1394.
7. Lo Vasco, V. R.; Longo, L.; Polonia, P., Phosphoinositide-specific Phospholipase C β1 gene deletion in bipolar disorder affected patient. *J Cell Commun Signal* **2013,** *7* (1), 25-29.
8. Kurian, M. A.; Meyer, E.; Vassallo, G.; Morgan, N. V.; Prakash, N.; Pasha, S.; Hai, N. A.; Shuib, S.; Rahman, F.; Wassmer, E.; Cross, J. H.; O'Callaghan, F. J.; Osborne, J. P.; Scheffer, I. E.; Gissen, P.; Maher, E. R., Phospholipase C beta 1 deficiency is associated with early-onset epileptic encephalopathy. *Brain* **2010,** *133* (10), 2964-2970.
9. Schoonjans, A.-S.; Meuwissen, M.; Reyniers, E.; Kooy, F.; Ceulemans, B., PLCB1 epileptic encephalopathies; Review and expansion of the phenotypic spectrum. *European Journal of Paediatric Neurology* **2016,** *20* (3), 474-479.
10. Narayanan, V.; Scarlata, S., Membrane Binding and Self-Association of α-Synucleins. *Biochemistry* **2001,** *40* (33), 9927-9934.
11. Golebiewska, U.; Scarlata, S., High pressure promotes alpha-synuclein aggregation in cultured neuronal cells. *FEBS Letters* **2015,** *589* (21), 3309-3312.
12. Philip, F.; Sahu, S.; Caso, G.; Scarlata, S., Role of Phospholipase C-β in RNA interference. *Adv Biol Regul* **2013,** *53* (3), 319-330.
13. Li, L.; Gu, W.; Liang, C.; Liu, Q.; Mello, C. C.; Liu, Y., The Translin-TRAX complex/C3PO is a ribonuclease in tRNA processing. *Nat Struct Mol Biol* **2012,** *19* (8), 824-830.
14. Liu, Y.; Ye, X.; Jiang, F.; Liang, C.; Chen, D.; Peng, J.; Kinch, L. N.; Grishin, N. V.; Liu, Q., C3PO, an Endoribonuclease That Promotes RNAi by Facilitating RISC Activation. *Science* **2009,** *325* (5941), 750-753.
15. Park, A. J.; Havekes, R.; Fu, X.; Hansen, R.; Tudor, J. C.; Peixoto, L.; Li, Z.; Wu, Y.-C.; Poplawski, S. G.; Baraban, J. M.; Abel, T., Learning induces the translin/trax RNase complex to express activin receptors for persistent memory. *eLife* **2017,** *6*, e27872.
16. Pratt, A. J.; MacRae, I. J., The RNA-induced Silencing Complex: A Versatile Gene-silencing Machine. *J. Biol. Chem.* **2009,** *284* (27), 17897-17901.
17. Jo, Myung H.; Shin, S.; Jung, S.-R.; Kim, E.; Song, J.-J.; Hohng, S., Human Argonaute 2 Has Diverse Reaction Pathways on Target RNAs. *Molecular Cell* **2015,** *59* (1), 117-124.
18. Protter, D. S. W.; Parker, R., Principles and Properties of Stress Granules. *Trends in Cell Biology* **2016,** *26* (9), 668-679.
19. Babar, I. A.; Slack, F. J.; Weidhaas, J. B., miRNA modulation of the cellular stress response. *Future Oncology* **2008**.

20. Buchan, J. R.; Parker, R., Eukaryotic Stress Granules: The Ins and Out of Translation. *Molecular Cell* **2009,** *36* (6), 932.
21. Anderson, P.; Kedersha, N., Stress granules. *Current biology : CB* **2009,** *19* (10), R397-8.
22. Wheeler, J. R.; Matheny, T.; Jain, S.; Abrisch, R.; Parker, R., Distinct stages in stress granule assembly and disassembly. *Elife* **2016,** *5*.
23. Lin, Y.; Protter, David S. W.; Rosen, Michael K.; Parker, R., Formation and Maturation of Phase-Separated Liquid Droplets by RNA-Binding Proteins. *Molecular Cell* **2015,** *60* (2), 208-219.
24. Decker, C. J.; Parker, R., P-Bodies and Stress Granules: Possible Roles in the Control of Translation and mRNA Degradation. *Cold Spring Harb Perspect Biol* **2012,** *4* (9), a012286.
25. Gareau, C.; Martel, D.; Coudert, L.; Mellaoui, S.; Mazroui, R., Characterization of Fragile X Mental Retardation Protein granules formation and dynamics in Drosophila. *Biol Open* **2012,** *2* (1), 68-81.
26. Kim, D. Y.; Reynaud, J. M.; Rasalouskaya, A.; Akhrymuk, I.; Mobley, J. A.; Frolov, I.; Frolova, E. I., New World and Old World Alphaviruses Have Evolved to Exploit Different Components of Stress Granules, FXR and G3BP Proteins, for Assembly of Viral Replication Complexes. *PLOS Pathogens* **2016,** *12* (8), e1005810.
27. Hauser, A. S.; Attwood, M. M.; Rask-Andersen, M.; Schioth, H. B.; Gloriam, D. E., Trends in GPCR drug discovery: new agents, targets and indications. *Nat Rev Drug Discov* **2017,** *16* (12), 829-842.
28. Ruz, C.; Alcantud, J. L.; Vives Montero, F.; Duran, R.; Bandres-Ciga, S., Proteotoxicity and Neurodegenerative Diseases. *Int J Mol Sci* **2020,** *21* (16).
29. Kruger, R.; Muller, T.; Riess, O., Involvement of alpha-synuclein in Parkinson's disease and other neurodegenerative disorders. *J Neural Transm (Vienna)* **2000,** *107* (1), 31-40.
30. Hackelberg, S.; Oliver, D., Metabotropic Acetylcholine and Glutamate Receptors Mediate PI(4,5)P2 Depletion and Oscillations in Hippocampal CA1 Pyramidal Neurons in situ. *Sci Rep* **2018,** *8* (1), 12987.
31. Ratti, S.; Follo, M. Y.; Ramazzotti, G.; Faenza, I.; Fiume, R.; Suh, P. G.; McCubrey, J. A.; Manzoli, L.; Cocco, L., Nuclear phospholipase C isoenzyme imbalance leads to pathologies in brain, hematologic, neuromuscular, and fertility disorders. *J Lipid Res* **2019,** *60* (2), 312-317.
32. Kind, P. C.; Kelly, G. M.; Fryer, H. J.; Blakemore, C.; Hockfield, S., Phospholipase C-beta1 is present in the botrysome, an intermediate compartment-like organelle, and Is regulated by visual experience in cat visual cortex. *J Neurosci* **1997,** *17* (4), 1471-80.
33. Matthews, K. A.; Xu, W.; Gaglioti, A. H.; Holt, J. B.; Croft, J. B.; Mack, D.; McGuire, L. C., Racial and ethnic estimates of Alzheimer's disease and related dementias in the United States (2015-2060) in adults aged >/=65 years. *Alzheimers Dement* **2019,** *15* (1), 17-24.
34. Larson, T. C.; Kaye, W.; Mehta, P.; Horton, D. K., Amyotrophic Lateral Sclerosis Mortality in the United States, 2011-2014. *Neuroepidemiology* **2018,** *51* (1-2), 96-103.
35. Maenner, M. J.; Shaw, K. A.; Baio, J.; EdS; Washington, A.; Patrick, M.; DiRienzo, M.; Christensen, D. L.; Wiggins, L. D.; Pettygrove, S.; Andrews, J. G.; Lopez, M.; Hudson, A.; Baroud, T.; Schwenk, Y.; White, T.; Rosenberg, C. R.; Lee, L. C.; Harrington, R. A.; Huston, M.; Hewitt, A.; PhD; Esler, A.; Hall-Lande, J.; Poynter, J. N.; Hallas-Muchow, L.; Constantino, J. N.; Fitzgerald, R. T.; Zahorodny, W.; Shenouda, J.; Daniels, J. L.; Warren, Z.; Vehorn, A.; Salinas, A.; Durkin, M. S.; Dietz, P. M., Prevalence of Autism Spectrum Disorder

Among Children Aged 8 Years - Autism and Developmental Disabilities Monitoring Network, 11 Sites, United States, 2016. *MMWR Surveill Summ* **2020,** *69* (4), 1-12.

2 Chapter 2 – Background

Lela Jackson[1], Androniqi Qifti[1], Katherine M. Pearce[1] and Suzanne Scarlata[1]

1 - Department of Chemistry & Biochemistry, Worcester Polytechnic Institute, Worcester, MA

The following subsections appear in Jackson *et al.* "Regulation of bifunctional proteins in cells: Lessons from the phospholipase Cβ/G protein pathway" *Protein Science.* (2019) and are reproduced here with permission. L.J., A.Q., K.P. and S.S. worked together to develop an outline of the paper. L.J. developed the C3PO/RISC related sections. L.J & A.Q developed the stress granule formation related sections including the model. A.Q. developed the Gαq stabilization section through caveolae. K.P. developed the calcium signaling related section.

2.1 Abstract

Some proteins can serve multiple functions depending on different cellular conditions. An example of a bifunctional protein is inositide-specific mammalian phospholipase Cβ (PLCβ). PLCβ is activated by G proteins in response to hormones and neurotransmitters to increase intracellular calcium. Recently, alternate cellular function(s) of PLCβ have become uncovered. However, the conditions that allow these different functions to be operative are unclear. Like many mammalian proteins, PLCβ has a conserved catalytic core along with several regulatory domains. These domains modulate the intensity and duration of calcium signals in response to external sensory information and allow this enzyme to inhibit protein translation in a noncatalytic manner. In this review, we first describe PLCβ's cellular functions and regulation of the switching between these functions, and then discuss the thermodynamic considerations that offer insight into how cells manage multiple and competitive associations allowing them to rapidly shift between functional states.

2.2 PLCβ generates Ca^{2+} signals in response to extracellular signals

Most sensory information is received and processed by the G protein signaling system.[1] This pathway allows external hormones and neurotransmitters to elicit different cell responses, such as movement or morphology changes. G protein pathways are initiated when an extracellular agent binds to its specific G protein coupled receptor (GPCR). GPCRs are a large family of seven transmembrane proteins that interact and respond to a diverse array of ligands that include hormones, neurotransmitters, vasodilators, many pharmaceutical agents, and light. Ligand binding allows GPCRs to activate their associated G proteins by catalyzing the exchange of GDP for GTP on the Gα subunits peripherally bound to the plasma membrane.[2-3] Heterotrimeric G proteins are composed of three subunits (α, β, and γ). In the GTP-bound state, Gα has a ~50-fold weaker affinity to Gβγ subunits,[4] which destabilizes the heterotrimer leaving the Gα and Gβγ to separately bind to and activate specific proteins. Once the complex is destabilized, the Gα and the Gβγ subunits each act as effectors on specific targets. Depending on the Gα subunit family, Gα will act to stimulate or inhibit adenylyl cyclase (AC), activate phosphoinositide-specific phospholipase C (PI-PLC), or regulate RhoA proteins. Alternatively, Gβγ subunits are thought to play a role in calcium channel

activity, and regulate protein kinases and small G proteins, such as ERK1/2, JNK, phosphoinositide-3 kinase (PI3K), and mitogen-activated protein kinases (MAPKs).[5]

In contrast to the ~800 different GPCRs, there are only four families of heterotrimeric G proteins that are classified by their Gα subunits.[6] PLCβ is the main effector of Gαq,[7] and activation of Gαq increases the binding affinity of PLCβ ~20–40-fold (Figure 2.1).[8] Gαq is coupled to receptors for neurotransmitters such as dopamine and acetylcholine, as well as hormones that mediate vasoconstriction and inflammation, such as bradykinin and angiotensin II. PLCβ is soluble but binds to membranes, where it catalyzes the hydrolysis of phosphatidylinositol 4,5 bisphosphate (PIP_2), which is found at low levels in the plasma membrane.[9] PIP_2 hydrolysis catalyzed by PLCβ leads to two products: the lipid portion, diacylglycerol, which activates protein kinase C, and the soluble head group, 1,4,5 inositol trisphosphate (IP_3). IP_3 diffuses to the endoplasmic reticulum (ER) where it binds to IP_3 receptors. These receptors are Ca^{2+} channels and when IP_3 binds, they open, releasing Ca^{2+} from intracellular stores into the cytoplasm. This increased level of calcium changes the activity of a wide range of enzymes that carry out key cellular events such as generating action potentials and neurotransmission in neurons, or initiating muscle contraction.[10-12] Besides being activated by Gαq, two of the four known isoforms of PLCβ can be activated by Gβγ subunits.[13] Although Gβγ subunits have the potential to be released by any G protein family, release is generally associated with Gαi subunits thus connecting PLCβ and calcium signals to large and diverse array of GPCRs.

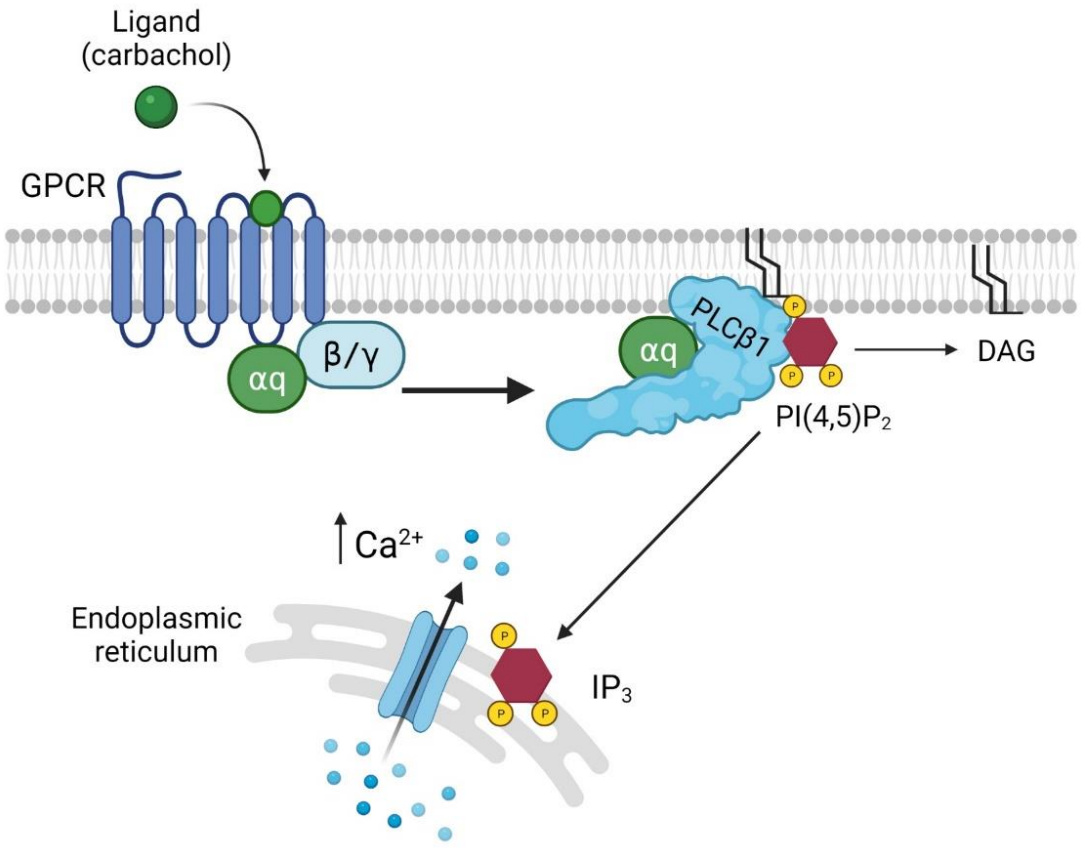

Figure 2.1 Cartoon of the Gαq/PLCβ signaling system showing simultaneous activation of PLCβ by both Gβγ and Gα subunits. (See references[14-15]) (Created with BioRender.com)

In order to access its substrate, PLCβ must bind to the plasma membrane. Binding of PLCβ to model membranes is strong and fairly nonspecific with partition coefficients ranging from 10 to 100 μM.[16] This range of affinities suggests a transient membrane association in the range of 0.1 to 1 s.[17-18] Studies using purified proteins and model membranes suggest that PLCβ initially binds to membranes where it diffuses and hops along the membrane until it encounters Gαq.[16] It is unclear whether a similar scenario occurs in cells since the amount of membrane available for binding may be lower, and if this is the case, PLCβ will bind directly to Gαq. Once activated, the affinity between Gαq and PLCβ1 increases 20-fold.[4] The high affinity between Gαq and PLCβ (K_d ~1 nM) is attributed to the tucking of Gαq into a nook between the C2 domain and C-terminal tail (Figure 2.2) of PLCβ1.[19]

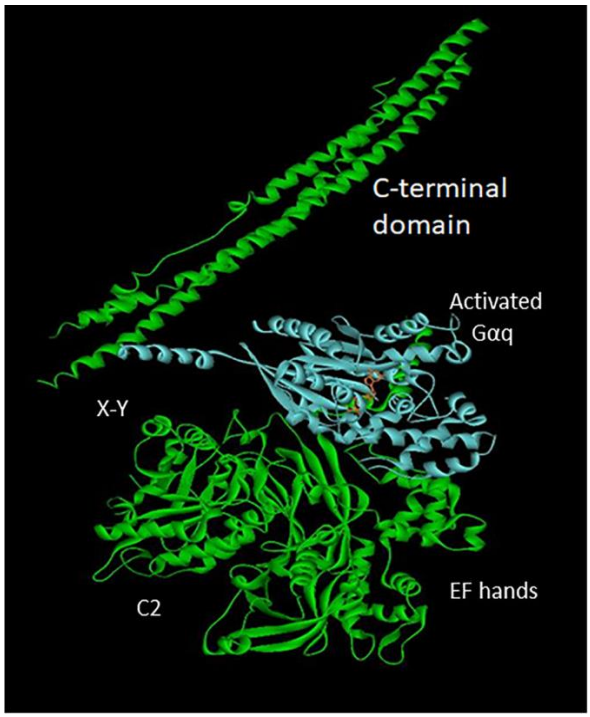

Figure 2.2 Crystal structure (PDB Id: 4GNK) of the PLCβ3 (green) -Gαq (blue) complex showing the extended C-terminal domain and where the various domains are indicated. Missing is an unstructured 52aa connector between the C2 and C-terminal domains.

The initial activation of PLCβ and subsequent calcium release results in a series of coordinated events involving changes in protein associations, modifications, and localization.[20] Calcium release is enhanced by two major effects.[11] One is the activation of PLCδ. PLCδ has a similar structure as PLCβ but is not activated by G proteins. Instead, PLCδ becomes highly active when calcium levels in the cell rise, synergizing PLCβ activity.[21] Additionally, increased calcium opens calcium-activated calcium channels on the plasma membrane, allowing external calcium to enter the cell.[22]

2.3 The domain structure of PLCβ allows multi-functionality

Like most mammalian signaling proteins, PLCβ is composed of several conserved domains (Figure 2.3). At the N-terminus is the pleckstrin homology (PH) which mediates activation by Gβγ. This domain is followed by two EF hands and the catalytic domain. Immediately following the catalytic domain is the C2 domain and a long 400 amino acid coiled-coil domain that comprises

the C-terminal domain. This region is distinctive of PLCβ enzymes and confers Gαq activation to the catalytic core. Gαq binds to the C-terminal domain close to the C2 domain (Figure 2.2), leaving the long coiled coil extension to potentially interact with other species. As described below, it is this noncatalytic C-terminal region that allows PLCβ to impact protein translation.[23-24]

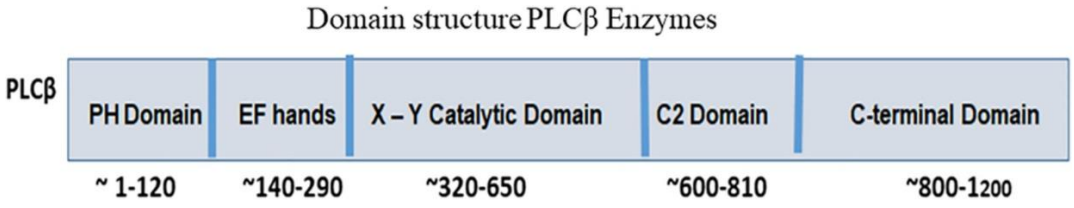

Figure 2.3 Schematic of the domain structure of PLCβ along with the amino acid number.

2.4 PLCβ has an atypical cytosolic population that impact protein translation

Even though PLCβ1 binds strongly to model membranes, cultured cells have a significant level of PLCβ in the cytosol (Figure 2.4). In previous years, the function of this cytosolic population was unclear because the activity of PLCβ in the absence of activated Gαq is very low, especially compared to PLCδ. To understand the role, if any, of this cytosolic population, our lab set out to identify novel binding partners of cytosolic PLCβ using two unbiased approaches: a yeast two hybrid study and identification of proteins associated with cytosolic PLCβ in an antibody pull-down.

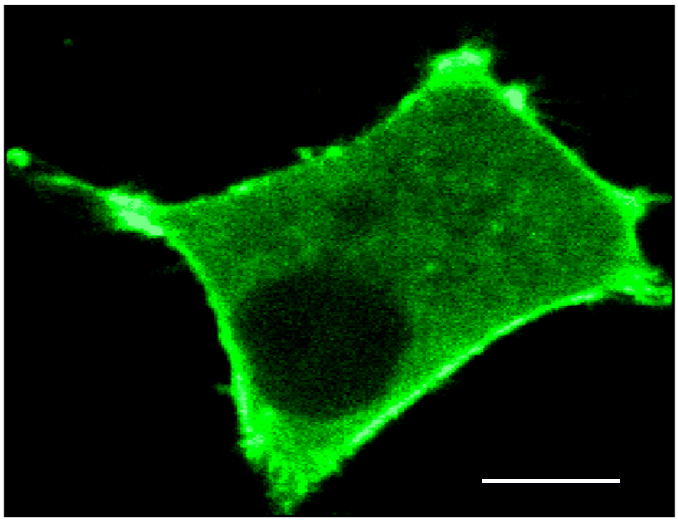

Figure 2.4 eGFP-PLCβ1 expressed in a differentiated PC12 cell showing the prominent plasma membrane and cytosolic populations. Scale bar=10 μm.

2.5 PLCβ inhibits the promoter of RNA-induced silencing, C3PO, to impact post-translational gene regulation

A search for cytosolic PLCβ1 binding partners was first carried out by a yeast two-hybrid study using the C-terminal region as bait with the idea that an unknown cytosolic partner might activate PLCβ in a similar manner as Gαq and allow the enzyme to modify the PIP_2 levels in internal membranes. These studies identified the nuclease TRAX (translin-associated factor X).[25] TRAX is a small helical protein that shuttles between the cytoplasm and nucleus.[26] TRAX is always found complexed with the oligonucleotide binding protein translin in a 6:2 (translin:TRAX) octamer called C3PO (Component 3 Promoter of the RNA Induced Silencing Complex), and expression of the two proteins is linked.[27] C3PO is found in all cells with similar structure from sponges to humans (Figure 2.5[28]). The C3PO octamer is a dimer of tetramers with the oligonucleotide binding site located in a channel between the two hemispheres.[29] Single or double stranded oligonucleotides bind nonspecifically to the translin subunits where they are subsequently hydrolyzed by the TRAX subunits. PLCβ was found to bind primarily to the TRAX subunits at a 1:1 (C3PO:PLCβ) stoichiometry and a K_d ~8 nM.[25, 30] PLCβ1 binding blocks the release of product, inhibiting release and C3PO activity.

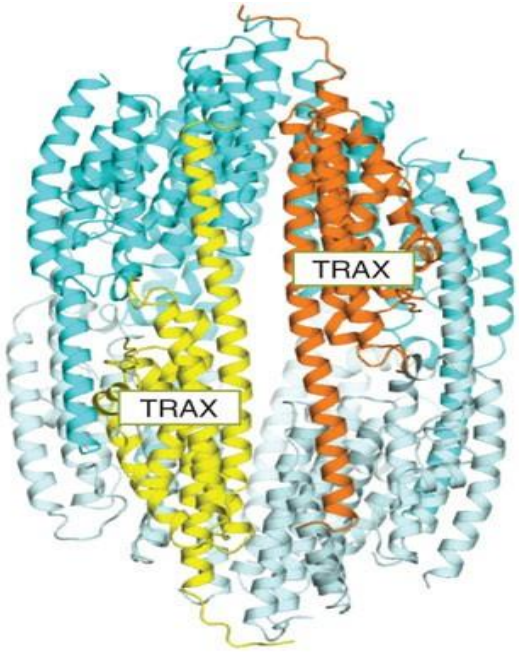

Figure 2.5 Structure of human C3PO where translin subunits are in blue and TRAX subunits are in yellow/orange. PDB Id: 3PJA.

While the exact cellular role of C3PO is under debate, there is evidence that C3PO promotes the activity of the RNA-induced silencing complex, RISC.[31] RISC is a ribonucleoprotein complex that silences gene expression by cleaving and degrading mRNA. Its activity is initiated by the RNase III enzyme Dicer to process dsRNA into ~22 nucleotide microRNA's (miRNA or miR).[32-33] For degradation to happen, a guide strand of miRNA acts as a template for a complementary mRNA passenger strand to bind. With perfect pairing, Argonaute 2 (Ago2) will nick the miRNA passenger strand and C3PO will help further degrade it, allowing the complementary mRNA to hybridize to the guide strand. Once this happens, Ago2 will nick the mRNA between the 10th and 11th nucleotide, causing it to be degraded.[34-35] If the guide strand does not match the mRNA perfectly, the Ago2-mRNA complex will stall and form aggregates, such as stress granules (Figure 2.6).

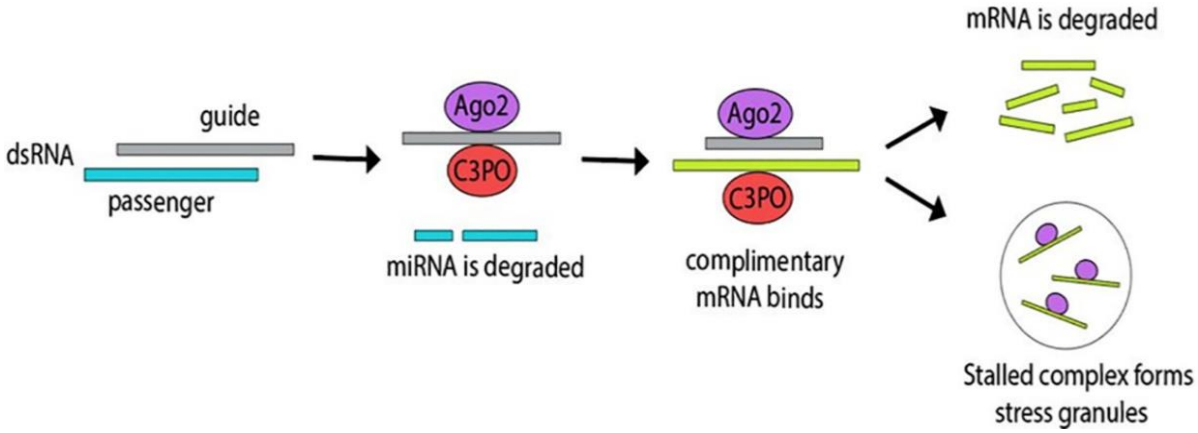

Figure 2.6 RNA silencing as a result of cleavage of miRNA byAgo2 and degradation by C3PO.

In general, inhibition of C3PO by PLCβ can reverse silencing by exogenously added siRNAs, although this is not always the case. Part of the selectivity of the oligonucleotides that are silenced by PLCβ is dictated by the relative concentration of the specific miR, the presence of any competing miRs, and the stability of the miRs. Insight into the conditions that allow PLCβ to impact hydrolysis of specific oligonucleotides can be found in the thermodynamic cycle.[36]

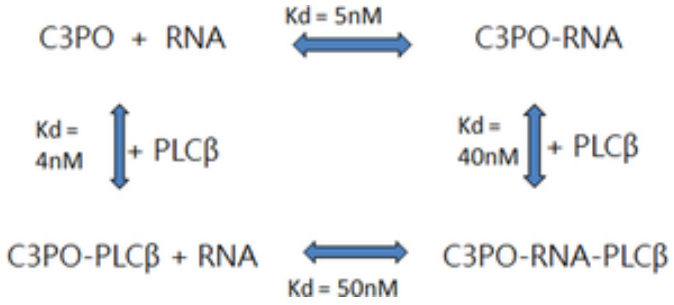

Figure 2.7 Schematic of PLCβ1, C3PO and RNA binding.

The schematic shown in Figure 2.7 lists the association of RNA to C3PO, of PLCβ to C3PO and formation of ternary complexes where the K_d values are taken from model oligonucleotides.[36] The studies show that miRs that are slowly hydrolyzed (i.e., high melting T, high GC content) and are held in the active site of C3PO for relatively long times, are subject to inhibition by PLCβ.

Alternately, less stable RNAs whose hydrolysis and product release occur during the off-rate of PLCβ, are unaffected by PLCβ binding.

In cultured neuronal cells under basal conditions, only a minor population of PLCβ binds C3PO. However, when sympathetic neurons from pheochromocytoma of rat adrenal medulla (PC12) cells, a common model for neuronal cell development,[37] are induced to differentiate, PLCβ increases its association to C3PO, and these complexes diminish as differentiation ends.[38] Surprisingly, loss of either PLCβ or C3PO reverses differentiation causing stem cell markers to be expressed and shifting miR populations to those associated with the differentiated state. These results suggest that small amounts of PLCβ-C3PO complexes are required to maintain the differentiated state.

It is important to stress the dynamics of PLCβ in inhibiting RNA-induced silencing. Activation of Gαq shifts PLCβ away from C3PO allowing silencing to continue, whereas transfection of siRNAs, promotes cytosolic localization and reduces calcium signals (Figure 2.8[39]). Thus, PLCβ is in dynamic equilibrium between these two partners.

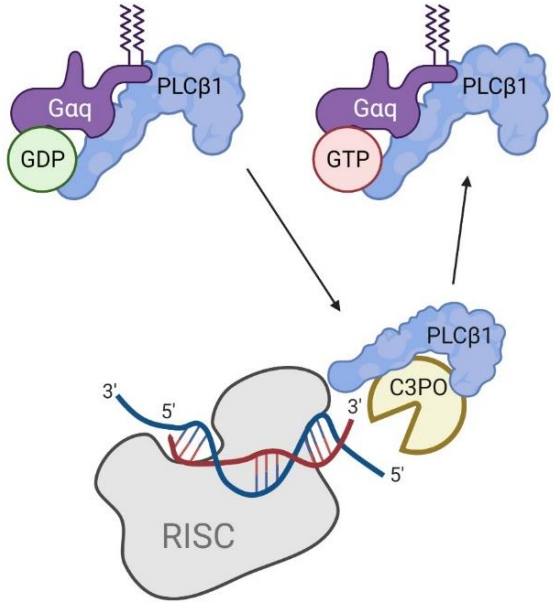

Figure 2.8 Cartoon showing the exchange of the PM and cytosolic populations of PLCβ. (Created with BioRender.com)

2.6 PLCβ impacts stress granule assembly

While the functional significance of PLCβ-C3PO association is traced to shifting miR populations to establish and maintain neuronal differentiation, under basal conditions, only a minor population of PLCβ associates with C3PO suggesting that PLCβ may have additional roles. To identify additional functions, we set out to identify additional binding partners. To this end, we isolated the cytosolic fractions of both undifferentiated PC12 cells and A10 cells (smooth muscle cell line derived from thoracic aorta of rats) and pulled-down PLCβ with a monoclonal antibody to identify the bound proteins by mass spectrometry. Surprisingly, we find that approximately one third of the bound proteins are classified as stress granule proteins.[40]

Stress granules are membraneless aggregates of stalled mRNA that prioritize protein synthesis until the stress is relieved.[41] Cells try to alleviate environmental stressors such as a change in osmotic pressure, heat, or oxidative stress by localizing untranscribed miRs into compact granules.[41-42] These granules do not have an encapsulating membrane or envelope, and are effective in partitioning themselves from the cytosol and other organelles in a liquid-like state. Stress granules give the cell an opportunity to sort mRNAs and decide whether they should be degraded, stored, or translated.[31, 43] It is important to note that assembly and disassembly of stress granules are vital to healthy neuronal function and plasticity, and the inability to disassemble has been associated with some types of neurological diseases.[44]

Stress granules are mainly composed of untranslated mRNA, but also include proteins such as Argonaute 2 (Ago2), polyadenylate binding protein 1 (PABPC1), fragile X mental retardation proteins 1 and 2 (FXR1/2), Ras, GTPase activating protein-binding Protein 1 (G3BP1), and multiple eukaryotic translation initiation factors.[44-46] We find that all of these proteins are bound to cytosolic PLCβ1.[40] Furthermore, stress granules are independent of P bodies (processing bodies), which are similar membraneless aggregates that traditionally do not contain translation initiation factors and only store degraded mRNA.[47]

Our studies show that reducing cytosolic levels of PLCβ1 by downregulation or by activating Gαq to drive PLCβ to the membrane, increases the formation of stress granules containing Ago2,

PABPC1 and G3BP1 in several types of cultured cells (Figure 2.9).[40] These observations suggest that the binding of PLCβ to stress granule proteins helps to prevent their aggregation.[48] The composition of the stress granules formed by the loss of cytosolic PLCβ and the identities of the transcripts contained are under investigation.

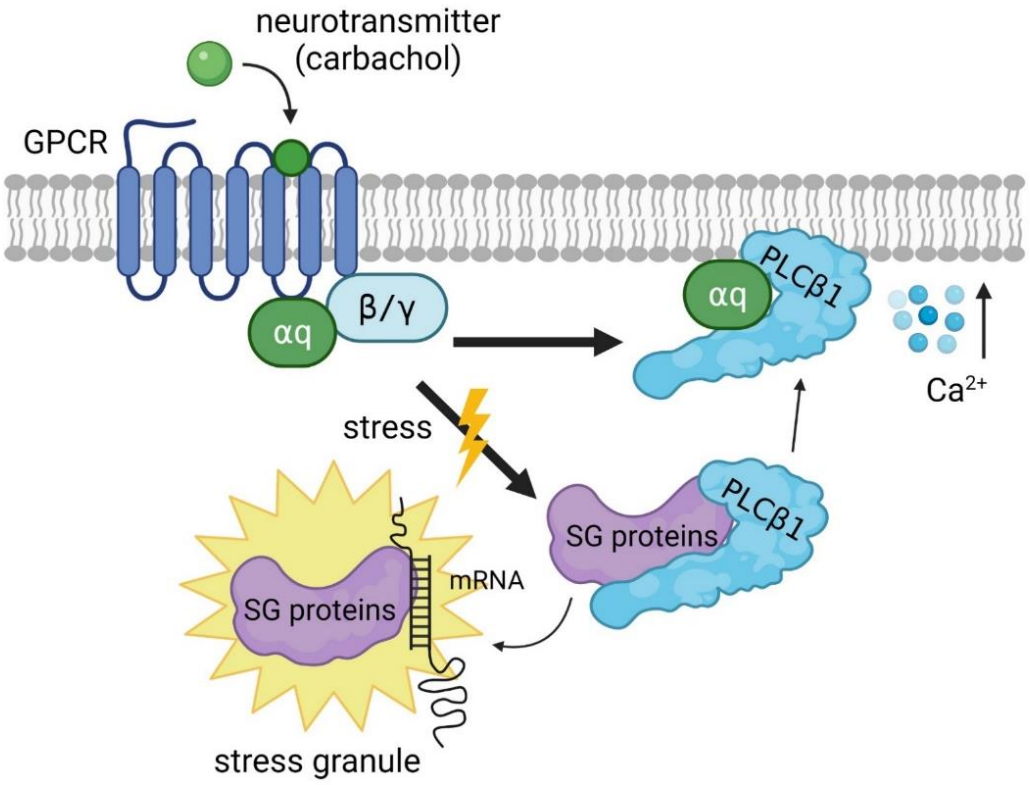

Figure 2.9 Model of PLCβ1's dynamic exchange between G proteins on the plasma membrane and stress granules. (Created with BioRender.com)

2.7 Model for the role of cytosolic PLCβ

When PLCβ1 is bound to C3PO, many small, interfering RNAs (siRNAs) fail to downregulate protein expression.C3PO competes with Gαq for the same binding site on PLCβ1,[48] so it is believed that the role of PLCβ1issplitbetween the plasma membrane, when binding with Gαq, or the cytosol when interacting with C3PO or stress granule proteins. Thus, PLCβ1 binding to Gαq reverses its inhibition of C3PO while binding to C3PO inhibits calcium signaling through Gαq activation.[48] The need to shuttle PLCβ1 between the cytosol and plasma membrane depends on

the concentration of these proteins within the cell and these processes are especially important to under-stand since they may impact key events, such as PC12 cell differentiation

Another surprising, but more limited function of PLCβ is to inhibit CDK16, which is a neuronal and testis-specific cyclin-dependent kinase that inhibits an inhibitor of proliferation, p27kip.[49-50] At the onset of PC12 cell differentiation, expression of PLCβ1 increases several-fold.[38] Besides binding to C3PO to promote differentiation, this bolus of PLCβ also binds to CDK16 to inhibit proliferation.[39] The mechanism of inhibition is not clear. Based on testing of several cell lines, it appears that the ability of PLCβ1 to impact proliferation is limited to neuronal cells where CDK16 is expressed.

2.8 Controlling the translation of PLCβ1's plasma membrane versus cytosolic function

Transition between PLCβ's two functions, that is, G protein/Ca^{2+} signaling on the plasma membrane versus inhibition of RNA-induced silencing in the cytosol, is primarily controlled by the activation of Gαq, which may override all of PLCβ's cytosolic functions. However, switching between these functions is subject to other cellular factors.

2.8.1 Control Gαq/GPCR localization

The localization of Gαq/GPCR will affect the localization of the plasma membrane population of PLCβ that exchanges with the cytosolic population. Several studies have shown that GPCRs are not homogeneous on the plasma membrane but can sequester in distinct areas, and the factors that control localization are numerous. First, it has been found that the shape of the cell regulates GPCR/Gαq localization affecting both signal transduction processes within the cell and second messenger dynamics between the plasma membrane (PM) and the endoplasmic reticulum.[51] An example of differences in calcium release in the body and neurons of PC12 cells is shown in Figure 2.10. Localization patterns may play important roles in cells with varied morphologies such as neurons and podocytes. It is notable that in neurons GPCRs play an important role in presynaptic and postsynaptic signaling leading to their necessity to be localized all along the cell not just located within the synaptic cleft.[20] These findings lead to the interesting idea that localization of

the receptors and their attached G proteins on tips and protrusions of cells may help sequester PLCβ from C3PO and stress granule proteins eliminating PLCβ's cytosolic function.

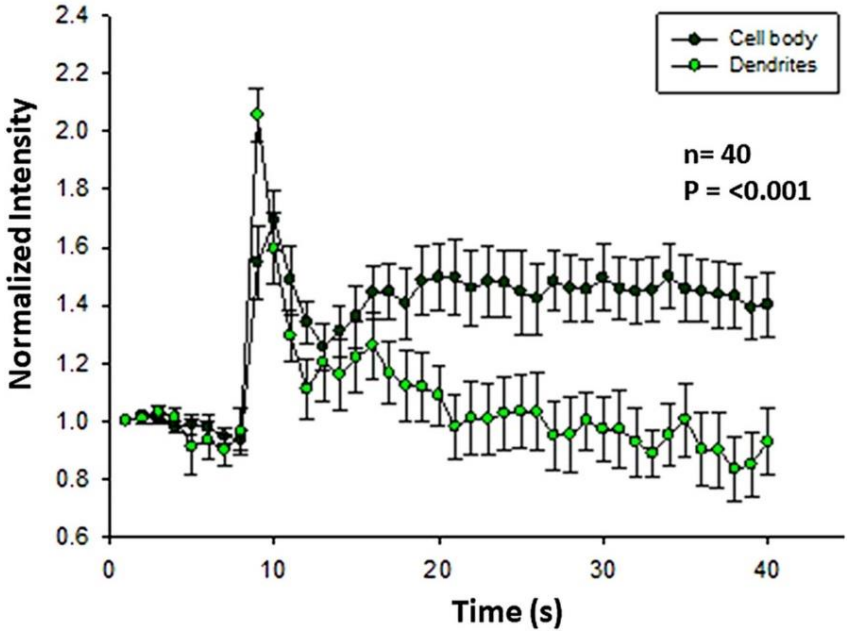

Figure 2.10 Differences in calcium signals in the dendrites versus the cell body of PC12 cells upon acetylcholine stimulation, from Garwain and Scarlata, unpublished

2.8.2 Stabilization of Gαq

The most stable and well-characterized microdomains on the plasma membrane are caveolae, and it has been shown that the presence of caveolae has profound effects on Gαq/PLCβ signaling.[52] Caveolae are protein dense invaginations on the plasma membrane. Structurally, caveolae are composed of caveolin-1 (Cav1) and/or caveolin-3 (Cav-3) where Cav-3 is muscle specific along with other proteins.[53-54] Caveolin molecules only penetrate the inner leaflet in a "U" shape, and aggregation of ~140 of these proteins results in the invaginations that are a hallmark of these domains.[55-56]

Several signaling complexes localize to caveolae leading to the idea that caveolae helps sequester and organize functionally related proteins.[54, 57-59] Our lab has found that Cav-1 or -3 specifically binds Gαq and their affinity increases when Gαq is activated.[60] The stabilization of activated Gαq

by Cav1/3, coupled with release of Gβγ from caveolae domains during the activation cycle, has the net effect of prolonging PLCβ activation and increasing the extent and duration of Ca^{2+} responses.[61] The interaction between Cav1/3 not only localizes Gαq to caveolae domains, but also in turn allows Gαq to scaffold its associated GPCRs leading to a localized and potentially synergistic response.[62]

Caveolae are prominent in smooth muscle cells and provide mechanical strength by flattening during stretch to provide more membrane area.[63-64] We have found that the flattening of these domains by mechanical stretch or hypo-osmotic conditions eliminates stabilization of activated Gαq by caveolin molecules reducing Ca^{2+} signals.[65-66] Additionally, osmotic stress reduces the cytosolic level of PLCβ eliminating its cytosolic function.[40] Thus, caveolae have the potential to regulate the cytosolic versus plasma membrane functions of PLCβ by modulating the localization of Gαq and the duration of its activated state (Figure 2.11).

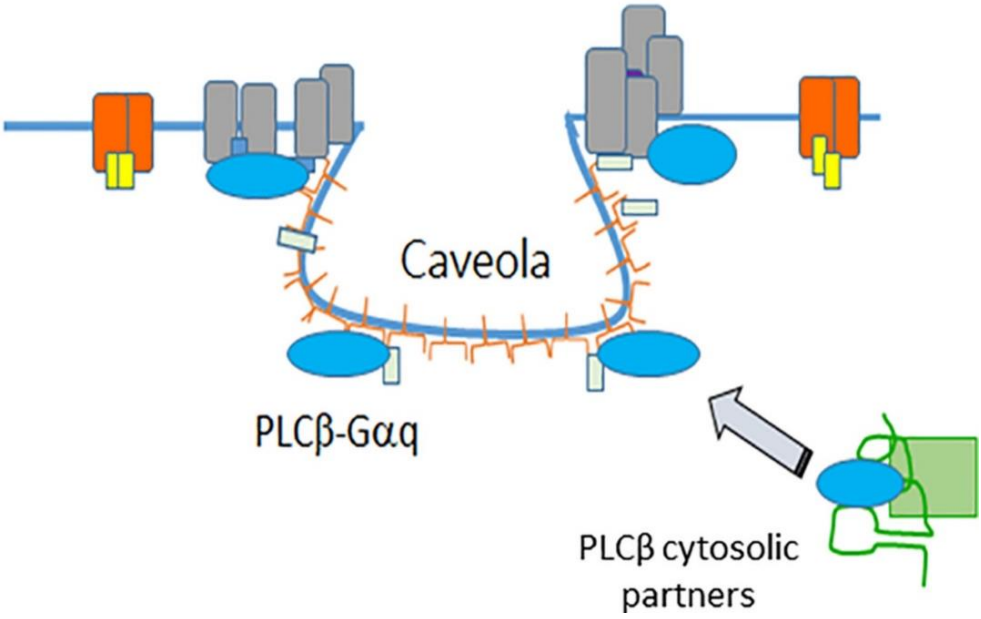

Figure 2.11 Model depicting localization of PLCβ (blue), and Gαq (light gray) and their corresponding GPCRs (dark gray) in caveolae where caveolin molecules are in red. GPCRs coupled to other G proteins are in red and yellow

2.9 Predicting the impact of Gαq/PLCβ activation on calcium signals versus protein translation

Being able to delineate the factors that regulate the localization and activation of Gαq is a first step in predicting the ability of PLCβ to generate calcium responses or modulating protein translation. While present day methods are moving toward accurate quantification of the molecular identities, quantities and localization of proteins in cells, these values can only be estimated. Nevertheless, we can formulate a thermodynamic analysis that should be applicable in predicting the regulation of multifunctional proteins.

2.10 Functional switching of proteins

PLCβ is an example of a protein that has multiple cellular functions that switch upon activation, growth, differentiation, or other cellular events. Functional switching involves three key factors: (a) *Changes in the local concentration of protein and its relative partners*; (b) *Changes in relative affinities*; *and* (c) *Changes in the concentration and relative affinities of extraneous but competing proteins*.

The most simple analysis assumes that the observed PLCβ function stems from the relative plasma membrane versus cytosolic concentrations resulting from two competing bimolecular associations; one that impacts Ca^{2+} signals and one that impacts protein translation (PT). The key feature for PLCβ, and possibly other systems, is that simultaneous binding of Gαq and C3PO does not occur (PLCβ's interaction region with other cytosolic partners has not yet been determined).

The equilibria of PLCβ's function (K_f), can be considered as the ratio of the concentration of PLCβ bound to Gαq (PLCβ-Gαq) versus C3PO and other cytosolic partners (PLCβ-CP).

$$K_f=[PLC\beta\cdot G\alpha q]/[PLC\beta\cdot CP]$$

Where these complexes are described by the dissociation constants associated with PLCβ's calcium function (K_d[f-Ca^{2+}]) or PLCβ's cytosolic function (K_d[f-CP]):

$$PLC\beta + G\alpha q = PLC\beta \cdot G\alpha q; \qquad K_d(f \cdot Ca^{2+}) = ([PLC\beta]*[G\alpha q])/[PLC\beta \cdot G\alpha q]$$

$$PLC\beta + CP = PLC\beta \cdot CP \qquad K_d(f \cdot CP) = ([PLC\beta]*[CP])/[PLC\beta \cdot CP]$$

Substituting and rearranging gives

$$Kf = [G\alpha q]*K_d(f \cdot Ca^{2+})/[CP]*K_d(f \cdot CP)$$

The above expression shows that the observed function of PLCβ is surprisingly independent of concentration and only dependent of the relative cellular concentration of the competing partners. The dissociation constants for the PLCβ-Gαq (both in its inactivated and activated states) complexes and the complexes formed between PLCβ and C3PO and/or the putative stress granule binding partner eukaryotic initiation factor 5A, have been measured using purified proteins.[4, 25, 40] More relevant dissociation constants can be obtained using cell extracts that will allow for quantification of the dissociated species and their complexes. We know that the binding of C3PO to PLCβ1 is stronger than Gαq(GDP) but weaker than Gαq(GTP), and these differences are within a 10-fold range allowing cells to switch PLCβ functions as needed depending on cellular circumstances. These expressions are regulated by three major factors.

2.11 The local concentration of protein and its relative partners; effects of compartmentalization

Cell compartmentalization allows cells to sequester components to promote some interactions while preventing others. For the case of PLCβ, compartmentalization takes the form of concentrating PLCβ's main partner, Gαq on the PM surface. PLCβ association with Gαq in this compartment is regulated by its intrinsic membrane binding, which enhances its association with Gαq by a reduction of dimensionality.

$$PLC(cytosol) = PLC\beta(PM)$$

$$PLC(PM) + G\alpha q = PLC\beta \cdot G\alpha q(PM)$$

The concentrating effect of the plasma membrane has been previously treated[4] by considering that membrane-bound proteins are confined in a reduced volume (v) in relation to the bulk volume (V_b). The relationship between the amount of protein bound to a membrane, $[P]_{(membrane)}$ to its unbound concentration in the bulk $[P]_{(bulk)}$ effect can be expressed

$$[P]_{(membrane)}=[P]_{(bulk)}*(V_b/v)$$
$$v=4\pi r^2 d$$

Where v is the reduced volume of a spherical membrane with a known radius (r) and diameter (d). The apparent dissociation constant will be reduced by:

$$K_d=(V_b/v)K_{app}$$

This equation quantifies the increased affinity of two membrane-bound proteins versus their association in bulk solution and can be readily modified to a single membrane-bound species or multiple membrane associations. Analysis for proteins reconstituted on lipid vesicles is straightforward but more challenging for cellular systems because of uncertainty in the membrane surface area that the protein is confined; that is, proteins might diffuse in a limited surface area due to protein barriers, be confined to a domain such as caveolae, and/or a combination of the two. While these parameters are important for integral membrane proteins such as GPCRs, peripheral membrane proteins such as PLCβ undergo dissociation and reassociation events as dictated by their partition coefficients. Gαq, which is stably bound to the membrane by two palmitoyl groups[67] and bound to GPCR, has much more stable binding. Despite these complications, single molecule measurements may be used to estimate the amount of protein per surface area and the impact of plasma membrane partitioning on protein affinities.

In the case of Gαq/PLCβ association in cells, it is not clear whether the observed plasma membrane population is bound to membrane or Gαq. While PLCβ partitions to model bilayers with the partition coefficient, Kp ~1–10 μM[16] the amount of lipid available for binding is unclear. Thus, it is likely that the plasma membrane population PLCβ is complexed to Gαq in both its deactivated and activated, and this is supported by FRET studies.[68]

2.12 Changes in relative affinities

All cellular events can be traced to changes in protein association due to changes in affinity. These changes in affinity can be brought about by the binding of ligands to extracellular or intracellular targets, phosphorylation/dephosphorylation, ATP hydrolysis, and so forth. For the Gαq/PLCβ pathway, activation of Gαq increases its affinity for PLCβ 20-fold,[4] which is stronger than the affinity measured for PLCβ /C3PO,[25] and possibly the affinities with other cytosolic proteins. Notably, the cumulative affinities of these cytosolic proteins may not completely compete with activated Gαq. Thus, the net effect of Gαq activation is to shift cytosolic populations of PLCβ to the membrane surface and away from cytosolic partners. Additionally, because Gαq resides on the quasi two-dimensional surface of a membrane, increase in affinity is enhanced.

Measuring affinities of proteins is difficult in intact cells and changes in affinities are taken from data using purified proteins, but it is assumed that the magnitude of the changes in affinity seen in solution occur in cells. Besides affinities, it is important to estimate the local concentrations of the associating proteins, which depend on the number of molecules, the compartmentalization and competing proteins (*see below*). One method to estimate relative affinities is by measuring the loss in FRET between two labeled proteins as known amounts of competitors using fluorescent-tagged proteins. These estimates are certain to become more quantitative as more sophisticated methods are available.

2.13 Concentration and relative affinities of extraneous, competing proteins

The least known variable in predicting exchange of protein partners in the complex milieu of the cell is the presence of competing proteins. Some of these interactions may have unclear functional relevance. It is likely that many of these interactions Here, we discuss several types of competing associations that might simplify analysis when predicting the switching of bifunctional proteins.

2.13.1 The presence of multiple isoforms of a given enzyme localized in the same compartment

Some cells express multiple isoforms of a protein that localize in similar compartments which, because of slightly varying affinities and activation profiles, allow cells to fine-tune responses. This is certainly the case for PLCβ where many cells express several isoforms at varying levels. Solution studies show that PLCβ1-3 bind to Gαq within an order of magnitude.[4] Additionally, all bind to Gβγ subunits but their activation profiles are very different; PLCβ1 is not activated by Gβγ while PLCβ2-3 are activated 2–10-fold.

When considering multiple isoforms of a protein and the affinities between the partners involved in the switching are not large, it is easiest to consider the isoforms as a single species that has a range of dissociation constants.

2.13.2 Competitors whose binding overlaps a primary binding site

If a competitive protein binds to a partner, there would be less of the partner available for binding and functional switching. The impact will depend on its affinity and local concentration. We can estimate these effects:

For the association of A and B: $A + B = AB$

$$K(AB) = [AB]/([A] * [B])$$

If competitor C binds to B: $C + B = CB$

$$K(CB) = [BC]/([C] * [B])$$

Substituting and rearranging gives

$$K(AB)/K(CB) = ([AB]/[A]) * ([BC]/[C])$$

Thus, in order for a reaction of weaker affinity to affect the primary reaction, the local concentration must compensate for the lower affinity.

2.13.3 Competitors whose binding only partially overlap the binding site

Many proteins have multiple binding sites that include the binding of other proteins, such as those discussed above, or allow partial exposure of the binding site. The degree of exposure will shift the impact from negligible for a small degree of occlusion to the equations above for complete exclusion

2.14 Conclusions and take-home lessons

PLCβ is an example of a protein that has evolved to perform multiple functions in cells. These interdependent functions allow cells to respond in multiple and complementary ways to extracellular sensory information, that is, through pathways that involve calcium fluxes and through changes in the translation of different proteins. While the primary calcium function has been well characterized, PLCβ's secondary functions are just beginning to be uncovered.

Multifunctional proteins switch between various cellular roles through changes in protein associations. These changes may be brought about by chemical modifications, such as phosphorylation, or local changes in concentration of a protein partner through the appearance of an activated cofactor or changes in compartmentalization. Although we are still far from accurate quantitation of the factors that allow functional switching in living cells and tissue, we have begun to formulate analysis from when they become available.

2.15 Acknowledgments

The authors are grateful for support from NIH GM 116187 and the Richard Whitcomb foundation.

2.16 References

1. Hepler, J. R.; Gilman, A. G., G-proteins. *Trends Biochem. Sciences* **1992,** *17*, 383-387.
2. Jong, Y. I.; Harmon, S. K.; O'Malley, K. L., Intracellular GPCRs Play Key Roles in Synaptic Plasticity. *ACS Chem Neurosci* **2018,** *9* (9), 2162-2172.
3. Devi, L. A., Heterodimerization of G-protein-coupled receptors: pharmacology, signaling and trafficking. *Trends in Pharmacological Sciences* **2001,** *22* (10), 532-537.
4. Runnels, L. W.; Scarlata, S., Determination of the affinities between heterotrimeric G protein subunits and their phospholipase C- β effectors. *Biochemistry* **1999,** *38*, 1488-1496.
5. Penela, P.; Ribas, C.; Sanchez-Madrid, F.; Mayor, F., Jr., G protein-coupled receptor kinase 2 (GRK2) as a multifunctional signaling hub. *Cell Mol Life Sci* **2019,** *76* (22), 4423-4446.
6. Neves, S. R.; Ram, P. T.; Iyengar, R., G Protein Pathways. *Science* **2002,** *296* (5573), 1636-1639.
7. Lee, C. H.; Park, D.; Wu, D.; Rhee, S. G.; Simon, M. I., Members of the Gq alpha subunit gene family activate phospholipase C beta isozymes. *J Biol Chem* **1992,** *267* (23), 16044-7.
8. Drin, G.; Scarlata, S., Stimulation of phospholipase C[beta] by membrane interactions, interdomain movement, and G protein binding -- How many ways can you activate an enzyme? *Cellular Signalling* **2007,** *19* (7), 1383-1392.
9. Bittner, M. A.; Holz, R. W., Phosphatidylinositol-4,5-bisphosphate: actin dynamics and the regulation of ATP-dependent and -independent secretion. *Mol Pharmacol* **2005,** *67* (4), 1089-98.
10. Dickinson, G. D.; Ellefsen, K. L.; Dawson, S. P.; Pearson, J. E.; Parker, I., Hindered cytoplasmic diffusion of inositol trisphosphate restricts its cellular range of action. *Sci Signal* **2016,** *9* (453), ra108.
11. Rosenberg, S. S.; Spitzer, N. C., Calcium Signaling in Neuronal Development. *Cold Spring Harb Perspect Biol* **2011,** *3* (10).
12. Stiber, J. A.; Rosenberg, P. B., The role of store-operated calcium influx in skeletal muscle signaling. *Cell Calcium* **2011,** *49* (5), 341-349.
13. Park, D.; Jhon, D.; C., L.; Lee, K.; Rhee, S. G., Activation of Phospholipase C Isozymes by G Protein βγ Subunits. *J. Biol. Chem.* **1993,** *268* (7), 4573-4576.
14. Philip, F.; Kadamur, G.; Silos, R. G.; Woodson, J.; Ross, E. M., Synergistic Activation of Phospholipase C-²3 by G±q and G²³ Describes a Simple Two-State Coincidence Detector. *Current biology : CB* **2010,** *20* (15), 1327-1335.
15. Cabrera-Vera, T. M.; Vanhauwe, J.; Thomas, T. O.; Medkova, M.; Preininger, A.; Mazzoni, M. R.; Hamm, H. E., Insights into G Protein Structure, Function, and Regulation. *Endocr Rev* **2003,** *24* (6), 765-781.
16. Runnels, L. W.; Jenco, J.; Morris, A.; Scarlata, S., Membrane binding of phospholipases C-β_1 and C-β_2 is independent of phosphatidylinositol 4,5-bisphosphate and the α and βγ subunits of G proteins. *Biochemistry* **1996,** *35* (51), 16824-32.
17. Yang, B.; Pu, M.; Khan, H. M.; Friedman, L.; Reuter, N.; Roberts, M. F.; Gershenson, A., Quantifying transient interactions between Bacillus phosphatidylinositol-specific phospholipase-C and phosphatidylcholine-rich vesicles. *J Am Chem Soc* **2015,** *137* (1), 14-7.
18. Suzuki, K. G.; Fujiwara, T. K.; Edidin, M.; Kusumi, A., Dynamic recruitment of phospholipase C gamma at transiently immobilized GPI-anchored receptor clusters induces IP3-Ca2+ signaling: single-molecule tracking study 2. *J Cell Biol* **2007,** *177* (4), 731-42.

19. Lyon, A. M.; Dutta, S.; Boguth, C. A.; Skiniotis, G.; Tesmer, J. J., Full-length Galpha(q)-phospholipase C-beta3 structure reveals interfaces of the C-terminal coiled-coil domain. *Nat Struct Mol Biol* **2013,** *20* (3), 355-62.
20. Huang, Y.; Thathiah, A., Regulation of neuronal communication by G protein-coupled receptors. *FEBS Lett* **2015,** *589* (14), 1607-19.
21. Rebecchi, M.; Pentylana, S., Structure, function and control of phosphoinositide-specific phospholipase C. *Physiological Reviews* **2000,** *80*, 1291-1335.
22. Hill-Eubanks, D. C.; Werner, M. E.; Heppner, T. J.; Nelson, M. T., Calcium signaling in smooth muscle. *Cold Spring Harb Perspect Biol* **2011,** *3* (9), a004549.
23. Wu, D.; Jiang, H.; Katz, A.; Simon, M. I., Identification of critical regions on phospholipase C-beta 1 required for activation by G-proteins. *J Biol Chem* **1993,** *268* (5), 3704-9.
24. Lyon, A. M.; Tesmer, J. J. G., Structural insights into phospholipase C-β function. *Molecular pharmacology* **2013,** *84* (4), 488-500.
25. Aisiku, O. R.; Runnels, L. W.; Scarlata, S., Identification of a Novel Binding Partner of Phospholipase Cβ1: Translin-Associated Factor X. *PLoS One* **2010,** *5* (11).
26. Cho, Y. S.; Chennathukuzhi, V. M.; Handel, M. A.; Eppig, J.; Hecht, N. B., The Relative Levels of Translin-associated Factor X (TRAX) and Testis Brain RNA-binding Protein Determine Their Nucleocytoplasmic Distribution in Male Germ Cells. *J. Biol. Chem.* **2004,** *279* (30), 31514-31523.
27. Yang, S.; Cho, Y. S.; Chennathukuzhi, V. M.; Underkoffler, L. A.; Loomes, K.; Hecht, N. B., Translin-associated Factor X Is Post-transcriptionally Regulated by Its Partner Protein TB-RBP, and Both Are Essential for Normal Cell Proliferation. *J. Biol. Chem.* **2004,** *279* (13), 12605-12614.
28. Ye, X.; Huang, N.; Liu, Y.; Paroo, Z.; Huerta, C.; Li, P.; Chen, S.; Liu, Q.; Zhang, H., Structure of C3PO and mechanism of human RISC activation. *Nat Struct Mol Biol* **2011,** *18* (6), 650-657.
29. Tian, Y.; Simanshu, D. K.; Ascano, M.; Diaz-Avalos, R.; Park, A. Y.; Juranek, S. A.; Rice, W. J.; Yin, Q.; Robinson, C. V.; Tuschl, T.; Patel, D. J., Multimeric assembly and biochemical characterization of the Trax–translin endonuclease complex. *Nat Struct Mol Biol* **2011,** *18* (6), 658-664.
30. Sahu, S.; Philip, F.; Scarlata, S., Hydrolysis Rates of Different Small Interfering RNAs (siRNAs) by the RNA Silencing Promoter Complex, C3PO, Determines Their Regulation by Phospholipase Cβ. *J. Biol. Chem.* **2014,** *289* (8), 5134-5144.
31. Liu, Y.; Ye, X.; Jiang, F.; Liang, C.; Chen, D.; Peng, J.; Kinch, L. N.; Grishin, N. V.; Liu, Q., C3PO, an Endoribonuclease That Promotes RNAi by Facilitating RISC Activation. *Science* **2009,** *325* (5941), 750-753.
32. Lo Vasco, V. R.; Longo, L.; Polonia, P., Phosphoinositide-specific Phospholipase C β1 gene deletion in bipolar disorder affected patient. *J Cell Commun Signal* **2013,** *7* (1), 25-29.
33. Kurian, M. A.; Meyer, E.; Vassallo, G.; Morgan, N. V.; Prakash, N.; Pasha, S.; Hai, N. A.; Shuib, S.; Rahman, F.; Wassmer, E.; Cross, J. H.; O'Callaghan, F. J.; Osborne, J. P.; Scheffer, I. E.; Gissen, P.; Maher, E. R., Phospholipase C beta 1 deficiency is associated with early-onset epileptic encephalopathy. *Brain* **2010,** *133* (10), 2964-2970.
34. Golebiewska, U.; Scarlata, S., High pressure promotes alpha-synuclein aggregation in cultured neuronal cells. *FEBS Letters* **2015,** *589* (21), 3309-3312.
35. Narayanan, V.; Scarlata, S., Membrane Binding and Self-Association of α-Synucleins. *Biochemistry* **2001,** *40* (33), 9927-9934.

36. Sahu, S.; Williams, L.; Perez, A.; Philip, F.; Caso, G.; Zurawsky, W.; Scarlata, S., Regulation of the activity of the promoter of RNA-induced silencing, C3PO. *Protein Science* **2017,** *26* (9), 1807-1818.
37. Greene, L. A.; Tischler, A. S., Establishment of a noradrenergic clonal line of rat adrenal pheochromocytoma cells which respond to nerve growth factor. *Proc Natl Acad Sci U S A* **1976,** *73* (7), 2424-2428.
38. Garwain, O.; Scarlata, S., Phospholipase Cβ-TRAX Association Is Required for PC12 Cell Differentiation. *J. Biol. Chem.* **2016,** *291* (44), 22970-22976.
39. Scarlata, S.; Singla, A.; Garwain, O., Phospholipase Cβ Interacts With Cytosolic Partners to Regulate Cell Proliferation. *Adv Biol Regul* **2018,** *67*, 7-12.
40. Qifti, A.; Jackson, L.; Singla, A.; Garwain, O.; Scarlata, S., Stimulation of phospholipase Cbeta1 by Galphaq promotes the assembly of stress granule proteins. *Sci Signal* **2021,** *14* (705), eaav1012.
41. Philip, F.; Sahu, S.; Caso, G.; Scarlata, S., Role of Phospholipase C-β in RNA interference. *Adv Biol Regul* **2013,** *53* (3), 319-330.
42. Li, L.; Gu, W.; Liang, C.; Liu, Q.; Mello, C. C.; Liu, Y., The Translin-TRAX complex/C3PO is a ribonuclease in tRNA processing. *Nat Struct Mol Biol* **2012,** *19* (8), 824-830.
43. Park, A. J.; Havekes, R.; Fu, X.; Hansen, R.; Tudor, J. C.; Peixoto, L.; Li, Z.; Wu, Y.-C.; Poplawski, S. G.; Baraban, J. M.; Abel, T., Learning induces the translin/trax RNase complex to express activin receptors for persistent memory. *eLife* **2017,** *6*, e27872.
44. Pratt, A. J.; MacRae, I. J., The RNA-induced Silencing Complex: A Versatile Gene-silencing Machine. *J. Biol. Chem.* **2009,** *284* (27), 17897-17901.
45. Babar, I. A.; Slack, F. J.; Weidhaas, J. B., miRNA modulation of the cellular stress response. *Future Oncology* **2008**.
46. Buchan, J. R.; Parker, R., Eukaryotic Stress Granules: The Ins and Out of Translation. *Molecular Cell* **2009,** *36* (6), 932.
47. Hyman, A. A.; Weber, C. A.; Julicher, F., Liquid-liquid phase separation in biology. *Annu Rev Cell Dev Biol* **2014,** *30*, 39-58.
48. Decker, C. J.; Parker, R., P-Bodies and Stress Granules: Possible Roles in the Control of Translation and mRNA Degradation. *Cold Spring Harb Perspect Biol* **2012,** *4* (9), a012286.
49. Mikolcevic, P.; Sigl, R.; Rauch, V.; Hess, M. W.; Pfaller, K.; Barisic, M.; Pelliniemi, L. J.; Boesl, M.; Geley, S., Cyclin-Dependent Kinase 16/PCTAIRE Kinase 1 Is Activated by Cyclin Y and Is Essential for Spermatogenesis. *Molecular and Cellular Biology* **2012,** *32* (4), 868-879.
50. Yanagi, T.; Matsuzawa, S.-i., PCTAIRE1/PCTK1/CDK16: a new oncotarget? *Cell Cycle* **2015,** *14* (4), 463-464.
51. Rangamani, P.; Lipshtat, A.; Azeloglu, Evren U.; Calizo, Rhodora C.; Hu, M.; Ghassemi, S.; Hone, J.; Scarlata, S.; Neves, Susana R.; Iyengar, R., Decoding Information in Cell Shape. *Cell* **2013,** *154* (6), 1356-1369.
52. Weinstein, H.; Scarlata, S., The correlation between multidomain enzymes and multiple activation mechanisms--the case of phospholipase Cbeta and its membrane interactions. *Biochim Biophys Acta* **2011,** *1808* (12), 2940-7.
53. Gratton, J. P.; Bernatchez, P.; Sessa, W. C., Caveolae and caveolins in the cardiovascular system. *Circ Res* **2004,** *94* (11), 1408-17.
54. Bastiani, M.; Parton, R. G., Caveolae at a glance. *J Cell Sci* **2010,** *123* (22), 3831-3836.

55. Murthy, K. S.; Makhlouf, G. M., Heterologous desensitization mediated by G protein-specific binding to caveolin. *J Biol Chem* **2000,** *275* (39), 30211-9.
56. Echarri, A.; Del Pozo, M. A., Caveolae - mechanosensitive membrane invaginations linked to actin filaments. *J Cell Sci* **2015,** *128* (15), 2747-58.
57. Anderson, R. G., The caveolae membrane system. *Annu.Rev.Biochem.* **1998,** *67*, 199-225.
58. Kovtun, O.; Tillu, V. A.; Ariotti, N.; Parton, R. G.; Collins, B. M., Cavin family proteins and the assembly of caveolae. *J Cell Sci* **2015,** *128* (7), 1269-1278.
59. Schlegel, A.; Volonte, D.; Engelman, J. A.; Galbiata, F.; Mehta, P.; Zhange, X.-L.; Scherer, P.; Lisanti, M. P., Crowded little caves: structure and function of caveolae. *Cell Signal.* **1998,** *10*, 457-463.
60. Sengupta, P.; Philip, F.; Scarlata, S., Caveolin-1 alters Ca2+ signal duration through specific interaction with the G{alpha}q family of G proteins. *J Cell Sci* **2008,** *121* (9), 1363-1372.
61. Guo, Y.; Golebiewska, U.; Scarlata, S., Modulation of Ca2+ Activity in Cardiomyocytes through Caveolae-G[alpha]q Interactions. *Biophysical Journal* **2011,** *100* (7), 1599-1607.
62. Calizo, R. C.; Scarlata, S., A role for G-proteins in directing G-protein-coupled receptor-caveolae localization. *Biochemistry* **2012,** *51* (47), 9513-23.
63. Sinha, B.; Köster, D.; Ruez, R.; Gonnord, P.; Bastiani, M.; Abankwa, D.; Stan, R. V.; Butler-Browne, G.; Vedie, B.; Johannes, L.; Morone, N.; Parton, R. G.; Raposo, G.; Sens, P.; Lamaze, C.; Nassoy, P., Cells Respond to Mechanical Stress by Rapid Disassembly of Caveolae. *Cell* **2011,** *144* (3), 402-413.
64. Yang, L.; Scarlata, S., Super-resolution Visualization of Caveola Deformation in Response to Osmotic Stress. *J Biol Chem* **2017,** *292* (9), 3779-3788.
65. Guo, Y.; Yang, L.; Haught, K.; Scarlata, S., Osmotic Stress Reduces Ca2+ Signals through Deformation of Caveolae. *J Biol Chem* **2015,** *290* (27), 16698-707.
66. Qifti, A.; Garwain, O.; Scarlata, S., Mechanical Stretch Redefines Membrane Galphaq-Calcium Signaling Complexes. *J Membr Biol* **2019,** *252* (4-5), 307-315.
67. Wedegaertner, P.; Wilson, P.; Bourne, H., Lipid modifications of trimeric G proteins. *J.Biol.Chem.* **1995,** *270*, 503-506.
68. Dowal, L.; Provitera, P.; Scarlata, S., Stable association between G alpha(q) and phospholipase C beta 1 in living cells. *J Biol Chem* **2006,** *281* (33), 23999-4014.

3 Chapter 3 – Stimulation of phospholipase Cβ1 by Gαq promotes the assembly of stress granule proteins

Androniqi Qifti[†1], Lela Jackson[†1], Ashima Singla[1], Osama Garwain[1] and Suzanne Scarlata[1]

† - These authors contributed equally to this work

1 - Department of Chemistry & Biochemistry, Worcester Polytechnic Institute, Worcester, MA

The following subsections appear in Qifti & Jackson *et al.* "Stimulation of phospholipase Cβ1 by Gαq promotes the assembly of stress granule proteins" *Science Signaling.* (2021) and are reproduced here with permission. Supporting information from the manuscript can be found in the appendix. Sections with an asterisk (*) indicate additional sections not included in the original publication. A.Q., L.J., A.S., O.G. and S.S. designed experiments and interpreted the data. A.Q., L.J., and S.S. developed the signaling model and developed the manuscript. L.J. conducted and analyzed the following experiments: GFP immunoprecipitation, FLIM/FRET, number and brightness of eGFP-G3BP1 in PC12 cells and mass spectrometry analysis. A.Q. conducted and analyzed the following experiments: western blots, PLC cytosolic relocalization, PABPC1 and Ago2 particle analysis in live and fixed PC12 cells, PABPC1 particle analysis in A10 cells, number and brightness of eGFP-Ago2 in PC12 and WKO-3M22 cells and dynamic light scattering. O.G. conducted and analyzed the following experiments: immunoprecipitation of PABPC1 and Ago2, FLIM/FRET, and co-localization experiment between Ago2 and PABPC1. A.S. conducted the mass spectrometry experiment and calcium release experiment.

3.1 Abstract

During adverse conditions, mammalian cells suppress protein production by sequestering the translational machinery in membrane-less organelles known as stress granules. Here, we found that activation of the G protein subunit Gαq promoted the formation of particles that contained stress granule proteins through a mechanism linked to a cytosolic fraction of phospholipase Cβ1 (PLCβ1). In experiments with PC12 and A10 cells, we showed that under basal conditions, cytosolic PLCβ1 bound to stress granule–associated proteins, including PABPC1, eIF5A, and Ago2. Knockdown of cytosolic PLCβ1 with siRNA or promoting its relocalization to the plasma membrane by activating Gαq resulted in the formation of particles containing these stress granule–associated proteins. Our studies showed that the composition of these particles resembled those formed under osmotic stress and were distinct from those formed in response to other types of stress. Our results fit a simple thermodynamic model in which cytosolic PLCβ1 solubilizes stress granule proteins such that its movement to activated Gαq releases these proteins to enable the formation of stress granules. Together, our data suggest a link between Gαq-coupled signals and protein translation through stress granule formation.

3.2 Introduction

When cells are subjected to environmental stresses, they halt the production of many housekeeping proteins to preserve resources for the synthesis of proteins that will help the cell alleviate the particular stress. These stalled translation complexes, called stress granules, are thought to act as triage sites that protect non-translated mRNAs from degradation until the stress is removed while enabling the synthesis of other proteins.[1-2] Stress granules are distinct from processing bodies (P-bodies) that store and process mRNA, although these have also been observed under nonstress conditions. Depending on the cellular conditions, the mRNA held in these stalled complexes may be degraded, translated, or stored until needed. In addition, studies in yeast subjected to hypo-osmotic stress found that P-bodies and stress granules may form hybrid structures,[3] although this behavior has not yet been observed in higher eukaryotes. Physically, stress granules are phase-separated domains composed of non-translating mRNAs, translation initiation complexes, PABPC1, and many additional mRNA-related proteins.[4] They consist of a packed core with loosely associated peripheral proteins.[5] Stress granules appear when cells are subjected to

environmental conditions such as cold or heat shock, exposure to toxic molecules, oxidative stress, hypo- or hyperosmolarity, ultraviolet irradiation, or nutrient deprivation. The molecular mechanisms that transduce these different stresses into the cellular interior remain largely unresolved. Although stress granules appear in many types of cells, we focused here on those that form in mammalian cells. Stress granules have been implicated in the pathogenesis of various diseases, such as cancer, neurodegeneration, and viral infections.[1, 6] Many stress granule proteins contain disordered regions, which play important roles in the liquid-like nature of stress granules. Neuronal cells, in particular, contain many proteins with disordered regions, and so, it is expected that some neurological diseases (for example, amyotrophic lateral sclerosis) have been attributed to the abnormal stability of stress granules.[7] Thus, it is important that cells have mechanisms to prevent the premature formation of stress granules, as well as to ensure their reversible assembly and disassembly.

Whereas stress granules primarily contain proteins associated with translation, note that Argonaut 2 (Ago2) can be found in these regions,[8] Ago2 is the main nuclease component of the RNA-induced silencing complex (RISC).[9] Ago2 binds to small interfering RNAs (siRNAs) in their double-stranded form and holds the guide strand after the passenger strand is degraded to enable hybridization with a target mRNA. If pairing between the passenger strand and the mRNA is perfect, as is the case with exogenous siRNAs, then Ago2 will undergo conformational changes that result in mRNA degradation. Alternatively, if pairing is imperfect, as is frequently the case for endogenous microRNAs (miRNAs), the conformational changes that enable Ago2 nuclease activity do not occur, which results in the formation of a stalled complex.[10] Thus, the formation and stability of these stalled complexes and their incorporation into stress granules alter protein populations, which may modify downstream protein-protein interactions that may ultimately change the properties of the cell.

The mechanisms through which environmental changes are transduced into the cell to promote stress granule formation are unclear and are likely to differ with different types of stress. Here, we showed that extracellular signals can affect stress granule formation through heterotrimeric guanine nucleotide–binding proteins (G proteins) to stall protein translation. Signaling through G proteins is initiated when external ligands bind to their target G protein–coupled receptors

(GPCRs), which activates intracellular Gα subunits. The Gαq family of G proteins is activated by GPCRs for agents such as acetylcholine, dopamine, bradykinin, serotonin, and histamine.[11-12] Activated Gαq, in turn, activates phospholipase Cβ (PLCβ), which catalyzes the hydrolysis of the signaling lipid phosphatidylinositol-4,5-bisphosphate, which eventually results in an increase in intracellular calcium (Ca^{2+}) signaling. There are four known members of the PLCβ family, which differ in their tissue distribution and their ability to be activated by G proteins.[12] Here, we focused on PLCβ1, which is the isoform most highly activated by Gαq and is prominent in neuronal tissue. Whereas the major population of PLCβ1 lies at the plasma membrane, where it binds to Gαq and accesses its substrate, PLCβ1 is also found in the cytosol in every cell type examined and under different conditions.[13-14]

We previously found that cytosolic PLCβ1 binds to C3PO, the Promoter of RNA-induced silencing, and showed that this binding can reverse the RNA-induced silencing of specific genes.[14-15] The association between these two proteins occurs in the same region through which Gαq binds to PLCβ1 and is upstream of the active site. Thus, although the catalytic activity of PLCβ1 is not affected by the binding of C3PO, its ability to be activated by Gαq is eliminated. Subsequent studies showed that the association between PLCβ1 and C3PO is critical for PC12 cell differentiation;[16-17] however, little or no association is seen in non-differentiating cells, leading to the question of whether cytosolic PLCβ1 has other binding partners. We also found that PLCβ1 binds to and inhibits a neuronal-specific enzyme required for cellular proliferation, cyclin-dependent kinase 16 (CDK16),[18-19] and that this association enables cells to cease proliferation and transition into a differentiated state.[17] Again, this association is confined to a specific event that drives neuronal cells out of stemness, and suggests that under non-proliferating, non-differentiating conditions, cytosolic PLCβ1 serves some other function. Here, we showed that a major population of cytosolic PLCβ1 was bound to stress granule–associated proteins and that this binding prevented premature stress granule formation. Removal of PLCβ1 from the cytoplasm in response to stress or by Gαq-mediated stimulation promoted stress particle assembly. The interaction between PLCβ1 and stress granule proteins suggests a previously uncharacterized feedback mechanism between the external environment and the protein translation machinery.

3.3 Results

3.3.1 PLCβ1 binds to stress granule–associated proteins

We began this work by performing experiments to determine previously uncharacterized binding partners of cytosolic PLCβ1 in PC12 cells under non-differentiating conditions. Our approach was to isolate the cytosolic fractions of unsynchronized, undifferentiated PC12 cells and use a monoclonal antibody to pull down proteins bound to PLCβ1. We collected the PLCβ1-bound proteins and identified them by mass spectrometry (MS) analysis. Unexpectedly, we found that ~30% of the total proteins associated with cytosolic PLCβ1 were markers for stress granules[1, 20] and we determined the percentage of their contribution to the total intensity (Figure 3.1A). In contrast, control studies with cytosolic fractions of cells with reduced amounts of PLCβ1 identified nonspecific proteins, such as tubulin, actin, and mitochondrial proteins.

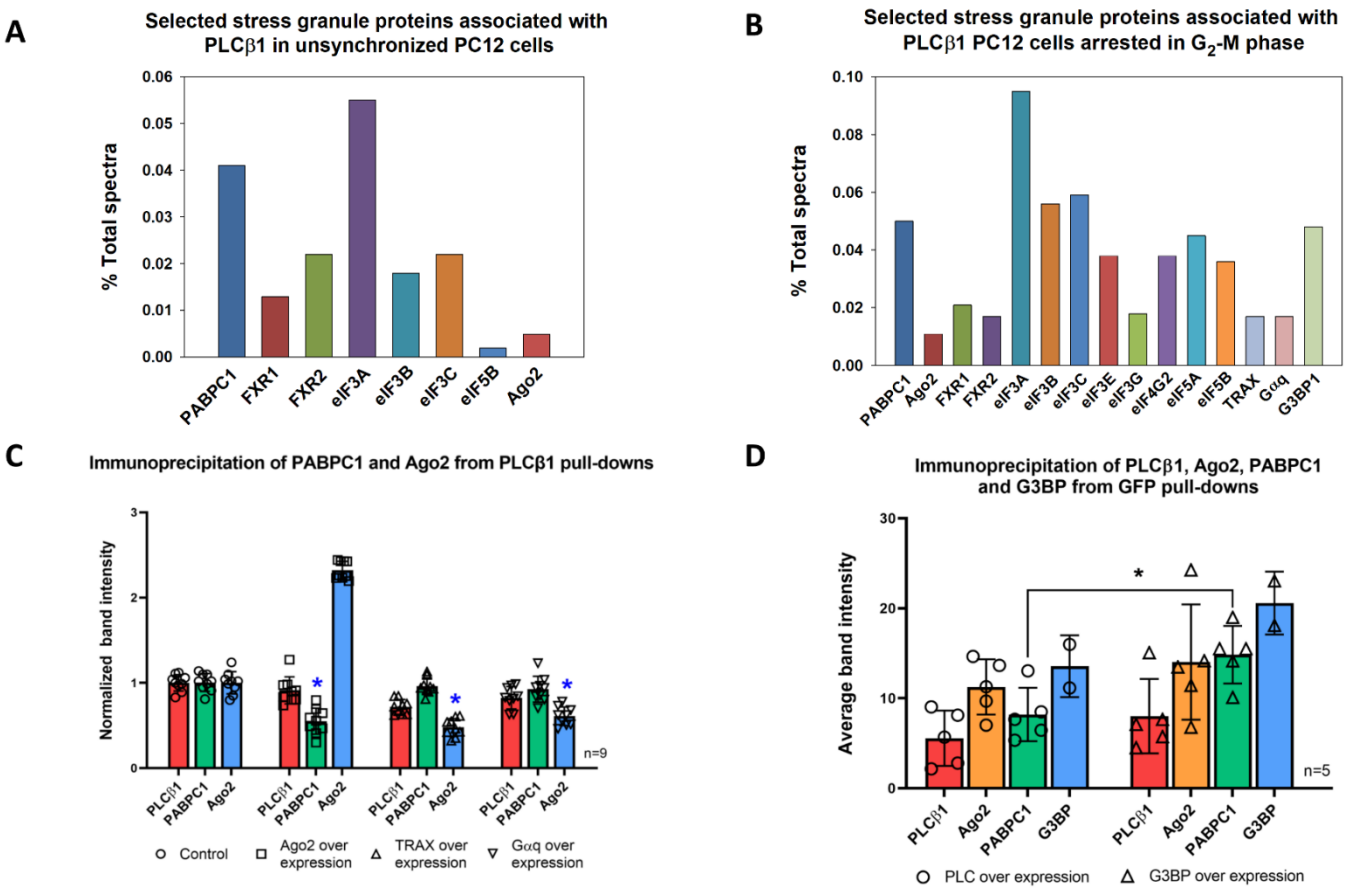

Figure 3.1 Major binding partners of PLCβ1 in PC12 cells (**A** and **B**). Proteins associated with PLCβ1 were pulled down with a monoclonal antibody from the cytosolic fractions of unsynchronized PC12 cells primarily in the G_1 phase (**A**) or PC12 cells arrested in the G_2-M phase (**B**) and then subjected to MS analysis. The relative amounts of the indicated proteins were calculated as described in Materials and Methods. All of the proteins identified in (**A**), except for eIF5B, were also found in an identical experiment in which proteins associated with Ago2 were pulled down. Proteins that were found to be phosphorylated included (**A**) FXR2 and (**B**) eIF3A, eIF3B, and eIF3C. Data were gathered from a single set of MS measurements, and key features were validated biochemically as described in the text. (**C** and **D**) The cytosolic fractions of undifferentiated PC12 cells that were untransfected (control) or were transfected to overexpress Ago2, TRAX, or constitutively active Gαq were incubated with a monoclonal anti-PLCβ1 antibody to pull down PLCβ1-associated proteins. The pull-down samples (10 μg) were then analyzed by Western blotting with antibodies against PLCβ1, PABC1, and Ago2, as indicated in the representative blots (Figure S3.1), and a compilation of the relative intensities of the bands of interest was determined by densitometry (see Materials and Methods). Data are means ± SD of eight experiments. *=P<0.001. The relative amounts of C3PO and Gαq that were pulled down with PLCβ1 were not significantly different from that of PABPC1: P=0.81 and P=0.54, respectively. (**D**) A similar study to that described in (**C**) was performed with a monoclonal anti-GFP antibody to isolate either eGFP-PLCβ1 or eGFP-G3BP1 and their associated proteins from whole transfected PC12 cells. The relative amounts of the indicated proteins that were pulled down were determined by densitometry. Data are means ± SD of five experiments for PLCβ1, PABPC1, and Ago2 and of two experiments for G3BP1. Full-sized Western blots for representative samples can be seen in Figure S3.2.

These studies (Figure 3.1A) were performed with unsynchronized cells where ~90% were in the G1 phase.[17] However, our previous studies suggested that PLCβ1 may change binding partners as cells move through the cell cycle.[17] Additionally, PLCβ1 has a nuclear population that may exchange with the cytosolic one.[21] Therefore, we repeated the studies in cells in which the nuclear population of PLCβ1 was also available for binding by arresting cells in the G_2-M phase, during which the nuclear matrix has broken down (Figure 3.1B). Again, we found that 32% of the proteins bound to PLCβ1 were markers for stress granules, with the most prominent being eukaryotic initiation factor 5A (eIF5A) and polyadenylate binding protein C1 (PABPC1) (Figure 3.1B). Additionally, other stress granule and translation proteins appeared in both groups, including FXR1/2, G3BP1, and other eIF proteins. Note that Ago2, which is associated with both RISCs and stress granules,[8] appeared in these cells.

The proteomics studies described earlier are only indicative of potential protein partners of PLCβ1, because the candidates were identified under nonphysiological conditions. Therefore, we verified

the binding of PLCβ1 to stress granule proteins through several other methods. First, we again performed pull-down experiments with the same monoclonal antibody that we used earlier, and we detected the association of two stress granule proteins by Western blotting analysis. The first, PABPC1, is an established marker for stress granules.[20] The second, Ago2, moves into granules under stress conditions.[8] Using unsynchronized, undifferentiated PC12 cells, we verified that PABPC1 and Ago2 bound to PLCβ1 (Figure 3.1C-D). We then determined whether the amounts of these proteins changed when two of the established binding partners of PLCβ1, Gαq and C3PO, were over-expressed (Figure 3.1C and figure S3.1). We found that the amount of Ago2 that bound to PLCβ1 was reduced when that of either of the binding partners was increased, suggesting that Ago2 bound to similar regions of PLCβ1. However, the amount of PABPC1 that was pulled down with PLCβ1 did not significantly change with over-expression of either Gαq or C3PO (P = 0.81 and P = 0.54, respectively) and was reduced when Ago2 was over-expressed. The simplest interpretation of these data is that the interaction between PLCβ1 and PABPC1 differs from that between PLCβ1 and Ago2, and that the reduction in PABPC1 abundance in cells overexpressing Ago2 may be due to a redistribution of the PLCβ1 pool.

We wanted to verify that similar results could be obtained from experiments in which a different PLCβ1 antibody was used. Noting that PLCβ1 differs from other PLCβ family members mainly in the long 400 amino acid C-terminal domain to which Gαq and C3PO bind, and where some stress granule proteins may bind, we repeated the pull-down experiments under conditions in which antibody binding to its epitope in PLCβ1 would not occlude any potential binding partners. Specifically, we transfected undifferentiated, unsynchronized PC12 cells with a plasmid expressing eGFP-PLCβ1 where the eGFP tag is tethered to the N terminus of PLCβ1 and performed the pull-down experiments with anti-eGFP antibody. The results (Figure 3.1C-D and figure S3.2) showed associations between PLCβ1 and PABPC1, Ago2, and G3BP1. Together, these data support the idea that cytosolic PLCβ1 interacts with stress granule-associated proteins.

3.3.2 PLCβ1 associates with Ago2 but not G3BP1 in live cells

Our earlier studies suggested that the interaction between PLCβ1 and Ago2 might be modulated by G protein stimulation and cellular events associated with C3PO. Keeping in mind that C3PO promotes RNA-induced silencing, we set out to characterize the factors that regulated the PLCβ1-

Ago2 association. We first isolated the cytosolic fractions of unsynchronized, undifferentiated PC12 cells, pulled down proteins associated with Ago2, and identified them by MS. We found that PLCβ1 was included in the data set. Note that all of the proteins that were associated with PLCβ1 (Figure 3.1A) were also pulled down with Ago2.

We measured the extent of the association between PLCβ1 and Ago2 in live PC12 cells by Förster resonance energy transfer (FRET) as monitored by fluorescence lifetime imaging microscopy (FLIM). In this method, FRET efficiency is determined by the reduction in the time that the donor spends in the excited state, or the fluorescence lifetime, before transferring energy to an acceptor fluorophore.[22] If the donor molecule is excited with light that has a modulated intensity, the lifetime can be determined by the reduction in modulated intensity (M) as well as the shift in phase (φ) of the emitted light. If FRET occurs when the donor is in the excited state, the fluorescence lifetime will be reduced as indicated by a reduced change in modulation and phase shift. The amount of FRET can then be directly determined from the raw data by plotting the lifetimes in each pixel in the image on a phasor plot [S versus G, where $S = M*\sin(\varphi)$ and $G = M*\cos(\varphi)$].[23] In these plots, the lifetimes in each pixel in a FLIM image will fall on the phasor arc for a single population. However, when two or more lifetimes are present, the points will be a linear combination of the fractions, with the points inside the phase arc that move towards the right due to shortened lifetimes such as when FRET occurs. Note that phasor representation is simply the Fourier transform of the lifetime decay curves but readily displays lifetimes directly from raw data without the need for model-dependent fitting of the lifetimes or other corrections.

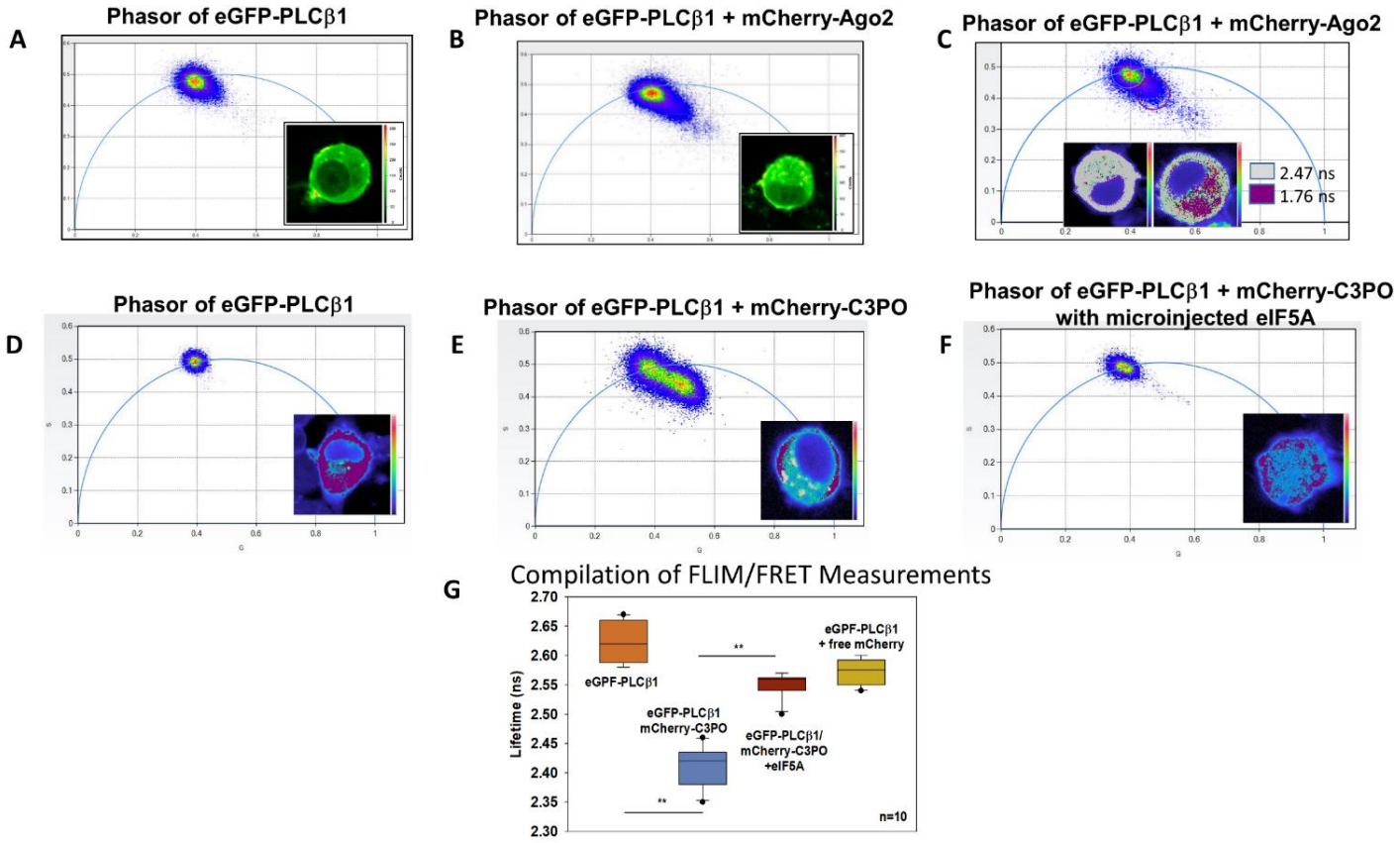

Figure 3.2 Binding of PLCβ1 to Ago2 and eIF5A in PC12 cells. (**A** to **C**) Representative phasor plots from transfected PC12 cells expressing (**A**) eGFP-PLCβ1 alone or (**B**) eGFP-PLCβ1 and mCherry-Ago2. The raw lifetimes are plotted in polar coordinates, as indicated from the phase and modulated fluorescence lifetimes (see Results). Each point in the phasor plots corresponds to the lifetime of the eGFP-PLCβ1 emission measured in each pixel from the corresponding cell image shown in the graph. Images are representative of five to eight cells from three independent experiments. (**C**) A phasor diagram in which the non-FRET and FRET points are selected and the pixels are shown in the cell images. (**D**) Example of a phasor plot and the corresponding image from a FLIM measurement of eGFP-PLCβ1 expressed in a PC12 cell. The heatmap indicates eGFP signal intensity. (**E**) A similar study to that described in (**B**) except that PC12 cells were cotransfected with plasmids expressing eGFP-PLCβ1 and mCherry-C3PO (TRAX). Purple dots indicate pixels represented in the phasor plot. (**F**) A similar study to that described in (**E**) except that this cell was microinjected with purified, unlabeled eIF5A. (**G**) Compilation of eGFP-PLCβ1 lifetime result from two independent studies with n=10 cells for each study and in which free mCherry was used as a negative control. Comparison of data before and after eIF5A micro-injection was statistically significant: **=P<0.001.

Thus, we generated the phasor plot and the corresponding image of a PC12 cell expressing eGFP-PLCβ1 presenting the phase and modulation lifetime of each pixel in the image (Figure 3.2A-C). As expected for a single lifetime species, all points fell on the phasor arc (Figure 3.2A). When we repeated this experiment with cells expressing both eGFP-PLCβ1 and mCherry-Ago2, where mCherry is a FRET acceptor, the average donor lifetime was reduced from 2.5 to 1.7 ns and the points moved inside the phasor (Figure 3.2B). This reduction in lifetime and movement of the points into the phasor showed the occurrence of FRET between the probes. Because the amount of FRET depends on the distance between the fluorophores to the sixth power and given that the distance at which 50% transfers for the eGFP-mCherry pair is ~30 Å,[24] our results suggest a direct interaction between PLCβ1 and Ago2 in the cytosol. We could select points in the phasor plots and visualize their localization in the cell image. We found that the points corresponding to FRET, and thus eGFP-PLCβ1:mCherry-Ago2 complexes, were localized in the cytoplasm (Figure 3.2C). In contrast, points corresponding to eGFP-PLCβ1 alone were found both on the plasma membrane and in the cytoplasm. Additionally, we tested the extent of the association between eGFP-PLCβ1 and eGFP-G3BP1 using homo-FRET or FRET between identical species. No changes in lifetime, and thus no FRET, were detected (Figure S3.3). This absence of FRET indicates that the two fluorophores were separated by more than ~45 Å, which suggests that any association between the two proteins is indirect.

3.3.3 eIF5A binds to PLCβ1 competitively with C3PO and Gαq

To remain cytosolic, stress granule proteins would need to bind to PLCβ1 in a manner competitive with Gαq or it would localize to the plasma membrane. We previously showed that PLCβ1 binds to C3PO through the same C-terminal region with which it binds to Gαq,[15] and that competition between C3PO and Gαq regulates the ability of PLCβ1 to generate Ca^{2+} signals through Gαq activation or the ability of siRNAs to promote silencing, respectively.[25] With this in mind, we searched the proteins identified in our MS analysis for stress granule proteins that could sequester PLCβ1 from Gαq. We noted that eIF5A, which is a GTP-activating protein,[26] has homologous regions to the GTPase region of Gαq and appeared in our MS screen as a PLCβ1-binding protein, so we chose it for further testing.

In an initial study, we purified PLCβ1 and covalently labeled it with a FRET donor, Alexa Fluor 488. We then purified eIF5A, labeled it with the FRET acceptor Alexa Fluor 594, and measured the association between the two proteins in solution by fluorescence titrations similarly to previous studies.[27] We found that the two proteins bound to each other with strong affinity (K_d = 27 ± 5 nM). However, when we formed the Alexa 488-PLCβ1-C3PO complex and titrated Alexa 594-eIF5A into the solution, we could not detect FRET (Figure S3.4). This result suggests that eIF5A binds to the same region of PLCβ1 as does C3PO, and similarly, to Gαq.[15] To determine whether eIF5A competed with C3PO for binding to PLCβ1 in cells, we transfected PC12 cells with plasmids expressing eGFP-PLCβ1 and mCherry-TRAX to produce fluorescent C3PO.[28] We detected an association between the two proteins by FLIM/FRET measurements (Figure 3.2D-E). We then microinjected purified eIF5A into the cells to increase its intracellular concentration by ~10 nM and found that FRET was eliminated (Figure 3.2F). This result suggests that eIF5A displaces C3PO from PLCβ1 and that both proteins bind to a similar region of PLCβ1 (Figure 3.2G).

We confirmed our hypothesis that eIF5A binds to the C-terminal region of PLCβ1 in experiments with purified proteins in solution. In these studies, we formed the eIF5A-PLCβ1 complex, chemically cross-linked the proteins, digested the samples, separated the fragments by electrophoresis, and sequenced the peptides by MS (Figure S3.5). We found several interaction sites between the two proteins, but one of the most prominent was between residues 1085 to 1095 of PLCβ1and residues 97 to 103 of eIF5A, which are expected to be close to the Gαq activation region. Together, these studies suggest that eIF5A competes with both Gαq and C3PO for binding to PLCβ1 and thus could direct PLCβ1 to complexes containing stress granule proteins.

3.3.4 PLCβ1, Ago2 and C3PO form tertiary complex *

To understand how the interactions between PLCβ1, Ago2 and C3PO are related we continued FLIM/FRET experiments. Combinations of the three proteins were overexpressed using plasmid transfections with the FRET pair eGFP and mCherry in differentiated PC12 cells. FRET was detected through a decrease in fluorescence lifetime that occurs when Ago2 binds to C3PO (Figure 3.3A & D) and PLCβ1 binds to both C3PO (Figure 3.3B & E) and Ago2 (Figure 3.3C). Interestingly, knockdown of PLCβ1 results in loss of interactions between eGFP-Ago2 and

mCherry-C3PO (Figure 3.3A) while knocking down Ago2 in cells expressing eGFP-PLCβ1 and mCherry-C3PO (Figure 3.3B), or knocking down C3PO in cells expressing eGFP-PLCβ1 and mCherry-Ago2 (Figure 3.3C) does not impact PLCβ1 binding. To test the idea that PLCβ1 helps promote C3PO / Ago2 association further, carbachol stimulation was used to drive PLCβ1 away from its cytosolic binding partners. Cells stimulated with carbachol behaved similarly to those transfected with PLCβ1 siRNA, resulting in a loss of interaction between Ago2-C3PO (Figure 3.3D), suggesting that PLCβ1 is crucial for the formation of the PLCβ1-Ago2-C3PO ternary complex. Cells expressing eGFP-PLCβ1 and mCherry-C3PO show an even closer interaction between the proteins after carbachol stimulation in the cytosol (Figure 3.3E), suggesting that the PLCβ1 population that is more tightly bound to C3PO does not translocate to the plasma membrane (Figure 3.3F).

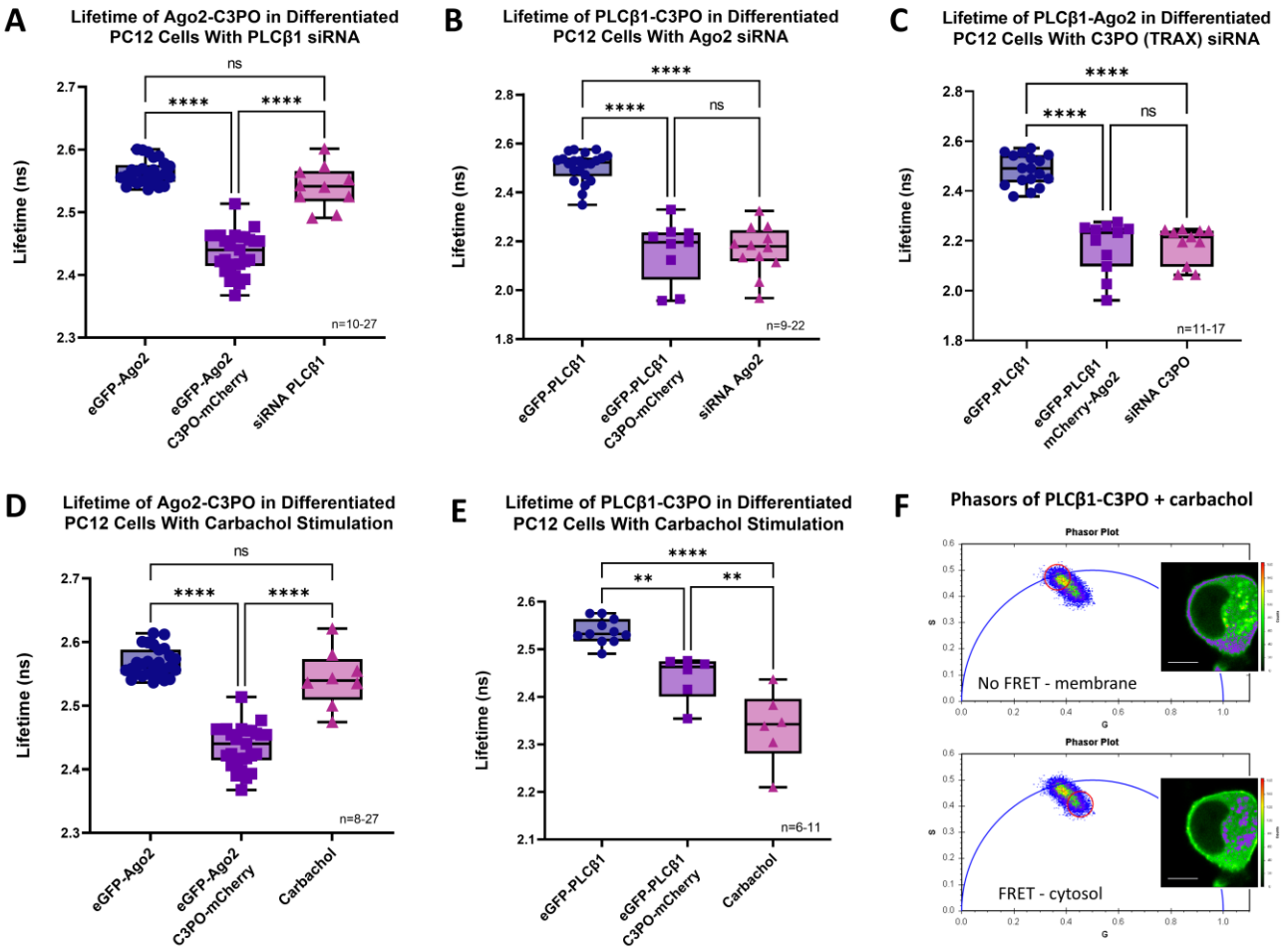

Figure 3.3 Binding of PLCβ1 or Ago2 to C3PO in differentiated PC12 cells. (**A**) Comparison of data after cotransfection with eGFP-Ago2 and mCherry-C3PO was statistically significant. Interaction diminishes after PLCβ1 siRNA transfection. Data were collected from three independent experiments with n=10-27 cells. (**B**) Similar study as described in (**A**), but comparing data after cotransfection with eGFP-PLCβ1 and mCherry-C3PO. Interaction remains after Ago2 siRNA transfection. Data were collected from three independent experiments where n = 9-22 cells. (**C**) Similar study as described in (**A**) but comparing data after cotransfection with eGFP-PLCβ1 and mCherry-Ago2. Interaction remains after C3PO (TRAX) siRNA transfection. Data were collected from three independent experiments where n=11-17 cells. (**D**) Similar study as described in (**A**), where interaction is detected between eGFP-Ago2 and mCherry-C3PO. Interaction diminishes after carbachol stimulation. Data were collected from three independent experiments where n=8-27 cells. (**E**) Similar study as described in (**B**), where interaction is detected between eGFP-PLCβ1 and mCherry-C3PO. Interaction becomes stronger after carbachol stimulation. Data were collected from three independent experiments where n=6-11 cells. (**F**) Representative phasor plot of cells expressing eGFP-PLCβ1 and C3PO-mCherry with carbachol stimulation, where pixels circled correspond to purple pixels highlighted in the cell image. ***=P≤0.001, ****=P≤0.0001.

Because FLIM/FRET measurements rely on the use of fluorescent pairs, we optimized further imaging studies to include a third proteins in our measurements by adding an unlabeled PLCβ1 plasmid in a transfection with eGFP-Ago2 and mCherry-C3PO in differentiated PC12 cells. By this method, we were able to determine how PLCβ1 impacts Ago2-C3PO interactions when PLCβ1 is also in excess. We detected a decreased lifetime after eGFP-Ago2 and mCherry-C3PO cotransfection, and stronger binding indicated by further significant decrease in lifetime when untagged PLCβ1 was present (Figure 3.4A). Stimulating these cells with carbachol resulted in an even further decrease in lifetime, indicating that PLCβ1 is vital to the interaction between these three proteins as interaction is strongest within the cytosol (Figure 3.4B).

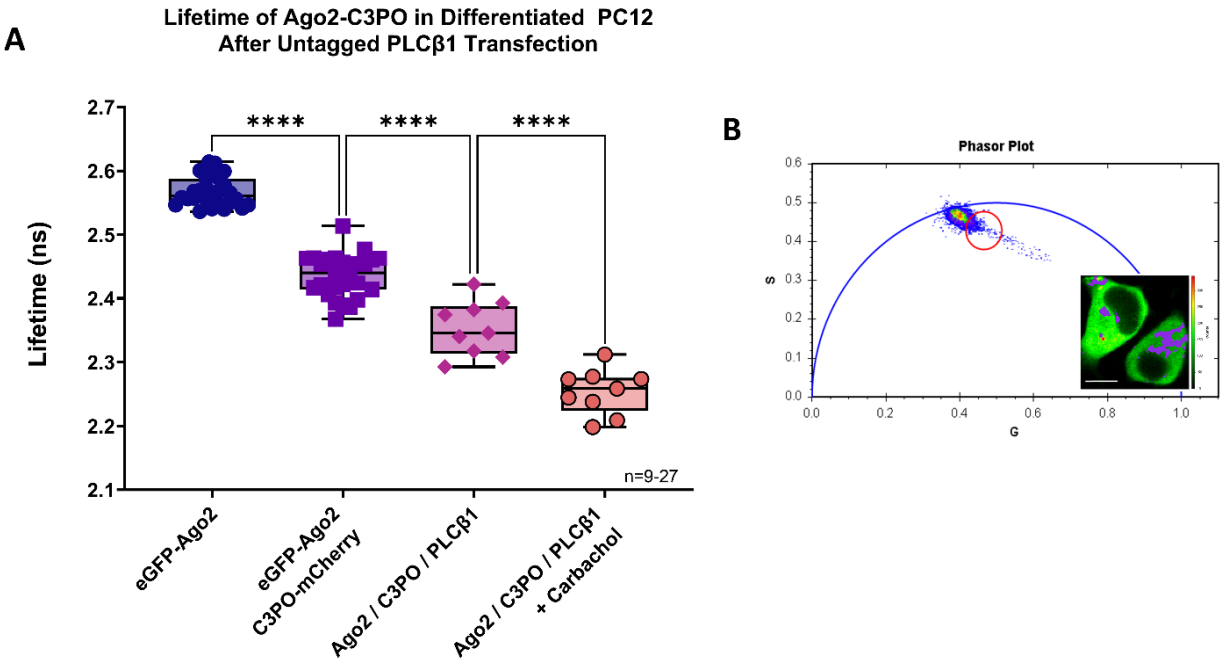

Figure 3.4 Binding between Ago2 and C3PO increases when PLCβ1 is overexpressed. (**A**) Comparison of data after cotransfection with eGFP-Ago2 and mCherry-C3PO (TRAX) shows decrease in fluorescence lifetime. Additionally, overexpressing untagged PLCβ1, as well as applying carbachol stimulation results in further binding between Ago2 and C3PO (TRAX). Data were collected from three independent experiments with n=9-27 cells. ****=P≤0.0001. (**B**) Representative phasor plot where pixels circled correspond to purple pixels in the cell image. These regions denote interaction between eGFP-Ago2 and mCherry-C3PO remaining in the cytosol after carbachol stimulation. Scale bar=10 μm.

3.3.5 Osmotic stress has different effects on PLCβ1 isoforms

To determine whether PLCβ1 could affect stress granule formation, we subjected cells to mild, hypo-osmotic stress (300 to 150 mOsm), which we previously showed has reversible effects on the Gαq-PLCβ signaling pathway in muscle cells (Figure 3.5A-E).[29-30] We first determined whether hypo-osmotic stress affected the association between PLCβ1 and stress granule proteins within 5 min before adaptive changes in the cell occurred.

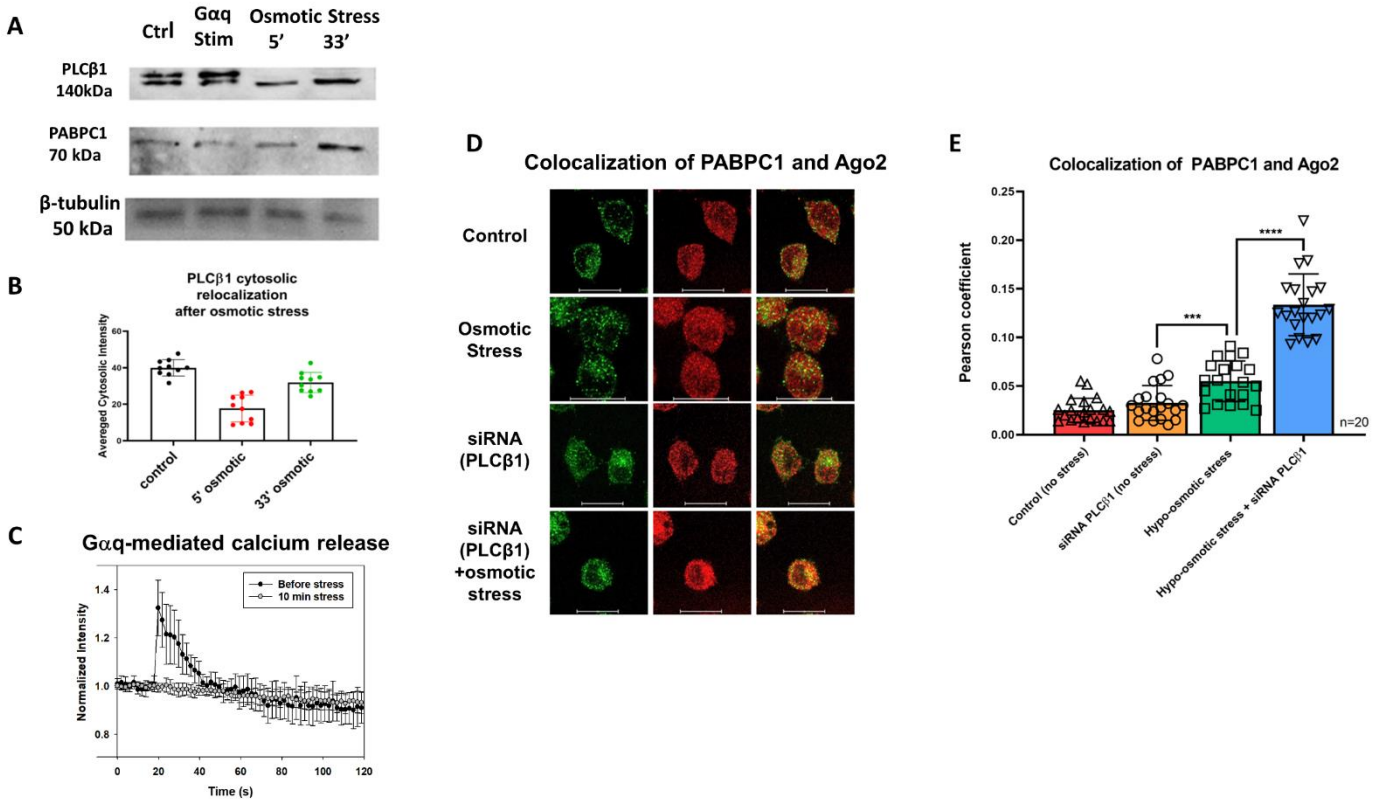

Figure 3.5 The effect of osmotic stress on cytosolic PLCβ1 in PC12 cells. (**A**) Representative Western blotting analysis of the cytosolic fractions of PC12 cells for PLCβ1, where PLCβ1a is the upper band of the doublet and PLCβ1b is the lower band. Cells were subjected to 10 min of incubation with 5 μM carbachol to stimulate Gαq activity or were subjected to osmotic stress (150 mOsm) for 5 and 30 min. PABPC1 and β-tubulin bands are shown for comparison. (**B**) Results of a study in which undifferentiated PC12 cells transfected to express eGFP-PLCβ1 were subjected to osmotic stress as indicated, and changes in cytosolic fluorescence intensity in a slice in the middle of the cell were quantified. Data are from nine independent experiments. Compared to control cells, those subjected to osmotic stress for 5 min had significantly different fluorescence intensity ($P < 0.001$). (**C**) Analysis of the change in Ca^{2+} release when PC12 cells labeled with Calcium Green were stimulated with 5 μM carbachol under basal conditions (300 mOsm) and hypo-osmotic stress (150 mOsm) for 10 min. Data are from n=12 cells from three experiments,

and bars indicate SD. (**D**) Images of PC12 cells immunostained for Ago2 (green) and PABPC1 (red) under basal conditions (control), when the osmolarity was lowered from 300 to 150 mOsm (osmotic stress), and when cells that had been treated with siRNA(PLCβ1) were subjected to normal conditions or osmotic stress. Scale bars=20 μm. (**E**) Compiled colocalization data showing the extent of colocalization of PABPC1 and Ago2 in cells from the experiments shown in (**D**). Data are from three experiments with 20 cells per experiment. ***=P=0.002 and ****=P≤0.001.

Of the two major subtypes of PLCβ1 (1a and 1b), the 1a form is the best characterized and most prevalent subtype, having additional residues in its C terminus (residues 1142 to 1216) compared to the 1b isoform.[31] Although both isoforms are similarly activated by Gαq, some studies showed differences in their localization, although these differences appear to be cell type–specific.[32-34] We found that 5 min of exposure of PC12 cells to osmotic stress caused a marked reduction in PLCβ1a abundance, whereas the amount of PLCβ1b was relatively unchanged (Figure 3.5A). Gαq stimulation by the addition of carbachol did not affect the abundance of either isoform. Tracking the total amount of PLCβ1 with an antibody that recognizes both isoforms, we found that the cytosolic fraction of PLCβ1 was preferentially reduced by osmotic stress (Figure 3.5B). Considering that the half-life of total PLCβ1 in PC12 cells is 20 min,[17] our findings (Figure 3.5A-B) suggest that osmotic stress enhances PLCβ1a degradation. After 30 min of stress, the abundance of PLCβ1b increased compared to that in control cells, as did the amount of PABPC1, but PLCβ1a abundance remained low as the cells adapted (Figure 3.5B). Because we could not distinguish between the 1a and 1b isoforms of PLCβ1 in most of our experiments, we will refer only to PLCβ1.

We determined the ability of hypo-osmotic stress to affect Ca^{2+} signals generated by Gαq in response to 1 μM carbachol. Using the fluorescent calcium indicator, Calcium Green (see Materials and Methods), we first verified that reducing the osmolarity from 300 to 150 mOsm did not affect the intracellular Ca^{2+} concentration. However, osmotic stress quenched the increase in Ca^{2+} signaling in response to activation of the Gαq-PLCβ1 pathway (Figure 3.5C). This loss was consistent with the reduced PLCβ1 abundance in cells under hypo-osmotic stress.

3.3.6 The abundance of cytosolic PLCβ1 affects stress granule assembly

It is possible that PLCβ1 binds to stress granule–associated proteins to prevent the premature assembly of stress particles. To test this idea, we followed stress granule formation in PC12 cells under hypo-osmotic stress by counting the number of particles that formed in undifferentiated,

unsynchronized PC12 cells using a 100x objective lens under normal (300 mOsm) and hypo-osmotic (150 mOsm) conditions. Note that at this resolution, we may not have captured the formation of small particles,[5] and we might have observed the assembly of primary particles, as well as the fusion of small pre-formed ones. In our experiments, we analyzed particle numbers and sizes in 1.0-µm slices though several cells and reported particle sizes in area as seen for each slice. Note also that converting the particles into three dimensions and analyzing the particles gave identical results but with reduced resolution.

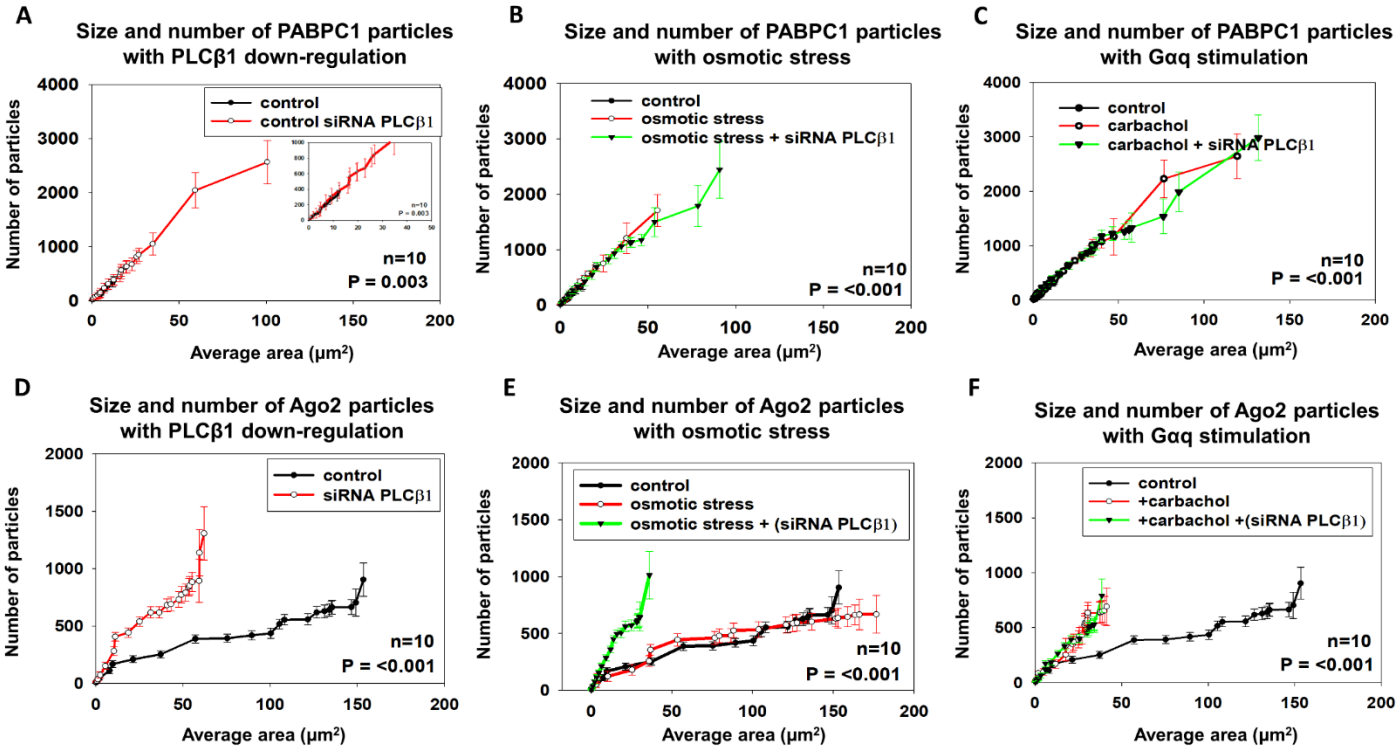

Figure 3.6 The effect of PLCβ1 on the formation of PABPC1- and Ago2-associated particles in PC12 cells. (**A** to **C**) The sizes and numbers of particles associated with monoclonal anti-PABPC1 in the cytosol of fixed and immunostained PC12 cells were measured with a 100× objective and analyzed by ImageJ software (see Materials and Methods). (**A**) Treatment of cells with siRNA(PLCβ1) relative to mock-transfected controls. Inset: An enlarged version of the plot is shown to enable better comparison. (**B**) Analysis of the effect of osmotic stress (150 mOsm, 5 min) on the size and number of PABPC1-associated particles in control PC12 cells and in PC12 cells treated with siRNA(PLCβ1). (**C**) Analysis of the effect of Gαq stimulation by treatment with 5 µM carbachol on the size and number of PABPC1-associated particles in control PC12 cells and in PC12 cells treated with siRNA(PLCβ1). (**D** to **F**) Size and number of Ago2-associated particles as determined by immunofluorescence analysis with a monoclonal antibody for cells that were treated with siRNA(PLCβ1) and compared to control cells (**D**). Control cells subjected to 5 min of

osmotic stress (150 mOsm) were compared to cells treated with siRNA(PLCβ1) under osmotic stress (**E**). Control cells treated with 5 μM carbachol to stimulate Gαq were compared to cells treated with siRNA(PLCβ1) and stimulated with 5 μM carbachol (**F**). Data are an average of three independent experiments that each sampled 10 cells. Error bars represent SD. The P values compare control conditions to the specific condition and were determined by ANOVA.

We fixed PC12 cells under normal and hypo-osmotic conditions and stained them with monoclonal antibodies against the stress granule marker, PABPC1. In this analysis, we measured the size and number of particles in each slice of a confocal volume (see Materials and Methods) and plotted the additive values of these data. Thus, the highest value plotted (Figure 3.6) corresponds to the total area of the cell occupied by stress granule particles. In control cells, PABPC1 antibody staining showed ~750 particles that were less than 25 μm^2 in area (Figure 3.6A). When PLCβ1 abundance was reduced by siRNA, we observed an increase in PABPC1 particle size from 25 to 100 μm^2, suggesting that the loss of PLCβ1 promoted the formation of larger particles. When we applied osmotic stress to the cells, we observed an increase in the number of PABC1-containing particles between 25 and 50 μm^2 in area (Figure 3.6B) However, osmotic stress did not change the size or number of PABC1-containing particles in cells in which PLCβ1a had been reduced, suggesting that osmotic stress and the loss of PLCβ1 were not additive effects. In another series of experiments, we stimulated cells with carbachol to activate Gαq (Figure 3.6C). We found that such stimulation induced the formation of a high number of particles of up to ~150 μm^2 in area and that reducing PLCβ1 abundance did not substantially affect either the size or number of PABPC1-containing particles. Together, these findings suggest that depletion of cytosolic PLCβ1, through siRNA treatment, osmotic stress, or recruitment to activated Gαq, promoted the incorporation of PABPC1 into larger aggregates. We then used immunofluorescence analysis to test the effect of PLCβ1 on the size and number of particles associated with Ago2. For Ago2, the number of smaller particles substantially increased when PLCβ1 abundance was reduced (Figure 3.6D). Unlike PABPC1-associated particles, the size and number of Ago2-associated particles were not affected by osmotic stress, although an increase in the number of small particles was still seen when PLCβ1 abundance was reduced (Figure 3.6E). Additionally, carbachol-dependent stimulation of Gαq resulted in an increase in the number of Ago2-containing small particles (Figure 3.6F).

The experiments described earlier were performed with fixed, stained cells. We also followed particle formation in live PC12 cells transfected with plasmids expressing mCherry-Ago2 or eGFP-G3BP1. Although the number and areas of the particles varied somewhat with the extent of transfection, the results showed the same trend as those from the immunostained samples (Figure S3.6A-B), that Gαq stimulation or osmotic stress increased the number of Ago2-associated smaller particles. These studies suggest that reduction of cellular PLCβ1 abundance increases the number of particles of proteins associated with stress granules. Whereas the increase in particle assemblies could be due to the loss of cellular PLCβ1, it may also be due to the removal of PLCβ1 from pre-formed particles. To address this question, we transfected PC12 cells with plasmid expressing eGFP-PLCβ1 and analyzed their particles (Figure S3.6C). We could not detect many particles less than 400 μm^2 in area, beyond which, the number the number of particles increased to ~1000. No substantial differences were found in cells subjected to osmotic stress. These data suggest that PLCβ1 does not associate with large particles in the cell.

The differences in the size and number of PABPC1- versus Ago2- or G3BP1-containing particles suggest that they might partition into different types of granules. We tested this idea by monitoring the effect of both PLCβ1 and osmotic stress on the colocalization between Ago2 and PABPC1 (Figure 3.5D-E). Under normal osmolarity, we found little colocalization between the proteins in cells either with endogenous amounts of PLCβ1 or in cells in which PLCβ1 was knocked down. However, when the cells were subjected to osmotic stress, colocalization between Ago2 and PABPC1 increased, and this increase was greater in cells in which PLCβ1 was knocked down. These results suggest that PABPC1 and Ago2 form distinct particles that may begin to fuse or associate under high stress conditions, such as loss of cytosolic PLCβ1 or osmotic stress.

3.3.7 Assembly of Ago2- and G3BP1-containing aggregates depends on the type of environmental stress

It is probable that osmotic stress produces granules that are different in size, number, and composition than those produced by other stresses. We compared the formation of Ago2- and G3BP1-containing particles under different types of stress by number & brightness (N&B) analysis (see Materials and Methods). This method measures the number of fluorescent molecules

associated with a diffusing particle in live cells[35]. Thus, N&B measurements of cells expressing eGFP-Ago2 would indicate the conditions that promote the formation of aggregates.

We followed Ago2 aggregation in PC12 cells subjected to various stress conditions (Figure 3.7A-C). Subjecting cells to osmotic stress shifted the distribution of eGFP-Ago2 particles to the point where ~60% of the eGFP-Ago2 were significantly larger than monomers (Figure 3.7B). Note that these Ago2-containing particles formed throughout the cytoplasm, and that only 75 to 80% of the cells showed aggregation. We compared the aggregation of eGFP-Ago2 in cells subjected to other stresses: cold shock (12^{o}C for 1 hour), heat shock (40^{o}C for 1 hour), treatment with 0.5 mM arsenite for 10 min (Figure S3.7A -C), and oxidative stress (1 mM $CoCl_2$ for 8 hours; Figure S3.7D). Unlike osmotic stress, these other stresses produced changes in all of the cells observed; however, eGFP-Ago2 aggregates were seen as a few large particles rather than being evenly distributed through the cell. In a final series of experiments, we stimulated cells under normal conditions with carbachol to activate Gαq and promote the relocalization of cytosolic PLCβ1 to the plasma membrane (Figure 3.7C). Unlike for the other stresses, we observed the formation of small eGFP-Ago2 aggregates distributed throughout the cytosol. This behavior was seen in every cell tested. These data suggest that different stresses, including Gαq activation, result in patterns of formation of particles containing multiple Ago2 molecules. We also viewed the aggregation of eGFP-G3BP1 expressed in undifferentiated, unsynchronized PC12 cells (Figure 3.7D-G). Unlike cells expressing eGFP-Ago2, PC12 cells expressing eGFP-G3BP1 showed aggregation under untreated conditions, (Figure 3.7D), and the extent of this aggregation increased with hypo-osmotic stress (Figure 3.7E), treatment with PLCβ1-specific siRNA, (3.7F), and carbachol treatment (Figure 3.5G). Unlike the punctate pattern seen for eGFP-Ago2, eGFP-G3BP1 aggregates were more diffuse and occurred close to the plasma membrane, suggesting that eGFP-G3BP1 was present in a range of different stress granules.

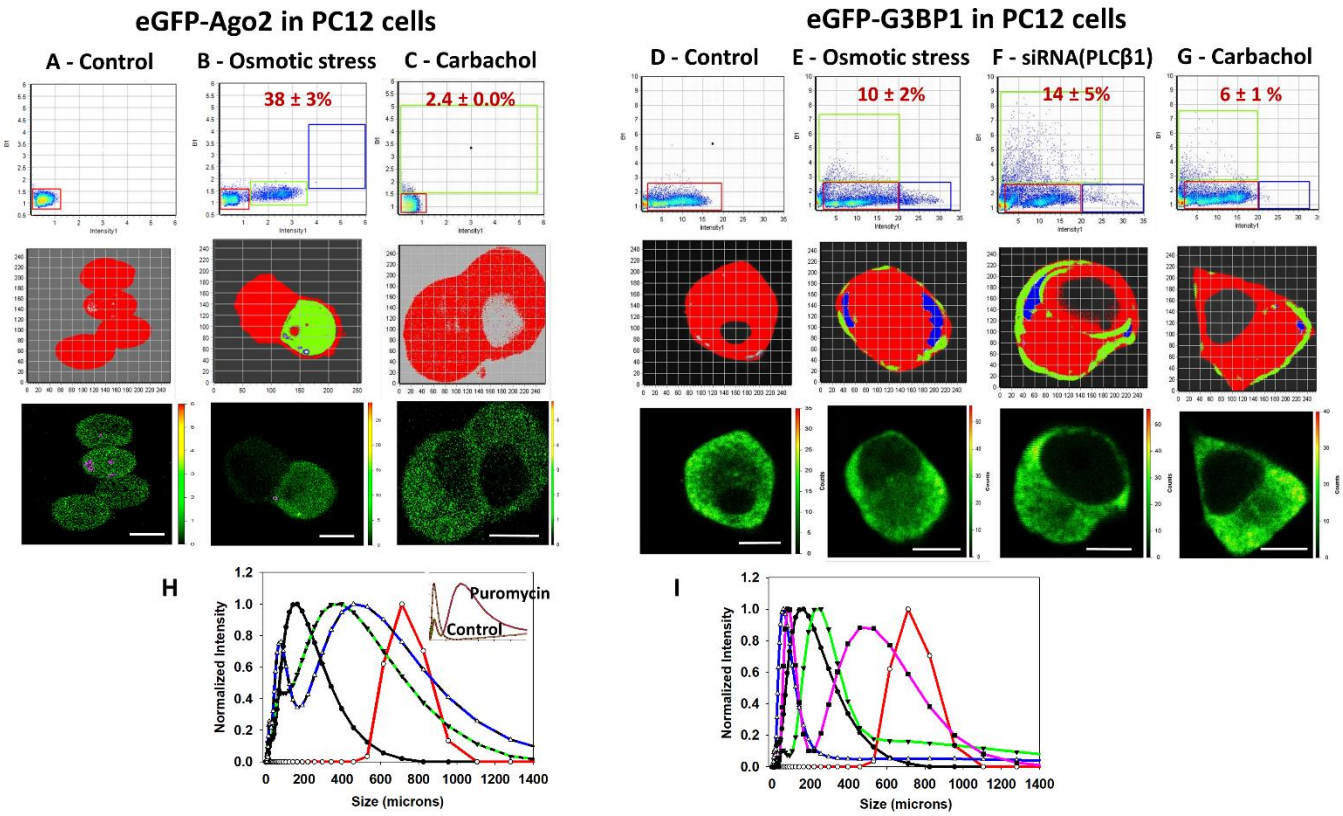

Figure 3.7 Aggregation of Ago2 and G3BP1 in PC12 cells as monitored by N&B analysis. (**A** to **G**) N&B studies of PC12 cells expressing eGFP-Ago2 (**D** to **C**) and eGFP-G3BP1 (**D** to **G**) and subjected to the indicated conditions. Top: The graphs display N&B values for each pixel, where the y axis corresponds to the brightness of the particle and the x axis shows particle intensity. The pixels contained in the red boxes are the values found for free eGFP and correspond to monomeric eGFP-Ago2 (**A** to **C**) or eGFP-G3BP1 (**D** to **G**). Points outside the red boxes, shown in green and blue, where the percentages are given in red font in the upper panels, correspond to higher-order species of Ago2 or G3BP1. Middle: Images show the pixels corresponding to monomeric (red) and higher-order eGFP-Ago2 or eGFP-G3BP1 aggregates (green and blue) from the data shown in the graphs directly above. Bottom: Images are from fluorescence microscopy analysis with ISS software. The purple pixels denote Ago2 or G3BP1 aggregates. Data in (**A**) and (**D**) show control cells (n=8 experiments); data in (**B**) and (**E**) show cells subjected to hypo-osmotic stress (150 mOsm, 5 min) (n=8 experiments), and data in (C) and (**G**) show cells subjected to carbachol stimulation (5 μM, 10 min) (n=5 experiments). Data in (**F**) show cells treated with siRNA(PLCβ1) (n=4 experiments). Scale bars=10 μm. (**H**) The size distribution of cytosolic RNAs isolated from the indicated PC12 cells was measured by DLS for control conditions (black), hypo-osmotic stress (150 mOsm, 5 min; green), overexpression of constitutively active Gαq (blue), and treatment with siRNA(PLCβ1) (pink). Inset: DLS spectra of cytosolic RNAs extracted from control cells and from cells treated with puromycin; the x-axis range is from 0 to 3000 nm. (**I**) Size distribution of cytosolic RNAs where data for control cells (black) are included for easier comparison to cells subjected to hypo-osmotic stress (150 mOsm, 5 min; red), heat shock at 40°C for 1 hour (green), cold shock at 12°C for 1 hour (blue), and treatment with 0.5 mM arsenite for 10 min (pink). Inset:

Comparison of control and puromycin-treated cells. Normalized data are shown. Each sample was scanned three times with 10 min per run. The numbers of independent samples were six (control), two (PLCβ1 knockdown, Gαq overexpression, heat shock, cold shock, arsenite), and four (hypo-osmotic stress).

3.3.8 Cytosolic PLCβ1 abundance affects the size of cytosolic RNAs

The formation of stress granules is expected to be accompanied by an increase in the size distribution of cytosolic RNA as mRNA accumulates due to the arrest of translation. We measured the sizes of cytosolic RNA by dynamic light scattering (DLS) (Figure 3.7H-I). Subjecting cells to osmotic stress caused a significant shift to larger sizes. Reducing PLCβ1 abundance resulted in a small peak at low molecular weights and a broad peak at larger sizes that was shifted to the right when compared to that for the control cells. This small peak was consistent with enhanced C3PO activity due to the relief of inhibition by PLCβ1.[27] Over-expressing Gαq resulted in a similar behavior as did treatment with siRNA (PLCβ1). As a control, we measured the DLS spectra of cytosolic RNA from untreated cells and in cells treated with the antibiotic puromycin, which halts mRNA translation, rendering mRNA in stress granules.[36] The RNAs from puromycin-treated cells were almost two-fold greater in molecular weight compared to those in control cells and showed a small peak that corresponded to the sizes seen in control cells. These data (Figure 3.7H-I) are consistent with the translational arrest and the accumulation of higher molecular weight RNAs that occurred when PLCβ1 abundance was reduced.

3.3.9 Cytosolic PLCβ1 abundance affects stress granules in smooth muscle cells

Myocytes and other cell types may experience changes in osmotic conditions during their lifetime. With this in mind, we extended our studies to two different smooth muscle cell types: rat aortic smooth muscle (A10) cells and Wistar-Kyoto rat 3M22 (WKO-3M22) cells. We identified PLCβ1-associated proteins in A10 cells under control conditions and after 5 min of osmotic stress by pulling down PLCβ1 complexes with a monoclonal antibody and identifying the proteins by MS analysis. A large fraction of the proteins pulled down with PLCβ1 are associated with transcription, which is most likely due to the nuclear population of PLCβ.[37] The stress granule–associated proteins were less abundant than the transcription-associated proteins. Many of the stress granule–associated proteins were also found in PC12 cells, for example, PABPC1 and eIF5A (Figure 3.8A), whereas others, such as Ago2 and FXR, were not detected. We repeated these experiments with

A10 cells that had been subjected to hypo-osmotic stress for 5 min before undergoing lysis. We detected a loss of almost all of the transcription-associated proteins and most of the stress granule–associated proteins (Figure 3.8B). These results suggest that PLCβ1 binds to stress granule–associated proteins in A10 cells, as well as in PC12 cells, and that osmotic stress results in their release from PLCβ1. Whereas the cellular amount of PLCβ1 in A10 cells was reduced by osmotic stress, this effect was much lower than that in PC12 cells (Figure S3.8).

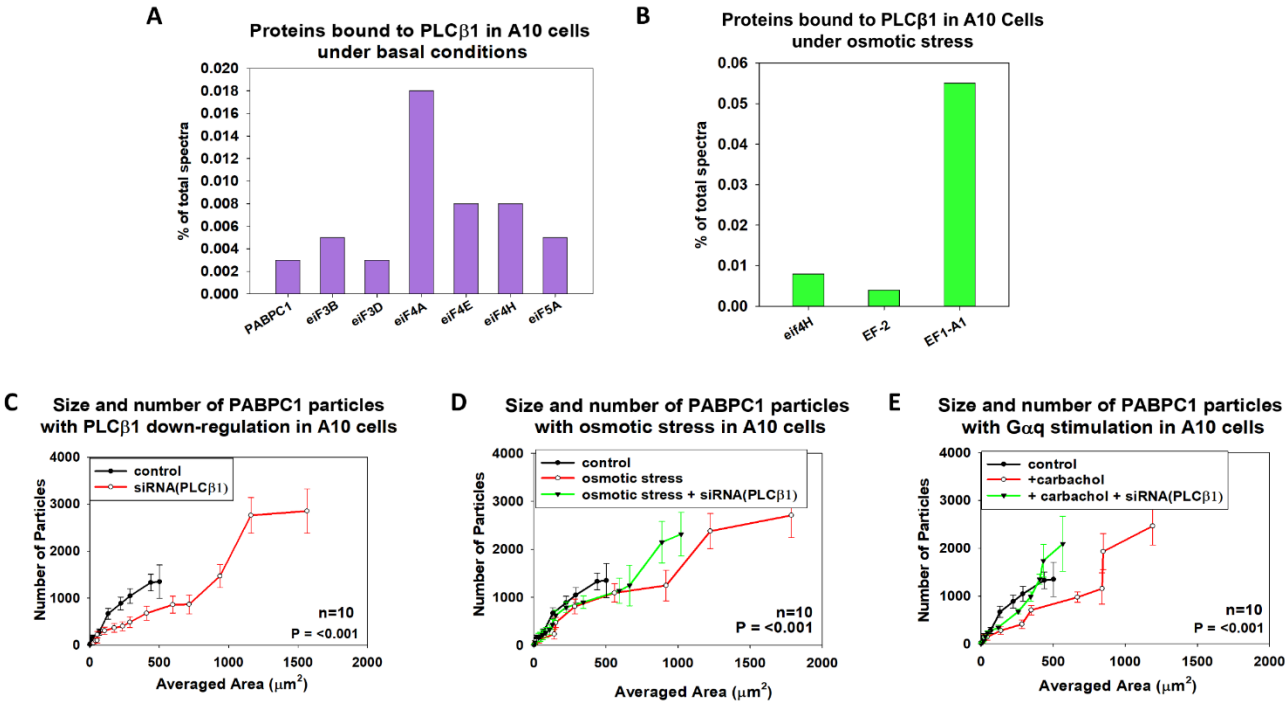

Figure 3.8 The effect of PLCβ1 on stress granule formation in A10 cells. (**A** and **B**) MS analysis of the proteins associated with PLCβ1 in A10 cells under normal osmotic conditions (**A**) and after being subjected to hypo-osmotic stress (150 mOsm) for 5 min (**B**). The full dataset is shown in table S6. (**C**-**E**) Analysis of the sizes and numbers of particles associated with anti-PABPC1 in the cytosol of control A10 cells and A10 cells treated with siRNA(PLCβ1) as measured with a 100× objective and analyzed with ImageJ software (see Materials and Methods). The indicated cells were analyzed under basal conditions (**C**), after being subjected to osmotic stress (150 mOsm) (**D**), and after treatment with 5 μM carbachol to stimulate Gαq (**E**). All measurements are an average of three independent experiments, with 10 cells sampled per experiment. Error bars indicate SD. P values were determined by ANOVA.

We then measured the formation of PABPC1 particles in A10 cells in which the cytosolic abundance of PLCβ1 was perturbed, such as by osmotic stress, siRNA(PLCβ1) treatment, and Gαq stimulation (Figure 3.8C-E). These cells exhibited particles that were ~10-fold larger than those in PC12 cells. Similar to PC12 cells, reducing PLCβ1 abundance in the A10 cells resulted in the formation of larger particles, which also occurred because of osmotic stress. In addition, stimulation with carbachol (to activate Gαq) also resulted in a significant increase in the number of larger particles. Together, these data indicate that the size and number of PABPC1-containing particles depend on the abundance of PLCβ1 in the cytosol.

Both osmotic stress and carbachol also promoted the formation of Ago2-containing particles in WKO-3M22 cells. We analyzed the N&B results of these cells subjected to osmotic stress, carbachol stimulation (Figure 3.9A-C), and arsenite (Figure S3.9). As occurred with PC12 cells, both osmotic stress and carbachol stimulation promoted Ago2 aggregation in the WKO-3M22 cells, whereas arsenite stress had only a minor effect (Figure S3.9). Reducing the abundance of PLCβ1 promoted Ago2 aggregation in both control (Figure 3.9D-E) and arsenite-stressed cells (Figure S3.9). In a final series of experiments, we monitored shifts in the sizes of cytosolic RNA in WKO-3M22 cells subjected to osmotic stress or carbachol stimulation and found statistically significant increases in the RNA sizes under both conditions (Figure 3.9F). Note that the particles and cytosolic RNAs in WKO-3M22 cells appeared to be larger than those found in PC12 cells (Figure 3.7 versus Figure 3.9).

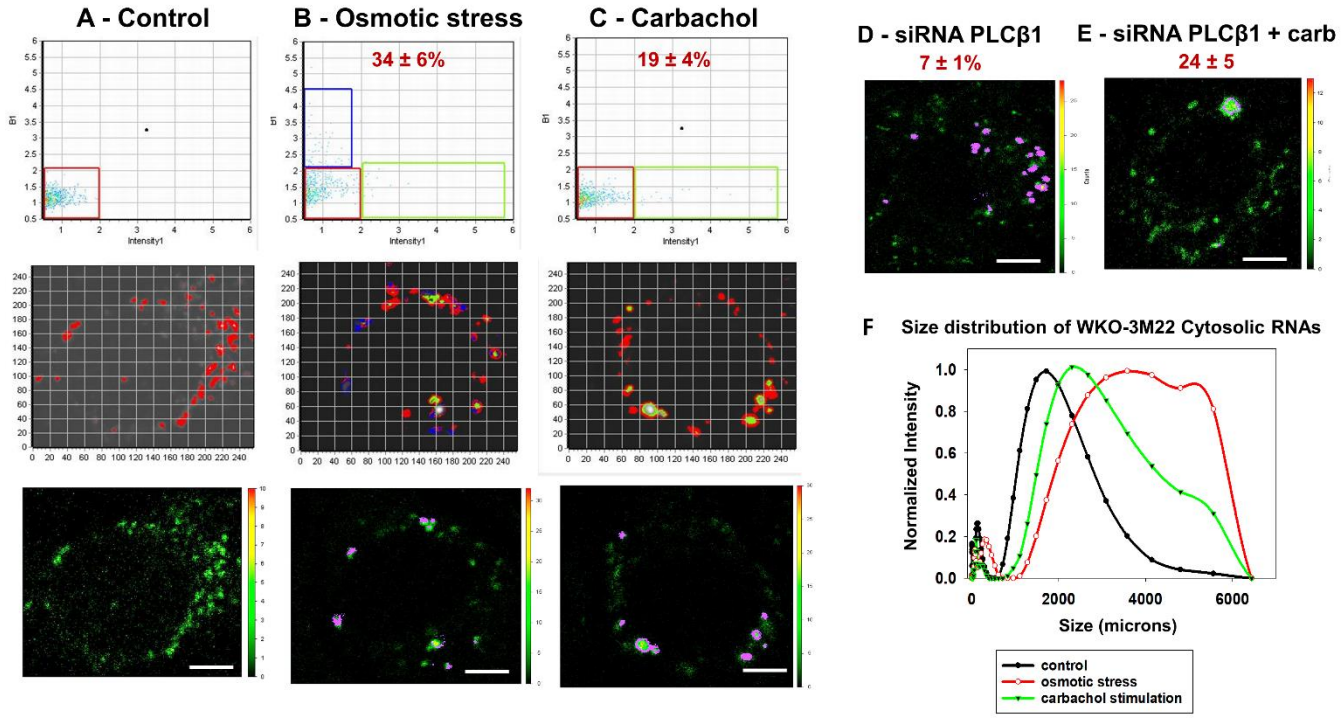

Figure 3.9 N&B analysis of eGFP-Ago2 aggregation in WKO-3M22 cells. (**A** to **C**) N&B analysis of brightness versus intensity for PC12 cells under the indicated condi-tions with the pixels of the colored boxes corresponding to specific regions in the cells (middle). Bottom: Corresponding fluorescence microscopy images. Red boxes correspond to monomeric eGFP-Ago2 as determined by free eGFP. Points outside this box and in the green and blue boxes correspond to higher-order species and where the percentage of aggregation is given in red. Data in (**A**) show control cells; data in (**B**) show cells subjected to hypo-osmotic stress (150 mOsm, 5 min), and data in (**C**) show cells subjected to carbachol stimulation (5 μM, 10 min). (**D** and **E**) Data in (**D**) show cells treated with siRNA(PLCβ1), whereas data in (**D**) and (**E**) show cells treated with siRNA(PLCβ1) and stimulated with osmotic stress (150 mOsm). Data are from three experiments with nine cells analyzed per experiment. (**F**) Plot of the size distribution of cytosolic RNAs of WKO-3M22 cells as measured by DLS for control conditions (black), osmotic conditions (150 mOsm, 5 min; red), and stimulation of Gαq with carbachol (5 μM, 10 min; green).

3.3.10 Stress granule formation depends on the abundance of PLCβ1

To understand the dependence of stress granule formation on the abundance of PLCβ1, we assumed that eIF5A was the primary contact between PLCβ1 and stress granule–associated proteins; however, eIF5B or another factor might be involved. We can then express the partitioning of eIF5A from the cytosol (c) to the particulate phase (p) as:

$$Kp = \frac{eIF5A^p}{eIF5A^c}$$

where eIF5A^p is the stress granule phase, also termed *G*. The total amount of eIF5A is given by:

$$\mathrm{E_T} = \mathrm{eIF5A^p} + \mathrm{eIF5A^c},$$

$$\text{where } \mathrm{eIF5A^c} = \mathrm{eIF5^{free}} + \text{eIF5A-PLC}\beta.$$

We can then express the association between PLCβ and eIF5A in terms of a bimolecular dissociation constant:

$$K_d = \frac{[PLC\beta][eIF5A]}{[PLC\beta - eIF5A]}$$

In this equation, PLCβ refers to cytosolic PLCβ. We only considered the cytosolic population and not the membrane-bound population in accordance with our results showing that the loss of cytosolic PLCβ appeared to promote stress granule formation. Thus, the total cytosolic amount of PLCβ is given by:

$$\mathrm{P_T} = \mathrm{PLC\beta^{free}} + \text{PLC}\beta\text{-eIF5A}$$

If we combine these equations to determine the relationship between the number of particles and the concentration of PLCβ, we obtain an equation that is quadratic in *G* (eIF5A).

$$G^2\left(1 + \frac{1}{K_p}\right) + G\left(P_T - E_T + K_pK_d + K_d\right) - K_pK_dE_T = 0$$

To give:

$$G = \frac{-\left(P_T - E_T + K_d\left(1 + K_p\right)\right) \pm \sqrt{P_T^2 + E_T^2 + K_d^2\left(1 + K_p\right)^2 + 2K_d\left(1 + K_p(P_T + E_T)\right) - 2P_T E_T}}{\left(\frac{2\left(1 + K_p\right)}{K_p}\right)}$$

To determine the applicability of this model, we first needed to estimate values for *G*. We found a linear dependence between the number of particles and the average area of the particles for PABPC1 in PC12 and in A10 cells (Figure 3.10A-B). This linearity enabled us to estimate *G* using either of these measurements. Note that this linearity did not occur for Ago2-containing particles for which stress primarily increased the number of particles rather than their size (Figure 3.6).

We could estimate the total amount of cytosolic PLCβ by single molecule fluorescence measurements comparing the intensity of eYFP-PLCβ1 to an intensity scale constructed with Alexa488 as measured with a multiphoton laser in a fluorescence correlation instrument (see Materials and Methods). Briefly, we measured the number of eYFP-PLCβ1 molecules diffusing in a specific confocal volume after calibration with Alexa488. Note that we typically over-express ~two-fold more protein as indicated by Western blotting analysis. Our measurements enabled us to estimate a cytosolic eYFP-PLCβ1 concentration of ~43 nM in PC12 cells and ~49 nM in A10 cells, which was reduced to 10 to 15 nM under hypo-osmotic conditions. This decline can be compared with the ~2.5-fold reduction in cytosolic PLCβ1 abundance that occurred in response to carbachol stimulation (Figure 3.10B) and the 80 to 90% reduction in PLCβ1 abundance caused by siRNA treatment[38] as seen in S3.10. Although these values for PLCβ1 are approximate, we used them to determine its dependence on stress granules as expressed as G^2. These data (Figure 3.10C) showed the dependence of the size and number of stress granules when cytosolic changes of PLCβ1 abundance occur.

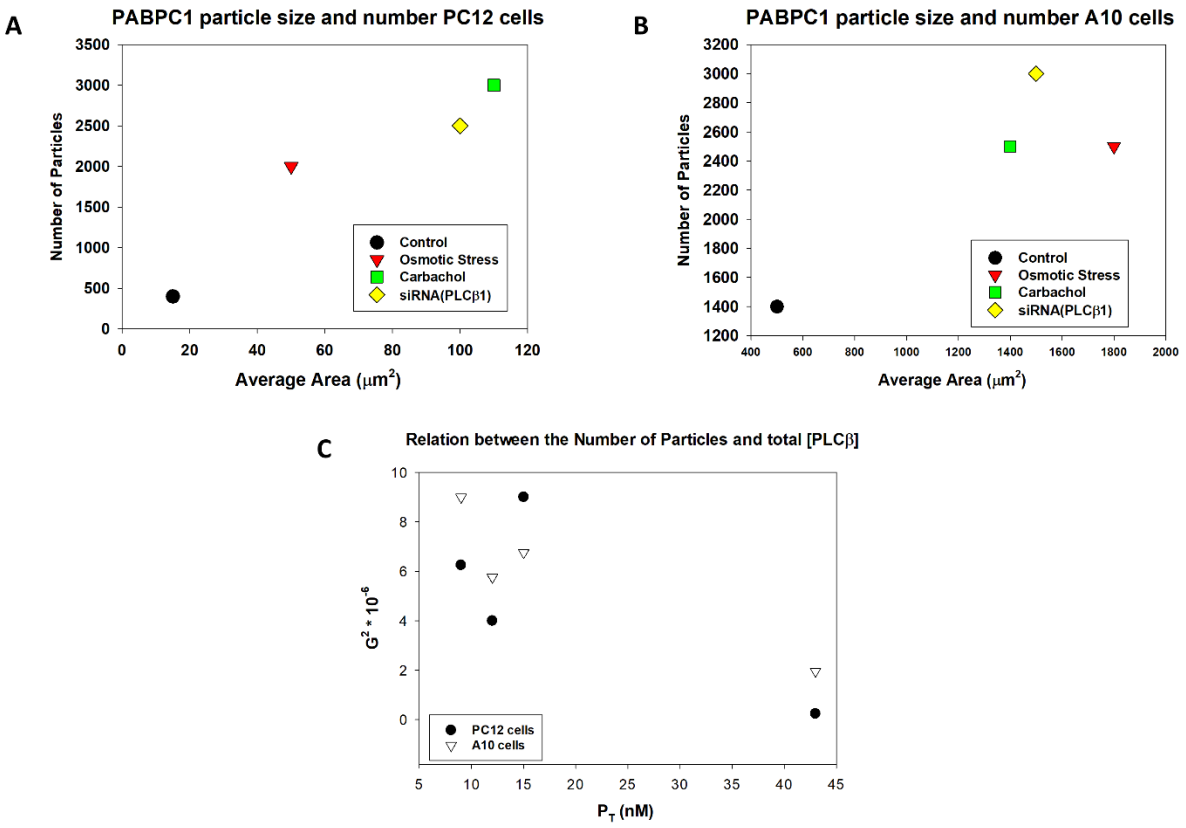

Figure 3.10 Relationship between particle formation and PLCβ1 abundance. (**A** and **B**) Analysis of the relationship between the number of PABPC1 particles and their average area in (**A**) PC12 cells and (**B**) A10 cells that were treated as indicated. (**C**) Analysis of the relationship between the number of PABPC1 particles determined in Figure 3.6 (**A** to **C**) and Figure 3.8 (**C** to **E**) and the estimated concentration of total cytosolic PLCβ1 in PC12 and A10 cells, where the intensity is compared to a calibration scale using Alexa Fluor 488 and measuring in confocal volume in an FCS instrument.

3.4 Discussion

The experiments presented here support the idea that cells direct signals through the reversible sequestration of proteins in membrane-less organelles. In some cases, these structures promote protein-protein interactions by reducing the local concentration and mobility of the proteins, whereas in other cases they effectively halt a functional pathway.[39-40] In this work, we showed that the atypical cytosolic population of PLCβ1 organized particles containing stress granule proteins in response Gαq signals. The specific types of stress granules that resulted from Gαq-PLCβ1 signals appeared to be similar to those that occurred under osmotic stress but were distinct from

those resulting from cold or heat shock, oxidative stress, or arsenite treatment. Our findings suggest that PLCβ1 regulates the entry of Ago2 and other stress granule proteins into particulates through a simple thermodynamic binding mechanism that is competitive with Gαq and that is dependent on the cytosolic concentration of PLCβ.

The traditional function of PLCβ is to generate Ca^{2+} signals in response to signaling molecules that lead to the activation of Gαq, such as acetylcholine, dopamine, serotonin, melatonin, histamine, and angiotensin II. Note that without Gαq stimulation, the enzymatic activity of PLCβ1 is very low, and because Gαq resides at the plasma membrane and is not found in the cytosol, cytosolic PLCβ1 is not expected to be a substantial modifier of inositol phospholipids in internal membranes. Thus, any effect of these cytosolic binding partners on the enzymatic function of PLCβ1 would be immaterial; however, their ability to regulate its access to Gαq may be important for Ca^{2+} generation.

PLCβ1 plays multiple roles in cellular functions that are usually attributed to its enzymatic function. Studies showed that PLCβ1 can localize to the nucleus to regulate cell growth and differentiation, possibly through modulation of PIP_2 abundance in the nuclear envelope.[41-42] We previously found that a stable, cytosolic population of PLCβ1 affects various cell functions, such as RNA silencing and neuronal cell differentiation and proliferation independently of its catalytic activity.[43-44] These alternative cytosolic functions of PLCβ only occur at specific and limited times in the cell cycle. For this reason, we set out to determine whether cytosolic PLCβ1 binds to other proteins in non-differentiating cells under non-stimulated conditions. With these parameters in mind, we used a proteomics approach to uncover potential interacting proteins and validated some of these interactions in live cells. Our experiments showed that under basal conditions, cytosolic PLCβ1 interacted with stress granule–associated proteins in intact cultured cells.

Stress granules are RNA-protein aggregates that enable cells to halt the translation of mRNAs encoding nonessential proteins when the cells are subjected to environmental stress. We found that many of the proteins that associated with PLCβ1 in complexes directly contribute to RNA-processing and ribosome assembly, and that these proteins were found in PLCβ1-containing complexes isolated from PC12 cells and A10 cells. During the initiation stage of mRNA

translation, the polyadenylate binding protein PABP binds to the tail of the mRNA, which then associates with eIF4, enabling the mRNA-protein complex to bind to the 40*S* subunit.[45] A cytosolic form of PABP, PABPC1, was found in our PLCβ1 pulldown assay together with eIF4 subtypes, which bind to PABPC1 (see https://www.uniprot.org/uniprot/P11940). Several other eIF proteins were also identified in our analysis.

An important step in the progression of translation is the hydrolysis of GTP on eIF2, which is catalyzed by the GTPase activity of eIF5. Our results suggest that eIF5A may be a primary binding partner to mediate the association of PLCβ1 with stress granule proteins. eIF5A is found at very high abundance in cells arrested at the G2/M checkpoint when protein translation is expected to be low. eIF5A has several regions in its sequence that are homologous to those of Gαq, including a region through which Gαq directly binds to PLCβ (amino acid residues 147 to 162), as indicated by homologous sequence alignment and chemical cross-linking.[46] We directly tested the association between PLCβ1 and eIF5A in experiments with purified proteins. Not only was the PLCβ1-eIF5A binding affinity in the same range as the affinity between PLCβ1 and C3PO,[15] but the binding was competitive both in solution and in cells. Because the site in PLCβ1 through which it binds to C3PO overlaps with its binding site for Gαq, the association of PLCβ1 with eIF5A should depend on the extent of Gαq activation, and this behavior was observed in our experiments. Thus, in the absence of Gαq stimulation, a population of cytosolic PLCβ1 may associate with eIF5A until specific events, such as cellular differentiation, cause PLCβ1 binding to shift to C3PO and inhibit RNA-induced silencing.

We found that cytosolic PLCβ1 also bound to Ago2 as seen in our pull-down studies, co-immunoprecipitation experiments, and FRET/FLIM analysis. Our ability to disrupt the PLCβ1-Ago2 interaction by the addition of purified eIF5A is suggestive of a direct interaction. Ago2 is the key nuclease component of the RISC,[47] and our previous work suggested an association between PLCβ1, C3PO and Ago2.[14] FLIM/FRET measurements suggest that these three proteins form a ternary complex where PLCβ1 is necessary for the interaction of Ago2 and C3PO as they exchange RNA (Figure 3.11). When carbachol stimulation or environmental stress drives a large population of PLCβ1 to the plasma membrane, cytosolic binding partners are released, but it appears that a small fraction of PLCβ1 remains cytosolic and persists in binding. These residual

cytosolic interactions may be partially responsible for the different composition of stress granules formed under different conditions. In neuronal tissue, endogenous levels of PLCβ1 are significantly higher than that of both Ago2 and C3PO. Ensembl reports 18 transcripts associated with PLCβ1, a level to be considered enhanced brain specificity for this gene. However, low brain specificity is seen for Ago2 and C3PO with only 3 and 2 transcript copies identified respectively (see https://www.proteinatlas.org/). Considering PLCβ1 is the most highly expressed protein involved in this ternary system, it is not surprising that changes in interaction between Ago2-C3PO are detected as a result of knockdown of PLCβ1. Sequence alignment of Ago2 and the TRAX subunits of C3PO shows four homologous regions ranging from ~20 to 40 amino acid residues in length and from 21 to 30% identity and 40 to 56% homology (residues 2 to 54, 87 to 119, 202 to 228, and 109 to 136 in C3PO and residues 788 to 826, 555 to 598, 188 to 202, and 831 to 858 in Ago2). Note that at least three of the C3PO regions are potential interaction sites for binding to PLCβ1, and at least one of these may be available for binding to PLCβ1-Ago2.[27] By this argument, it is possible that PLCβ1 directly binds to Ago2 through interactions similar to those through which it binds to C3PO.

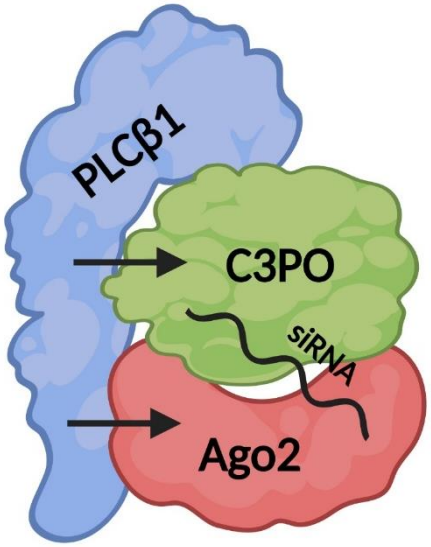

Figure 3.11 Model of PLCβ1s interaction with cytosolic binding partners. Under basal conditions, PLCβ1 is found to bind both Ago2 and C3PO to regulate RISC function and stress granule formation. Stimulation by carbachol removes a large population of PLCβ1 from the cytosol and residual cytosolic protein binds the remaining fraction of C3PO and Ago2 tightly. (Created with BioRender.com)

We determined whether PLCβ1 affected stress granule formation by monitoring the behavior of two established stress granule markers, Ago2 and PABPC1. We initially used mild osmotic stress that may occur physiologically. Hypo-osmotic stress initiates a series of cellular events to reduce the number of osmolytes in the cell, such as the synthesis of glycogen from glucose, as well as ion flow.[48] Whereas we expected osmotic strength to change the ability of PLCβ1 to interact with stress granule proteins by causing changes in tertiary or quaternary structure, we were surprised to find a large reduction in PLCβ1a abundance in PC12 cells when osmotic stress was initially applied, although this effect was far less pronounced in A10 cells. The PLCβ1a and PLCβ1b isoforms differ by ~20 amino acids in the C-terminal region, but they are similarly activated by Gαq. Piazzi *et al*. found that PLCβ1b, but not PLCβ1a, prevents cell death under oxidative conditions by affecting the amounts of key signaling proteins.[49] Additionally, these two PLCβ1 isoforms may localize differently depending on cell type.[31-34, 50-51] Whereas our experiments could not adequately distinguish between these two isoforms, it would be interesting to investigate any separate roles they may play in stress granule formation. Note that in addition to the changes in PLCβ1 abundance or properties that occurred because of osmotic stress, we also varied cytosolic PLCβ1 abundance by stimulating Gαq to recruit PLCβ1 from the cytosol to the plasma membrane, and we also reduced total PLCβ1 abundance with siRNA(PLCβ1). All of these methods showed a connection between cytosolic PLCβ1 abundance and the formation of particles.

Our experiments showed that the stress granules formed by osmotic stress differed from those formed in response to other stresses. Whereas we observed a substantial assembly of Ago2 under osmotic stress, we found that arsenite, oxidative stress, and temperature shock produced particles that contained monomeric Ago2. In addition, osmotic stress resulted in a large increase in the size distribution of cytosolic RNAs, whereas arsenite, oxidative stress, and temperature shock did not. Studies in *S. cerevisiae*[3] indicate that hypo-osmotic stress promotes the formation of particles composed of markers of both P-bodies and stress granules, supporting our findings that subjecting mammalian cells to hypo-osmotic stress forms particles with compositions that differ from those formed in response to other types of stress. Our results also suggest that these latter granules, which have low Ago2 content and are rich in proteins associated with RNA-processing, such as G3BP, are poised to prevent the translation of mRNAs whose protein products would not survive arsenite stress or oxidation, such as those involved in phosphorylation.[52] In contrast, Ago2-rich granules,

whose formation is mediated by the Gαq-PLCβ1 pathway, may shift translation to mRNAs whose protein products enable cells to better respond to external signals. Thus, unlike arsenite or other stresses, Gαq activation may give rise to more physiologically relevant particles.

We monitored the appearance of stress granules under hypo-osmotic conditions structurally by fluorescence imaging and functionally by the accumulation of large cytosolic RNAs. Wheeler *et al*. showed that initially, stress granules are small and grow in size in a time-dependent manner [5]. Here, we resolved particles greater than 10 μm^2 in area that formed in the cytoplasm, and the size and number of these particles did not vary between 5 and 10 min after stress induction. Additionally, whereas a very small population of eGFP-PLCβ1 incorporated into particles of ~400 μm^2, these were unchanged under conditions of osmotic stress, suggesting that PLCβ1 might deliver proteins into particles without incorporating into them. PABPC1 was associated with a high number of aggregates whose numbers were affected by the abundance of cytosolic PLCβ1 as determined by immunofluorescence analysis. Formation of Ago2-associated particles, as monitored by both immunofluorescence and live-cell imaging, was sensitive to Gαq stimulation but not to other stresses. Furthermore, the formation of stress granules associated with G3BP1, which did not appear to bind directly to PLCβ1, appeared to be sensitive to cytosolic PLCβ1 abundance and showed extensive and diffuse aggregation. These data suggest that cells respond to Gαq activation by sequestering Ago2, G3BP1, and other proteins into stress granules to halt the production of specific proteins.

Our results also suggest that the stress granules generated by Gαq activation are more similar to those formed by reducing PLCβ1 abundance or inducing osmotic stress in terms of Ago2 aggregates and are distinct from those produced by thermal or oxidative stress. Specifically, cold, heat, oxidative, or arsenite stress did not result in Ago2 aggregation and did not substantially affect the sizes of cytosolic RNAs, even though oxidative stress reduced the abundance of PLCβ1 together with that of many cellular proteins.[53] Our results are consistent with the variability of stress granule composition formed in response to different types of stress.[36, 54-55] Our studies also suggest that a loss of cytosolic PLCβ1 may arrest the translation of mRNAs for specific proteins by promoting the formation of mRNA-Ago2–associated stress granules. The idea that sustained

Gαq activation can regulate the production of specific proteins is intriguing and a comprehensive study of all of the transcripts affected by PLCβ1 is underway.

Neurons and cardiomyocytes are long-lived cells, and their viability depends on the reversible assembly of stress granules. We used PC12 cells as a model for the role of stress granules in neurological diseases and A10 cells as a model for muscle cells that regularly experience changes in osmolarity. We also used WYK-3M22 rat aortic smooth muscle cells as another model of muscle cells, which is used as the normotensive control for spontaneously hypertensive rats, which are a common model of hypertension.[56] We found a similar set of stress-related proteins in PLCβ1-containing complexes in the two cell lines, with the exception of neural-specific proteins and RISC proteins, such as Ago2 and C3PO. Thus, PLCβ1 may serve a similar role in many cell types by mediating stress granule formation but not in regulating RNA processing.

We constructed a simple thermodynamic model in which the partitioning of eIF5A into particulates is regulated by its association with PLCβ1, but we note that eIF5A can easily be replaced with Ago2. The expression derived from this model shows the scope by which PLCβ1 could affect stress granule formation. Specifically, if the total amount of eIF5A is much greater than that of PLCβ1, then stress granule formation will be independent of PLCβ1. Considering the high concentration of ribosomes in cells, it is difficult to estimate the amount of eIF5A that would be available to bind to PLCβ1. We know that microinjection studies that delivered ~10 nM eIF5A into cells resulted in the displacement of C3PO from PLCβ1, which can give us a quantitative handle for future studies. Regardless of the specific nature of eIF5A and its associated proteins, our data suggest that there is a concentration range of PLCβ1 that sensitizes cells to stress granule formation and that this range is under the control of Gαq activation. Additionally, endogenous amounts of PLCβ1 may help to control premature stress responses.

In summary, our studies suggest a model in which cytosolic PLCβ1 binds to stress granule protein complexes to keep these proteins disperse under basal conditions. Activation of Gαq shifts the cytosolic population of PLCβ1 to the plasma membrane, displacing stress granule proteins and promoting the formation of particles. This dynamic nature of PLCβ1 is consistent with FCS studies showing the rapid movement of the enzyme between the cytosol and plasma membrane.[27] We

propose a model (Figure 3.12) in which cells use cytosolic PLCβ1 abundance to regulate the formation and timing of protein synthesis and to prevent the formation of irreversible aggregates. Note that the quenching of Gαq-PLCβ1–dependent Ca^{2+} signals in cells under osmotic stress suggests that the stress granules may effectively block this signaling pathway.

We previously found that PLCβ1 plays an important but uncharacterized role in neuronal cell development. Specifically, the expression of PLCβ1a increases substantially within the first 24 hours of PC12 cell differentiation and then slowly decreases,[16] leading to the question of why its abundance is so variable. PLCβ1 is highly expressed in neuronal tissue in which dysfunction in stress granule assembly has been implicated in disease.[57-58] Our data suggest that PLCβ1 may act as a chaperone to keep stress granule proteins dispersed under basal conditions. Note that reductions in the amount PLCβ1 are associated with a host of neurological disorders that may result from disruptions in Ca^{2+} signaling and the proliferation and differentiation of neuronal cells.[59-62] Schizophrenia and suicide specifically involve varying amounts of PLCβ1a and PLCβ1b in the prefrontal cortex.[61] Note also that the PLCβ1-associated proteins identified here play important roles in neuronal function. FXR proteins are associated with the most common form of hereditary mental retardation,[63-64] whereas eIF5A is associated with neuronal growth and brain development.[65] It is interesting to speculate about connections between PLCβ1-associated neurological disorders and those associated with FXR and eIF5A, which may involve dysfunction in stress granule assembly and disassembly.

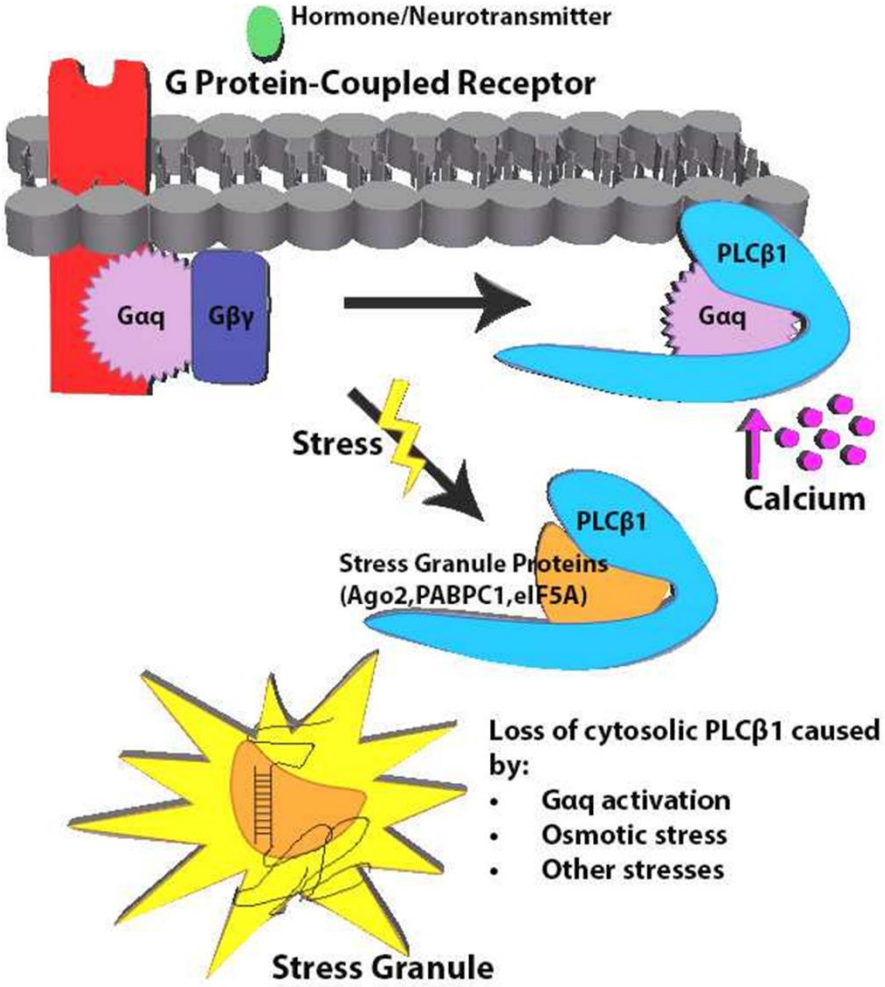

Figure 3.12 Model of the multiple interactions of PLCβ1 in cells. Under basal conditions, PLCβ1 is distributed both at the plasma membrane and in the cytosol where it may interact with stress granule–associated proteins. The activation of Gαq (through the stimulation of a GPCR by its ligand) promotes the movement of PLCβ1 to the plasma membrane, thereby releasing the stress granule–associated proteins and promoting particle formation.

3.5 Materials & methods

3.5.1 Cell culture

Rat pheochromocytoma (PC12) and rat aortic smooth muscle (A10) cells were obtained from the American Type Culture Collection (ATCC). Wistar-Kyoto rat 3M22 (WKO-3M22) cells, originally obtained from ATCC, were a gift from M. Rolle (Department of Biomedical Engineering, Worcester Polytechnic Institute). PC12 cells were cultured in high-glucose Dulbecco's modified Eagle's medium (DMEM; Gibco) with 10% heat-inactivated horse serum (Gibco) and 5% fetal bovine serum (FBS; Atlanta Biologicals). A10 cell lines were cultured in high-glucose DMEM with 10% FBS and 1% sodium pyruvate. WKO-3M22 cell lines were cultured in high-glucose DMEM (Corning) without L-glutamine with 10% FBS, 1% sodium pyruvate, 1% nonessential amino acids (VWR), and 1% L-glutamine (VWR). All cells were incubated at 37°C in 5% CO_2. Cells were synchronized in the G_2-M phase as described previously.[17] Briefly, 2 mM thymidine was added to the cells for 24 hours, after which the medium was removed and replaced by fresh complete culture medium for 8 hours, which was followed by the addition of nocodazole (40 ng/ml).

3.5.2 Plasmids

The EGFP-hArgonaute-2 (eGFP-Ago2) plasmid was purchased from Addgene (plasmid no. 21981) and was prepared in the laboratory of P. Sharp (Massachusetts Institute of Technology). The mCherry-Ago2 plasmid was a gift from A. Weaver (Vanderbilt University). EGFP-G3BP1 was purchased from Addgene (plasmid, no. 119950) and was prepared in the laboratory of J. Chao (Friedrich Miescher Institute). The mCherry-TRAX-C1 plasmid was constructed by inserting the complementary DNA (cDNA) encoding *TRAX* between the Bam HI and Eco RI restriction sites in the mCherry-C1 backbone with T4 DNA ligase (NEB). Cell transfections with plasmids and siRNAs were performed with Lipofectamine 3000 (Invitrogen) in antibiotic-free medium. The culture medium was changed to one containing antibiotic (1% penicillin-streptomycin) 12 to 18 hours after transfection. For every FLIM experiment, two separate samples were prepared: donor alone and donor in the presence of acceptor.

3.5.3 Co-immunoprecipitations

PC12 cells were lysed in buffer containing 1% Triton X-100, 0.1% SDS, 1× protease inhibitor cocktail, and 10 mM tris (pH 7.4), after which 200 μg of soluble protein was incubated with 2 μl of anti-PLCβ1 or anti-Ago2 antibody overnight at 4°C. After the addition of 20 mg of protein A-Sepharose 4B beads (Invitrogen), the mixture was gently rotated for 4 hours at 4°C. Beads were washed three times with lysis buffer, and bound proteins were eluted with sample buffer for 5 min at 95°C. Precipitated proteins were loaded onto two 10% polyacrylamide gels. After SDS–polyacrylamide gel electrophoresis (SDS-PAGE), one gel was transferred to nitrocellulose membranes and proteins were detected by Western blotting analysis with anti-PLCβ1 (D-8, Santa Cruz Biotechnology) and anti-Ago2 (Abcam, ab32381, lot# GR3195666-1) antibodies.

3.5.4 Application of stress conditions

For hypo-osmotic stress conditions, the culture medium was diluted with 50% water for 5 min before it was removed and replaced with Hanks' balanced salt solution (HBSS) for imaging. For the arsenite treatment, a stock solution of 100 mM arsenite in water was prepared. Cells were exposed to a final concentration of 0.5 mM arsenite for 10 min before the medium was removed and replaced by HBSS for imaging. For heat shock conditions, cells were incubated at 40°C for 1 hour, whereas for cold shock, cells were incubated at 12°C for 1 hour. For the oxidative stress treatment, a stock solution of 1 M $CoCl_2$ was prepared, and the cells were exposed to a final concentration of 1 mM $CoCl_2$ for 12 to 16 hours (overnight) at 37°C before the medium was removed. Treatment of both PC12 cells and WKO-3M22 cells with puromycin (20 μg/liter) was performed for 30 min at 37°C.

3.5.5 FRET studies between purified PLCβ1 and eIF5A

PLCβ1 was purified by overexpression in human embryonic kidney (HEK) 293 cells as previously described.[28] Purification of eIF5A was performed as described previously.[26] Purified eIF5A in a pET28-mhl vector was expressed in bacteria [Rosetta 2(DE3)plysS] by inoculating 100 ml of an overnight culture grown in Luria-Bertani medium into 2 liters of Terrific Broth medium in the presence of kanamycin (50 μg/ml) and chloramphenicol (25 μg/ml) at 37°C. When the culture reached an optical density at 600 nm (OD 600) of ~3.0, the temperature of the medium was reduced to 15°C and the culture was treated with 0.5 mM isopropyl-β-D-thiogalactopyranoside (IPTG) to

induce protein production. The cells were allowed to grow overnight before they were harvested and stored at −80°C. Frozen cells from 1.8 liters of TB culture were thawed, resuspended in 150 ml of lysis buffer [20 mM Hepes (pH 7.5), 300 mM NaCl, 5% glycerol, 2 mM β-mercaptoethanol (BME), 5 mM imidazole, 0.5% CHAPS, protease inhibitor cocktail, and 5 μl of deoxyribonuclease], and lysed with a panda homogenizer. The lysate was centrifuged at 30,000*g* for 45 min, added to a cobalt column in binding buffer [20 mM Hepes (pH 7.5), 300 mM NaCl, 5% glycerol, 2 mM BME, and 5 mM imidazole], and equilibrated in 4 × 1 ml of a 50% slurry of cobalt resin. We passed 150 ml of supernatant through each cobalt column at about 0.5 ml/min; washed first with 20 mM Hepes (pH 7.5), 300 mM NaCl, 5% glycerol, 2 mM BME, and 30 mM imidazole and second with 20 mM Hepes (pH 7.5), 300 mM NaCl, 5% glycerol, 2 mM BME, and 75 mM imidazole; and eluted with 20 mM Hepes (pH 7.5), 300 mM NaCl, 5% glycerol, 2 mM BME, and 300 mM imidazole. Protein-protein associations were assessed by FRET using sensitized emission. Briefly, PLCβ1a and eIF5A were covalently labeled on their N termini with Alexa Fluor 488 and Alexa Fluor 594 (Invitrogen), respectively, and the increase in acceptor emission when the samples were excited at the donor wavelength in the presence of Alexa Fluor 488–PLCβ1 was measured. Studies were repeated by prebinding catalytically inactive C3PO with Alexa Fluor 488–PLCβ1.

3.5.6 Mass spectrometry

MS measurements were performed at the University of Massachusetts Medical School as previously described.[66] Cytosolic fractions were isolated from cells, and proteins that bound to monoclonal anti-PLCβ1a antibody (Santa Cruz Biotechnology, D-8) were separated by electrophoresis. Protein bands were isolated by cutting the gels into 1 mm–by–1 mm pieces, which were placed in 1.5-ml Eppendorf tubes with 1 ml of water for 30 min. The water was removed, and 200 μl of 250 mM ammonium bicarbonate was added. Disulfide bonds were reduced by incubation with dithiothreitol at 50°C for 30 min, which was followed by the addition of 20 μl of 100 mM iodoacetamide for 30 min at room temperature. The gel slices were washed twice with 1-ml water aliquots. The water was then removed, 1 ml of 50:50 50 mM ammonium bicarbonate:acetonitrile was placed in each tube, and the samples were incubated at room temperature for 1 hour. The solution was then removed, and 200 μl of acetonitrile was added to each tube, at which point the gel slices turned white and became opaque. The acetonitrile was

removed, and the gel slices were further dried in a SpeedVac (Savant Instruments Inc.). Gel slices were rehydrated in 100 µl of sequencing-grade trypsin (4 ng/µl; Sigma-Aldrich) in 0.01% ProteaseMAX Surfactant (Promega):50 mM ammonium bicarbonate. Additional bicarbonate buffer was added to ensure complete submersion of the gel slices. Samples were incubated at 37°C for 18 hours. The supernatant of each sample was then removed and placed into a separate 1.5-ml Eppendorf tube. Gel slices were further extracted with 200 µl of 80:20 acetonitrile:1% formic acid. The extracts were combined with the supernatants of each sample. The samples were then completely dried down in a SpeedVac. Tryptic peptide digests were reconstituted in 25 µl of 5% acetonitrile containing 0.1% (v/v) trifluoroacetic acid and separated on a nanoACQUITY (Waters) ultraperformance liquid chromatograph. Briefly, a 2.5-µl injection was loaded in 5% acetonitrile containing 0.1% formic acid at 4.0 µl/min for 4.0 min onto a 100–µm–inner diameter (I.D.) fused-silica precolumn packed with 2 cm of 5-µm (200 Å) Magic C18AQ (Bruker-Michrom) and eluted with a gradient at 300 nl/min onto a 75-µm I.D. analytical column packed with 25 cm^3 of 3-µm (100 Å) Magic C18AQ particles to a gravity-pulled tip. The solvents used were solvent A [water (0.1% formic acid)] and solvent B [acetonitrile (0.1% formic acid)]. A linear gradient was developed from 5% solvent A to 35% solvent B in 90 min. Ions were introduced by positive electrospray ionization through a liquid junction into a Q Exactive hybrid mass spectrometer (Thermo Fisher Scientific). Mass spectra were acquired over mass/charge ratio (*m*/*z*) 300 to 1750 at 70,000 resolution (*m*/*z* 200), and data-dependent acquisition selected the top 10 most abundant precursor ions for tandem MS by higher-energy C-trap dissociation fragmentation using an isolation width of 1.6 Da, a collision energy of 27, and a resolution of 17,500. Raw data files were peak-processed with Proteome Discoverer software (version 2.1, Thermo Fisher Scientific) before undergoing database searching with Mascot Server (version 2.5) against the Uniprot_Rat database. Search parameters included trypsin specificity with two missed cleavages or no enzymatic specificity. The variable modifications of oxidized methionine, pyroglutamic acid for N-terminal glutamine, phosphorylation of serine and threonine, N-terminal acetylation of the protein, and a fixed modification for carbamidomethyl cysteine were considered. The mass tolerances were 10 ppm (parts per million) for the precursor and 0.05 Da for the fragments. Search results were then loaded into the Scaffold Viewer (Proteome Software Inc.) for peptide/protein validation and label-free quantitation. These data were analyzed using percentage of total spectra in Scaffold4 software before plotting with SigmaPlot 14.

3.5.7 Number and brightness (N&B) measurements

N&B theory and measurement were fully described previously.[35] Experimentally, we collected ~100 cell images in which we viewed either free eGFP (control) or eGFP-Ago2 at a resolution of 66 nm per pixel and at a rate of 4 μs per pixel. Regions of interest (256 × 256 box) were analyzed from a 320 × 320 pixel image. Offset and noise were determined from the histograms of the dark counts performed every two measurements. N&B data were analyzed with SimFC software (www.lfd.uci.edu).

3.5.8 N&B analysis

N&B defines the number of photons associated with a diffusing species by analyzing the variation of the fluorescence intensity in each pixel in the cell image. In this analysis, the apparent brightness, *B*, in each pixel is defined as the ratio of the variance, σ, over the average fluorescence intensity <*k*>

$$B=\sigma 2/<k>$$

and

$$<k>=\varepsilon n$$

where *n* is the number of fluorophores. The determination of the variance in each pixel is obtained by rescanning the cell image ~100 times as described earlier. The average fluorescence intensity, <*k*>, is directly related to the molecular brightness, ε, in units of photons per second per molecule, and *n*. *B* can also be expressed as

$$B=\epsilon+1$$

The apparent number of molecules, *N*, is defined as

$$N=\epsilon n/(\epsilon+1)$$

3.5.9 Fluorescence lifetime imaging measurements

FLIM measurements were performed on the dual-channel confocal fast FLIM (Alba version 5; ISS Inc.) equipped with photomultipliers and a Nikon Eclipse Ti-U inverted microscope. A 60× Plan Apo (1.2 numerical aperture, water immersion) objective and a mode-locked, two-photon titanium-sapphire laser (Tsunami; Spectra-Physics) were used in this study. The lifetime of the laser was calibrated each time before experiments by measuring the lifetime of Atto 435 in water

with a lifetime of 3.61 ns (reference) at 80, 160, and 240 MHz. The samples were excited at 800/850 nm, and emission spectra were collected through a 525/50 band-pass filter. For each measurement, the data were acquired until the photon count was >300. Fluorescence lifetimes were calculated by allowing ω = 80 MHz

$$\tau = S/(G*2\pi*\omega)$$

3.5.10 Statistical analysis

Data were analyzed with the SigmaPlot 13 and GraphPad Prism 9 statistical packages, which included the Student's *t* test and one-way analysis of variance (ANOVA).

3.5.11 Dynamic light scattering

DLS measurements were performed on a Malvern Panalytical Zetasizer Nano ZS instrument. For these experiments, mRNA from PC12 cells was extracted with the QIAGEN Mini Kit (catalog no. 74104) according to the manufacturer's instructions. Before the mRNA was extracted, the cells were exposed to stress, treated with siRNA(PLCβ1a), or transfected with plasmid expressing constitutively active GαqRC.[67] For these measurements, about 50 μl of extracted mRNA in RNase-free water was added in a Hellma fluorescence quartz cuvette (QS-3.00mm). Each sample was run three times for 10 min per run. Control samples were repeated six times, the PLCβ knockdown sample was repeated twice, and the Gαq overexpression sample was repeated once.

3.5.12 Particle analysis

Samples were imaged with a 100×/1.49 oil total internal reflection fluorescence (TIRF) objective to microscopically count the number of particles per μm^2 formed under different conditions. For each condition, 10 to 20 cells were randomly selected, and *z*-stack measurements were taken (1.0 μm per frame). Analysis was performed with ImageJ and Fiji ImageJ software in two ways. First, each measurement was thresholded before analyzing, and the number of particles per frame per measurement was averaged. Second, all *z*-stack measurements were combined to generate a three-dimensional image for each sample before analyzing the number of particles per sample and averaging the results. Both methods produced identical results.

3.5.13 Microinjection studies

Microinjection of a solution of 100 nM eIF5A into PC12 cells was performed with an Eppendorf FemtoJet microinjector mounted on Nikon Eclipse Ti-U inverted confocal microscope under 0.35-psi pressure and 0.5 s per injection.

3.5.14 Immunofluorescence

Cells were fixed with 3.7% formaldehyde, permeabilized with 0.1% Triton X-100 in PBS, and then blocked with 10% goat serum, 5% bovine serum albumin, and 50 mM glycine in PBS. Cells were then stained with the appropriate primary antibodies (Abcam), incubated for 1 hour, washed, and treated with a secondary antibody for 1 hour. After another wash, the cells were viewed on a Zeiss Meta 510 laser confocal microscope. Data were analyzed with Zeiss LSM software and ImageJ. The secondary antibodies used were Alexa Fluor 488–conjugated anti-rabbit antibody for Ago2 and Alexa Fluor 647–conjugated anti-mouse antibody for PABPC1.

3.5.15 Ca^{2+} signal imaging

Single-cell Ca^{2+} measurements were performed by labeling the cells with Calcium Green (Thermo Fisher Scientific), incubating the cells in HBSS for 45 min, and then washing the cells twice with HBSS. The release of intracellular Ca^{2+} in live PC12 cells was initiated by the addition of 2 μM carbachol before imaging the time series on a Zeiss LSM 510 confocal microscope with excitation at 488 nm using the time series mode as previously described.[68]

3.5.16 Western blotting

Samples were placed in six-well plates and collected in 250 μl of lysis buffer, which included NP-40 and protease inhibitors as mentioned earlier. Sample buffer was added at 20% of the total volume. After SDS-PAGE, proteins were transferred to nitrocellulose membranes (Bio-Rad). The primary antibodies used included the following: anti-PLCβ1 (Santa Cruz Biotechnology, sc-5291), anti-Ago2 (Abcam, ab32381), anti-PABPC1 (Santa Cruz Biotechnology, sc-32318), anti-G3BP1 (Santa Cruz Biotechnology, sc-81940), anti-actin (Abcam, ab8226), anti-HSP90 (Santa Cruz Biotechnology, sc-69703), anti-eGFP (Santa Cruz Biotechnology, sc-8334), and siRNA PLCβ1 (Ambion, 4390771). Membranes were treated with antibodies diluted 1:1000 in 0.5% milk and washed three times for 5 min each before applying the appropriate secondary antibody (anti-mouse

or anti-rabbit; Santa Cruz Biotechnology) at a 1:2000 dilution. Membranes were washed three times for 10 min each before being imaged on a Bio-Rad ChemiDoc imager to determine the relative band intensities. Band intensities were measured at several sensitivities and exposure times to ensure that the intensities were in a linear range. Data were analyzed with ImageJ software.

3.6 Acknowledgements

The authors thank M. Rolle (WPI) for the WKO-3M22 cells and E. Bafaro (WPI) for her help in cloning mCherry-TRAX, S. Yerramilli (WPI) for help with the N&B experiments and his helpful comments throughout this work, and G. Fiorentino (WPI) for her help in gathering data. S.S. is also a Professor Emeritus at Stony Brook University, NY, USA. Funding: The authors are grateful for the support of NIH GM116187. O.G. was supported by a Richard Whitcomb Fellowship.

3.7 References

1. Anderson, P.; Kedersha, N., RNA granules. *J Cell Biol* **2006,** *172* (6), 803-808.
2. Protter, D. S. W.; Parker, R., Principles and Properties of Stress Granules. *Trends in Cell Biology* **2016,** *26* (9), 668-679.
3. Shah, K. H.; Varia, S. N.; Cook, L. A.; Herman, P. K., A Hybrid-Body Containing Constituents of Both P-Bodies and Stress Granules Forms in Response to Hypoosmotic Stress in Saccharomyces cerevisiae. *PLoS One* **2016,** *11* (6), e0158776.
4. Khong, A.; Matheny, T.; Jain, S.; Mitchell, S. F.; Wheeler, J. R.; Parker, R., The Stress Granule Transcriptome Reveals Principles of mRNA Accumulation in Stress Granules. *Molecular Cell* **2017,** *68* (4), 808-820.e5.
5. Wheeler, J. R.; Matheny, T.; Jain, S.; Abrisch, R.; Parker, R., Distinct stages in stress granule assembly and disassembly. *Elife* **2016,** *5*.
6. Anderson, P.; Kedersha, N., Stress granules. *Current Biology 19* (10), R397-R398.
7. Ramaswami, M.; Taylor, J. P.; Parker, R., Altered Ribostasis: RNA-Protein Granules in Degenerative Disorders. *Cell* **2013,** *154* (4), 727-736.
8. Detzer, A.; Engel, C.; Wunsche, W.; Sczakiel, G., Cell stress is related to re-localization of Argonaute 2 and to decreased RNA interference in human cells. *Nucleic Acids Res* **2011,** *39* (7), 2727-41.
9. Hammond, S. M.; Caudy, A. A.; Hannon, G. J., Post-transcriptional gene silencing by double-stranded RNA. *Nat Rev Genet* **2001,** *2* (2), 110-9.
10. Lopez-Orozco, J.; Pare, J. M.; Holme, A. L.; Chaulk, S. G.; Fahlman, R. P.; Hobman, T. C., Functional analyses of phosphorylation events in human Argonaute 2. *RNA (New York, N.Y.)* **2015,** *21* (12), 2030-2038.
11. Suh, P.; Park, J.; Manzoli, L.; Cocco, L.; Peak, J.; Katan, M.; Fukami, K.; Kataoka, T.; Yun, S.; Ryu, S., Multiple roles of phosphoinositide-specific phospholipase C isozymes. *BMB reports* **2008,** *41*, 415-34.
12. Rebecchi, M.; Pentylana, S., Structure, function and control of phosphoinositide-specific phospholipase C. *Physiological Reviews* **2000,** *80*, 1291-1335.
13. Dowal, L.; Provitera, P.; Scarlata, S., Stable association between G alpha(q) and phospholipase C beta 1 in living cells. *J Biol Chem* **2006,** *281* (33), 23999-4014.
14. Philip, F.; Guo, Y.; Aisiku, O.; Scarlata, S., Phospholipase Cβ1 is linked to RNA interference of specific genes through translin-associated factor X. *The FASEB Journal* **2012,** *26* (12), 4903-4913.
15. Aisiku, O. R.; Runnels, L. W.; Scarlata, S., Identification of a Novel Binding Partner of Phospholipase Cβ1: Translin-Associated Factor X. *PLoS One* **2010,** *5* (11).
16. Garwain, O.; Scarlata, S., Phospholipase Cβ-TRAX Association Is Required for PC12 Cell Differentiation. *J. Biol. Chem.* **2016,** *291* (44), 22970-22976.
17. Garwain, O.; Valla, K.; Scarlata, S., Phospholipase Cbeta1 regulates proliferation of neuronal cells. *FASEB J* **2018,** *32* (5), 2891-2898.
18. Yanagi, T.; Krajewska, M.; Matsuzawa, S.-i.; Reed, J. C., PCTAIRE1 Phosphorylates p27 and Regulates Mitosis in Cancer Cells. *Cancer Research* **2014,** *74* (20), 5795-5807.
19. Yanagi, T.; Matsuzawa, S.-i., PCTAIRE1/PCTK1/CDK16: a new oncotarget? *Cell Cycle* **2015,** *14* (4), 463-464.
20. Mahboubi, H.; Stochaj, U., Cytoplasmic stress granules: Dynamic modulators of cell signaling and disease. *Biochim Biophys Acta* **2017,** *1863* (4), 884-895.

21. Cocco, L.; Martelli, A. M.; Gilmour, R. S.; Rhee, S. G.; Manzoli, F. A., Nuclear phospholipase C and signaling. *Biochim Biophys Acta* **2001,** *1530* (1), 1-14.
22. Lakowicz, J., *Principles of Fluorescence Spectroscopy, Second Edition*. Plenum: New York, 1999.
23. Digman, M. A.; Caiolfa, V. R.; Zamai, M.; Gratton, E., The Phasor Approach to Fluorescence Lifetime Imaging Analysis. *Biophysical Journal* **2008,** *94* (2), L14-L16.
24. Patterson, G. H.; Piston, D. W.; Barisas, B. G., Forster distances between green fluorescent protein pairs. *Anal Biochem* **2000,** *284* 438-440.
25. Philip, F.; Sahu, S.; Golebiewska, U.; Scarlata, S., RNA-induced silencing attenuates G protein-mediated calcium signals. *FASEB J* **2016,** *30* (5), 1958-67.
26. Paulin, F. E.; Campbell, L. E.; O'Brien, K.; Loughlin, J.; Proud, C. G., Eukaryotic translation initiation factor 5 (eIF5) acts as a classical GTPase-activator protein. *Current biology : CB* **2001,** *11* (1), 55-9.
27. Sahu, S.; Williams, L.; Perez, A.; Philip, F.; Caso, G.; Zurawsky, W.; Scarlata, S., Regulation of the activity of the promoter of RNA-induced silencing, C3PO. *Protein Science* **2017,** *26* (9), 1807-1818.
28. Sahu, S.; Philip, F.; Scarlata, S., Hydrolysis Rates of Different Small Interfering RNAs (siRNAs) by the RNA Silencing Promoter Complex, C3PO, Determines Their Regulation by Phospholipase Cβ. *J. Biol. Chem.* **2014,** *289* (8), 5134-5144.
29. Guo, Y.; Yang, L.; Haught, K.; Scarlata, S., Osmotic Stress Reduces Ca2+ Signals through Deformation of Caveolae. *J Biol Chem* **2015,** *290* (27), 16698-707.
30. Yang, L.; Scarlata, S., Super-resolution Visualization of Caveola Deformation in Response to Osmotic Stress. *J Biol Chem* **2017,** *292* (9), 3779-3788.
31. Bahk, Y. Y.; Lee, Y. H.; Lee, T. G.; Seo, J.; Ryu, S. H.; Suh, P. G., Two forms of phospholipase C-beta 1 generated by alternative splicing. *J. Biol. Chem.* **1994,** *269* (11), 8240-8245.
32. Bahk, Y.; Song, H.; Baek, K. J.; Park, B. Y.; Kim, H.; Ryu, S. H.; Suh, P. G., Localization of two forms of phospholipase Cβ1, a and b, in C6Bu-1 cells. *Biochem Biophys Acta* **1998,** *1389*, 76-80.
33. Kim, C. G.; Park, D.; Rhee, S. G., The role of carboxyl-terminal basic amino acids in $G_q\alpha$-dependent activation, particulate association, and nuclear localization of phospholipase C-β_1. *J Biol Chem* **1996,** *271* (35), 21187-92.
34. Grubb, D. R.; Vasilevski, O.; Huynh, H.; Woodcock, E. A., The extreme C-terminal region of phospholipase Cbeta1 determines subcellular localization and function; the "b" splice variant mediates alpha1-adrenergic receptor responses in cardiomyocytes. *Faseb j* **2008,** *22* (8), 2768-74.
35. Digman, M. A.; Dalal, R.; Horwitz, A. F.; Gratton, E., Mapping the Number of Molecules and Brightness in the Laser Scanning Microscope. *Biophys J* **2008,** *97*, 2320-2332.
36. Aulas, A.; Fay, M. M.; Lyons, S. M.; Achorn, C. A.; Kedersha, N.; Anderson, P.; Ivanov, P., Stress-specific differences in assembly and composition of stress granules and related foci. *J Cell Sci* **2017,** *130* (5), 927-937.
37. Cocco, L.; Faenza, I.; Fiume, R. M.; Gilmour, S. R.; Manzoli, F. A., Phosphoinositide-specific phospholipase C (PI-PLC) [beta]1 and nuclear lipid-dependent signaling. *Biochem Biophys Acta* **2006,** *1761*, 509-521.

38. Garwain, O.; Pearce, K. M.; Jackson, L.; Carley, S.; Rosati, B.; Scarlata, S., Stimulation of the Gαq/phospholipase Cβ1 signaling pathway returns differentiated cells to a stem-like state. *The FASEB Journal* **2020,** *34* (9), 12663-12676.
39. Case, L. B.; Zhang, X.; Ditlev, J. A.; Rosen, M. K., Stoichiometry controls activity of phase-separated clusters of actin signaling proteins. *Science* **2019,** *363* (6431), 1093-1097.
40. Huang, W. Y. C.; Alvarez, S.; Kondo, Y.; Lee, Y. K.; Chung, J. K.; Lam, H. Y. M.; Biswas, K. H.; Kuriyan, J.; Groves, J. T., A molecular assembly phase transition and kinetic proofreading modulate Ras activation by SOS. *Science* **2019,** *363* (6431), 1098-1103.
41. Cocco, L.; Manzoli, L.; Faenza, I.; Ramazzotti, G.; Yang, Y. R.; McCubrey, J. A.; Suh, P. G.; Follo, M. Y., Modulation of nuclear PI-PLCbeta1 during cell differentiation. *Adv Biol Regul* **2016,** *60*, 1-5.
42. Ramazzotti, G.; Faenza, I.; Fiume, R.; Billi, A. M.; Manzoli, L.; Mongiorgi, S.; Ratti, S.; McCubrey, J. A.; Suh, P. G.; Cocco, L.; Follo, M. Y., PLC-beta1 and cell differentiation: An insight into myogenesis and osteogenesis. *Adv Biol Regul* **2017,** *63*, 1-5.
43. Scarlata, S.; Garwain, O.; Williams, L.; Burguera, I. G.; Rosati, B.; Sahu, S.; Guo, Y.; Philip, F.; Golebiewska, U., Phospholipase Cbeta connects G protein signaling with RNA interference. *Adv Biol Regul* **2016,** *61*, 51-7.
44. Scarlata, S.; Singla, A.; Garwain, O., Phospholipase Cβ interacts with cytosolic partners to regulate cell proliferation. *Adv Biol Regul* **2017**.
45. Alberts, B.; Bray, D.; Lewis, J.; Raff, M.; Roberts, K.; Watson, J., *Molecular Biology of the Cell*. Garland: New York, 1994.
46. Lyon, A. M.; Tesmer, V. M.; Dhamsania, V. D.; Thal, D. M.; Gutierrez, J.; Chowdhury, S.; Suddala, K. C.; Northup, J. K.; Tesmer, J. J. G., An autoinhibitory helix in the C-terminal region of phospholipase C-β mediates Gαq activation. *Nat Struct Mol Biol* **2011,** *18*, 999-1005.
47. Hutvagner, G.; Simard, M. J., Argonaute proteins: key players in RNA silencing. *Nature Reviews Molecular Cell Biology* **2008,** *9*, 22.
48. Dietmar, K., Osmotic stress sensing and signaling in animals. *The FEBS Journal* **2007,** *274* (22), 5781-5781.
49. Piazzi, M.; Blalock, W. L.; Bavelloni, A.; Faenza, I.; Raffini, M.; Tagliavini, F.; Manzoli, L.; Cocco, L., PI-PLCβ1b affects Akt activation, cyclin E expression, and caspase cleavage, promoting cell survival in pro-B-lymphoblastic cells exposed to oxidative stress. *The FASEB Journal* **2015,** *29* (4), 1383-1394.
50. Martelli, A. M.; Gilmour, R. S.; Bertagnolo, V.; Neri, L. M.; Manzoli, L.; Cocco, L., Nuclear localization and signalling activity of phosphoinositidase C beta in Swiss 3T3 cells. *Nature* **1992,** *358* (6383), 242-5.
51. Filtz, T. M.; Grubb, D. R.; McLeod-Dryden, T. J.; Luo, J.; Woodcock, E. A., Gq-initiated cardiomyocyte hypertrophy is mediated by phospholipase Cβ1b. *The FASEB Journal* **2009,** *23* (10), 3564-3570.
52. Hughes, M. F., Arsenic toxicity and potential mechanisms of action. *Toxicology letters* **2002,** *133* (1), 1-16.
53. Guo, Y.; Scarlata, S., A Loss in Cellular Protein Partners Promotes α-Synuclein Aggregation in Cells Resulting from Oxidative Stress. *Biochemistry* **2013,** *52* (22), 3913-3920.
54. Youn, J. Y.; Dunham, W. H.; Hong, S. J.; Knight, J. D. R.; Bashkurov, M.; Chen, G. I.; Bagci, H.; Rathod, B.; MacLeod, G.; Eng, S. W. M.; Angers, S.; Morris, Q.; Fabian, M.; Cote, J. F.;

Gingras, A. C., High-Density Proximity Mapping Reveals the Subcellular Organization of mRNA-Associated Granules and Bodies. *Mol Cell* **2018,** *69* (3), 517-532.e11.
55. Jain, S.; Wheeler, Joshua R.; Walters, Robert W.; Agrawal, A.; Barsic, A.; Parker, R., ATPase-Modulated Stress Granules Contain a Diverse Proteome and Substructure. *Cell 164* (3), 487-498.
56. Lemire, J. M.; Covin, C. W.; White, S.; Giachelli, C. M.; Schwartz, S. M., Characterization of cloned aortic smooth muscle cells from young rats. *The American journal of pathology* **1994,** *144* (5), 1068-1081.
57. Wolozin, B., Physiological Protein Aggregation Run Amuck: Stress Granules and the Genesis of Neurodegenerative Disease. *Discovery medicine* **2014,** *17* (91), 47-52.
58. Chen, L.; Liu, B., Relationships between Stress Granules, Oxidative Stress, and Neurodegenerative Diseases. *Oxidative Medicine and Cellular Longevity* **2017,** *2017*, 10.
59. Hannan, A. J.; Kind, P. C.; Blakemore, C., Phospholipase C-β1 expression correlates with neuronal differentiation and synaptic plasticity in rat somatosensory cortex. *Neuropharmacology* **1998,** *37* (4–5), 593-605.
60. McOmish, C. E.; Burrows, E. L.; Howard, M.; Hannan, A. J., PLC-β1 knockout mice as a model of disrupted cortical development and plasticity: Behavioral endophenotypes and dysregulation of RGS4 gene expression. *Hippocampus* **2008,** *18* (8), 824-834.
61. Udawela, M.; Scarr, E.; Boer, S.; Um, J. Y.; Hannan, A. J.; McOmish, C.; Felder, C. C.; Thomas, E. A.; Dean, B., Isoform specific differences in phospholipase C beta 1 expression in the prefrontal cortex in schizophrenia and suicide. *npj Schizophrenia* **2017,** *3* (1), 19.
62. Kim, H.-j.; Koh, H.-Y., Impaired Reality Testing in Mice Lacking Phospholipase Cβ1: Observed by Persistent Representation-Mediated Taste Aversion. *PLoS One* **2016,** *11* (1), e0146376.
63. Agulhon, C.; Blanchet, P.; Kobetz, A.; Marchant, D.; Faucon, N.; Sarda, P.; Moraine, C.; Sittler, A.; Biancalana, V.; Malafosse, A.; Abitbol, M., Expression of FMR1, FXR1, and FXR2 genes in human prenatal tissues. *Journal of neuropathology and experimental neurology* **1999,** *58* (8), 867-80.
64. Bardoni, B.; Schenck, A.; Mandel, J.-L., The Fragile X mental retardation protein. *Brain Research Bulletin* **2001,** *56* (3), 375-382.
65. Huang, Y.; Higginson, D. S.; Hester, L.; Park, M. H.; Snyder, S. H., Neuronal growth and survival mediated by eIF5A, a polyamine-modified translation initiation factor. *Proc Natl Acad Sci U S A* **2007,** *104* (10), 4194-4199.
66. Iwata, S., Lee, J.W., Okada, K., Lee, J.K. Iwata, M., Rasmussen, B., Link T.A., Ramaswamy, S. and Jap, B.K., Complete at of the 11 subunit bovine mitochondrial cytochrome bc1 complex. *Science* **1998,** *281*, 64-71.
67. Hughes, T. E.; Zhang, H.; Logothetis, D.; Berlot, C. H., Visualization of a functional Gαq-green fluorescent protein fusion in living cells. *J.Biol.Chem.* **2001,** *276*, 4227-4235.
68. Calizo, R. C.; Scarlata, S., A role for G-proteins in directing G-protein-coupled receptor-caveolae localization. *Biochemistry* **2012,** *51* (47), 9513-23.

4 Chapter 4 – Activation of Gαq sequesters specific transcripts into Ago2 particles

Lela Jackson[1], Madison Rennie[1], Alison Poussaint[1] and Suzanne Scarlata[1]

1 - Department of Chemistry & Biochemistry, Worcester Polytechnic Institute, Worcester, MA

The following subsections appear in Jackson *et al.* "Activation of Gαq sequesters specific transcripts into Ago2 particles" *Scientific Reports.* (2022) and are reproduced here with permission. Supporting information from the manuscript can be found in the appendix. L.J., M.R., A.P. and S.S. designed experiments and interpreted the data. L.J. conducted and analyzed the following experiments: number and brightness, particle analysis, stress granule protein and RNA purifications, mass spectrometry analysis, RT-PCR and western blots. M.R. assisted with RT-PCR. A.P. conducted and analyzed the intrinsic FLIM experiment.

4.1 Abstract

The Gαq / phospholipase Cβ1 (PLCβ1) signaling system mediates calcium responses from hormones and neurotransmitters. While PLCβ1 functions on the plasma membrane, there is an atypical cytosolic population that binds Argonaute 2 (Ago2) and other proteins associated with stress granules preventing their aggregation. Activation of Gαq relocalizes cytosolic PLCβ1 to the membrane, releasing bound proteins, promoting the formation of stress granules. Here, we have characterized Ago2 stress granules associated with Gαq activation in differentiated PC12 cells, which have a robust Gαq/PLCβ1 signaling system. Characterization of Ago2-associated stress granules shows shifts in protein composition when cells are stimulated with a Gαq agonist, or subjected to heat shock or osmotic stress, consistent with the idea that different stresses result in unique stress granules. Purified Ago2 stress granules from control cells do not contain RNA, while those from heat shock contain many different mRNAs and miRs. Surprisingly, Ago2 particles from cells where Gαq was stimulated show only two transcripts, chromogranin B, which is involved in secretory function, and ATP synthase 5f1b, which is required for ATP synthesis. RT-PCR, western blotting and other studies support the idea that Gαq-activation protects these transcripts. Taken together, these studies show a novel pathway where Gαq/PLCβ regulates the translation of specific proteins.

4.2 Introduction

Binding of extracellular ligands such as acetylcholine, serotonin and histamine, to their specific G protein coupled receptor will activate Gαq, one of the four major G proteins pathways.[1] Gαq, in turn, activates phospholipase Cβ, which catalyzes the hydrolysis of the signaling lipid phosphoinositide 4,5 bisphosphate leading to an increase in intracellular calcium.[2] Along with this important membrane function, PLCβ1 has been shown to have a cytosolic population that binds to the Promoter of RNA-induced silencing, C3PO, as well as several proteins involved in stress granules formation.[3-4] Stress granules are halted ribosomal complexes that protect mRNAs under stress conditions such as arsenite treatment, heat / cold shock and osmotic stress.[5-7] Proteins that bind PLCβ1 include eFI5A, polyadenylate binding protein (PABPC1) and Ago2. Ago2 is additionally the main nuclease component of the RNA-induced silencing complex (RISC)[8] that degrades mRNA with the help of C3PO. When Ago2-bound mRNA pairs perfectly with a bound

miR, Ago2 transitions to an active conformation to hydrolyze the mRNA. However, if pairing is imperfect, it will form a stalled complex[9-11] resulting in stress granules.

Our recent study showed that reducing the cytosolic PLCβ1 population increases the number and size of particles containing Ago2 as well as the stress granule markers PABPC1 and G3BP1.[4, 12] Binding between PLCβ1 and stress granule proteins helps keep them disperse, while activation of Gαq promotes relocalization of cytosolic PLCβ1 to the plasma membrane, promoting release of bound proteins and the formation of stress granules. This mechanism suggests that Gαq may be connected to protein translation through cytosolic PLCβ1.

Here, we have characterized the composition of Ago2 stress granules formed in response to Gαq activation in differentiated PC12 cells and compared these to traditional stress responses. PC12 cells have a large endogenous expression of Gαq and PLCβ1, and although not neuronal in origin, when treated with nerve growth factor, the cells adopt neuronal morphology and secrete particles mimicking synaptic vesicles.[13-14] We find that Gαq activation produces stress granules that have a distinct protein composition as compared to other stresses. Also, unlike heat shock that contain different mRNA and miRs, Gαq stress granules contain only two major mRNA transcripts. Our studies show a surprising connection between physiological Gαq activation and protein translation.

4.3 Results

4.3.1 Activation of Gαq promotes stress responses in differentiated cells

Previous studies followed the formation of stress granules associated with Ago2 and PABCP1 by Gαq activation in undifferentiated PC12 cells as well as two other cell lines,[4] and here we extended these studies to differentiated PC12 cells. We first followed the assembly of the stress granule marker, eGFP-G3BP1, whose dimerization initiates stress granule formation.[15] These studies used time-lapse fluorescence imaging and assessed the number of fluorophores associated with a diffusing particle called Number and Brightness (N&B)[16] analysis. We find that the amount of eGFP-G3BP1 fluorescence intensity associated with diffusing particles increases with the loss of cytosolic PLCβ1 either by down-regulation, by relocalization to the membrane upon Gαq activation, or by osmotic stress which also reduces cytosolic PLCβ1 levels[4] (Figure 4.1A-D).

Although much of the G3BP1 aggregation that we see in N&B measurements is localized monomeric protein (denoted in blue text), there is also a fraction of detected oligomeric protein and that portion is reported in green text. It is important to note that we are inducing aggregation by different stresses where G3BP1 dimerization may play a lesser role. Additionally, aggregation of the fluorophore raises the possibility of photo physical mechanisms that reduce fluorescence such as homo transfer, which is highly likely given the close proximity of the fluorophores and/or self-quenching.

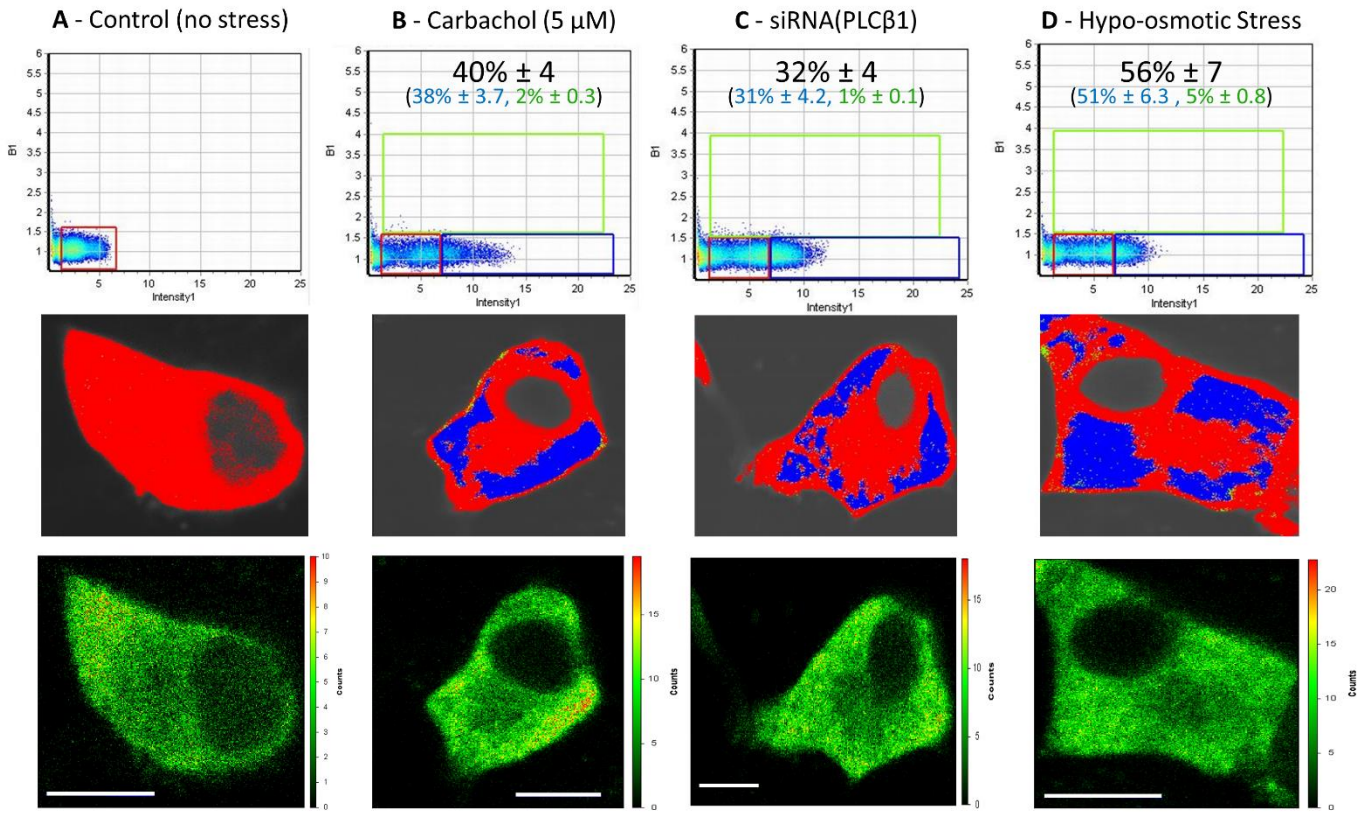

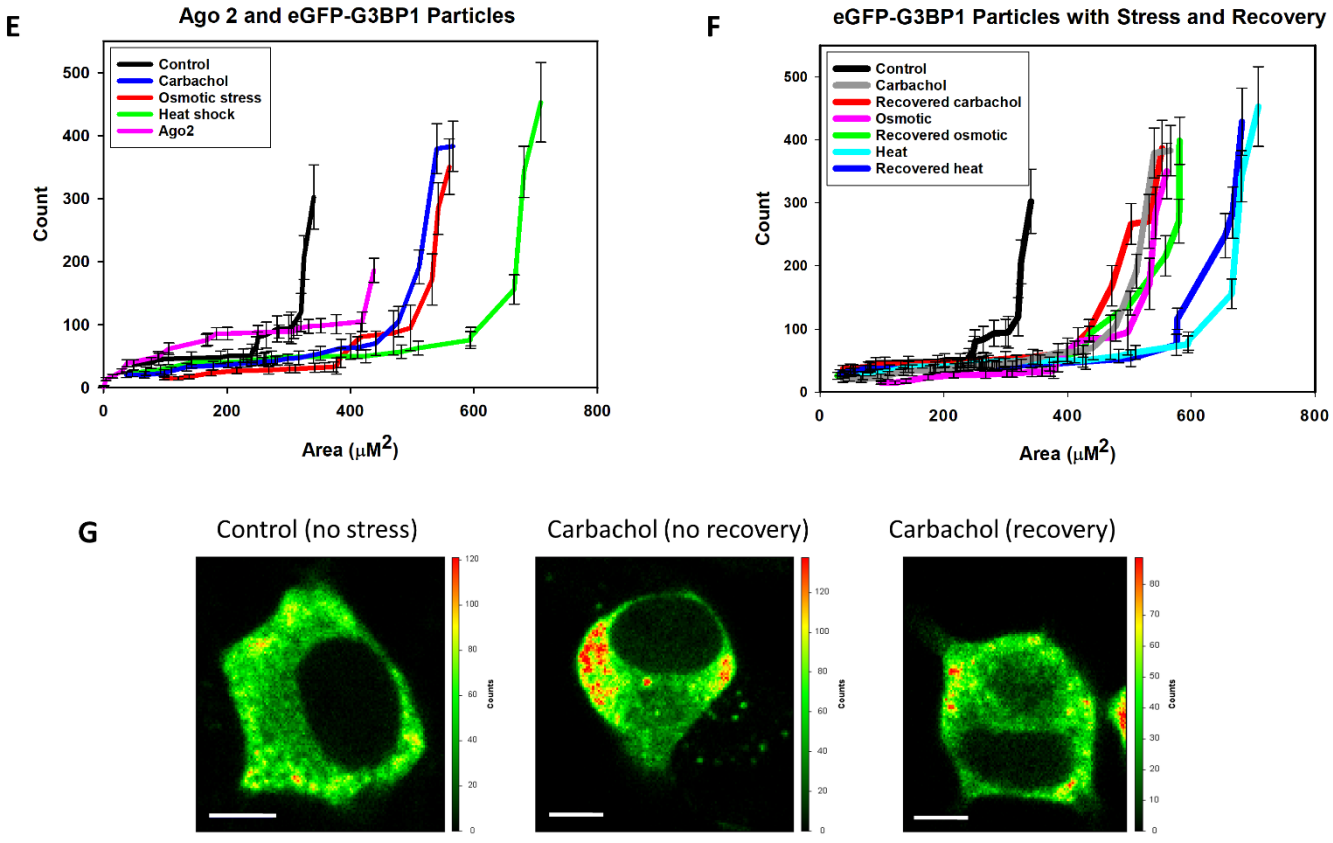

Figure 4.1 Aggregation of G3BP1 in differentiated PC12 cells. Cells transfected with eGFP-G3BP1 were at (A) control conditions, n=12; (B) activated Gαq by exposure to carbachol for 10 minutes, n=30; (C) treated with siRNA(PLCβ1), n=28; (D) subjected to hypo-osmotic stress (150 mOsm) for 5 minutes, n=14. The graphs in the top rows display N&B values for each pixel where the y-axis correspond to the brightness of the particle and the x-axis shows particle intensity. The pixels contained in the red boxes are the values found for free, non-aggregated eGFP. Points outside the red boxes shown in blue correspond to a high number of condensed monomeric protein, while points shown in green correspond to higher-order species of G3BP1 where the percent of pixels in these categories are given. Images in the middle rows show the pixels corresponding to free (red) and aggregated eGFP-G3BP1 (green and blue). Images in the bottom row are the corresponding fluorescence microscopy images. Total percent protein aggregation for each condition is reported in red text, while the portion of total aggregation derived from the green and blue boxes is reported in green and blue text, respectively. We note that a significant percent of cells in the carbachol (66%) and siRNA(PLCβ1) (54%) samples showed low (~2%) aggregation and only the percentages in the higher groups are shown. Scale bars=10 μm. (E) Cumulative values of the intensities (count) and size of eGFP-Ago2 or eGFP-G3P1particles in live cells under control conditions as determined by confocal imaging where the count values for Ago2 are reduced by 10 fold for scaling purposes. Also shown are eGFP-G3BP1 particle size and number in live cells immediately after carbachol treatment, hypo-osmotic stress or heat shock. For all conditions,

n=11 for eGFP-G3BP1 and n=12 for Ago2 where SD is shown. (F) eGFP-G3BP1 particle data shown in (E) along with data taken for cells that were treated to a stress condition and then allowed to recover at 37 ^{o}C for 30 minutes where n=11 and SE is shown. (G) Sample images of PC12 cells expressing eGFP-Ago2 with stimulation and recovery. Scale bars=10 μm.

Additionally, we followed the formation of larger eGFP-G3BP1 aggregates in live cells when subjected to Gαq stimulation, and compared these data to heat shock or osmotic stress by measuring their size and number by confocal imaging using a 100x objective (Figure 4.1E). As expected, we find a significant increase in the cumulative number and size of particles relative to control for all three stress conditions, consistent with stress granule formation.[15] The trends seen for eGFP-G3BP1 mirror previous studies[4] of Ago2 under stress conditions. Removing the stress and viewing the cells 30 minutes after recovery show little disassembly of the stress granules (Figure 4.1F). We note that G3BP1 particles formed under all conditions were stable for at least 30 minutes.

4.3.2 Characterization of proteins associated with Ago2 under stress conditions

We characterized the proteins associated with Ago2 stress granules. These studies were carried out by pulling down Ago2 with a monoclonal antibody from the cytosolic fraction of cells subjected to Gαq stimulation, hypo-osmotic stress or heat shock. The proteins contained in these Ago2 complexes were then identified by mass spectrometry. We found that Ago2 complexes isolated from cells under control conditions showed the highest number of bound proteins (~125) accounting for more than ~95% of the total protein (see Appendix, Table S4.1). However, cells subjected to Gαq stimulation, heat shock and osmotic stress conditions had far less different types of proteins bound to Ago2 (see Appendix, Tables S4.2-S4.4).

We grouped the Ago2 bound proteins into functional categories: mRNA associated, transcription factors, tRNA associated, RNA polymerase, stress proteins, heat shock and eukaryotic initiation and translation, and proteins sensitive to changes in intracellular calcium (Figure 4.2A-D) and we note that several cytoskeletal proteins appear. As expected, different conditions had different protein distributions relative to control. Proteins bound to Ago2 in cells subjected to heat shock and Gαq stimulation show an increased percentage of transcription factors, which is consistent with a halting of fundamental cellular events, whereas samples from cells subjected to osmotic

stress show conserved levels of proteins associated with tRNA, which is consistent with shifts in protein production to restore basal osmolality. Comparison of the most abundant proteins associated with Ago2 under each condition shows transcriptional enhancer factor TEF-5 to be the major binding partner followed by cytoskeletal and structural proteins (i.e. actin, desmoplakin, titin, dynein, nesprin), whose amounts shift slightly with each condition. Focusing on the ten most abundant proteins, Ago2 complexes formed under Gαq stimulation showed only one unique protein, polyubiquitin-B, while both Ago2 complexes under Gαq stimulation and osmotic stress contain Phe tRNA ligase, which is absent in control and heat shock samples.

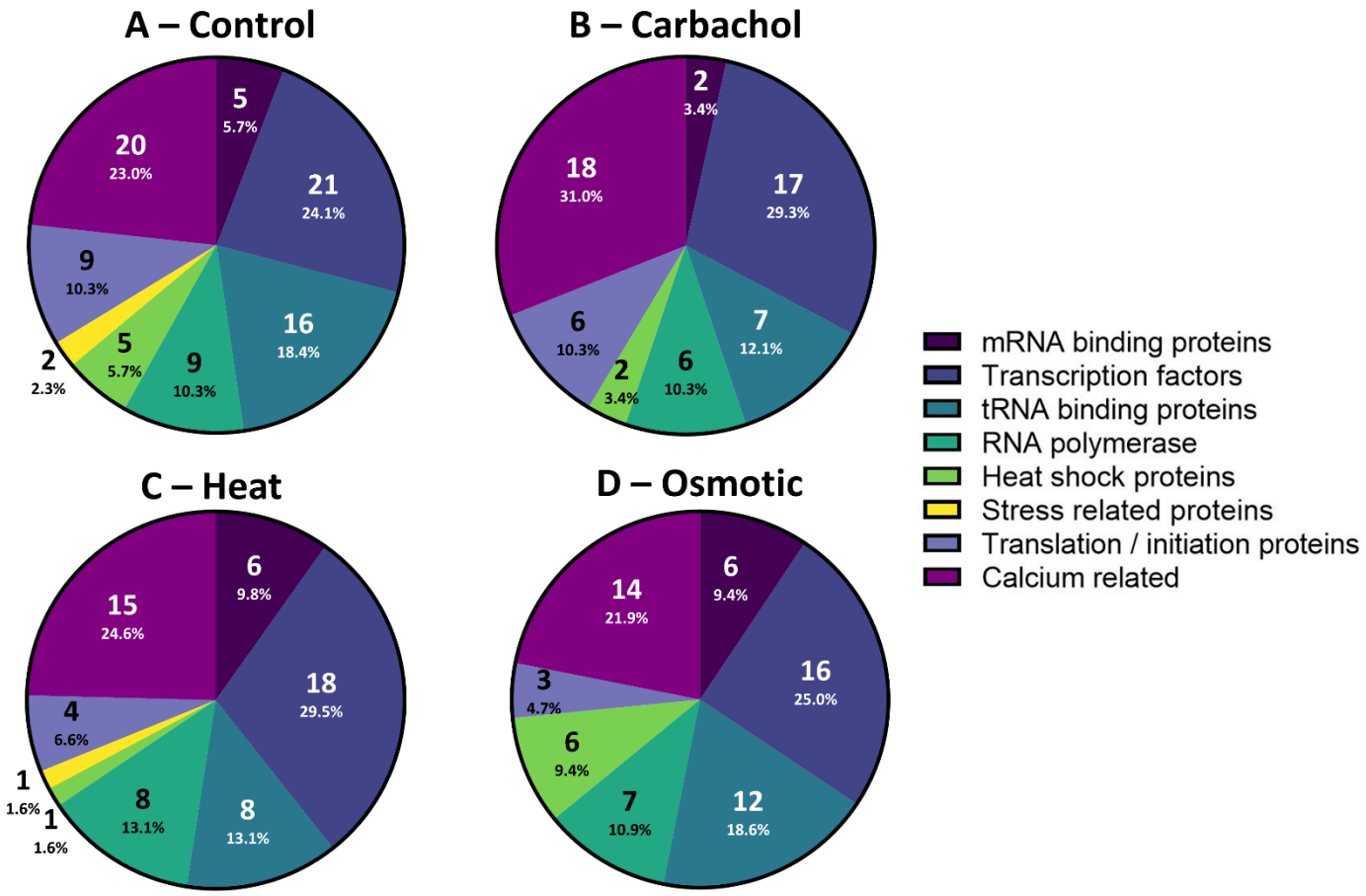

Figure 4.2 Distribution of Ago2 stress granule proteins under different stress. PC12 cells over expressing eGFP-Ago2 were exposed to **(A)** no stress, (**B**) carbachol activation of Gαq (10 min, 5μM), (**C**) heat shock (1hr, 42 °C), or (**D**) hypo-osmotic stress (150 mOsm, 5 min). Ago2 particles were pulled down for cytosolic fractions using a monoclonal GFP antibody. Purified stress granules were then subject to mass spectrometry analysis and results were filtered by the following

categories: mRNA binding proteins, transcription factors, tRNA binding proteins, RNA polymerases, heat shock proteins, stress related proteins, and translation/initiation proteins, and calcium-sensitive proteins where the values in the segment corresponds to the number of the total amount of Ago2-bound proteins.

4.3.3 Gαq activation is associated with Ago2 particles that contain specific transcripts

We sequenced the RNAs contained in Ago2 particles characterized above (See Appendix, Tables S4.5-S4.6). We could not detect RNA in Ago2 complexes pulled-down from control cells consistent with the absence of stable stress granules under basal conditions. In contrast, Ago2 particles from cells stimulated with Gαq or subjected to heat shock contained measurable amounts of RNAs, and these were isolated and sequenced. We found these two conditions yielded were very different results; in the Gαq-stimulated samples, only two transcripts of the ~50 most abundant RNAs were seen, *chromogranin A/B* (*CHGa/b*) and *ATP synthase 5f1b* (*ATP5f1b*). In contrast heat shock samples contained an assortment of different mRNAs and miRs. These results suggest that Ago2 particles formed in response to Gαq sequester specific transcripts, while those formed from heat are non-specific.

We extended the above studies by measuring changes in the total cellular levels by RT-PCR under different conditions. Levels of *CHGb* and *ATP5f1b* with carbachol stimulation were measured. Because carbachol stimulates Gαi as well as Gαq, we treated cells with pertussis toxin to inactivate Gαi signals and did not see changes in *CHGb* or *ATP5f1b* levels. We additionally carried out other controls including stimulation of Gαi rather than Gαq by isoproterenol, and measurements of *tau* mRNA since this transcript is not found in Ago2 complexes in cells subjected to Gαq stimulation or heat shock, although protein levels of tau are influenced by the PLCβ1/Gαq pathway by a mechanism independent of stress granules.[17]

In Figure 4.3, we compare cytosolic levels of *ATP5f1b, CHGb* and *tau* under control, Gαq stimulation, heat shock, osmotic stress and Gαi stimulation. Compared to controls, we find the heat shock and osmotic stress significantly reduce the levels of all four genes subjected to stress, while levels of *ATP5f1b* and *CHGb* are protected upon Gαq activation. These data are consistent with specific protection from degradation or translation of *ATP5f1b* and *CHGb* in Ago2 stress

granules formed upon Gαq activation. Activation of Gαi, increases *ATP5f1b* and *CHGb* and does not affect *tau*, consistent with its role in promoting growth pathways.[18]

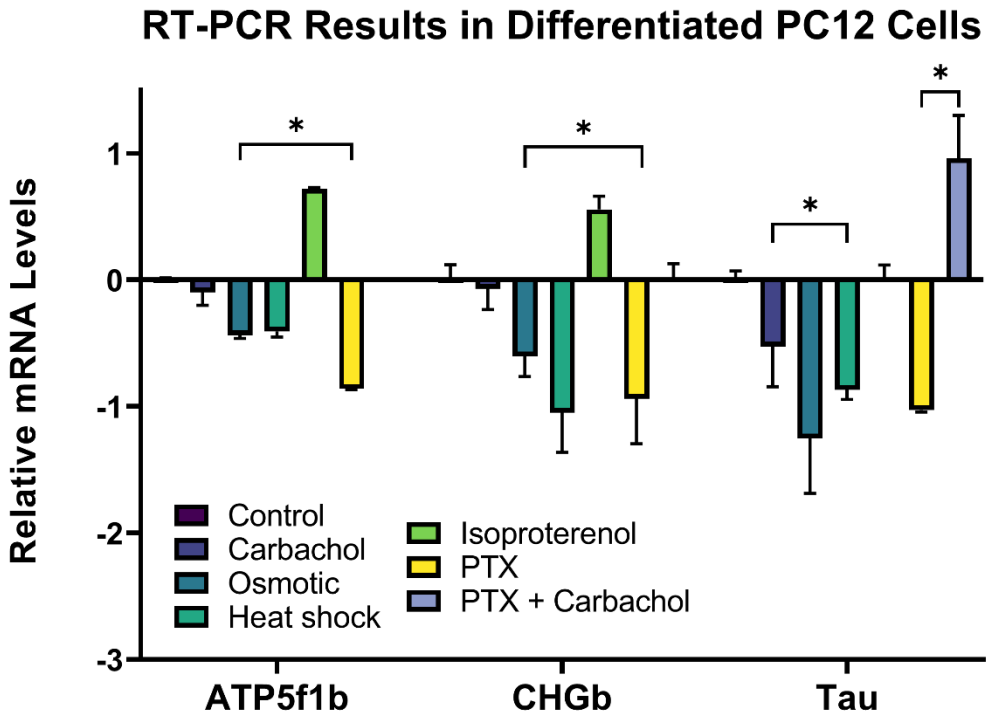

Figure 4.3 *ATP5f1b* and *CHGb* mRNA levels in cells under stress. RT-PCR results showing the relative levels of gene expression in PC12 cells of *ATP5f1b*, *CHGb* and *tau* (as a negative control) in differentiated PC12 cells exposed to different stress conditions (carbachol stimulation, hypo-osmotic stress, heat shock, isoproterenol as a Gαi stimulant and pertussis toxin (PTX) to eliminate effects of Gαi), where * denotes P≤0.001 and n=3-9 and SE is shown.

4.3.4 Impact of Gαq stimulation on ATP51b and Chga/b proteins levels

We measured changes in the protein levels of CHGb and ATP5f1b in cells subjected to different environmental stress (Figure 4.4). Because changes in protein levels are subject to many post-synthetic modifications and regulatory mechanisms besides translation, we added other conditions to better assess the role of Gαq stimulation. MG132 proteasome inhibitor was used as a pre-treatment before stress, as the rate of our target protein turnover is short (~1 hour)[19] resulting in a lack of accumulation of protein when long term stress is applied. In one series of studies, PLCβ1 was down-regulated to promote Ago2 particle formation without Gαq activation,[4] and but this did

not change protein levels. Additionally, no changes are seen in cells where Gαq was stimulated for 10 min or 30 min. However, heat shock, osmotic stress and stimulation of Gαi by isoproterenol all impact protein levels. The lack of change in CHGb and ATP5f1b with Gαq stimulation as opposed to other stress conditions suggests that that the Gαq/PLCβ pathway only influences longer-term changes in mRNA through Ago2 stress granules and not short-term protein levels.

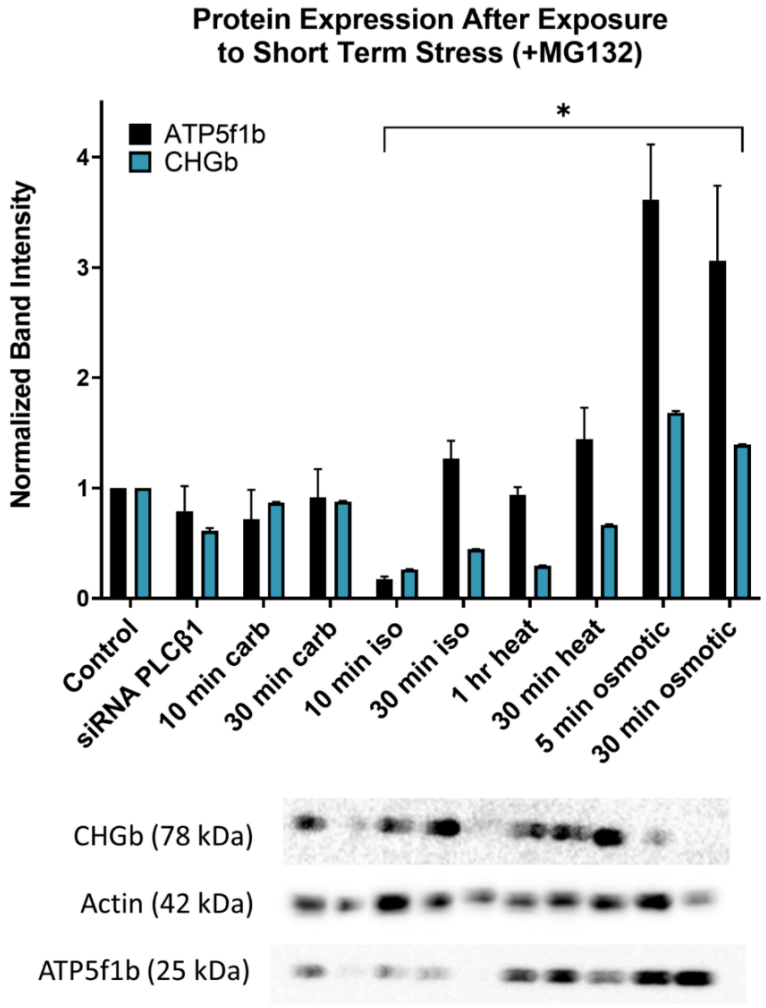

Figure 4.4 Protein levels of ATP5f1b and CHGb in cells under stress. PC12 cells, either untransfected or treated with siRNA(PLCβ1) for 48 hrs, were stimulated with carbachol or isoproterenol for Gαq or Gαi activation, respectively, or subjected to heat shock or hypo-osmotic stress, followed treatment with MG132 to prevent protein degradation before by lysis and western blotting where n=3, * denotes P values between 0.01 and <0.001 and SE is shown.

In a final series of studies, we assessed the protection of ATP5f1b with Gαq stimulation, by monitoring changes in the redox state of cells to assess mitochondria health and ATP production. These experiments measured changes in intrinsic fluorescence contributed mainly by NAD(P)H and FADH reflecting the optical redox state of mitochondria (see [20]). NADH, which is generated through the Krebs cycle, has a longer-lived fluorescence compared to other intrinsic fluorophores (see [21]). We measured the intrinsic fluorescence of cells under different stress conditions and found that while the lifetime of cells treated with carbachol to activate Gαq is the same as control, cells subjected to osmotic stress, isoproterenol or heat trend towards higher values (Figure 4.5). This higher lifetime is consistent with a transfer of ATP production to the Krebs cycle in response to reduced ATP synthase activity. These results support the idea that ATP5fb1 levels are protected with Gαq stimulation in contrast to other stresses.

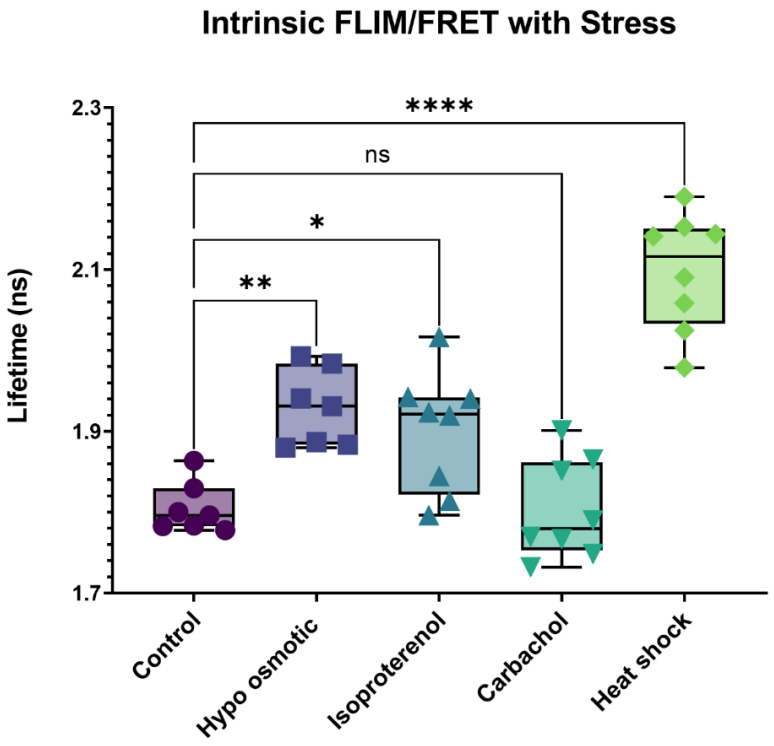

Figure 4.5 Intrinsic FLIM measurements to evaluate mitochondrial health. Untransfected, differentiated PC12 cells were exposed to carbachol, osmotic stress and heat shock before imaging at 740 nm excitation using a two photon laser, and measuring the autofluorescence lifetime by phase-modulation where n=8. P values were calculated using one-way ANOVA analysis comparing the specific sample with control. *=P≤0.05, **=P≤0.01, ***=P≤0.001, ****=P≤0.0001.

4.4 Discussion

Mammalian Gαq and its analogs in other species play a key role in generating cellular responses by increasing levels of intracellular calcium.[18] In this study, we have uncovered a novel pathway in which Gαq may control specific mRNA translation. Our studies show that in differentiated PC12 cells, Gαq activation sequesters two mRNAs important for endocrine function and cellular energy in Ago2 stress granules.

The basis of this pathway stems from the multifunctional nature of PLCβ1. PLCβ1 has several conserved structural domains surrounding the catalytic domain along with a long 400aa tail that is required for Gαq binding, and that can mediate binding to cytosolic partners (see [22]). One of these confirmed partners is the Promoter of RNA-induced silencing, C3PO,[23-24] which is inhibited by PLCβ1 binding.[3, 25-27] In recent work, we characterized the proteins bound to cytosolic PLCβ1 in undifferentiated PC12 cells and found roughly 30% of bound proteins are identified as stress granules proteins, including Ago2, PABPC1, eIF5a and G3BP1.[4, 28] These studies showed that reducing the cytosolic level of PLCβ1 either by down-regulation, osmotic stress or Gαq activation allowed for the release of bound proteins and promoted the formation of stress granules. While stress granules protect mRNA from degradation during stress conditions,[5] it is surprising these particles form under routine physiological responses generated by Gαq. This observation prompted us to determine whether the stress granules formed upon Gαq activation had a specific physiological impact on cells.

Our previous studies using undifferentiated PC12 cells and two muscle cell lines, A10 and WKO-3M22, showed that Gαq activation promotes the assembly of stress granules as indicated by established markers, G3BP1 and PABPC1, as well as Ago2[4] (see [15, 29-32]). Those studies identified Ago2 as either a direct or indirect binding partner of PLCβ1 by pull down studies and by FRET using tagged proteins, and showed Ago2 particles that grew in size and number under various stress conditions. Here, we show similar stress granule assembly as followed by the marker protein G3BP1 and that these particles that are stable for at least 30 minutes under our conditions.

Formation of stress granules depends not only on the environmental conditions, but also on the nature of the bound miRs and mRNA,[8, 12, 31, 33] and we reasoned that the binding of these species may be influenced by proteins that reside in stress granules. To this end, we characterized the proteins associated with Ago2 stress granules using a proteomics approach. Additionally, because previous studies suggested that different stresses form stress granules with distinct composition,[29] here we identified proteins in Ago2-associated stress granules in cells subjected to Gαq stimulation, osmotic stress and heat. We find that the shifts in composition were surprisingly minor especially considering their different cumulative responses. All stress conditions found that TEF-5 is a major binding partner of Ago2. TEF-5 is a transcriptional enhancer factor that works through the hippo pathway to inhibit proliferation,[34] and its association with Ago2 may serve to regulate TEF-5 translation to the nucleus. Comparing the top ten proteins in the Ago2 proteomics data sets, we find only one unique protein for Gαq stimulation, polyubiquitin-B, which impacts protein turn-over as well as various signaling cascades.[35] It is notable that stress granules formed with carbachol stimulation have a higher percentage of calcium-sensitive proteins.

Under control conditions, we find that Ago2 is associated with many proteins, but these complexes do not contain RNA meaning that they are not true stress granules. The observation that only two major transcripts (*ATP5f1b* and *CHGb*) are sequestered in Ago2 transcripts formed in response to Gαq stimulation was surprising. Our N&B studies found ~40% of G3BP1 aggregated with carbachol stress but we note that only 30% of the cells responded. By comparing the amount by total cellular *ATP5f1b* with the amount isolated in Ago2 particles per cell as determined by PCR where there was little loss in total Ago2, we find that at least 5% of this mRNA transcript is contained in stress granules. However, this value does not account for loss of RNA in the RNAseq measurements, and because our data show complete protection of this transcript, we suspect the value is much higher. It is important to note that we also find that cell recover very little after the stress is removed for 30 minutes implying a relatively long-term protection of these transcripts. Thus, if a larger cell population responds by increasing or repeating stimulation, then a much higher percent of the transcripts will be protected. By this argument, repeated stress would cause a significant population of transcripts to accumulate in Ago2 stress granules impacting cell function.

Maintaining cellular energy production during and after signaling is important, and the functional impact of preserving *ATP5f1b* during Gαq stimulation is seen though the preservation of the redox state (Figure 4.5). Similarly, Gαq is found in many cell types with endo- and exocrine function, and preservation of CHGa/b, which mediates vesicle formation, is expected. Of course, these studies focused on differentiated PC12 cells that have secretory function,[14] but it is very likely that other cell types will sequester other mRNAs upon Gαq stimulation.

The selection of these two specific transcripts by Ago2 stress granules is unclear and is under investigation. Because Gαq stimulation results in an increase in intracellular calcium, it is possible that distinct calcium sensitive proteins contained in the Ago2 stress granules that form, are directly or indirectly responsible for specifically recruiting these transcripts. A model connecting Gαq activation and the two transcripts sequestered in the Ago2 stress granules formed is shown in Figure 4.6.

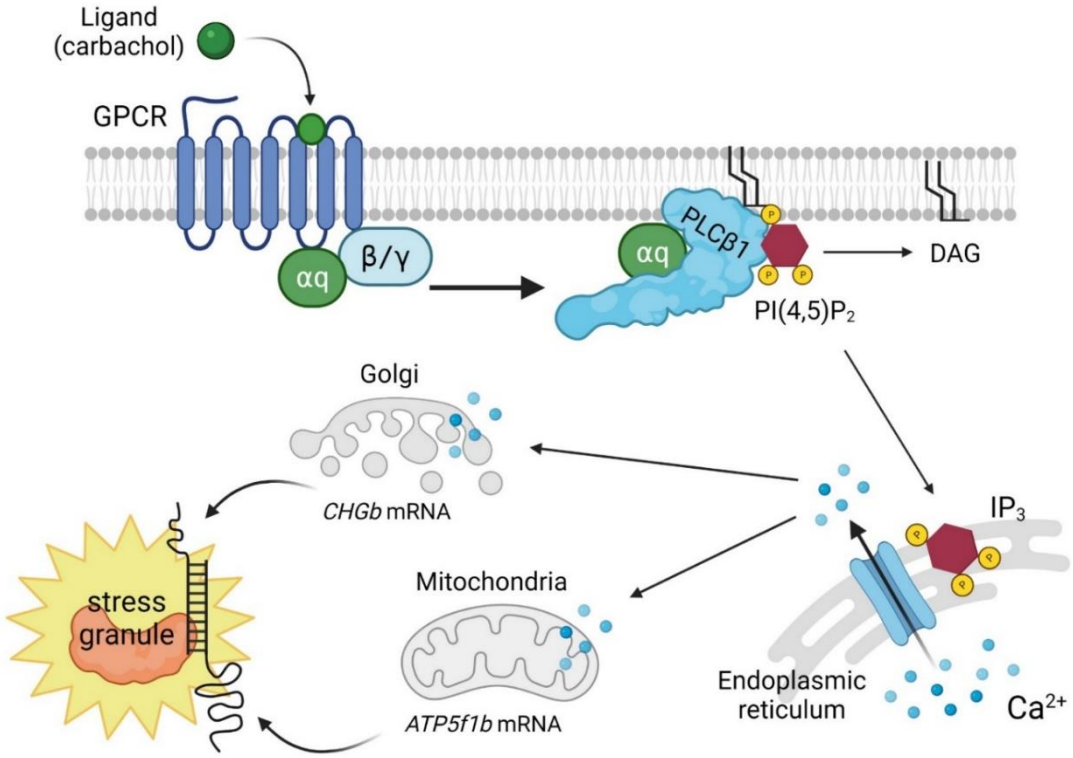

Figure 4.6 Model connecting the Gαq pathway with specific transcripts sequestered with activation. When PLCβ1 is activated by Gαq, Ca^{2+} is released. This excess calcium is believed to flood the mitochondria and Golgi, leading to the movement of *CHGa/b* and *ATP5f1b* mRNA into stress granules. (Created with BioRender.com)

PLCβ1 is associated with loss of proliferation and differentiation[36-37] and these effects are likely to be due to its interaction with C3PO and Ago2, as well as mediating calcium signals. We have previously identified miRs associated PLCβ1 down-regulation in PC12 cells[38] and found that down-regulating PLCβ1 levels results in substantial reduction in miR101a and miR101b, which may regulate ATP synthase 5B[39] and miR-22 levels by 20%, which regulates *CHGb.*[40] The loss of these miRs, along with the observation that loss of cytosolic PLCβ1 or sustained activation of Gαq returns PC12 cells to the undifferentiated state, may indicate that the increased number of stress granules may sequester mRNAs important for defining cell phenotype.

4.5 Materials & methods

4.5.1 Cell culture

PC12 cells were cultured in high glucose DMEM (Gibco) with 10% heat inactivated horse serum (Gibco), 5% fetal bovine serum (Atlanta Biologicals) and 1% Penicillin/Streptomycin (Gibco). Cells were treated with 0.1 ug/mL nerve growth factor (Bon Opus) for ~48 hours in media containing 1% heat inactivated horse serum and 1% antibiotic to induce differentiation. All cells were incubated at 37 °C in 5% CO2. Cells below passage 10 were used for all experiments.

4.5.2 Plasmids

EGFP-hArgonaute2 (eGFP-Ago2) was purchased from Addgene (plasmid # 21981) and was prepared in the laboratory of Philip Sharp (MIT). G3BP1-GFP was purchased from Addgene (plasmid # 119950) and was prepared in the laboratory of Jeffrey Chao (Friedrich Miescher Institute). siRNA(PLCβ1) was from Dharmacon (smartpool # L-092936-02-0005). Plasmid transfections and siRNA knockdowns were done using Lipofectamine 3000 (Invitrogen) in antibiotic free media. Medium was changed to one containing antibiotic (1% Penicillin/Streptomycin) 4-12 hours post-transfection.

4.5.3 Stress conditions

Cells were exposed to carbachol or isoproterenol stimulation at a final concentration of 5 μm for 10 minutes. For hypo-osmotic stress, the culture medium was diluted from 300 mOsm to 150 mOsm with 50% water for 5 minutes. For heat shock, cells were incubated at 42 °C for 1 hour.

Pertussis toxin (Invitrogen, cat # PHZ1174) was incubated in cell media at a concentration of 100 ng/mL for 24 hours before applying 10 minute carbachol stimulation.

4.5.4 Number and brightness (N&B) measurements

N&B defines the number of photons associated with a diffusing species by analyzing the variation of the fluorescence intensity in each pixel in the cell image, and full details about the method and analysis can be found in.[16] In these studies, we collected ~100 cell images viewing either free eGFP (control) or eGFP-G3BP1 at a 66 nm/pixel resolution and at a rate of 4 μs/pixel (see[4]). Images obtained were 256x256 pixels. The size of the SimFCS4 boxes used was determined by the amount of monomeric protein seen in unstressed controls. Any pixels on the B vs I plot that were outside of this region were determined to be protein aggregation due to the stress applied. Percent aggregation was calculated based off of total number of pixels outside of the control (red box) region, divided by the total number of pixels in the cell. The percent aggregation corresponding to either oligomerization (pixels contained in the green box) or aggregated monomeric protein (pixels contained in the blue box) are also reported using text in the respective color. N&B samples were imaged on dual-channel confocal (Alba version 5, ISS Inc.) using a two-photon titanium-sapphire laser and a Nikon Eclipse Ti-U inverted microscope as described.[38] All measurements were taken at 850 nm wavelength using RICS/N&B mode on VistaVision software. Samples were imaged at room temperature. Number and Brightness (N&B) data were analyzed with SimFC4 software (www.lfd.uci.edu) where the brightness, B, in each pixel refers to the ratio of the variance, σ, over the average fluorescence intensity <k>:

$$B = \sigma 2 / < k >$$

and

$$< k > = \epsilon n$$

where n is the number of fluorophores. The variance in each pixel is obtained by rescanning the cell image ~100 times. The average fluorescence intensity, <k>, is directly related to the molecular brightness, ε, in units of photons per second per molecule. Data taken at various sampling times (50 frames/30 seconds, vs 200 frames/90 seconds) were compared, and yielded identical results.

4.5.5 Particle analysis

Samples were imaged with a 100X/1.49 oil TIRF objective to microscopically count the number of particles per μm2 formed under different conditions. For each condition, 10 to 20 cells were randomly selected, and z-stack measurements were taken (1.0 μm/frame). Analysis was performed with ImageJ and Fiji ImageJ software either by thresholding before analyzing, and averaging the number of particles per frame per measurement or by combining z-stack measurements to generate a 3D image for each sample before analyzing the number of particles per sample and averaging the results. Both methods produced identical results.

4.5.6 Mass spectrometry

Ago2 stress granules were purified from PC12 cells electroporated with eGFP-Ago2 then differentiated with NGF for ~48 hours using the protocol described by Wheeler *et al.*[41] Six 150 mm dishes of cells were used per condition. Immunoprecipitation was done using GFP antibody (Santa Cruz Biotechnology, sc-9996) with protein A dynabeads and elution buffer (Invitrogen,cat #10006D). Following short gel electrophoresis and band excision, mass spectrometry was performed at UMass Medical School Mass Spectrometry Facility. Bound proteins were reported using Scaffold software. Each protein in this report had a minimum of one total spectrum count measured for at least one condition.

4.5.7 eCLIP transcript sequences

PC12 cells were transfected with eGFP-Ago2 using electroporation (Bio-Rad Gene Pulser Xcell) with one pulse in a 0.4 cm gap cuvette (Bio-Rad, cat #1652088) in complete media and plated at ~50% confluency to leave room for neurite growth. Cells were stressed and crosslinked using 254 nm ultraviolet light. Treated cells were collected from at least four 150 mm culture dishes per sample condition. Lysis was done on fresh, non-frozen cell pellets using 100 μL lysis buffer supplemented with RNase inhibitor and protease inhibitor tablets (Roche). A 10 μL portion of each lysate was used to extract total RNA (Zymo Clean and Concentrator) which was then tested for RNA integrity using RNA Fragment Analyzer services at University of Massachusetts Medical School Molecular Biology Core Lab. The remaining lysate was immunoprecipitated using mouse Ago2 antibody. Subsequent western blots, RNA cleanup and library construction was done using Eclipse Bioinnovation protocol v1.01R, storing samples at -80 °C overnight when necessary.

Sample quantity was evaluated by qPCR. Libraries were sequenced at UMass Medical School Deep Sequencing Core using Illumina HiSeq 4000 system. All reagents were supplied by Eclipse Bioinnovations unless otherwise specified.

4.5.8 RT-PCR

For each condition, one 100 mm dish was used for total RNA extraction. Cells were differentiated and stressed before isolating RNA using RNeasy Mini Kit (Qiagen, Cat #74104) with DNase digestion (Qiagen, cat #79254). CDNA synthesis was done using MiniAmp Thermal Cycler (Applied Biosystems). Purified RNA sample concentrations were measured by Nanodrop and 1 µg RNA was incubated with dNTP (New England Biolabs, cat #N0447S), random hexamers (Thermo Scientific, cat #SO142), and nuclease free water (Invitrogen, cat #AM9930), at 65 °C for 5 minutes. After the first incubation, 5x First Strand Buffer, DTT (Invitrogen cat #18080093) and RNase inhibitor (Invitrogen, cat #AM2694) were added to the mixture and incubated at 25 °C for 2 minutes. After the second incubation, 1 µL Superscript III Reverse Transcriptase (Invitrogen, cat #18080093) was added and the mixture was incubated at 25 °C for 10 minutes, 42 °C for 50 minutes, and 70 °C for 15 minutes. CDNA was stored at -20 °C overnight or used immediately at a dilution of 1:20 in nuclease free water for RT-PCR experiments with Luna Universal Master Mix (New England Biolabs, cat #M3003L), nuclease free water, and custom ATP5f1b and CHGb primers (ITD). For positive and negative controls, 18S ribosomal subunit and tau primers were used.

ATP5f1b	F:	5′-GTCCAGTTCGATGAGGGATTAC-3
	R:	5′-CCAGTACTTTCTGGCCTCTAAC-3′
CHGb	F:	5′-TGCTTGCTTGAGGGTAGATAAG-3′
	R:	5′-TGGGAACTAGATGGGTAGAGAG-3′
Tau	F:	5′-CAGGACAGGAAATGACGAGAAG-3′
	R:	5′-CAGGGACATGGGTGATGTTATC-3′
18S	F:	5′-ACGTCTGCCCTATCAACTTTC-3′
	R:	5′-CCGCGGTCCTATTCCATTATT-3′

4.5.9 Western blotting

We used an establish procedure[38] with modifications. Samples were grown in 100 mm dishes plates and were treated with MG132 at a final concentration of 250 nM 24 hours before collection. Cells were stressed and then collected in 250 μl of NP-40 lysis buffer [150 mM NaCl, 50 mM Tris (pH=8.0), 1% NP40, protease inhibitor]. The primary antibodies used included: anti-ATP5f1b (Abcam, ab117991), anti-Chgb (Abcam, ab150354), anti-actin (Santa Cruz, sc-47778).

4.5.10 Fluorescence lifetime imaging measurements (FLIM)

Phase modulation FLIM measurements were performed on the dual-channel confocal fast FLIM (Alba version 5, ISS Inc.) using a two-photon titanium-sapphire laser and a Nikon Eclipse Ti-U inverted microscope as described.[38] The lifetime of the laser was calibrated each time before experiments by measuring the lifetime of Atto 425 in water with a lifetime of 3.61 ns at 80, 160, and 240 MHz. The samples were excited at 740 nm for intrinsic measurements, and emission spectra were collected through a 525/50 bandpass filter. For each measurement, the data were acquired until the photon count was >100 for measurements of intrinsic fluorescence.

4.5.11 Statistical analysis

Data were analyzed with the Sigma Plot 14.5 and Graphpad Prism 9 statistical packages, which included the student's *t* test and one-way analysis of variance (ANOVA).

4.6 References

1. Exton, J. H., Cell signalling through guanine-nucleotide-binding regulatory proteins (G proteins) and phospholipases. [Review] [110 refs]. *European Journal of Biochemistry* **1997,** *243* (1-2), 10-20.
2. Suh, P.; Park, J.; Manzoli, L.; Cocco, L.; Peak, J.; Katan, M.; Fukami, K.; Kataoka, T.; Yun, S.; Ryu, S., Multiple roles of phosphoinositide-specific phospholipase C isozymes. *BMB reports* **2008,** *41*, 415-34.
3. Philip, F.; Guo, Y.; Aisiku, O.; Scarlata, S., Phospholipase Cβ1 is linked to RNA interference of specific genes through translin-associated factor X. *The FASEB Journal* **2012,** *26* (12), 4903-4913.
4. Qifti, A.; Jackson, L.; Singla, A.; Garwain, O.; Scarlata, S., Stimulation of phospholipase Cbeta1 by Galphaq promotes the assembly of stress granule proteins. *Sci Signal* **2021,** *14* (705), eaav1012.
5. Anderson, P.; Kedersha, N., RNA granules. *J Cell Biol* **2006,** *172* (6), 803-8.
6. Mahboubi, H.; Stochaj, U., Cytoplasmic stress granules: Dynamic modulators of cell signaling and disease. *Biochim Biophys Acta* **2017,** *1863* (4), 884-895.
7. Panas, M. D.; Ivanov, P.; Anderson, P., Mechanistic insights into mammalian stress granule dynamics. *J Cell Biol* **2016,** *215* (3), 313-323.
8. Hutvagner, G.; Simard, M. J., Argonaute proteins: key players in RNA silencing. *Nature Reviews Molecular Cell Biology* **2008,** *9*, 22.
9. Meister, G.; Landthaler, M.; Patkaniowska, A.; Dorsett, Y.; Teng, G.; Tuschl, T., Human Argonaute2 mediates RNA cleavage targeted by miRNAs and siRNAs. *Mol Cell* **2004,** *15* (2), 185-97.
10. Sen, G. L.; Blau, H. M., Argonaute 2/RISC resides in sites of mammalian mRNA decay known as cytoplasmic bodies. *Nat Cell Biol* **2005,** *7* (6), 633-6.
11. Sheu-Gruttadauria, J.; MacRae, I. J., Structural Foundations of RNA Silencing by Argonaute. *Journal of Molecular Biology* **2017,** *429* (17), 2619-2639.
12. Atwood, B. L.; Woolnough, J. L.; Lefevre, G. M.; Saint Just Ribeiro, M.; Felsenfeld, G.; Giles, K. E., Human Argonaute 2 Is Tethered to Ribosomal RNA through MicroRNA Interactions. *J. Biol. Chem.* **2016,** *291* (34), 17919-17928.
13. Dowal, L.; Provitera, P.; Scarlata, S., Stable association between G alpha(q) and phospholipase C beta 1 in living cells. *J Biol Chem* **2006,** *281* (33), 23999-4014.
14. Greene, L. A.; Tischler, A. S., Establishment of a noradrenergic clonal line of rat adrenal pheochromocytoma cells which respond to nerve growth factor. *Proc Natl Acad Sci U S A* **1976,** *73* (7), 2424-2428.
15. Yang, P.; Mathieu, C.; Kolaitis, R. M.; Zhang, P.; Messing, J.; Yurtsever, U.; Yang, Z.; Wu, J.; Li, Y.; Pan, Q.; Yu, J.; Martin, E. W.; Mittag, T.; Kim, H. J.; Taylor, J. P., G3BP1 Is a Tunable Switch that Triggers Phase Separation to Assemble Stress Granules. *Cell* **2020,** *181* (2), 325-345.e28.
16. Digman, M. A.; Dalal, R.; Horwitz, A. F.; Gratton, E., Mapping the Number of Molecules and Brightness in the Laser Scanning Microscope. *Biophys J* **2008,** *97*, 2320-2332.
17. Garwain, O.; Yerramilli, V. S.; Romero, K.; Scarlata, S., The Gαq/phospholipase Cβ signaling system represses tau aggregation. *Cell Signal* **2020,** *71*, 109620.
18. Hepler, J. R.; Gilman, A. G., G-proteins. *Trends Biochem. Sciences* **1992,** *17*, 383-387.

19. Malosio, M. L.; Giordano, T.; Laslop, A.; Meldolesi, J., Dense-core granules: a specific hallmark of the neuronal/neurosecretory cell phenotype. *J Cell Sci* **2004,** *117* (Pt 5), 743-9.
20. Chance, B.; Schoener, B.; Oshino, R.; Itshak, F.; Nakase, Y., Oxidation-reduction ratio studies of mitochondria in freeze-trapped samples. NADH and flavoprotein fluorescence signals. *J Biol Chem* **1979,** *254* (11), 4764-71.
21. Stringari, C.; Cinquin, A.; Cinquin, O.; Digman, M. A.; Donovan, P. J.; Gratton, E., Phasor approach to fluorescence lifetime microscopy distinguishes different metabolic states of germ cells in a live tissue. *Proc Natl Acad Sci U S A* **2011,** *108* (33), 13582-13587.
22. Jackson, L.; Qifti, A.; Pearce, K. M.; Scarlata, S., Regulation of bifunctional proteins in cells: Lessons from the phospholipase Cβ/G protein pathway. *Protein Science* **2020,** *29* (6), 1258-1268.
23. Liu, Y.; Ye, X.; Jiang, F.; Liang, C.; Chen, D.; Peng, J.; Kinch, L. N.; Grishin, N. V.; Liu, Q., C3PO, an Endoribonuclease That Promotes RNAi by Facilitating RISC Activation. *Science* **2009,** *325* (5941), 750-753.
24. Ye, X.; Huang, N.; Liu, Y.; Paroo, Z.; Huerta, C.; Li, P.; Chen, S.; Liu, Q.; Zhang, H., Structure of C3PO and mechanism of human RISC activation. *Nat Struct Mol Biol* **2011,** *18* (6), 650-657.
25. Aisiku, O. R.; Runnels, L. W.; Scarlata, S., Identification of a Novel Binding Partner of Phospholipase Cβ1: Translin-Associated Factor X. *PLoS One* **2010,** *5* (11), e15001.
26. Sahu, S.; Philip, F.; Scarlata, S., Hydrolysis Rates of Different Small Interfering RNAs (siRNAs) by the RNA Silencing Promoter Complex, C3PO, Determines Their Regulation by Phospholipase Cβ. *J. Biol. Chem.* **2014,** *289* (8), 5134-5144.
27. Sahu, S.; Williams, L.; Perez, A.; Philip, F.; Caso, G.; Zurawsky, W.; Scarlata, S., Regulation of the activity of the promoter of RNA-induced silencing, C3PO. *Protein Science* **2017,** *26* (9), 1807-1818.
28. Frame, M. D.; Dewar, A. M.; Calizo, R. C.; Qifti, A.; Scarlata, S. F., Nitrosative stress uncovers potent beta2-adrenergic receptor-linked vasodilation further enhanced by blockade of clathrin endosome formation. *Am J Physiol Heart Circ Physiol* **2018,** *314* (6), H1298-H1308.
29. Aulas, A.; Fay, M. M.; Lyons, S. M.; Achorn, C. A.; Kedersha, N.; Anderson, P.; Ivanov, P., Stress-specific differences in assembly and composition of stress granules and related foci. *J Cell Sci* **2017,** *130* (5), 927-937.
30. Chen, L.; Liu, B., Relationships between Stress Granules, Oxidative Stress, and Neurodegenerative Diseases. *Oxidative Medicine and Cellular Longevity* **2017,** *2017*, 10.
31. Detzer, A.; Engel, C.; Wunsche, W.; Sczakiel, G., Cell stress is related to re-localization of Argonaute 2 and to decreased RNA interference in human cells. *Nucleic Acids Res* **2011,** *39* (7), 2727-41.
32. Guillén-Boixet, J.; Kopach, A.; Holehouse, A. S.; Wittmann, S.; Jahnel, M.; Schlüßler, R.; Kim, K.; Trussina, I. R. E. A.; Wang, J.; Mateju, D.; Poser, I.; Maharana, S.; Ruer-Gruß, M.; Richter, D.; Zhang, X.; Chang, Y.-T.; Guck, J.; Honigmann, A.; Mahamid, J.; Hyman, A. A.; Pappu, R. V.; Alberti, S.; Franzmann, T. M., RNA-Induced Conformational Switching and Clustering of G3BP Drive Stress Granule Assembly by Condensation. *Cell* **2020,** *181* (2), 346-361.e17.
33. Broderick, J. A.; Salomon, W. E.; Ryder, S. P.; Aronin, N.; Zamore, P. D., Argonaute protein identity and pairing geometry determine cooperativity in mammalian RNA silencing. *RNA (New York, N.Y.)* **2011,** *17* (10), 1858-1869.

34. Mahoney, W. M., Jr.; Hong, J.-H.; Yaffe, M. B.; Farrance, I. K. G., The transcriptional co-activator TAZ interacts differentially with transcriptional enhancer factor-1 (TEF-1) family members. *The Biochemical journal* **2005,** *388* (Pt 1), 217-225.
35. Komander, D., The emerging complexity of protein ubiquitination. *Biochemical Society Transactions* **2009,** *37* (5), 937-953.
36. Garwain, O.; Scarlata, S., Phospholipase Cβ-TRAX Association Is Required for PC12 Cell Differentiation. *J. Biol. Chem.* **2016,** *291* (44), 22970-22976.
37. Garwain, O.; Valla, K.; Scarlata, S., Phospholipase Cβ1 regulates proliferation of neuronal cells. *The FASEB Journal* **2018,** *32* (5), 2891-2898.
38. Garwain, O.; Pearce, K. M.; Jackson, L.; Carley, S.; Rosati, B.; Scarlata, S., Stimulation of the Gαq/phospholipase Cβ1 signaling pathway returns differentiated cells to a stem-like state. *The FASEB Journal* **2020,** *34* (9), 12663-12676.
39. Zheng, S. Q.; Li, Y. X.; Zhang, Y.; Li, X.; Tang, H., MiR-101 regulates HSV-1 replication by targeting ATP5B. *Antiviral Res* **2011,** *89* (3), 219-26.
40. Friese, R. S.; Altshuler, A. E.; Zhang, K.; Miramontes-Gonzalez, J. P.; Hightower, C. M.; Jirout, M. L.; Salem, R. M.; Gayen, J. R.; Mahapatra, N. R.; Biswas, N.; Cale, M.; Vaingankar, S. M.; Kim, H.-S.; Courel, M.; Taupenot, L.; Ziegler, M. G.; Schork, N. J.; Pravenec, M.; Mahata, S. K.; Schmid-Schönbein, G. W.; O'Connor, D. T., MicroRNA-22 and promoter motif polymorphisms at the Chga locus in genetic hypertension: functional and therapeutic implications for gene expression and the pathogenesis of hypertension. *Human molecular genetics* **2013,** *22* (18), 3624-3640.
41. Wheeler, J. R.; Matheny, T.; Jain, S.; Abrisch, R.; Parker, R., Distinct stages in stress granule assembly and disassembly. *eLife* **2016,** *5*, e18413.

5 Chapter 5 – Live cell fluorescence imaging shows neurotransmitter activation promotes aggregation of the intracellular domain of amyloid precursor protein

Lela Jackson[†1], V. Siddartha Yerramilli[†1] and Suzanne Scarlata[1]

† - These authors contributed equally to this work

1 - Department of Chemistry & Biochemistry, Worcester Polytechnic Institute, Worcester, MA

The following subsections appear in Jackson & Yerramilli *et al.* "Live Cell Fluorescence Imaging Shows Neurotransmitter Activation Promotes Aggregation of the Intracellular Domain of Amyloid Precursor Protein" *Under review*. Sections with an asterisk (*) indicate additional sections not included in the original publication. L.J,, S.Y. and S.S. designed experiments and interpreted the data. L.J., S.Y and S.S. developed the signaling model and manuscript. L.J. conducted and analyzed the following experiments: stress granule RNA purification, RT-PCR and number and brightness. S.Y. conducted and analyzed the FCS experiments.

5.1 Abstract

Amyloid precursor protein (APP) is a major contributor to the pathology of Alzheimer's and other neurodegenerative diseases through the accumulation of extracellular plaques. Here, we have studied the response of the APP translation and aggregation of its intracellular domain when the Gαq/PLCβ signaling system is activated by neurotransmitters. Previously, our group discovered that PLCβ1 mediates stress granule aggregation through its association with cytosolic stress granule protein binding partners including Argonaute 2 (Ago2). Here, we report that APP mRNA was identified as being bound to Ago2 as a result of Gαq stimulation. Using RT-PCR and a molecular beacon that follows APP mRNA in live cells, we find that Gαq activation sequesters APP mRNA similar to the stress granule response found in heat shock and hypo-osmotic stress thereby shutting down the production of APP. Following the intracellular domain of eGFP-APP, we find that Gαq stimulation increases aggregation as followed by number and brightness analysis of single molecular fluorescence time series. Our studies additionally show that APP aggregation is promoted by mechanistic levels of proteins associated with stress responses and RNA silencing complexes.

5.2 Introduction

Amyloid precursor protein (APP) is a family of alternately spliced variants generated from the full-length protein APP (APP770). Altered processing of APP can give rise proteins prone to aggregation that contribute to the neurodegenerative effects seen in Alzheimer's and related diseases.[1] The most common variant in the brain, APP695, is a membrane-bound glycosylated protein that can be processed to yield a soluble extracellular protein by secretases, and/or truncated at the C-terminus to yield intracellular variants.[2-3] While the function of APP is unknown, it is thought that the membrane-bound N-terminal proteins mediate cell contacts and neurite growth.[1] Part of APP contains a β-amyloid region that is highly prone to aggregation, and these aggregates are thought to impair intracellular processes such as acetylcholine / calcium signaling through the Gαq pathway.[4] This pathway is activated when acetylcholine binds to muscarinic receptors on the cell surface. The ligand-bound receptors activates Gαq, which in turn activates phospholipase Cβ leading to activation of protein kinase C and an increase in intracellular calcium.[5-6]

Our lab has found that PLCβ, the effector of Gαq, has a cytosolic population in addition to a membrane population.[7-8] This cytosolic population has unique binding partners whose interactions change during Gαq activation. For example, it has been found that PLCβ binds to C3PO, the Promoter of the RNA-induced silencing complex (RISC), and this binding inhibits C3PO activity and reverses RICS activity towards specific genes.[8-11] Activation of Gαq relocalizes cytosolic PLCβ to the membrane releasing C3PO and promoting RISC activity. Additionally, cytosolic PLCβ also binds to stress granule proteins keeping them disperse until activation of Gαq promotes relocalization of the cytosolic PLCβ population to the plasma membrane.[8] Stress granules are halted ribosomal complexes that form when cells are subjected to stress, or as we have found, to Gαq activation (for review see [12]). Surprisingly, stress granules formed upon Gαq activation contain specific transcripts, unlike heat stress which sequesters many different RNAs. In differentiated PC12 cells, the transcripts sequestered by Gαq are *Atp5f1b* and *CHGa/b,*[13] along with small amounts of *plectin* and *APP* suggesting strong or prolonged activation of Gαq might impact cellular APP levels.

In this study, we establish a link between Gαq activation and *APP* mRNA and intracellular APP aggregation. We find that aside from increased calcium levels, cytosolic PLCβ and its binding partners play a role in regulating APP properties. Using differentiated PC12 cells, we find that both short- and long-term stimulation of Gαq alters *APP* transcript levels and increases the amount of the C-terminal fragment in the cytosol resulting in aggregation. These studies showing a molecular connection between Gαq activation and neurotoxicity.

5.3 Results

5.3.1 Long term Gαq stimulation protects APP transcripts

To determine whether stress granules protect APP mRNA, we have previously purified stress granules associated with Ago2 by subjecting cells to various conditions and pulling down Ago2 using a monoclonal antibody (see [13]). Under basal conditions, no RNA is found in Ago2 complexes, but subjecting cells to Gαq stimulation by carbachol and heat shock caused RNA to become sequestered in stress granules. In the top 100 RNAs listed, Gαq stimulation showed two major transcripts, *ATP5f1b* and *CHGa/b*. Two minor transcripts were included as part of the >100 listed, *plectin* and *APP* (see Supplemental information in [13]). While this result may suggest a translational link between Gαq and APP levels, it is very minor.

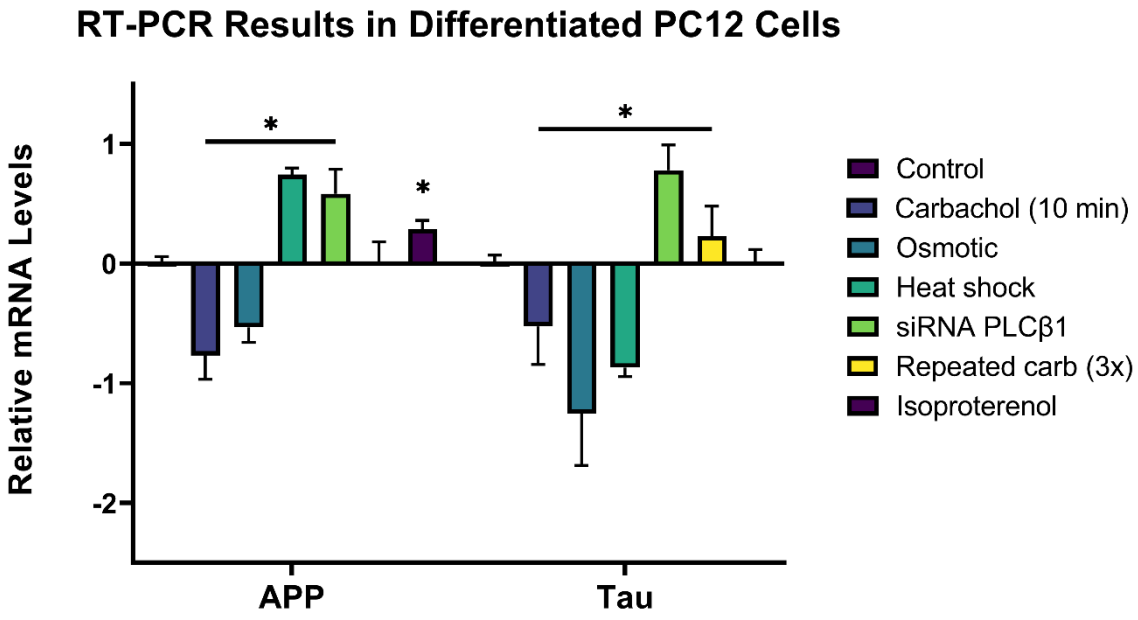

Figure 5.1 Changes in *APP* mRNA levels in cells under stress. RT-PCR results showing the relative levels of gene expression of *APP* and *tau* (as a negative control) in differentiated PC12 cells exposed to different stress conditions (10 minute carbachol stimulation, hypo-osmotic stress, heat shock, siRNA PLCβ1, 3x repeated carbachol stimulation and isoproterenol as a Gαi stimulant) where * denotes P<0.001, n=3-9 and SE is shown.

We determined changes in APP levels under varying conditions by RT-PCR in differentiated PC12 cells in comparison to tau, which is not connected to Gαq signaling, as a control. We find that APP levels change with Gαq stimulation, osmotic stress, heat stress and Gαi stimulation. However, when cells were stimulated with carbachol, washed and reactivated 3x, no changes in transcript levels were seen (Figure 5.1). This behavior is consistent with accumulation Gαq-associated stress granules that sequester APP. In contrast, tau, shows changes under all conditions except Gαi stimulation.

5.3.2 Repeated Gαq stimulation causes Ago2 stress granules to increase in size *

Testing particle formation of three stress granule proteins before stress and after repeated carbachol stimulation shows a decrease maximum particle size by 22% for PABPC1 stress granules, compared to a 0% change in particle size when tracking G3BP1, and a 17% increase in size of Ago2 particles (Figure 5.2A-C). Note that G3BP1 particles were tagged by overexpression of G3BP1-eGFP, while PABPC1 and Ago2 represent endogenous levels of protein in fixed immunostained differentiated PC12 cells.

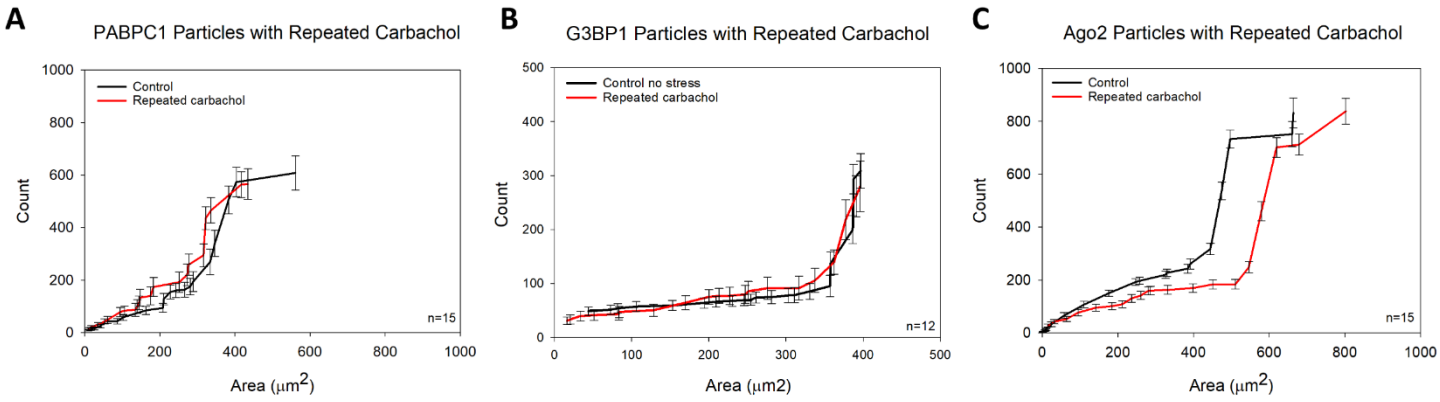

Figure 5.2 Size and number of stress granule proteins in differentiated PC12 cells with repeated carbachol stimulation. (**A**) PABPC1 (n=15, P≤0.05), (**B**) G3BP1 (n=12, P=0.358) and (**C**) Ago2 particle analysis (n=15, P≤0.05) SE is shown.

5.3.3 APP mRNA as visualized in real time is affected by stress conditions

We designed a beacon that is complementary to APP mRNA. The rationale for the design of the beacons has been described earlier.[14-15] Based on the selected loop region, the stem nucleotides were chosen to be 5'-CAUCUGUACAGUAAGAUG-3 using the pairing energies calculated with RNAfold software. The free energy of the thermodynamic ensemble is -4.25 kcal/mol and the melting temperature is 65.1 °C (Figure 5.3A). We obtained beacons that attached the quencher, Iowa Black Hole Quencher, and a fluorophore, FAM, at the 5' and 3' ends of the beacons to visualize and quantify changes in mRNA through fluorescence.

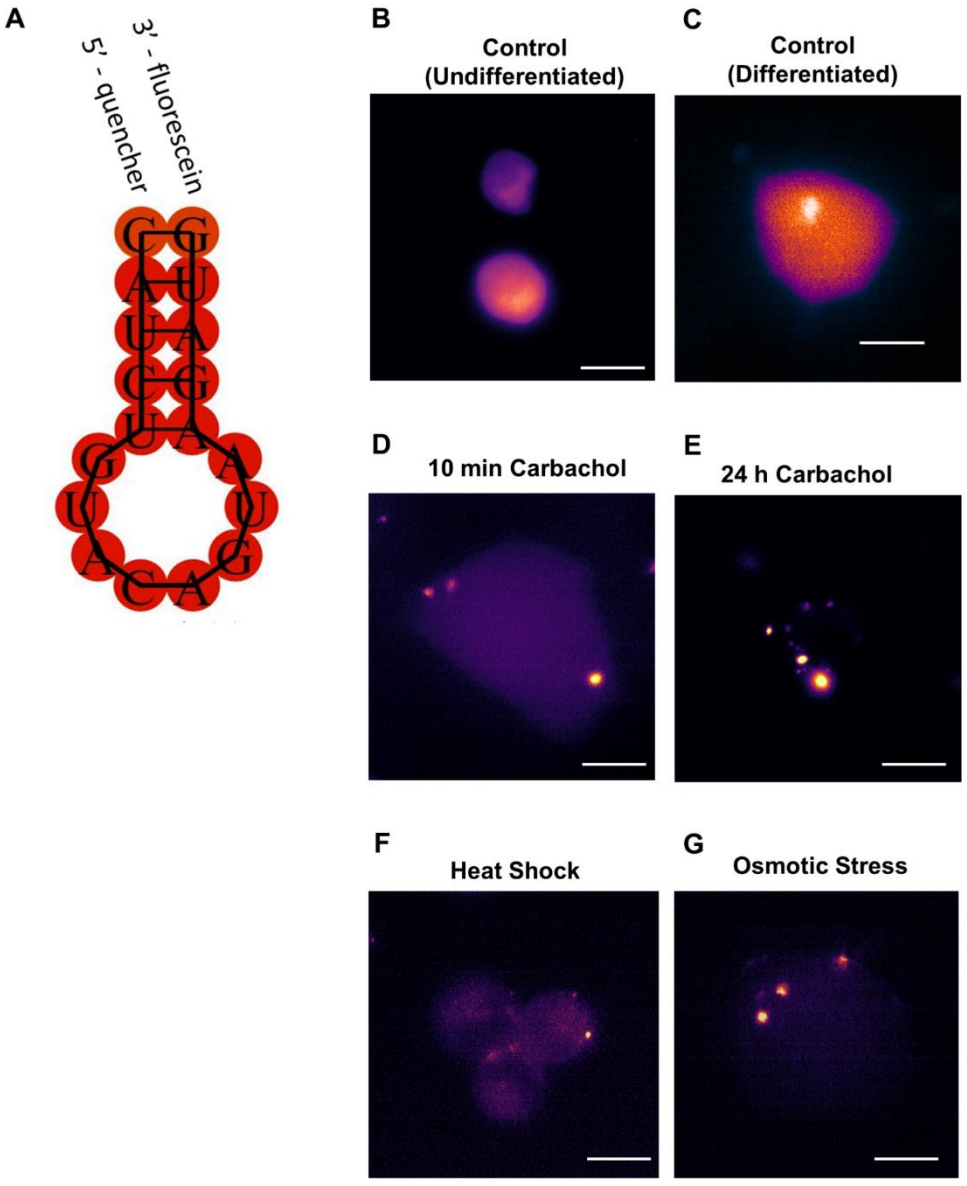

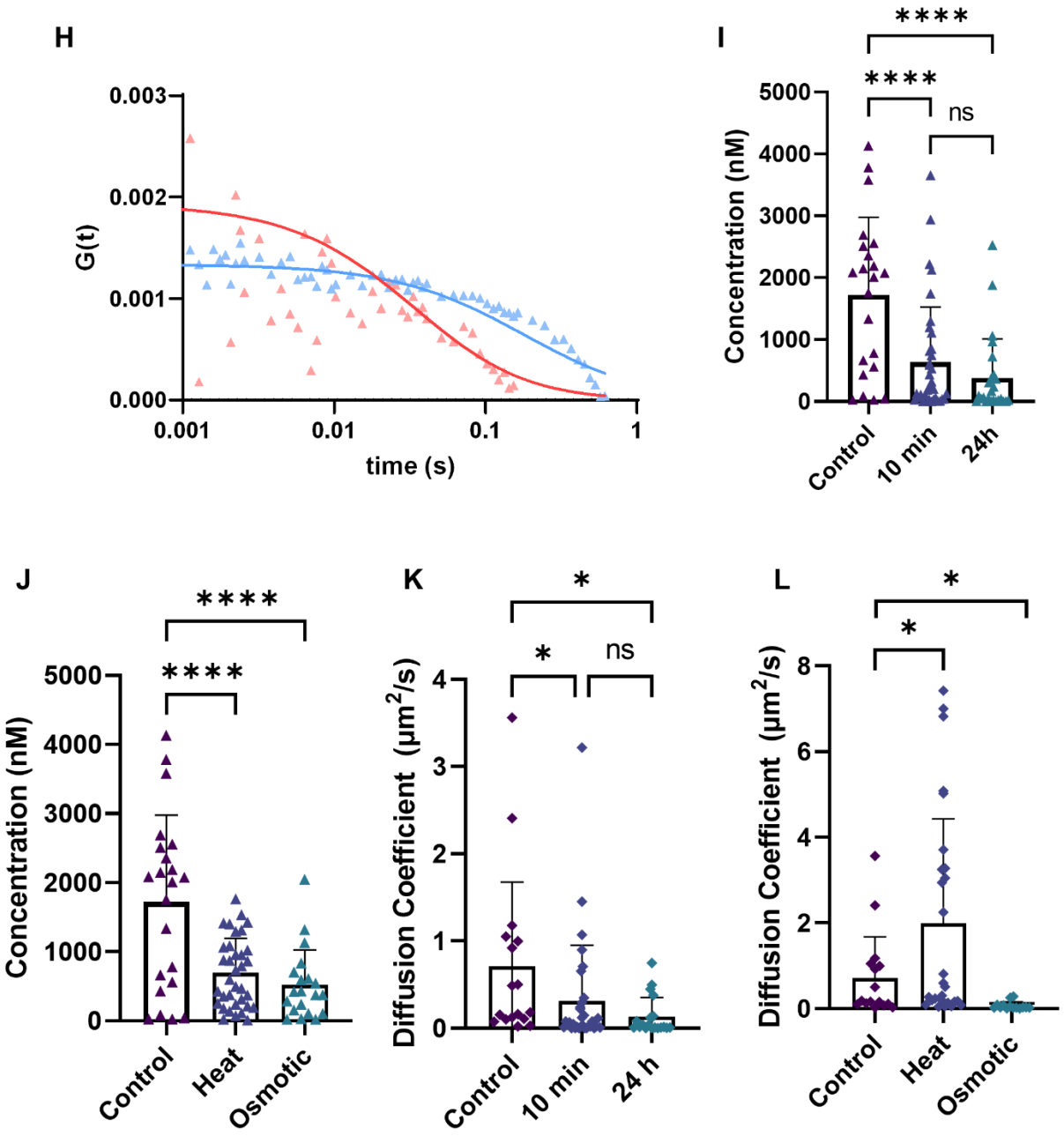

Figure 5.3 APP mRNA beacon aggregation is seen in cells under stress. (**A**) Illustration of the APP beacon with attached FAM-IBFQ fluorophores depicting its folded state. (**B-G**) Representative images of PC12 cells transfected with APP beacon showing APP mRNA localization as observed through dequenching of FAM fluorescence. The images include (**B**) undifferentiated PC12 cells; (**C**) differentiated PC12 cells (**D**) differentiated PC12 cells stimulated with 5 µM carbachol for 10 minutes; (**E**) differentiated PC12 cells stimulated with 2 µM carbachol for 24 hours; (**F**) differentiated PC12 cells exposed to (heat shock (42°C for 1 hour; (**G**) differentiated PC12 cells exposed to hypo-osmotic stress for 5 minutes. (**H**) Representative FCS

curves depicting the raw data and fitting of two measurements representative of lower (0.02 um2/s, blue) and higher (2.5 um2/s, red) diffusion coefficients using live differentiated PC12 cells one hour after transfection with the APP beacon. (**I**) The apparent 'concentration' of *APP* beacon derived from FCS correlation curves based on fluorescence intensity for beacon transfected into differentiated PC12 cells (**I**) stimulated with 5 µM carbachol for 10 minutes or with 2 µM carbachol for 24 hours in addition to basal differentiated PC12 cells. (**J**) cells exposed to hypo-osmotic stress for 5 minutes or exposed to excess heat (heat shock) at 42 C for 1 hour. (**K**) The diffusion coefficients of *APP* beacon derived from FCS correlation curves based in differentiated PC12 cells stimulated with 5 µM carbachol for 10 minutes or with 2 µM carbachol for 24 hours in addition to basal differentiated PC12 cells. (**L**) The diffusion coefficients of *APP* beacon particles derived from FCS correlation curves based on FAM-APP beacon fluorescence in differentiated PC12 cells exposed to osmotic stress for 5 minutes or exposed to excess heat (heat shock) at 42 C for 1 hour in addition to basal differentiated PC12 cells. *=P≤0.05, **=P≤0.01, ***=P≤0.001, and SE is shown. Scale bar=10 µm.

The APP beacon was transfected into PC12 cells using lipofectamine, which was previously found to be the optimal method to introduce RNA beacons into cells.[14] The transfected cells were imaged one hour after transfection at which point APP beacon fluorescence could be visualized. APP mRNA was found to be widely distributed in the cytoplasm of undifferentiated and differentiated PC12 cells (Figure 5.3B-C), noting absence of beacon fluorescence in neurites (Figure 5.3C). These fluorescent images also reveal that stress conditions including carbachol stimulation, heat shock and osmotic stress drastically affects the level and distribution of APP beacon fluorescencein differentiated PC12 cells. Specifically, the intensity the APP beacon becomes extremely low except for a few points of high intensity (Figure 5.3D-G). Comparing the beacon intensity with the RT-PCR results in Figure 5.1, which shows a reduction in APP transcripts a short time after carbachol stimulation and hypo-osmotic shock, but no change for longer times after carbachol stimulation and in increase with heat, we conclude that the large decreases in intensity mainly correspond to sequestration into stress granules rather than large scale degradation of the transcripts.

We quantified the dynamic properties of the APP beacon by fluorescence correlation spectroscopy which assess the diffusion and 'concentration' where the latter is related to the fluorescence intensity relative to a known concentration of a calibration probe (i.e. Alexa 488). These measurements (representative curves-Figure 5.3H), show that the diffusion coefficients and apparent concentration of the APP beacon is affected by all stress conditions (Figure 5.3I-L).

Carbachol stimulation (both 10 minutes and 24 hours (Figure 5.3I), heat shock and osmotic stress (Figure 5.3J) show a significant decrease in APP beacon fluorescence. The use of the APP beacon allows us to estimate the amount of APP mRNA sequestered in stress granules by the decrease in 'concentration', which we estimate to be ~70% for all stress conditions. Monitoring the diffusion coefficient the APP beacon with shows that the decrease in diffusion is consistent with sequestration of APP mRNA in stress granules (Figure 5.3K). It is notable that an increase in APP beacon diffusion occurs with higher temperature as seen for heat shock samples (Figure 5.3L).

5.3.4 Gαq activation increases APP protein processing and aggregation

We followed the properties of fluorescent intracellular APP domain during Gαq activation. We used a construct where an eGFP tag is attached to the C-terminus of APP-695 (see experimental procedures). Therefore, although the remaining extracellular domains of APP are overexpressed, these studies track only the C-terminal fragment (CTF) of the protein due to cleavage by γ-secretase. Under basal conditions, we find that the fluorescence intensity is fairly evenly distributed throughout the cytosol (Figure 5.4A). Stimulating cells with carbachol results in aggregation which remains high with long-term stimulation. Down-regulation of PLCβ1 greatly increases APP aggregation as does osmotic stress, which reduces the cytosolic population of PLCβ1 (Figure 5.4B-F). These results tie APP aggregation to both Gαq activation and cytosolic PLCβ1.We used Number and Brightness (N&B) analysis which monitors the number of fluorophores associated with a diffusing species.[16] In this analysis, we set the control sample to 'non-aggregated' values of N&B and then determined increases in these values which correspond to the aggregated form when the cells are subjected to carbachol stimulation. These values for the aggregation are given in Figure 5.4G, and the accompanying N&B plots show localization of protein aggregation as a result of stress.

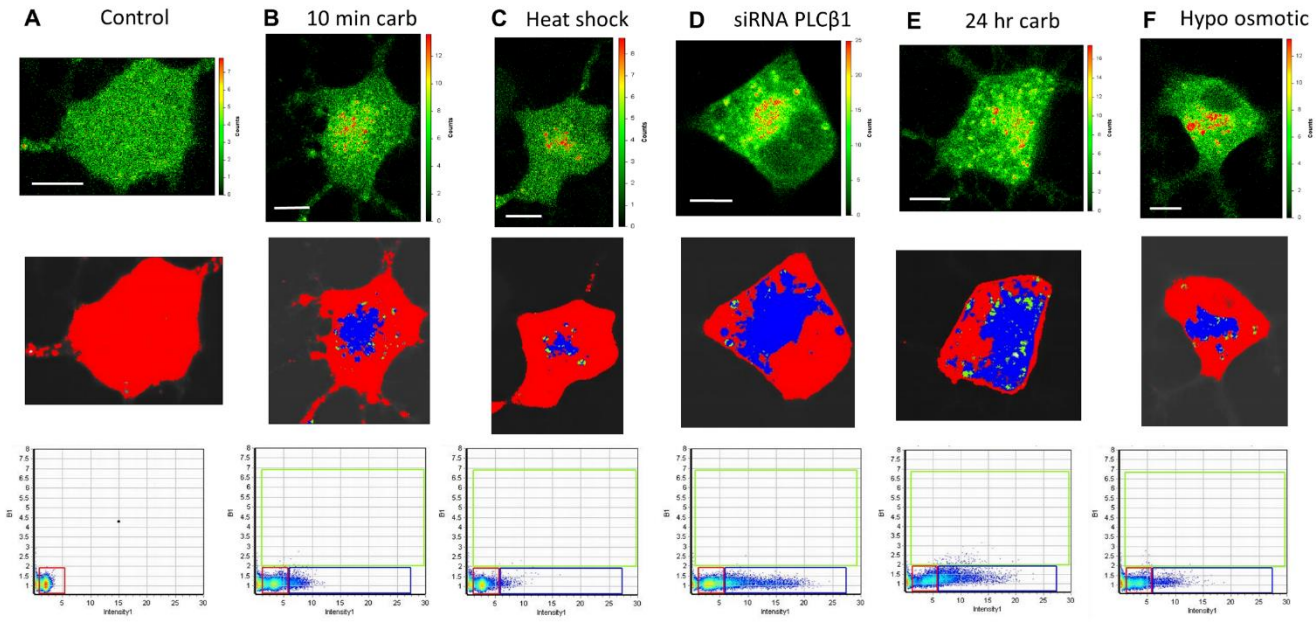

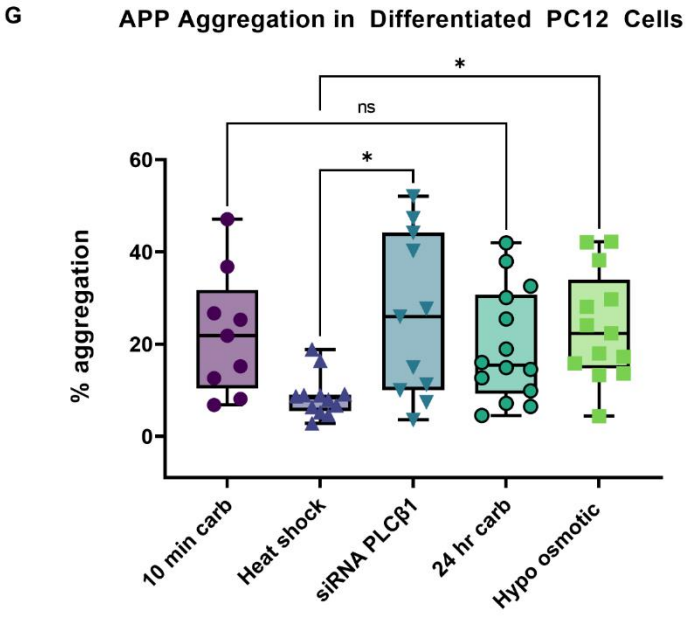

Figure 5.4 Aggregation of intracellular APP protein measured by N&B in cells exposed to environmental stress. Sample images (**A-F**) and compiled results (**G**) showing APP protein aggregation in differentiated cells exposed: 10 minutes carbachol stimulation, n=9; heat shock, n=12; hypo-osmotic stress, n=13; siRNA PLCβ1 transfection, n=11; and 24 hour carbachol stimulation, n=14. *=P≤0.05, **=P≤0.01, ***=P≤0.001, and SE is shown. Scale bar=10 µm.

Activation of Gαq by neurotransmitters reduces the level of cytosolic PLCβ1, and we carried out a series of studies to understand its contribution. We down-regulated two of PLCβ's cytosolic binding partners, C3PO and Ago2. C3PO is an octamer consisting of 6 translin and 2 TRAX subunits where the expression of TRAX and translin are linked.[17-18] Down-regulating TRAX, which will slow RISC activity, causes the fluorescent APP protein to have an initial aggregation that is no longer sensitive to carbachol stimulation (Figure 5.5A-D). Similarly, down-regulating Ago2, which interacts with both C3PO and PLCβ1,[19] will halt RISC activity and formation of Ago2 stress granules, and these results only show aggregation shortly after carbachol stimulation but not at longer times (Figure 5.5E-H). Over-expressing PLCβ1, which should inhibit RISC activity and reduce stress granule formation, increases aggregation under basal conditions (Figure 5.5I-L). The observation that changing the levels of cytosolic binding partners of PLCβ1 impact aggregation of APP suggests that cytosolic PLCβ in some way contributes to intracellular APP aggregation.

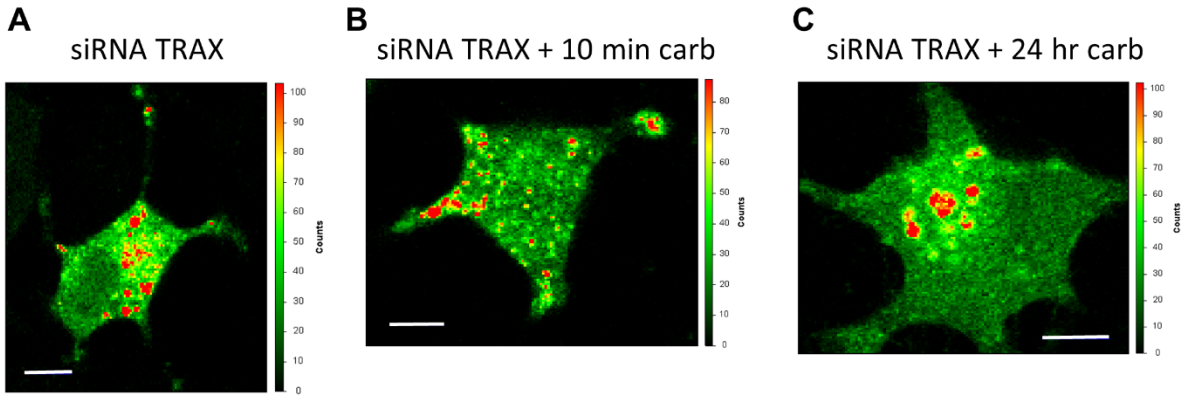
A
siRNA TRAX
B
siRNA TRAX + 10 min carb
C
siRNA TRAX + 24 hr carb
Counts

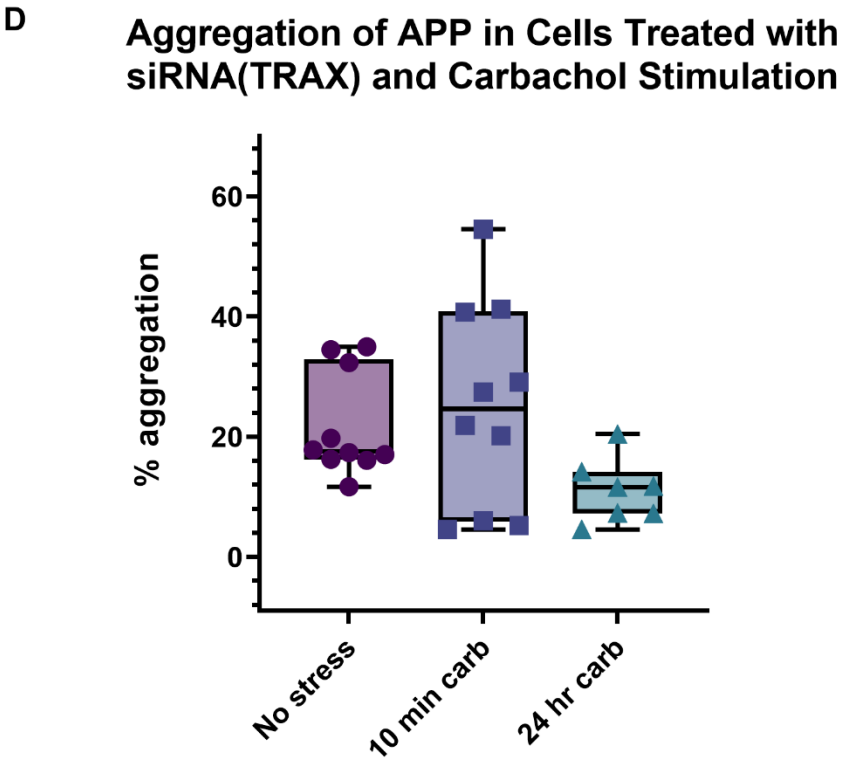
D
Aggregation of APP in Cells Treated with siRNA(TRAX) and Carbachol Stimulation
% aggregation
60
40
20
0
No stress
10 min carb
24 hr carb

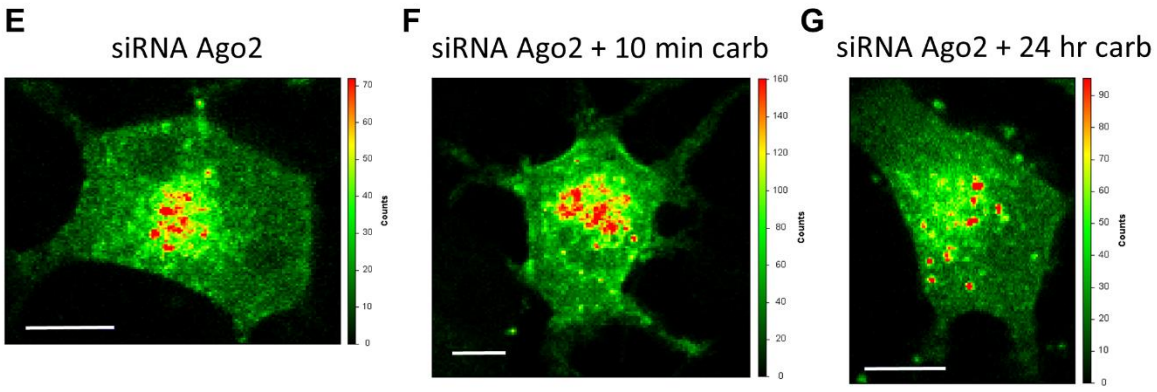
E
siRNA Ago2
F
siRNA Ago2 + 10 min carb
G
siRNA Ago2 + 24 hr carb
Counts

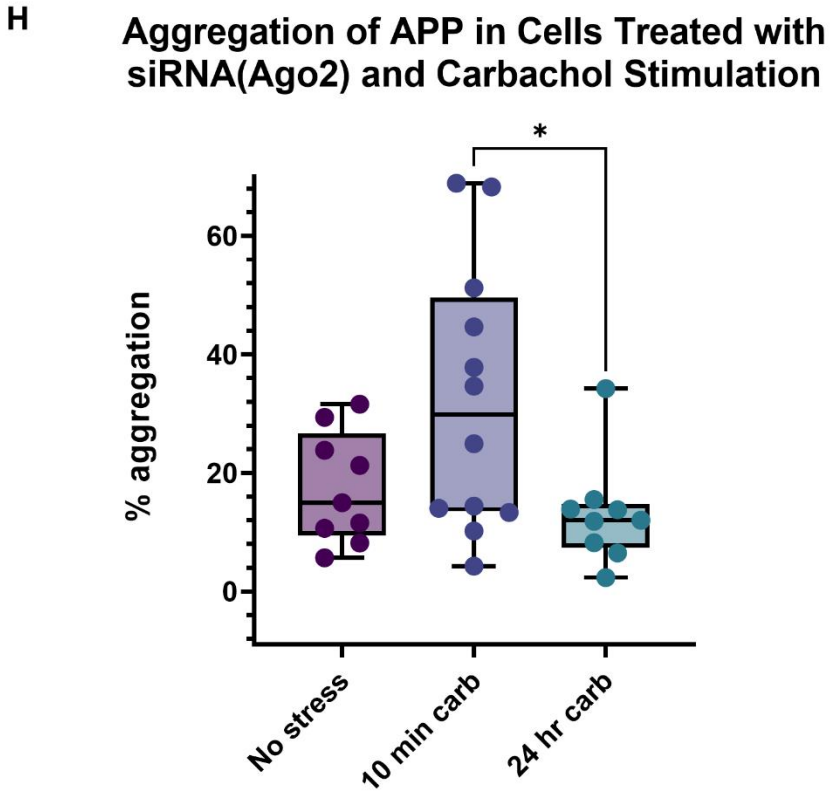
H
Aggregation of APP in Cells Treated with siRNA(Ago2) and Carbachol Stimulation
*
% aggregation
0
20
40
60
No stress
10 min carb
24 hr carb

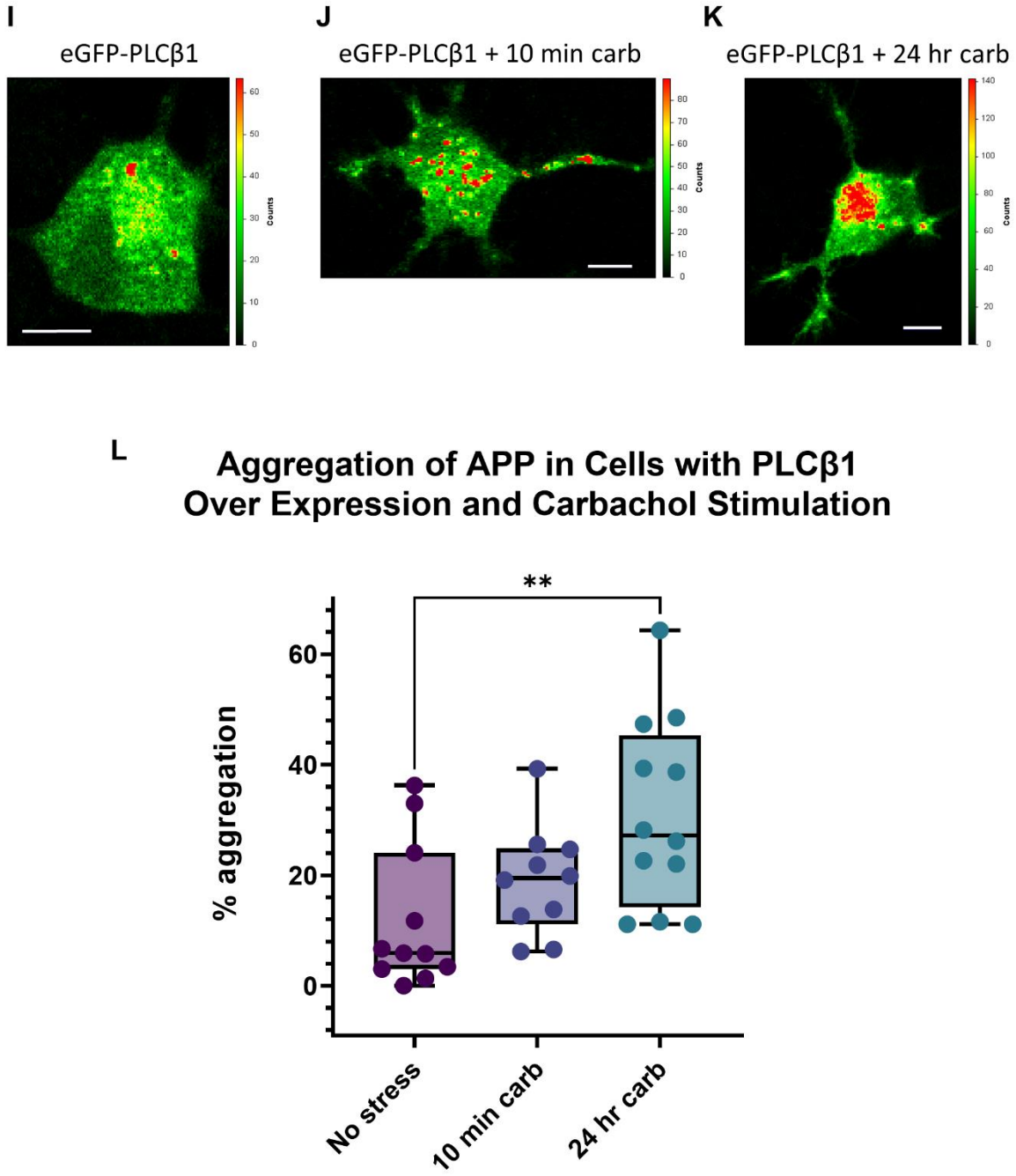

Figure 5.5 Aggregation of intracellular eGFP-APP measured by N&B in cells treated with siRNA(TRAX) and exposed to short and long term carbachol stimulation. Images of differentiated PC12 cells transfected with siRNA(TRAX) and intracellular eGFP-APP (**A**) control conditions (no stress); (**B**) exposure to carbachol for 10 minutes; (**C**) exposure to carbachol for 24 hours; and (**D**) complied results of aggregation determined by N&B where n=7-10. Images of differentiated PC12 cells transfected with siRNA(Ago2) under (**E**) control conditions (no stress); (**F**) exposure to carbachol for 10 minutes; (**G**) exposure to carbachol for 24 hours; and (**H**) complied results of

aggregation determined by N&B where n=9-12. Images of differentiated PC12 cells overexpressing eGFP-PLCβ1 under (**I**) control conditions (no stress); (**J**) exposure to carbachol for 10 minutes; (**K**) exposure to carbachol for 24 hours; and (**L**) complied results of aggregation determined by N&B where n=10-12. In (**D**) (**H**) and (**L**) SE is shown *=P≤0.05, **=P≤0.01, ***=P≤0.001. Scale bar=10 μm.

5.4 Discussion

In this study, we show that the Gαq signaling pathway, which is activated by acetylcholine, serotonin and other neurotransmitters, is involved in APP translation and aggregation of its intracellular domain. The effect of Gαq on APP aggregation has been monitored previously but not on the cellular level.[20] Rather than being solely mediated by increases in intracellular calcium, we find that aggregation of intracellular APP aggregation depends on cytosolic factors. First, we monitored *APP* transcripts. Using an RNA beacon to follow the accessibility of *APP* mRNA, we find that transcripts are unable for beacon detection presumably due to sequestration into stress granules caused by Gαq activation as well as more traditional cellular stresses. While these stresses sequester a large population of APP mRNA, prolonged or repeated Gαq activation results in a much more extensive sequestration seen in the beacon data and by RT-PCR. We see with fluorescence imaging that Ago2 particles increase in size, while G3BP1 particles don't change and PABPC1 particles decrease in size due to repeated stimulation. This suggests that Ago2's multiple functions play a role in stress granule aggregation, and more APP is recruited by Ago2 during repeated stress. Thus, stress conditions, as well as normal Gαq activation by neurotransmitters, will have the effect of reducing the production of APP.

We also followed a fluorescent-tagged APP who's transmembrane processing through γ-secretase activity produces an intracellular C-terminal fragment (CTF) tagged with eGFP.[21] Further processing produces two additional unlabeled domains including either a P3 or amyloid-β peptide, and a soluble N-terminal fragment (Figure 5.6). It is important to note that tracking of the CTF does not provide insight regarding amyloidogenic or non-amyloidogenic processing of the extracellular portion of APP. However, a completely cytosolic CTF is generated in the cases of both α and β-secretase cleavage and is involved with transcription regulation of genes related to Alzheimer's disease regardless of the production of extracellular amyloid-β.[22-24] This process happen through the CTF's suppression of miRs that control cell differentiation, a process similar

to that of PLCβ1 activation, and is favored in the APP695 isoform.[9, 23-24] Monitoring aggregation by N&B, we find that Gαq stimulation promotes aggregation which could result from two mechanisms. The primary role of Gαq activation is increasing intracellular calcium, and it is possible that APP processing and aggregation is influenced by calcium sensitive proteins. Activation of Gαq also relocalizes cytosolic PLCβ1 and we find that down-regulating PLCβ1's cytosolic partners renders GFP-APP695 insensitive to Gαq activation. This complex dependence of intracellular APP aggregation with levels of proteins stress granules and RNA-induced silencing proteins may correlates with its ability to impact endosomal events.[21, 25-26]

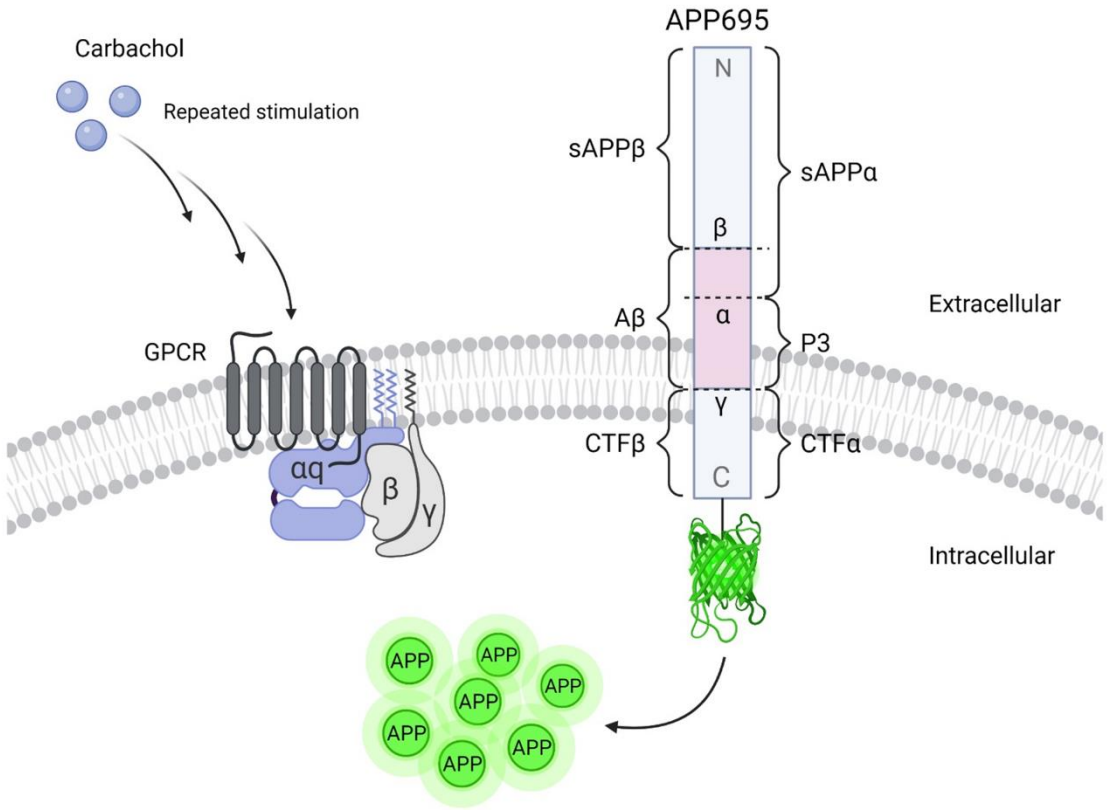

Figure 5.6 Model of APP aggregation due to repeated carbachol stress. When Gαq is activated, PLCβ1 shifts to the plasma membrane, releases cytosolic binding partners and allows for the formation of SGs. Carbachol stimulation results in two main mRNA SG components, however repeated stimulation accumulates a wider variety of mRNAs including *APP*. APP protein in aggregated in a similar way with extended and repeated Gαq stimulation. (Created with BioRender.com)

5.5 Materials & methods

5.5.1 Cell culture

PC12 cells were obtained from American Type Culture Collection (Manassas, VA, USA). DMEM (Invitrogen) with 10% horse serum from PAA (Ontario, Canada), 5% FBS (Atlanta Biological, Atlanta, GA), and 1% penicillin/streptomycin. Cells were incubated in 37 °C, 5% CO2, and 95% humidity. Differentiation was carried out in a medium of 1% horse serum, 1% penicillin/streptomycin and was initiated by the addition of nerve growth factor (NGF 7S) from Bon Opus. Medium was changed every 24 h. Transfection of plasmids, small interfering RNA (siRNA), or beacons was performed using Lipofectamine 3000 (Invitrogen) in antibiotic-free medium as per the manufacturer's instructions. A final concentration of 25 nM beacon was used for 0.5×10^6 cells in suspension in serum-free medium.

5.5.2 eCLIP transcript sequences

PC12 cells were transfected with eGFP-Ago2 using electroporation (Bio-Rad Gene Pulser Xcell) with one pulse in a 0.4 cm gap cuvette (Bio-Rad, cat #1652088) in complete media and plated at ~50% confluency to leave room for neurite growth. Cells were stressed and crosslinked using 254 nm ultraviolet light. Treated cells were collected from at least four 150 mm culture dishes per sample condition. Lysis was done on fresh, non-frozen cell pellets using 100 µL lysis buffer supplemented with RNase inhibitor and protease inhibitor tablets (Roche). A 10 µL portion of each lysate was used to extract total RNA (Zymo Clean and Concentrator) which was then tested for RNA integrity using RNA Fragment Analyzer services at University of Massachusetts Medical School Molecular Biology Core Lab. The remaining lysate was immunoprecipitated using mouse Ago2 antibody. Subsequent western blots, RNA cleanup and library construction was done using Eclipse Bioinnovation protocol v1.01R, storing samples at -80 °C overnight when necessary. Sample quantity was evaluated by qPCR. Libraries were sequenced at UMass Medical School Deep Sequencing Core using Illumina HiSeq 4000 system. All reagents were supplied by Eclipse Bioinnovations unless otherwise specified.

5.5.3 RT-PCR

For each condition, one 100 mm dish was used for total RNA extraction. Cells were differentiated and stressed before isolating RNA using RNeasy Mini Kit (Qiagen, Cat #74104) with DNase

digestion (Qiagen, cat #79254). CDNA synthesis was done using MiniAmp Thermal Cycler (Applied Biosystems). Purified RNA sample concentrations were measured by Nanodrop and 1 µg RNA was incubated with dNTP (New England Biolabs, cat #N0447S), random hexamers (Thermo Scientific, cat #SO142), and nuclease free water (Invitrogen, cat #AM9930), at 65 °C for 5 minutes. After the first incubation, 5x First Strand Buffer, DTT (Invitrogen cat #18080093) and RNase inhibitor (Invitrogen, cat #AM2694) were added to the mixture and incubated at 25 °C for 2 minutes. After the second incubation, 1 µL Superscript III Reverse Transcriptase (Invitrogen, cat #18080093) was added and the mixture was incubated at 25 °C for 10 minutes, 42 °C for 50 minutes, and 70 °C for 15 minutes. CDNA was stored at -20 °C overnight or used immediately at a dilution of 1:20 in nuclease free water for RT-PCR experiments with Luna Universal Master Mix (New England Biolabs, cat #M3003L), nuclease free water, and custom APP primer (ITD). For positive and negative controls, 18S ribosomal subunit and tau primers were used.

```
APP   F: 5′-GGGAGTTGGAAGGGCATAAA-3′
      R: 5′-GTGTGTGAGAGAGAGAGAGAGA-3′

Tau   F: 5′-CAGGACAGGAAATGACGAGAAG-3′
      R: 5′-CAGGGACATGGGTGATGTTATC-3′

18S   F: 5′-ACGTCTGCCCTATCAACTTTC-3′
      R: 5′-CCGCGGTCCTATTCCATTATT-3′
```

5.5.4 Particle analysis

Samples were imaged with a 100×/1.49 oil total internal reflection fluorescence (TIRF) objective to microscopically count the number of particles per µm^2 formed under different conditions. For each condition, 10 to 20 cells were randomly selected, and *z*-stack measurements were taken (1.0 µm per frame). Analysis was performed with ImageJ and Fiji ImageJ software in two ways. First, each measurement was thresholded before analyzing, and the number of particles per frame per measurement was averaged. Second, all *z*-stack measurements were combined to generate a three-dimensional image for each sample before analyzing the number of particles per sample and averaging the results. Both methods produced identical results. Live transfected cells, and fixed immunostained cells were used for comparison.

5.5.5 RNA beacons

The sequence for the APP beacon was derived from Ensemble ID ENSRNOG00000006997 and later verified using BLAST. The sequence we used for APP Beacon is 5'-CAUCUGUACAGUAAGAUG-3'. The beacon labeled with FAM (5(6)-carboxyfluorescein.) at the 5'end and Iowa-BHQ (black hole quencher) at the 3'end was purchased from IDT Technologies (Coralville, IA, USA). The sequences used for the oligonucleotides Beacons and oligonucleotides were dissolved into stock solutions and further diluted using DEPC water.

5.5.6 Fluorescence biophysics techniques

We also utilize techniques based on fluorescence fluctuation spectroscopy (FFS) that observes subtle changes in the intensities and movement of fluorescently labeled proteins in conjugation with fluorescent microscopy. One such technique is Fluorescence Correlation Spectroscopy (FCS) that was used in this study to characterize the differences in the mobility of micro-populations of proteins in small focal areas across a living cell at both basal and stimulated states. The movement of the fluorescently tagged proteins inside the excited focal volume generates a signal that is subsequently auto correlated to quantify physical quantities such as diffusion coefficients and concentrations.[27-29]

5.5.7 Fluorescence correlation spectroscopy (FCS)

FCS measurements on cells expressing fluorescent fusion protein using a 2-photon MaiTai laser (Spectra-Physics) (excitation 930 nm at 80 MHz) and a Nikon inverted confocal microscope in an ISS Alba System. The methodology of FCS has been discussed earlier.

5.5.8 Number and brightness (N&B) measurements

The Number and Brightness (N&B) analysis is a powerful tool that has been used previously to quantify graphically the aggregation state of diffusing proteins in living cells.[30-33] N&B analysis can determine of the number (N) of diffusing particles within a given focal area and the intrinsic brightness (B) of each particle represented by pixels in an image and provides providing a map of brightness for every pixel using the following equation. While we used B value as a measure of aggregation and oligomerization, it does not increase linearly with increased oligomerization. The mathematical equations that describe the apparent brightness B for every pixel are:

$$B = \frac{\sigma^2 - \sigma_0^2}{< I > - offset}$$

The methodology of N&B has been described earlier. Studies were performed by acquiring images of live cells plated on MatTek chambers (MatTek, MA, USA) using a 2-photon MaiTai laser (Spectra-Physics), a Nikon inverted confocal microscope in an ISS Alba System..

5.5.9 pEGFP-n1-APP plasmid information

N&B studies involved the use of live, differentiated PC12 cells transfected with pEGFP-n1-APP (Addgene plasmid #69924) which was prepared by Zita Balklava & Thomas Wassmer.[21] This construct was created by PCR amplification of APP695 from HeLa cells and includes pEGFP-n1 fused to the C-terminal backbone of the APP protein sequence at amino acids 2761-3477. Fluorescence indicates C-terminal fragments of the intracellular APP domain, however the entire APP protein is overexpressed, including two unlabeled extracellular fragments, P3 or amyloid-β depending on α or β-secretase cleavage respectively, as well as a soluble N-terminus fragment. Cells were transfected using Lipofectamine 3000 (Invitrogen) before NGF (Bon Opus) treatment for 48 hours in low serum media (DMEM + 1% horse serum, 1% antibiotics).

5.5.10 Statistical analysis

All data were analyzed using Prism 9 (GraphPad) using Student's t-test substituted by Mann-Whitney's rank sum test if the data was not normally distributed. A difference between two groups was considered statistically significant only with a p-value below 0.05.

5.6 Acknowledgements

The authors are grateful for the support of NIH GM116187 and Richard Whitcomb Fellowship.

5.7 References

1. O'Brien, R. J.; Wong, P. C., Amyloid precursor protein processing and Alzheimer's disease. *Annu Rev Neurosci* **2011,** *34*, 185-204.
2. Nguyen, K. V., The human beta-amyloid precursor protein: biomolecular and epigenetic aspects. *Biomol Concepts* **2015,** *6* (1), 11-32.
3. Schedin-Weiss, S.; Winblad, B.; Tjernberg, L. O., The role of protein glycosylation in Alzheimer disease. *FEBS J* **2014,** *281* (1), 46-62.
4. Sharma, K.; Pradhan, S.; Duffy, L. K.; Yeasmin, S.; Bhattarai, N.; Schulte, M. K., Role of Receptors in Relation to Plaques and Tangles in Alzheimer's Disease Pathology. *Int J Mol Sci* **2021,** *22* (23).
5. Exton, J. H., Cell signalling through guanine-nucleotide-binding regulatory proteins (G proteins) and phospholipases. [Review] [110 refs]. *European Journal of Biochemistry* **1997,** *243* (1-2), 10-20.
6. Suh, P.; Park, J.; Manzoli, L.; Cocco, L.; Peak, J.; Katan, M.; Fukami, K.; Kataoka, T.; Yun, S.; Ryu, S., Multiple roles of phosphoinositide-specific phospholipase C isozymes. *BMB reports* **2008,** *41*, 415-34.
7. Jackson, L.; Qifti, A.; Pearce, K. M.; Scarlata, S., Regulation of bifunctional proteins in cells: Lessons from the phospholipase Cbeta/G protein pathway. *Protein Sci* **2020,** *29* (6), 1258-1268.
8. Qifti, A.; Jackson, L.; Singla, A.; Garwain, O.; Scarlata, S., Stimulation of phospholipase Cbeta1 by Galphaq promotes the assembly of stress granule proteins. *Sci Signal* **2021,** *14* (705), eaav1012.
9. Garwain, O.; Pearce, K. M.; Jackson, L.; Carley, S.; Rosati, B.; Scarlata, S., Stimulation of the Gαq/phospholipase Cβ1 signaling pathway returns differentiated cells to a stem-like state. *The FASEB Journal* **2020,** *34* (9), 12663-12676.
10. Sahu, S.; Williams, L.; Perez, A.; Philip, F.; Caso, G.; Zurawsky, W.; Scarlata, S., Regulation of the activity of the promoter of RNA-induced silencing, C3PO. *Protein Science* **2017,** *26* (9), 1807-1818.
11. Philip, F.; Sahu, S.; Caso, G.; Scarlata, S., Role of Phospholipase C-β in RNA interference. *Adv Biol Regul* **2013,** *53* (3), 319-330.
12. Mahboubi, H.; Stochaj, U., Cytoplasmic stress granules: Dynamic modulators of cell signaling and disease. *Biochimica et Biophysica Acta (BBA) - Molecular Basis of Disease* **2017,** *1863* (4), 884-895.
13. Jackson, L.; Poussaint, A.; Scarlata, S., Neurotransmitter Activation Sequesters Specific mRNAs Into Stress Granules. *Scientific Reports* **2022,** *in press*.
14. Guo, Y.; Lu, Z.; Cohen, I. S.; Scarlata, S., Development of a universal RNA beacon for exogenous gene detection. *Stem Cells Transl Med* **2015,** *4* (5), 476-82.
15. Scarlata, S.; Yerramilli, V. S., Design of a Rapid and Reversible Fluorescence Assay to Detect Covid-19 and other Pathogens. **2022,** *10* (4).
16. Digman, M. A.; Dalal, R.; Horwitz, A. F.; Gratton, E., Mapping the Number of Molecules and Brightness in the Laser Scanning Microscope. *Biophys J* **2008,** *97*, 2320-2332.
17. Li, Z.; Wu, Y.; Baraban, J. M., The Translin/Trax RNA binding complex: clues to function in the nervous system. *Biochimica et biophysica acta* **2008,** *1779* (8), 479-485.
18. Jaendling, A.; Macfarlane, R., Biological roles of translin and translin-associated factor-X: RNA metabolism comes to the fore. *Biochem J* **2010,** *429*, 225-34.

19. Qifti, A.; Jackson, L.; Singla, A.; Garwain, O.; Scarlata, S., Stimulation of phospholipase Cbeta1 by Galphaq promotes the assembly of stress granule proteins. *Science Signaling* **2021,** *14* (705), eaav1012.
20. Roßner, S.; Ueberham, U.; Schliebs, R.; Regino Perez-Polo, J.; Bigl, V., The regulation of amyloid precursor protein metabolism by cholinergic mechanisms and neurotrophin receptor signaling. *Progress in Neurobiology* **1998,** *56* (5), 541-569.
21. Currinn, H.; Guscott, B.; Balklava, Z.; Rothnie, A.; Wassmer, T., APP controls the formation of PI(3,5)P(2) vesicles through its binding of the PIKfyve complex. *Cell Mol Life Sci* **2016,** *73* (2), 393-408.
22. Muller, T.; Meyer, H. E.; Egensperger, R.; Marcus, K., The amyloid precursor protein intracellular domain (AICD) as modulator of gene expression, apoptosis, and cytoskeletal dynamics-relevance for Alzheimer's disease. *Prog Neurobiol* **2008,** *85* (4), 393-406.
23. Shu, R.; Wong, W.; Ma, Q. H.; Yang, Z. Z.; Zhu, H.; Liu, F. J.; Wang, P.; Ma, J.; Yan, S.; Polo, J. M.; Bernard, C. C.; Stanton, L. W.; Dawe, G. S.; Xiao, Z. C., APP intracellular domain acts as a transcriptional regulator of miR-663 suppressing neuronal differentiation. *Cell Death Dis* **2015,** *6*, e1651.
24. Belyaev, N. D.; Kellett, K. A.; Beckett, C.; Makova, N. Z.; Revett, T. J.; Nalivaeva, N. N.; Hooper, N. M.; Turner, A. J., The transcriptionally active amyloid precursor protein (APP) intracellular domain is preferentially produced from the 695 isoform of APP in a {beta}-secretase-dependent pathway. *J Biol Chem* **2010,** *285* (53), 41443-54.
25. Choy, R. W.; Cheng, Z.; Schekman, R., Amyloid precursor protein (APP) traffics from the cell surface via endosomes for amyloid beta (Abeta) production in the trans-Golgi network. *Proc Natl Acad Sci U S A* **2012,** *109* (30), E2077-82.
26. Chaufty, J.; Sullivan, S. E.; Ho, A., Intracellular amyloid precursor protein sorting and amyloid-beta secretion are regulated by Src-mediated phosphorylation of Mint2. *J Neurosci* **2012,** *32* (28), 9613-25.
27. Golebiewska, U.; Nyako, M.; Woturski, W.; Zaitseva, I.; McLaughlin, S., Diffusion coefficient of fluorescent phosphatidylinositol 4,5-bisphosphate in the plasma membrane of cells. *Mol Biol Cell* **2008,** *19* (4), 1663-9.
28. Chiantia, S.; Ries, J.; Schwille, P., Fluorescence correlation spectroscopy in membrane structure elucidation. *Biochim Biophys Acta* **2009,** *1788* (1), 225-33.
29. Schwille, P., Fluorescence correlation spectroscopy and its potential for intracellular applications. *Cell Biochem Biophys* **2001,** *34* (3), 383-408.
30. Digman, M. A.; Dalal, R.; Horwitz, A. F.; Gratton, E., Mapping the number of molecules and brightness in the laser scanning microscope. *Biophys J* **2008,** *94* (6), 2320-32.
31. Ossato, G.; Digman, M. A.; Aiken, C.; Lukacsovich, T.; Marsh, J. L.; Gratton, E., A two-step path to inclusion formation of huntingtin peptides revealed by number and brightness analysis. *Biophys J* **2010,** *98* (12), 3078-85.
32. Plotegher, N.; Gratton, E.; Bubacco, L., Number and Brightness analysis of alpha-synuclein oligomerization and the associated mitochondrial morphology alterations in live cells. *Biochim Biophys Acta* **2014,** *1840* (6), 2014-24.
33. Planes, N.; Digman, M. A.; Vanderheyden, P.; Gratton, E.; Caballero-George, C., Number and brightness analysis to study spatio-temporal distribution of the angiotensin II AT1 and the endothelin-1 ETA receptors: Influence of ligand binding. *Biochim Biophys Acta Gen Subj* **2019,** *1863* (5), 917-924.

6 Chapter 6 – Conclusions, limitations & future work

6.1 Conclusions

PLCβ1 has proven to be a multifunctional protein, with a significant population working on the plasma membrane to regulate calcium signaling. However, this thesis focuses on the behavior of cytosolic PLCβ1, and its involvement in RNA induced silencing and stress responses. The first aim of this thesis, covered in chapter 3, focused on protein associations between cytosolic PLCβ1, Ago2 and C3PO, and the effects of their binding on gene silencing and stress granule formation. The second aim, introduced in chapter 4, identified trends in transcripts and proteins associated with Ago2 stress granules under different stress conditions. Chapter 5 expands aim 2 by exploring the incorporation of a gene highly associated with Alzheimer's disease into stress granule aggregates with prolonged and repeated Gαq activation.

When membrane bound PLCβ1 initiates an influx in calcium, organelles like mitochondria and Golgi that are associated with *ATP5f1b* and *CHGb* are flooded with calcium, causing these transcripts to move into SGs in an effort to avoid degradation. At the same time, activated Gαq causes cytosolic PLCβ1 to release binding partners involved in SG aggregation and RISC processing, and these proteins become free to carry out these functions. In the event of repeated neurotransmitter stimulation, which mimics the physiological condition that neurons experience regularly, additional mRNAs are recruited to Ago2 SGs including *APP*. Similarly, C-terminal fragments of APP protein are seen to aggregate with extended and repeated Gαq activation, suggesting that this protein may be included in SG particles as well. A model summarizing these events can be seen below in Figure 6.1

Understanding the role of PLCβ1 in mediating stress granule assembly and RISC function could be valuable in the field of neurodegeneration. The processes of SG assembly and disassembly impacts synapse formation and cell plasticity[1]. Therefore, understanding these processes may provide information needed to develop therapeutics concerning a broad range of diseases. Neurodegenerative diseases suspected to be impacted by stress granules include Alzheimer's disease (AD), amyotrophic lateral sclerosis (ALS), schizophrenia, Parkinson's disease and Autism

spectrum disorder (ASD).[2-6] Because the regulation of this process has the capability of impacting multiple fatal neurological disorders, it is critical to understand the behavior of PLCβ1 by Gαq activation to create effective treatments that could benefit more than 50 million Americans suffering from neurodegeneration.[7]

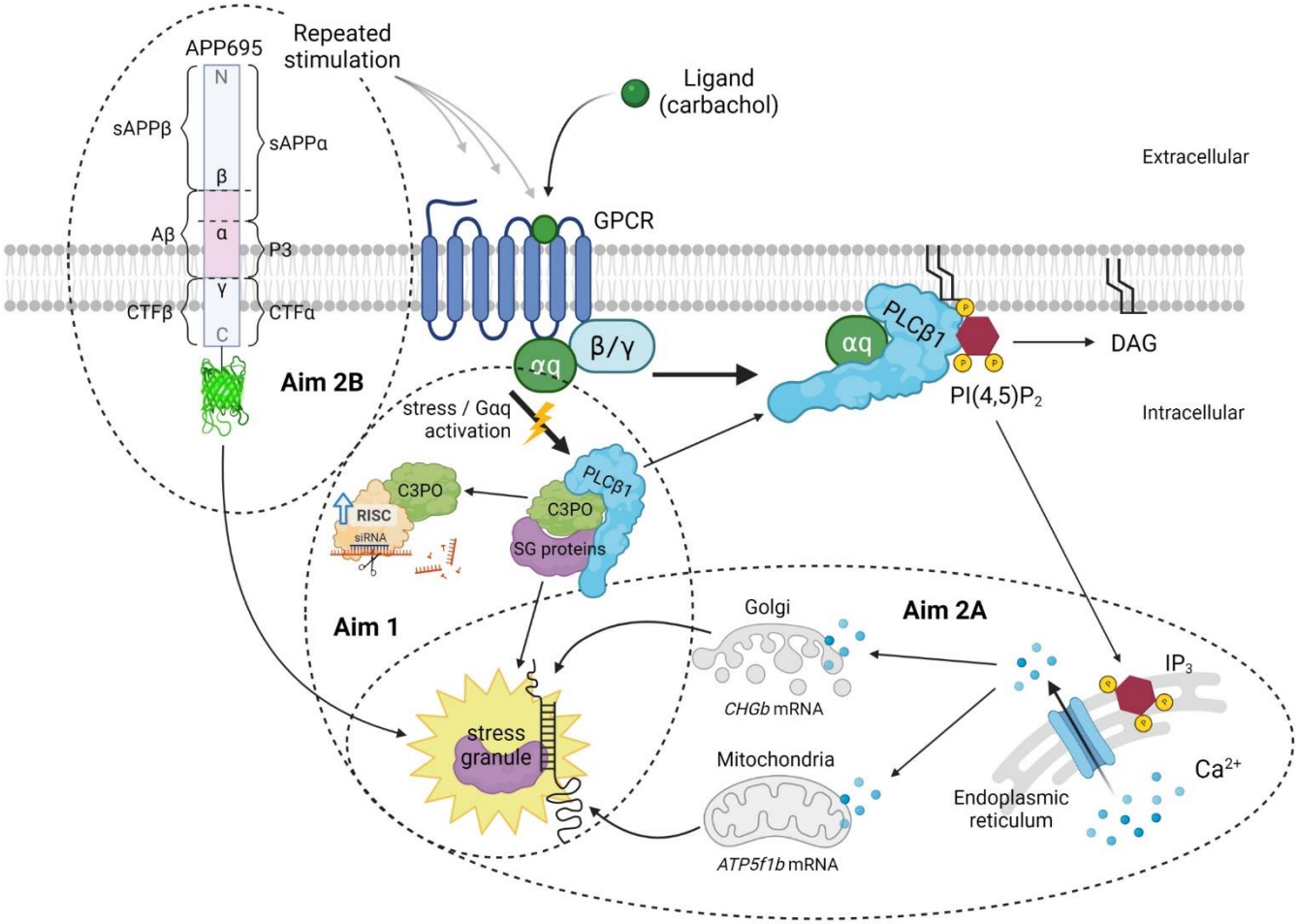

Figure 6.1 Summary model for this thesis. This model describes PLCβ1 activation on the plasma membrane, leading to an increase in calcium that disrupts the mitochondria and Golgi to move *ATP5f1b* and *CHGb* into SGs. This stimulation also causes PLCβ1 to release cytosolic binding partners which increases RISC activity and promotes the movement of proteins into SGs. Repeated Gαq activation causes C-terminal APP fragment to aggregate significantly within the cytosol.

6.1.1 Conclusions: Aim 1 (Chapter 3)

In chapter 3, we show a connection between PLCβ1 and stress granule formation. Identification of PLCβ1's cytosolic binding partners revealed that a significant portion of proteins contribute to assembly, stability and incorporation into stress granule aggregates. We used various methods including particle analysis, FLIM/FRET, dynamic light scattering and number and brightness to suggest that stress granules formed under different conditions contain different proteins and mRNAs. In our studies, the aggregation of stress granules was initiated through environmental stress and neurotransmitter stimulation within a physiological range, instead of non-physiological conditions that have traditionally been used to trigger SG formation such as arsenite treatment.[8] The loss of cytosolic PLCβ1 through multiple methods including siRNA transfection, carbachol stimulation and osmotic stress all resulted in increased protein aggregation. This led to the conclusion that PLCβ1 binds these proteins in the cytosol to mediate their release into SG aggregates.

Similarly, cytosolic PLCβ1 binds to and regulates activity of members of the RNA induced silencing complex. Component 3 promoter of RISC (C3PO) was previously found to be regulated by PLCβ1, resulting in changes in gene expression and cell phenotype.[9] This thesis looked at Ago2-C3PO associations and how these proteins simultaneously interact with PLCβ1. It was found that in the cytosol of PC12 cells, a ternary complex is formed between these proteins. Loss of Ago2 or C3PO does not interrupt PLCβ1-C3PO or PLCβ1-Ago2 interactions respectively, but loss of PLCβ1 results in the disassociation of Ago2-C3PO. Looking at Ago2-C3PO associations with excess PLCβ1 shows that a close interaction remains, even after loss of the majority of PLCβ1's cytosolic population. This result implies that PLCβ1 prioritizes its role on the plasma membrane, but when in excess, there is enough protein available to fulfill its job within the cytosol as well.

6.1.2 Conclusions: Aim 2A (Chapter 4)

Many biophysical methods were used in aim 1 to suggest that stress granules contain distinct mRNA and protein as a result of different types of stress. This chapter discusses specific trends in the mRNA and protein makeup of stress granules in cells exposed to different conditions. Ago2 stress granules were purified and mRNA was sequenced to provide more detailed information

about the way in which cells respond to stress. In cells exposed to heat shock, it appears that transcripts were randomly sequestered, but with carbachol stimulation we saw high levels of *ATP5f1b* and *CHGb* transcripts. Purified Ago2 stress granules were also analyzed by mass spectrometry, showing the highest percent conservation of proteins related to calcium and transcription factors in SGs formed by carbachol when compared to a non-stressed control. These findings suggest that the movement of PLCβ1 out of the cytosol to regulate calcium release through its role on the plasma membrane results in very high levels of calcium that may interfere with the normal function of organelles such as mitochondria or Golgi. This flooding of calcium could then cause the specific transcripts *ATP5f1b* and *CHGb* to become sequestered in the cytosol.

Furthermore, we were able to identify a timeline for stress granule formation under a variety of environmental stresses and stimulation in aim 1, but the time it takes for stress granule disassembly to occur was not well understood. In this portion of the thesis, we allowed 30 minutes recovery following stress before testing for the presence of stress granule aggregates. We discovered that none of the stress granules formed as a result of different environmental conditions were able to completely disassociate in this period of time. While further experiments are required to completely understand the rate at which stress granules disassemble, this does indicate that they persist significantly longer than the applied stress.

6.1.3 Conclusions: Aim 2B (Chapter 5)

In chapter 5, we determined that prolonged and repeated stress effectively moved high levels of *APP* into stress granule aggregates. APP is often associated with Alzheimer's disease, as β-secretase cleavage leads to the formation of extracellular neurotoxic β-amyloid fragments. There is an intracellular C-terminal fragment (CTF) that is created from, γ-secretase processing in the case of either β-secretase or α-secretase activity, however, most studies surrounding APP focus on the β-amyloid region of the protein, as it has a direct connection to AD. It is believed that similar to PLCβ1's association with C3PO, the CTF of APP controls differentiation of neuronal cells through regulation of miRs, but not much more is understood about the behavior of the CTF.[10] Considering neurons in humans and animals are constantly being stimulated by neurotransmitters, understanding the effects of repeated stimulation on APP is of high priority.

Our studies found that repeated Gαq activation results in both stress granules containing high levels of *APP* mRNA and also the aggregation of intracellular APP protein. Exposing cells to stress and allowing for incomplete recovery before applying more stress, or exposing cells to stress for long periods of time allows for *APP* mRNA to accumulate in greater quantities than with application of stress or stimulation only once.

6.2 Limitations

Although data was validated using multiple methods to get a greater understanding and perspective of this protein pathway, there were several limitations that may contributed to the experiments described in this work. This section will address some of these limitations and the factors that should be considered when planning experiments that are to be built from the work in this dissertation.

6.2.1 Limitations: Aim 1 (Chapter 3)

6.2.1.1 Particle analysis

In chapter 3, we designed a method to quantify the size and number of protein particles in cells that were fixed directly after the application of stress. Cells were then immunostained for a stress granule marking protein (i.e. Ago2, PABPC1) to indicate endogenous levels of stress granule aggregation as a result of different stresses. Live cells expressing tagged plasmids were also used (i.e. Ago2, G3BP1). Particle analysis could then be performed on cells by way of Z-stack imaging 1 μm thick slices at 100x magnification to ensure optimal resolution of aggregates on a two photon inverted confocal microscope. Images were analyzed to quantify the size and number of particles in each slice to account for multiple stress granules in a cell that may not be visualized by imaging in just one focal plane. Size and count of particles in slices were averaged among a population of cells, and sorted in ascending order to compare the distribution of data between minimum and maximum data points. Data for each condition were represented as a line graph with the size of particles plotted on the x-axis and number of particles on the y-axis.

It is important to note that with this style, a data point of the size of particles on the x-axis representing any given slice of a cell image does not necessarily correspond to the number of

particles in the same image slice on the y-axis. These data should be interpreted as independent datasets showing the distribution of particle size and number for the same cell images. After attempting to represent these data multiple different ways, including histograms and 3D reconstructions, it was determined that this type of line graph quantified both datasets in a way that was the simplest to compare, especially when looking at multiple environmental conditions.

When comparing live, transfected cells to fixed, stained cells there was often a significant shift in scaling of the axes due to the thresholding parameters applied during image analysis. This inconsistency is a result of higher levels of overexpressed protein detected in live cells, whereas there is not always a uniform distribution of fluorescence seen in stained samples. The image processing method used for particle analysis was identical for both live and fixed cells, but this detail becomes insignificant as data was compared statistically to other samples prepared under the same parameters.

Because a stress granule can be up to 2 μm in diameter, single particles often span more than one Z-stack slice. This is unavoidable when imaging, since the size and location of SG aggregates are unpredictable. This error is consistently carried through each measurement and for this reason, graphical representation of the range of data is preferred. These limitations carry over to particle analysis data reported in other chapters.

6.2.1.2 FLIM/FRET

FLIM/FRET is a method used to measure associations between two proteins in live cells. Although FLIM phasor plot analysis offers multiple advantages compared to other methods of measuring FRET, there were a few drawbacks when designing experiments for this thesis work. With FLIM/FRET, we could determine with high certainty the association between two proteins tagged with FRET pair fluorophores such as eGFP and mCherry. Proteins tagged with FRET pairs were necessary to determine associations due to a region of overlap of the donor's emission and acceptors excitation spectra.[11] Plasmids had to be constructed with this in mind and there were occasions in which we did not have constructs available to satisfy this requirement for the measurement of certain associations. Homo-FRET could be measured through increased intensity of two plasmids expressing eGFPs, but often phasor plot lifetimes did not reflect associations

accurately and/or in way that could be compared to our normal hetero-FRET measurements with confidence.[12] In addition, FRET between more than two proteins cannot be measured using our system. To avoid this issue, we overexpressed untagged protein that would alter associations while not interfering with fluorescent signals.

There are theoretical factors that complicate the FLIM/FRET measurements reported in chapter 3. It is unknown if the addition of siRNA by transfection affects the PLCβ1-C3PO-Ago2 complex, as we are measuring associations between members RISC which are constantly processing siRNAs. For this reason, multiple methods were used to drive PLCβ1 out of the cytosol to measure Ago2-C3PO protein associations including carbachol stimulation and hypo-osmotic stress. The impact of bound RNA to Ago2 and C3PO is actively being assessed by our group to further understand their role in these associations.

6.2.2 Limitations: Aim 2A (Chapter 4)

6.2.2.1 Number and brightness

Number and brightness is a technique used to measure protein oligomerization by measuring variance in diffusing fluorophores. In some cases, protein dimers and higher order oligomers that should be represented in our figures as an increase in pixels seen on the y-axis, or enclosed in the "green box" have the ability to self-quench.[13] This quenching results in loss of fluorescent signals, and therefore a lower percent aggregation is measured than may truly be occurring. This may be due to the fact that unlike many of the measurements reported in chapter 3 that measured WKO-3M22, A10 and undifferentiated PC12 cells, the N&B in chapters 4 & 5 measured differentiated PC12 cells. Note that differentiated PC12 cells express more PLCβ1 than undifferentiated PC12 cells, which may result in greater regulation of SG proteins in the cytosol, and therefore less oligomer aggregation detected. In addition, transfected cells are expressing a high amount of fluorescence, increase the possibility of self-quenching or homo-FRET. Even so, a significant percent aggregation of high intensity particles is seen overall as a result of cells experiencing stress or Gαq stimulation. Therefore, at the very least, we can confirm that high concentrations of monomeric protein are localizing to aggregates as a result of stress.

6.2.2.2 Mass spectrometry

In chapter 4, we report protein composition of purified Ago2 stress granules determined by mass spectrometry analysis. Because stress granules are such small fractions of whole cell lysate, an enormous amount of cell material was needed for this purification (six 150 mm dishes for each condition). This required a large amount of incubator space, media, NGF and plasmid to be consumed for this experiment. The procedure used as a guide for this purification did not specify what quantity of cells was appropriate for SG purification (see [14]). After multiple purification attempts combining frozen cell pellets grown in phases, using different stress granule protein antibodies for pulldown, different cell lines, and increasing the amount of material used to perform the purification, we discovered that using fresh, non-frozen cell pellets at the highest quantity possible was the most effective solution. Purification was eventually successful, as SG proteins were detected from samples via Western blotting. However little sample was detected by mass spectrometry. For these reasons, we compared the results from our screening against information in the mass spectrometry database, including data from multiple spectrums of previous Ago2 and PLCβ1 pulldowns. These data supplemented the purified SG samples spectrums and gave us a more complete understanding of proteins that likely are incorporated in mammalian cell stress granules. We then filtered out non-vertebrate species from the dataset and searched by protein function, instead of reporting specific proteins found under each condition.

Additionally, only the proteins stably associated with SG cores could be identified, as the dynamic nature of SG shells makes identification of loosely-bound proteins more difficult to isolate. However, identifying proteins incorporated in SG cores is still highly valuable, as these components are likely sequestered in greater concentrations that may cause significant changes in the function of these particular proteins or expression of specific genes.

6.2.2.3 eCLIP sequences

Similar mass spectrometry problems listed above regrading sample preparation were also experienced when sequencing purified Ago2 SG mRNA. It would have been preferred to compare more than two stress conditions for this sequencing report, however, not all samples yielded reliable results. Four 150 mm dishes of cells were plated for each condition for sequencing. This amount was far more material than was recommended in the protocol by manufacturer Eclipse

Bioinnovations, yet only two out of four samples yielded enough RNA to complete the sequencing with confidence (carbachol and heat). It appeared that for the control condition, the sample simply did not contain enough RNA due to the lack of stress granules formed since the nucleation of stress granules requires RNA. Some RNA binds Ago2 under basal conditions while gene processing, but it is significantly less than would be found in stress granules. For osmotic stress, it's possible that a portion of cells had been washed out of the dish as a result of changing cell media multiple times while applying this stress, leaving too little material to construct a useful library. With this said, we did have an environmental stress (heat) to compare to cells treated with carbachol to activate Gαq, which gave us a clear indication that different conditions result in different patterns of mRNAs that are sequestered by Ago2.

6.2.3 Limitations: Aim 2B (Chapter 5)

6.2.3.1 Fluorescent beacons

Fluorescent RNA beacons are a powerful tool for visualizing changes in RNA localization as a result of environmental stress and stimulation. With this technique, we could measure aggregation by fluorescence correlation spectroscopy (FCS) to validate whether *APP* mRNA moves into stress granules. Drawbacks of this technique include inability to track long term changes in mRNA dynamics, since binding between the mRNA and beacon is permanent once hybridization occurs. Nonetheless, the specificity of this technique demonstrated that *APP* mRNA does in fact move into SGs with repeated and extended carbachol stimulation and environmental stress, and the same result is seen with RT-PCR.

6.3 Future work

The finding that PLCβ1 has cytosolic binding partners involved in regulating RNAi and SG formation in neuronal cells has opened up many questions that go beyond the scope of this dissertation. Answering the questions posed below would provide valuable information regarding the way in which activated Gαq contributes to the onset of disease.

6.3.1 Future work: Aim 1 (Chapter 3)

The studies done in chapter 3 focused on the formation of stress granules but does not explore other factors including how long they persist before disassembly, and when or if PLCβ1 is involved in their reversal. There is much evidence that premature SG formation, and permanent aggregation is detrimental to the health of neuronal cell types, but we do not know what causes these types of inappropriate aggregates or if G-protein signaling is involved. Additionally, aside from protein signaling and LLPS, we know very little about the physical properties that help trigger the formation of SGs and how to control these parameters.

Because SGs are formed uniquely depending on the type of stress cells experience, the timeline of SG disassembly may also be unique to particular stresses. Our preliminary findings suggest that not only the stress applied but the age of the cell (i.e. number of passage) are highly relevant factors involved in the kinetics of SG disassembly. If we were to understand the conditions that result in rapid disassembly compared to the prolonged presence of SGs, and the extent of which this is exacerbated by aging, we could then study specific conditions and what unique physical properties result in the fastest SG breakdown.

It is known that SGs form in two parts, with a peripheral shell surrounding a tightly packed core. The core of SGs allows for little exchange of proteins, while the components contained in the shell are highly dynamic.[15] To expand on this, it would be interesting to know the physical properties that contribute to the ways in which the core and shell form, whether there is a universal process involved in driving the formation of SGs, and if shell components are specifically or randomly sequestered before diffusing. If there are consistencies in proteins necessary for the formation of multiple types of SGs, looking at how concentrations of these proteins impact the rate of disassembly could provide a correlation between the proteins that stabilize SG aggregates and the disassembly process. If this is not the case, other proteins may be involved in SG disassembly while not incorporating themselves into the aggregates, much like PLCβ1's role in SG formation. Understanding if there are specific proteins that trigger the release of SG aggregates would provide an opportunity to control the breakdown of SGs in situations in which they are not appropriately disassociating.

We have shown that PLCβ1 activation mediates the formation of SGs by moving PLCβ1 out of the cytosol. However, whether PLCβ1 plays a role in their disassembly, and the effect that increased levels of calcium has on SG formation and disassembly have not been identified. Tracking the effects that an increased or decreased presence of calcium has on SG aggregation may tell us more about how PLCβ1 activation is involved in the later parts of this timeline.

Future experiments also may include protein purification and cryo-EM imaging to understand structural details of PLCβ1-C3PO-Ago2 interactions and the impact that the presence or absence of siRNA has on this complex. With purified proteins, microinjections could be done to introduce active protein and validate FLIM/FRET associations.

6.3.2 Future work: Aim 2A (Chapter 4)

We understand that there are specific transcripts sequestered in Ago2 carbachol induced stress granules in differentiated PC12 cells, however we aren't entirely sure why these two transcripts are selected. We suspect that the increase in calcium as a result of Gαq activation plays a role, but further rationale for this process has not yet been discovered. This dissertation has looked at characterizing Ago2 specific stress granules since it is a multifunctional protein involved in both SG formation and RISC activity. However, many other stress granule proteins bind cytosolic PLCβ1, and the mRNAs and proteins bound most preferentially to those binding partners may differ from the results seen here.

In addition, it would be interesting to understand if *ATP5f1b* and *CHGb* are sequestered under carbachol stimulation in other cell types, as we suspect these results may be specific to neuroendocrine cells. Looking at cell lines other than PC12, or animal models could give a greater insight to phenotypic changes associated with diseases and the behavior of these mRNAs in other systems. If these two transcripts are specific to PC12 cell SGs, we would like to know if other neuronal cell lines also produce similar patterns of highly abundant transcripts after carbachol stimulation. Expanding these studies to include characterization of other stress conditions would also be valuable. In the same vein, gaining a more thorough understanding of proteins sequestered

in SGs under different conditions or in different model systems would also be useful to the understanding of neuronal stress response.

Future work regarding chapter 3 outlines the importance of understanding how aging and/or the type of stress applied are factors involved in disassociation of aggregates. Here, expanding chapter 4 could include looking specifically at levels of *ATP5f1b* and *CHGb* in old vs young cells to answer more questions about the specificity of these two mRNAs. In addition, do lower passage cells, or younger *C. elegans* respond differently to environmental stress than older samples? Do these two transcripts remain contained in PC12 SGs for longer or shorter periods of time as a result of age? What are other factors may become impacted by stress when dealing with sophisticated organisms such as *C. elegans* as opposed to cultured cells?

6.3.3 Future work: Aim 2B (Chapter 5)

There is still much to be understood about the impact of intracellular APP aggregation in general, as well as the effects it has due to repeated or extended stress on neurons. It would be valuable to know if identical treatment results in incorporation of *APP* mRNA into other neuronal stress granules, or if it's also present in differentiated PC12 cells after repeating different types of stress such as osmotic stress. Does this type of aggregation occur at higher rates with amyloidogenic or non-amyloidogenic processing in other areas of the APP protein? If so, does this process have a correlation with formation of extracellular plaques associated with AD?

By looking at components like *APP* that are seen to be incorporated in Ago2 SGs in low abundance, we may be able to understand more about the ways in which proteins and mRNAs move in and out of SG aggregations. For example, APP mRNA may loosely associate with Ago2 after a single carbachol stimulation by moving in and out of SG shells, whereas repeated or extended carbachol stimulation causes this mRNA to relocate into the core in higher quantities. Tracking mRNAs identified in lower abundance as a result of certain stress conditions using live cell time series imaging may give us a greater understanding of the dynamic nature of SG shells and how persistent SGs respond to these components with extended stress. We would also like to know what causes irreversible SGs to form, and if cells can contain irreversible and dynamic SGs simultaneously.

Aside from AD, many other neurodegenerative diseases have been linked to SG formation. Considering FXR1 and FXR2, two proteins highly associated with ASD, were also found to be binding partners of cytosolic PLCβ1, it could be interesting to test if continuous neurotransmitter activity impacts their aggregation in a way similar to that of intracellular APP. If so, does this result in phenotypic changes in cell morphology or organism behavior?

6.4 References

1. Martin, S.; Zekri, L.; Metz, A.; Maurice, T.; Chebli, K.; Vignes, M.; Tazi, J., Deficiency of G3BP1, the stress granules assembly factor, results in abnormal synaptic plasticity and calcium homeostasis in neurons. *J Neurochem* **2013,** *125* (2), 175-84.
2. Fernandes, N.; Eshleman, N.; Buchan, J. R., Stress Granules and ALS: A Case of Causation or Correlation? *Adv Neurobiol* **2018,** *20*, 173-212.
3. Li, Y. R.; King, O. D.; Shorter, J.; Gitler, A. D., Stress granules as crucibles of ALS pathogenesis. *J Cell Biol* **2013,** *201* (3), 361-72.
4. Daigle, J. G.; Lanson, N. A., Jr.; Smith, R. B.; Casci, I.; Maltare, A.; Monaghan, J.; Nichols, C. D.; Kryndushkin, D.; Shewmaker, F.; Pandey, U. B., RNA-binding ability of FUS regulates neurodegeneration, cytoplasmic mislocalization and incorporation into stress granules associated with FUS carrying ALS-linked mutations. *Hum Mol Genet* **2013,** *22* (6), 1193-205.
5. Monahan, Z.; Shewmaker, F.; Pandey, U. B., Stress granules at the intersection of autophagy and ALS. *Brain Res* **2016,** *1649* (Pt B), 189-200.
6. Lai, A.; Valdez-Sinon, A. N.; Bassell, G. J., Regulation of RNA granules by FMRP and implications for neurological diseases. *Traffic* **2020,** *21* (7), 454-462.
7. Brown, R. C.; Lockwood, A. H.; Sonawane, B. R., Neurodegenerative diseases: an overview of environmental risk factors. *Environ Health Perspect* **2005,** *113* (9), 1250-6.
8. Campos-Melo, D.; Hawley, Z. C. E.; Droppelmann, C. A.; Strong, M. J., The Integral Role of RNA in Stress Granule Formation and Function. *Front Cell Dev Biol* **2021,** *9*, 621779.
9. Garwain, O.; Pearce, K. M.; Jackson, L.; Carley, S.; Rosati, B.; Scarlata, S., Stimulation of the Gαq/phospholipase Cβ1 signaling pathway returns differentiated cells to a stem-like state. *The FASEB Journal* **2020,** *34* (9), 12663-12676.
10. Shu, R.; Wong, W.; Ma, Q. H.; Yang, Z. Z.; Zhu, H.; Liu, F. J.; Wang, P.; Ma, J.; Yan, S.; Polo, J. M.; Bernard, C. C.; Stanton, L. W.; Dawe, G. S.; Xiao, Z. C., APP intracellular domain acts as a transcriptional regulator of miR-663 suppressing neuronal differentiation. *Cell Death Dis* **2015,** *6*, e1651.
11. Bajar, B. T.; Wang, E. S.; Zhang, S.; Lin, M. Z.; Chu, J., A Guide to Fluorescent Protein FRET Pairs. *Sensors (Basel)* **2016,** *16* (9).
12. Zhou, Y.; Bai, Y.; Chen, C.; Dickenson, J. M., Processing of fluorescence lifetime image using modified phasor approach: homo-FRET from the acceptor. *J Fluoresc* **2013,** *23* (4), 725-32.
13. Lakowicz, J., *Principles of Fluorescence Spectroscopy, Second Edition*. Plenum: New York, 1999.
14. Wheeler, J. R.; Jain, S.; Khong, A.; Parker, R., Isolation of yeast and mammalian stress granule cores. *Methods* **2017,** *126*, 12-17.
15. Protter, D. S. W.; Parker, R., Principles and Properties of Stress Granules. *Trends Cell Biol* **2016,** *26* (9), 668-679.

7 Appendix

7.1 Chapter 3 supporting material

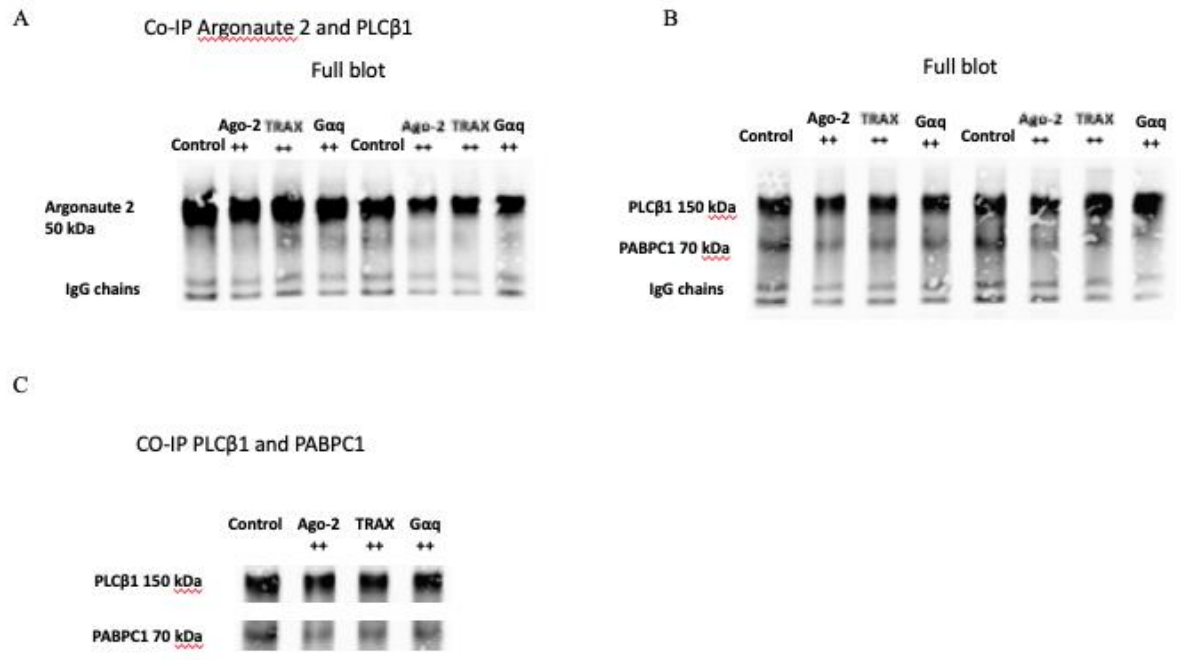

Figure S3.1 Western blotting analysis of proteins co-immunoprecipitated with Ago2 and PLCβ1. (**A** and **B**) Co-immunoprecipitation (CoIP) of PLCβ1 and Ago2 from the lysates of transfected PC12 cells expressing Ago2, TRAX, or Gαq as indicated. Antibodies used for CoIP and Western blotting are indicated. Blots are representative of two independent experiments. (**C**) CoIP of PLCβ1 and PABPC1 from the lysates of transfected PC12 cells expressing Ago2, TRAX, or Gαq as indicated. Antibodies used for CoIP and Western blotting are indicated. Blots are representative of two independent experiments.

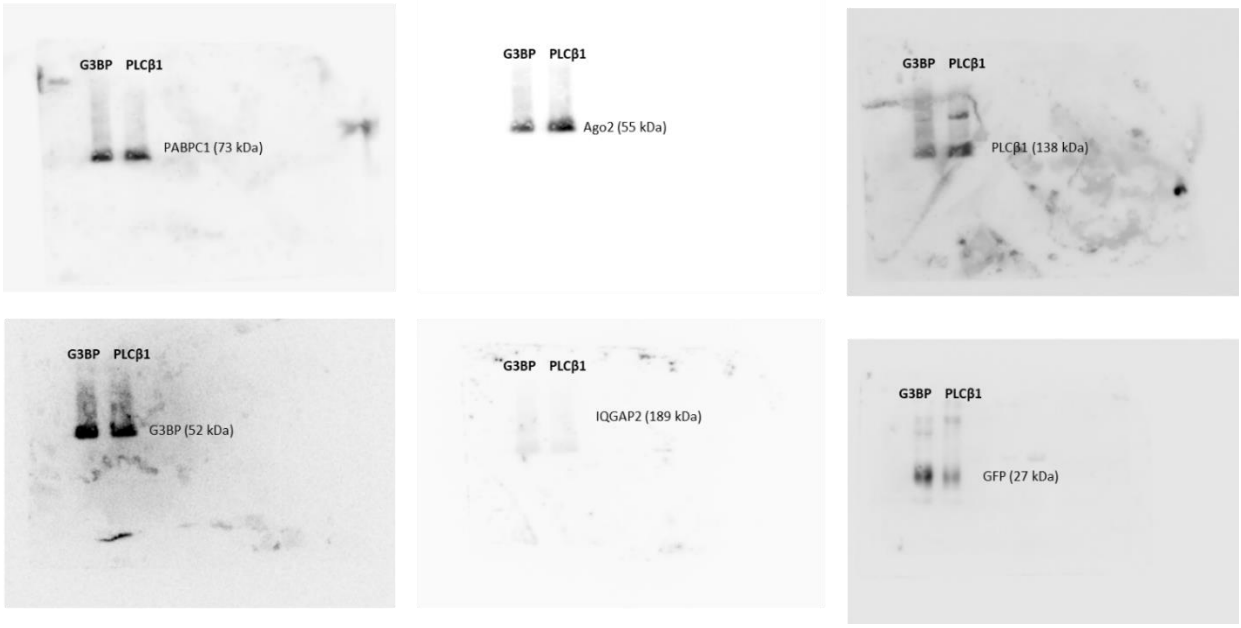

Figure S3.2 Pull-down of eGFP-PLCβ1 and eGFP-G3BP1 in PC12 cells. CoIP of GFP from the lysates of transfected PC12 cells expressing eGFP-PLCβ1 or eGFP-G3BP as indicated. Western blots are representative of five experiments for PLCβ1, PABPC1 and Ago2, and of two experiments for G3BP1. A nonbinding control, IQGAP2, was undetectable. Antibodies used for CoIP and Western blots are G3BP1, PABPC1, Ago2, PLCβ1, IQGAP2 and GFP.

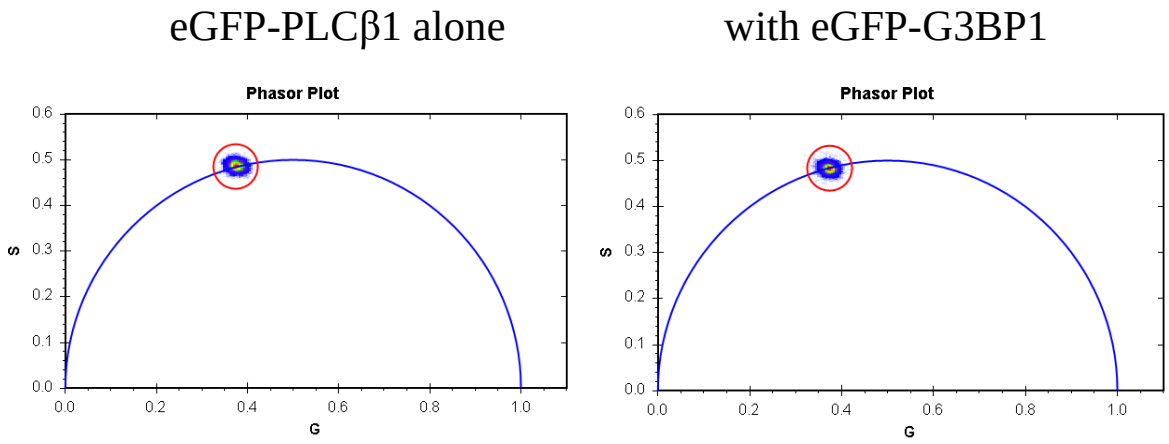

Figure S3.3 FLIM/FRET analysis showing the lack of association between eGFP-PLCβ and eGFP-G3BP1. Phasor plot of eGFP-PLCβ1 alone (left) and in cells cotransfected with plasmid encoding eGFP-G3BP1 (right), where the lifetime remained constant at 2.60 ns.

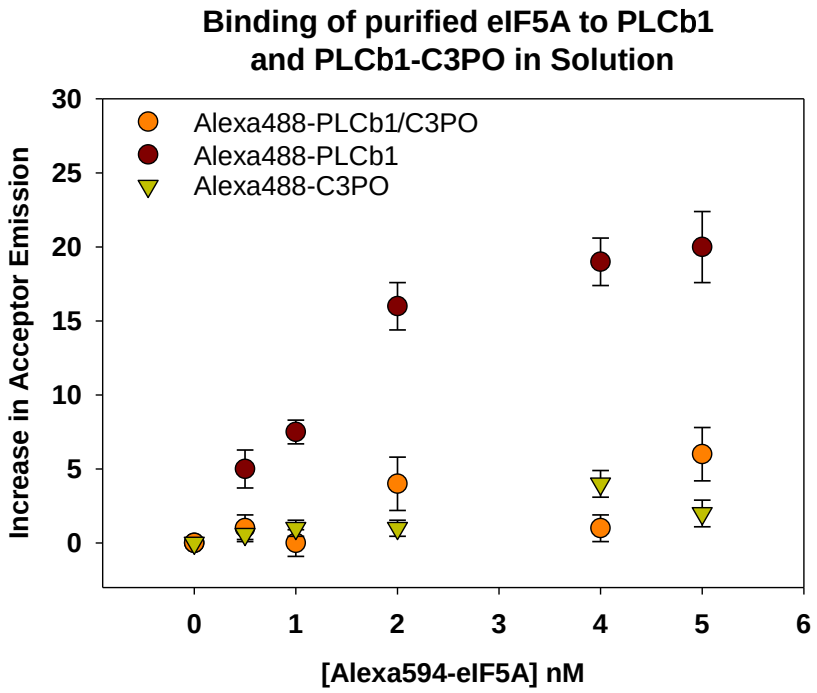

Figure S3.4 Competition between eIF5A and C3PO for binding to PLCβ1 in PC12 cells. Fluorescence binding studies showing changes in FRET between purified Alexa594-eIF5A titrated into solutions of Alexa488-PLCβ1(brown circles), the Alexa488-PLCβ1:C3PO complex (orange circles), or Alexa488-C3PO (green triangles). FRET was determined by subtracting the fluorescence intensity of Alexa594-eIF5A alone from its intensity in the presence of the different labeled proteins (sensitized emission). Data were corrected for background and are from three experiments; bars represent SD.

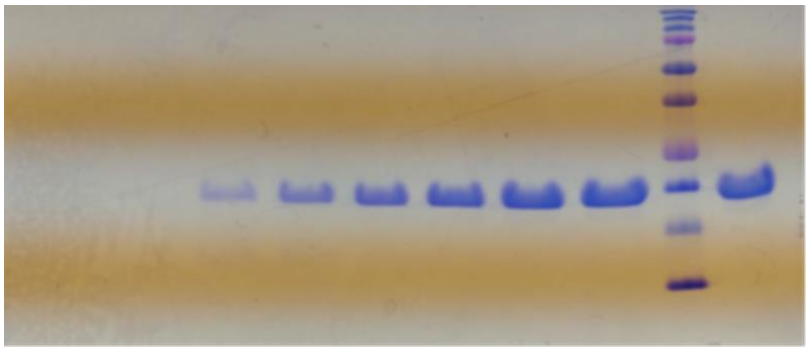

Figure S3.5 Analysis of eIF5A purity. Proteins were purified and labeled with fluorescent probes as described in the Materials and Methods. The Coomassie-stained SDS-PAGE gel shows the purity of eIF5A. Data are representative of 7 experiments.

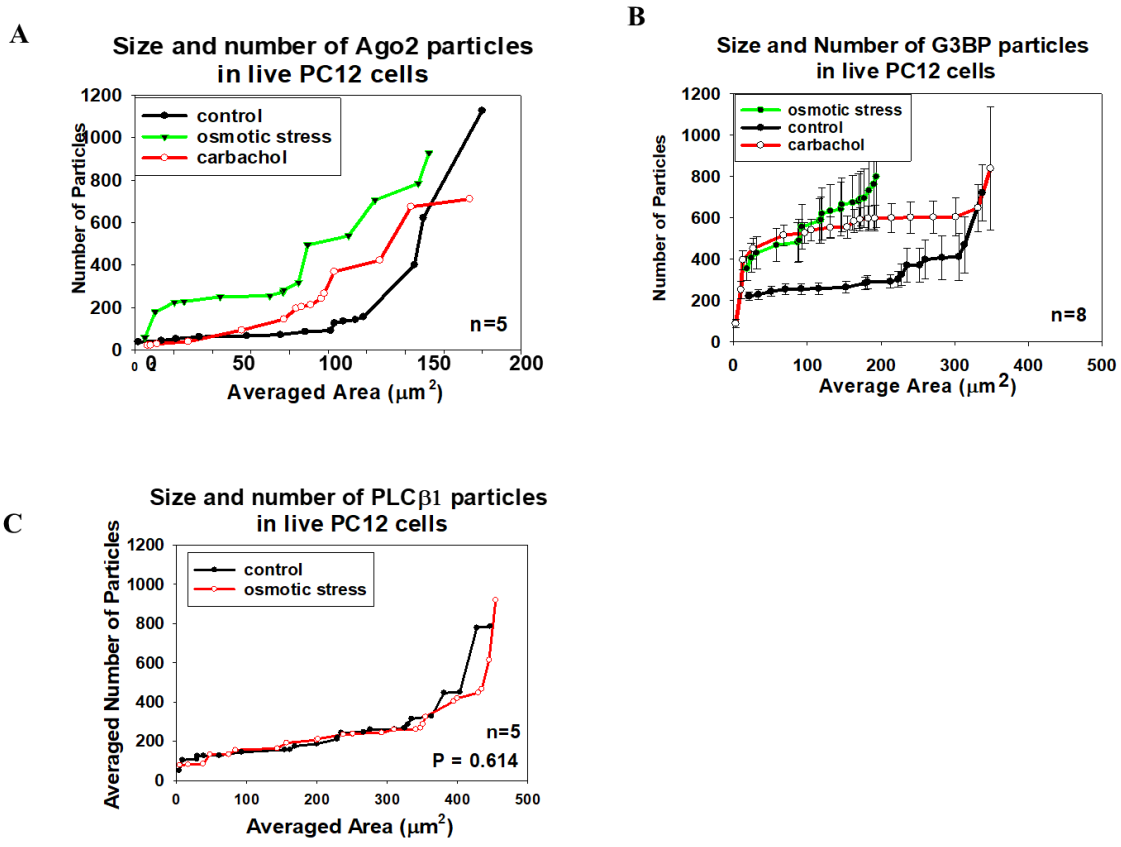

Figure S3.6 The effect of Gαq activation and hypo-osmotic stress on the formation of Ago2, G3BP1-, and PLCβ1-associated particles in PC12 cells. (**A**) Analysis of particles associated with mCherry-Ago2 in live PC12 cells under control conditions, after exposure to 150 mOsm osmotic stress for 5 min, and after stimulation with 5 μM carbachol. (**B**) Analysis of particles associated with eGFP-G3BP1 in live PC12 cells under control conditions, after exposure to 150 mOsm

osmotic stress for 5 min, and after stimulation with 5 µM carbachol. (**C**) Particles associated with eGFP-PLCβ1 in live cells under basal (300 mOsm) conditions and after osmotic stress (150 mOsm, 5 min). These data are an average of three independent experiments that each sampled five cells. For (**B**) and (**C**), bars indicate SD, whereas for (**A**), bars indicate SEM. The P values compare control versus osmotic stress conditions and were determined by ANOVA.

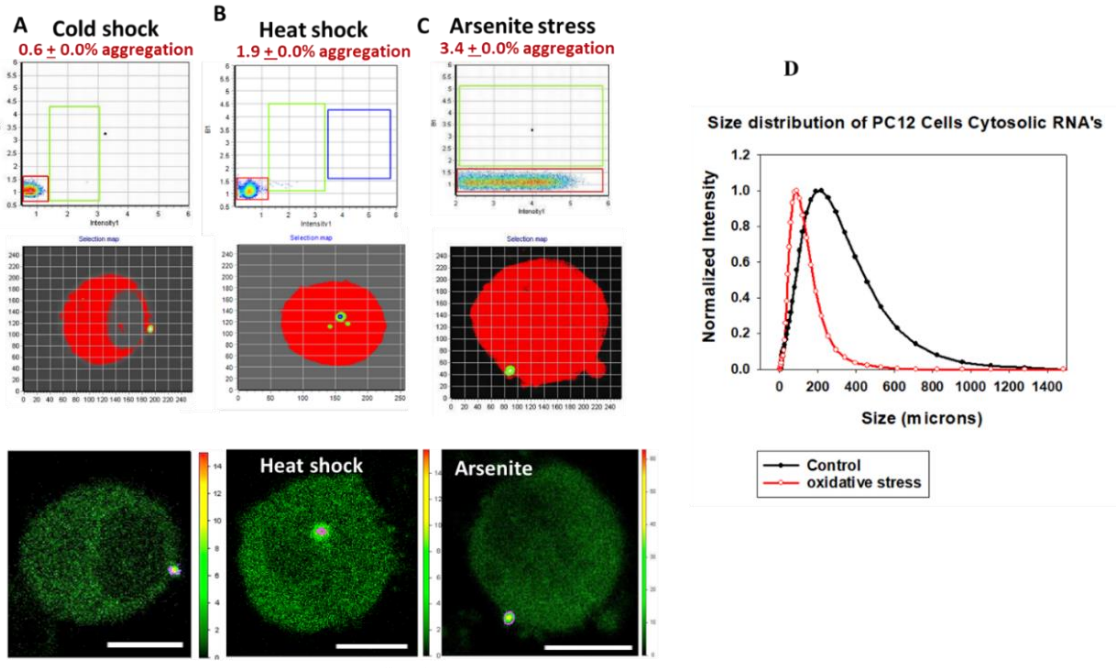

Figure S3.7 N&B analysis of eGFP-Ago2 aggregation in PC12 cells. (**A** to **C**) Data are from (**A**) cells subjected to cold shock at 12oC for 1 hour (n=six experiments), (**B**) cells subjected to heat shock at 40oC for 1 hour (n=six experiments); and (**C**) cells subjected to arsenite stress (0.5 mM, 10 min) (n=five experiments), Scale bars=10 µm. (**D**) The size distribution of cytosolic RNA isolated from PC12 cells was measured by dynamic light scattering (n=three experiments) for control conditions (black) and oxidative stress (1 mM CoCl2 for 12 to 16 hours, red).

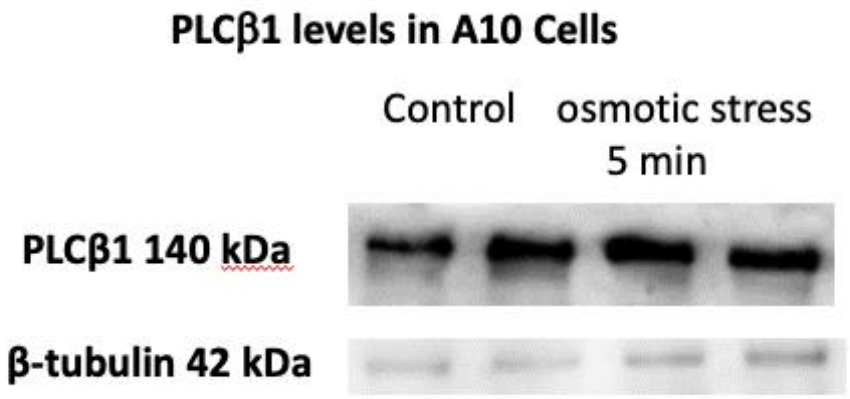

Figure S3.8 Western blot showing changes in the level of PLCβ1 in A10 cells under basal conditions and subjected to hypo-osmotic stress (150 mOsm for 5 min) (n=2). Densitometry comparing lanes 1 and 2 to 3 and 4, and accounting for differences in sample loading, show a 30-50% reduction in PLCβ1 levels.

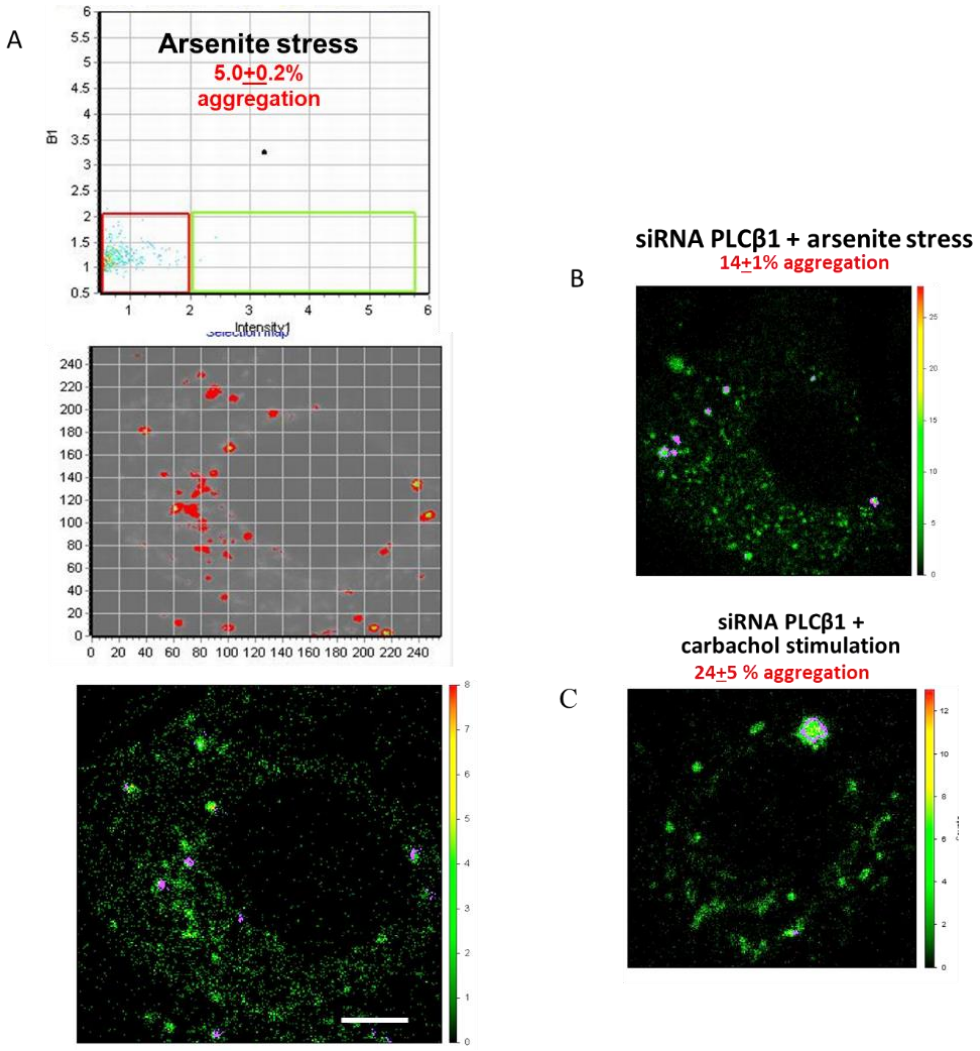

Figure S3.9 The effect of PLCβ1 on the formation of Ago2-associated particles in WKO-3M22 cells as monitored by N&B analysis. (**A**) N&B analysis of brightness versus intensity for PC12 cells under arsenite stress with the pixels of the colored boxes corresponding to specific regions in the cells with SIM-FCS 4. These cells were subjected to arsenite stress (0.5 mM for 10 min). Red boxes correspond to monomeric eGFP-Ago2 as determined by free eGFP. Points outside this box and in the green and blue boxes correspond to higher-order species. Scale bars=10 μm. The corresponding fluorescence microscopy images in ISS are shown. (**B** and **C**) Data in (**B**) show cells treated with siRNA(PLCβ1) and arsenite (0.5 mM for 10 min) whereas data in (**C**) show cells treated with siRNA(PLCβ1) and stimulated with carbachol (5 μM for 10 min). Data are from three experiments with nine cells analyzed per experiment.

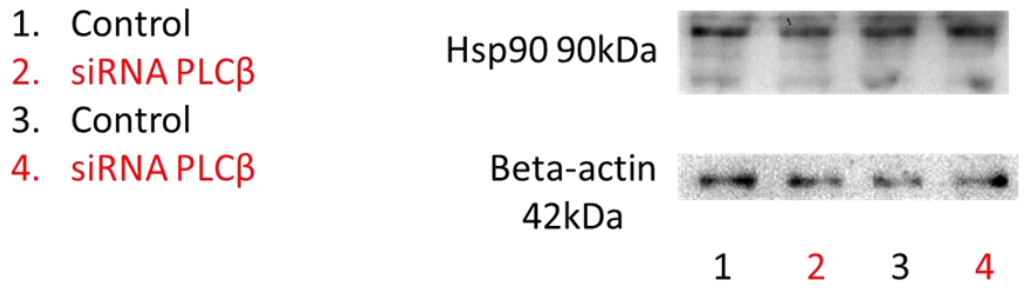

Figure S3.10 Effect of siRNA(PLCβ1) on Hsp90 abundance. Western blotting analysis of changes in Hsp90 abundance in undifferentiated PC12 cells that were treated with siRNA(PLCβ1). Cell treatments and Western blotting analysis were performed as described in the Results. Data are from two experiments.

7.2 Chapter 4 supporting material

Table S4.1 Proteins bound to Ago2 stress granules in non-stressed PC12 cells.

	Protein	Accession #	Alternate ID	M.W.	Spectrum count
mRNA related proteins:					
1	sp|Q3ZAV8|EDC4_RAT Enhancer of mRNA-decapping protein 4 OS=Rattus norvegicus OX=10116 GN=Edc4 PE=1 SV=1	sp|Q3ZAV8|EDC4_RAT (+2)	Edc4	153 kDa	99% (1)
2	tr|A0A091DGJ7|A0A091DGJ7_FUKDA mRNA-capping enzyme (Fragment) OS=Fukomys damarensis OX=885580 GN=H920_09191 PE=4 SV=1	tr|A0A091DGJ7|A0A091DGJ7_FUKDA (+6)	H920_09191	53 kDa	99% (1)
3	tr|A0A091DJ53|A0A091DJ53_FUKDA Pre-mRNA-splicing factor 38B OS=Fukomys damarensis OX=885580 GN=H920_15753 PE=4 SV=1	tr|A0A091DJ53|A0A091DJ53_FUKDA (+3)	H920_15753	59 kDa	99% (1)
4	tr|A0A1S3EQY6|A0A1S3EQY6_DIPOR regulation of nuclear pre-mRNA domain-containing protein 1B isoform X2 OS=Dipodomys ordii OX=10020 GN=Rprd1b PE=4 SV=1	tr|A0A1S3EQY6|A0A1S3EQY6_DIPOR (+3)	Rprd1b	35 kDa	99% (1)
5	tr|A0A1S3FCW4|A0A1S3FCW4_DIPOR pre-mRNA-processing factor 40 homolog B isoform X2 OS=Dipodomys ordii OX=10020 GN=Prpf40b PE=4 SV=1	tr|A0A1S3FCW4|A0A1S3FCW4_DIPOR (+2)	Prpf40b	98 kDa	99% (1)
Transcription factors:					
1	tr|A0A091CZI5|A0A091CZI5_FUKDA General transcription factor 3C polypeptide 2 OS=Fukomys damarensis OX=885580 GN=H920_15241 PE=3 SV=1	tr|A0A091CZI5|A0A091CZI5_FUKDA	H920_15241	162 kDa	100% (2)
2	tr|A0A0G2K7N8|A0A0G2K7N8_RAT Bromodomain PHD finger transcription factor OS=Rattus norvegicus OX=10116 GN=Bptf PE=1 SV=1	tr|A0A0G2K7N8|A0A0G2K7N8_RAT	Bptf	304 kDa	100% (2)
3	tr|A0A0P6JTL2|A0A0P6JTL2_HETGA HMG box transcription factor BBX isoform 1 OS=Heterocephalus glaber OX=10181 GN=BBX PE=4 SV=1	tr|A0A0P6JTL2|A0A0P6JTL2_HETGA (+1)	BBX	105 kDa	99% (2)
4	sp|F1LMN3-2|E2F8_RAT Isoform 2 of Transcription factor E2F8 OS=Rattus norvegicus OX=10116 GN=E2f8	sp|F1LMN3-2|E2F8_RAT (+2)	E2f8	94 kDa	99% (1)
5	sp|P0C6P6|TYY2_RAT Transcription factor YY2 OS=Rattus norvegicus OX=10116 GN=Yy2 PE=3 SV=1	sp|P0C6P6|TYY2_RAT (+4)	Yy2	42 kDa	99% (1)
6	sp|P46153|GATA6_RAT Transcription factor GATA-6 OS=Rattus norvegicus OX=10116 GN=Gata6 PE=1 SV=2	sp|P46153|GATA6_RAT (+1)	Gata6	59 kDa	99% (1)
7	sp|P70486|ATRX_RAT Transcriptional regulator ATRX (Fragment) OS=Rattus norvegicus OX=10116 GN=Atrx PE=1 SV=1	sp|P70486|ATRX_RAT	Atrx	59 kDa	99% (1)
8	sp|Q4QR87|DMRTC_RAT Doublesex- and mab-3-related transcription factor C1 OS=Rattus norvegicus OX=10116 GN=Dmrtc1 PE=2 SV=1	sp|Q4QR87|DMRTC_RAT	Dmrtc1	24 kDa	99% (1)
9	sp|Q561Q8|MED4_RAT Mediator of RNA polymerase II transcription subunit 4 OS=Rattus norvegicus OX=10116 GN=Med4 PE=2 SV=1	sp|Q561Q8|MED4_RAT (+3)	Med4	30 kDa	99% (1)
10	sp|Q66HG1|DMTF1_RAT Cyclin-D-binding Myb-like transcription factor 1 OS=Rattus norvegicus OX=10116 GN=Dmtf1 PE=2 SV=2	sp|Q66HG1|DMTF1_RAT (+4)	Dmtf1	84 kDa	99% (1)
11	sp|Q6AXU9|CNOT6_RAT CCR4-NOT transcription complex subunit 6	sp|Q6AXU9|CNOT6_RAT (+5)	Cnot6	63 kDa	99% (1)

	OS=Rattus norvegicus OX=10116 GN=Cnot6 PE=2 SV=1				
12	tr|A0A091CQ14|A0A091CQ14_FUKDA Transcription initiation factor TFIID subunit 7 OS=Fukomys damarensis OX=885580 GN=H920_19286 PE=4 SV=1	tr|A0A091CQ14|A0A091CQ14_FUKDA (+4)	H920_19286	40 kDa	99% (1)
13	tr|A0A091CQ91|A0A091CQ91_FUKDA Transcription factor NF-E2 45 kDa subunit OS=Fukomys damarensis OX=885580 GN=H920_17342 PE=3 SV=1	tr|A0A091CQ91|A0A091CQ91_FUKDA (+1)	H920_17342	41 kDa	99% (1)
14	tr|A0A091CYB9|A0A091CYB9_FUKDA Mediator of RNA polymerase II transcription subunit 11 OS=Fukomys damarensis OX=885580 GN=MED11 PE=3 SV=1	tr|A0A091CYB9|A0A091CYB9_FUKDA	MED11	13 kDa	99% (1)
15	tr|A0A091D225|A0A091D225_FUKDA Signal transducer and activator of transcription OS=Fukomys damarensis OX=885580 GN=H920_14054 PE=3 SV=1	tr|A0A091D225|A0A091D225_FUKDA	H920_14054	96 kDa	99% (1)
16	tr|A0A091D7D7|A0A091D7D7_FUKDA Pre-B-cell leukemia transcription factor 2 OS=Fukomys damarensis OX=885580 GN=H920_19927 PE=4 SV=1	tr|A0A091D7D7|A0A091D7D7_FUKDA	H920_19927	36 kDa	99% (1)
17	tr|A0A091D8Y4|A0A091D8Y4_FUKDA Transcription elongation factor A N-terminal and central domain-containing protein OS=Fukomys damarensis OX=885580 GN=H920_19321 PE=4 SV=1	tr|A0A091D8Y4|A0A091D8Y4_FUKDA	H920_19321	40 kDa	99% (1)
18	tr|A0A091DJB3|A0A091DJB3_FUKDA Transcription initiation factor TFIID subunit 13 OS=Fukomys damarensis OX=885580 GN=H920_07981 PE=4 SV=1	tr|A0A091DJB3|A0A091DJB3_FUKDA	H920_07981	13 kDa	99% (1)
19	tr|A0A091DWM1|A0A091DWM1_FUKDA Leucine-zipper-like transcriptional regulator 1 OS=Fukomys damarensis OX=885580 GN=H920_03876 PE=4 SV=1	tr|A0A091DWM1|A0A091DWM1_FUKDA (+1)	H920_03876	162 kDa	99% (1)
20	tr|A0A091DXE6|A0A091DXE6_FUKDA Transcription factor MafG OS=Fukomys damarensis OX=885580 GN=H920_02946 PE=3 SV=1	tr|A0A091DXE6|A0A091DXE6_FUKDA	H920_02946	25 kDa	99% (1)
21	tr|A0A091E162|A0A091E162_FUKDA General transcription factor IIF subunit 1 (Fragment) OS=Fukomys damarensis OX=885580 GN=H920_09738 PE=4 SV=1	tr|A0A091E162|A0A091E162_FUKDA (+1)	H920_09738	58 kDa	99% (1)
tRNA related proteins:					
1	sp|Q5U2R4|TM10C_RAT tRNA methyltransferase 10 homolog C OS=Rattus norvegicus OX=10116 GN=Trmt10c PE=2 SV=1	sp|Q5U2R4|TM10C_RAT	Trmt10c	48 kDa	99% (1)
2	sp|Q6P7B0|SYWC_RAT Tryptophan--tRNA ligase, cytoplasmic OS=Rattus norvegicus OX=10116 GN=Wars PE=1 SV=2	sp|Q6P7B0|SYWC_RAT (+2)	Wars	54 kDa	99% (1)
3	tr|A0A091CTZ7|A0A091CTZ7_FUKDA Valyl-tRNA synthetase OS=Fukomys damarensis OX=885580 GN=H920_17559 PE=3 SV=1	tr|A0A091CTZ7|A0A091CTZ7_FUKDA	H920_17559	279 kDa	99% (1)
4	tr|A0A091D935|A0A091D935_FUKDA Putative histidyl-tRNA synthetase, mitochondrial OS=Fukomys damarensis OX=885580 GN=H920_19277 PE=4 SV=1	tr|A0A091D935|A0A091D935_FUKDA	H920_19277	57 kDa	99% (1)
5	tr|A0A091DKK1|A0A091DKK1_FUKDA Putative tRNA (Adenine-N(1)-)-methyltransferase catalytic subunit TRMT61B OS=Fukomys damarensis OX=885580 GN=H920_15222 PE=4 SV=1	tr|A0A091DKK1|A0A091DKK1_FUKDA	H920_15222	53 kDa	99% (1)
6	tr|A0A091EFK3|A0A091EFK3_FUKDA rRNA/tRNA 2'-O-methyltransferase fibrillarin-like protein 1 OS=Fukomys damarensis OX=885580 GN=H920_04477 PE=3 SV=1	tr|A0A091EFK3|A0A091EFK3_FUKDA (+2)	H920_04477	29 kDa	99% (1)
7	tr|A0A091EHA5|A0A091EHA5_FUKDA tRNA (Uracil-5-)-methyltransferase like	tr|A0A091EHA5|A0A091EHA5_FUKDA (+2)	H920_03849	69 kDa	99% (1)

	protein A OS=Fukomys damarensis OX=885580 GN=H920_03849 PE=3 SV=1				
8	tr|A0A0P6K236|A0A0P6K236_HETGA Queuine tRNA-ribosyltransferase accessory subunit 2 OS=Heterocephalus glaber OX=10181 GN=QTRTD1 PE=3 SV=1	tr|A0A0P6K236|A0A0P6K236_HETGA (+2)	QTRTD1	40 kDa	99% (1)
9	tr|A0A1S3ENC1|A0A1S3ENC1_DIPOR tRNA-splicing endonuclease subunit Sen2 OS=Dipodomys ordii OX=10020 GN=Tsen2 PE=3 SV=1	tr|A0A1S3ENC1|A0A1S3ENC1_DIPOR	Tsen2	50 kDa	99% (1)
10	tr|A0A1S3F901|A0A1S3F901_DIPOR probable tRNA pseudouridine synthase 1 isoform X2 OS=Dipodomys ordii OX=10020 GN=Trub1 PE=3 SV=1	tr|A0A1S3F901|A0A1S3F901_DIPOR	Trub1	37 kDa	99% (1)
11	tr|A0A1S3FQU3|A0A1S3FQU3_DIPOR probable cysteine--tRNA ligase, mitochondrial OS=Dipodomys ordii OX=10020 GN=Cars2 PE=3 SV=1	tr|A0A1S3FQU3|A0A1S3FQU3_DIPOR	Cars2	62 kDa	99% (1)
12	tr|A0A1S3FRN5|A0A1S3FRN5_DIPOR tRNA methyltransferase 10 homolog A OS=Dipodomys ordii OX=10020 GN=Trmt10a PE=4 SV=1	tr|A0A1S3FRN5|A0A1S3FRN5_DIPOR	Trmt10a	39 kDa	99% (1)
13	tr|A0A1S3FSX0|A0A1S3FSX0_DIPOR probable tRNA methyltransferase 9-like protein OS=Dipodomys ordii OX=10020 GN=Kiaa1456 PE=4 SV=1	tr|A0A1S3FSX0|A0A1S3FSX0_DIPOR	Kiaa1456	50 kDa	99% (1)
14	tr|F1M9C9|F1M9C9_RAT Histidyl-tRNA synthetase 2, mitochondrial OS=Rattus norvegicus OX=10116 GN=Hars2 PE=1 SV=1	tr|F1M9C9|F1M9C9_RAT	Hars2	57 kDa	99% (1)
15	tr|M0R4L6|M0R4L6_RAT Glutamyl-tRNA(Gln) amidotransferase subunit B, mitochondrial OS=Rattus norvegicus OX=10116 GN=Gatb PE=1 SV=1	tr|M0R4L6|M0R4L6_RAT	Gatb	62 kDa	99% (1)
16	tr|Q5XI86|Q5XI86_RAT Peptidyl-tRNA hydrolase 2 OS=Rattus norvegicus OX=10116 GN=Ptrh2 PE=1 SV=1	tr|Q5XI86|Q5XI86_RAT	Ptrh2	20 kDa	99% (1)
RNA polymerases:					
1	sp|Q68FQ7|RPAP3_RAT RNA polymerase II-associated protein 3 OS=Rattus norvegicus OX=10116 GN=Rpap3 PE=1 SV=1	sp|Q68FQ7|RPAP3_RAT	Rpap3	75 kDa	100% (2)
2	sp|Q561Q8|MED4_RAT Mediator of RNA polymerase II transcription subunit 4 OS=Rattus norvegicus OX=10116 GN=Med4 PE=2 SV=1	sp|Q561Q8|MED4_RAT (+3)	Med4	30 kDa	99% (1)
3	tr|A0A091CM74|A0A091CM74_FUKDA DNA-directed RNA polymerase I subunit RPA34 OS=Fukomys damarensis OX=885580 GN=H920_19646 PE=4 SV=1	tr|A0A091CM74|A0A091CM74_FUKDA	H920_19646	54 kDa	99% (1)
4	tr|A0A091CYB9|A0A091CYB9_FUKDA Mediator of RNA polymerase II transcription subunit 11 OS=Fukomys damarensis OX=885580 GN=MED11 PE=3 SV=1	tr|A0A091CYB9|A0A091CYB9_FUKDA	MED11	13 kDa	99% (1)
5	tr|A0A091DKK2|A0A091DKK2_FUKDA DNA-directed RNA polymerase subunit OS=Fukomys damarensis OX=885580 GN=H920_05967 PE=3 SV=1	tr|A0A091DKK2|A0A091DKK2_FUKDA	H920_05967	194 kDa	99% (1)
6	tr|A0A091DT96|A0A091DT96_FUKDA DNA-directed RNA polymerase III subunit RPC5 OS=Fukomys damarensis OX=885580 GN=H920_05042 PE=4 SV=1	tr|A0A091DT96|A0A091DT96_FUKDA	H920_05042	83 kDa	99% (1)
7	tr|A0A0S3NTA3|A0A0S3NTA3_9MURI RRN3 RNA polymerase I transcription factor homolog OS=Tokudaia muenninki OX=742503 GN=RRN3 PE=4 SV=1	tr|A0A0S3NTA3|A0A0S3NTA3_9MURI (+1)	RRN3	75 kDa	99% (1)
8	tr|A0A1S3GHX3|A0A1S3GHX3_DIPOR DNA-directed RNA polymerases I, II, and III subunit RPABC3 isoform X2 OS=Dipodomys ordii OX=10020 GN=Polr2h PE=4 SV=1	tr|A0A1S3GHX3|A0A1S3GHX3_DIPOR	Polr2h	14 kDa	99% (1)

9	tr|D3ZYB6|D3ZYB6_RAT DNA-directed RNA polymerase OS=Rattus norvegicus OX=10116 GN=Polrmt PE=3 SV=2	tr|D3ZYB6|D3ZYB6_RAT	Polrmt	136 kDa	99% (1)
Heat shock proteins:					
1	sp|O88600|HSP74_RAT Heat shock 70 kDa protein 4 OS=Rattus norvegicus OX=10116 GN=Hspa4 PE=1 SV=1	sp|O88600|HSP74_RAT (+1)	Hspa4	94 kDa	99% (1)
2	tr|A0A091DFA4|A0A091DFA4_FUKDA Heat shock 70 kDa protein 12A (Fragment) OS=Fukomys damarensis OX=885580 GN=H920_09610 PE=4 SV=1	tr|A0A091DFA4|A0A091DFA4_FUKDA (+2)	H920_09610	74 kDa	99% (1)
3	tr|A0A0P6IYL2|A0A0P6IYL2_HETGA Heat shock factor-binding protein 1 OS=Heterocephalus glaber OX=10181 GN=HSBP1 PE=4 SV=1	tr|A0A0P6IYL2|A0A0P6IYL2_HETGA (+1)	HSBP1	9 kDa	99% (1)
4	tr|A0A0P6JD03|A0A0P6JD03_HETGA Heat shock 70 kDa protein 1A/1B OS=Heterocephalus glaber OX=10181 GN=HSPA1A PE=3 SV=1	tr|A0A0P6JD03|A0A0P6JD03_HETGA	HSPA1A	70 kDa	99% (1)
5	tr|G5BWP2|G5BWP2_HETGA Heat shock cognate 71 kDa protein OS=Heterocephalus glaber OX=10181 GN=GW7_16362 PE=4 SV=1	tr|G5BWP2|G5BWP2_HETGA	GW7_16362	14 kDa	99% (1)
Stress proteins:					
1	tr|A0A091DZQ9|A0A091DZQ9_FUKDA Oxidative stress-induced growth inhibitor 1 OS=Fukomys damarensis OX=885580 GN=H920_02833 PE=4 SV=1	tr|A0A091DZQ9|A0A091DZQ9_FUKDA	H920_02833	92 kDa	99% (1)
2	tr|G5BFX7|G5BFX7_HETGA Oxidative stress-induced growth inhibitor 1 OS=Heterocephalus glaber OX=10181 GN=OSGIN1 PE=4 SV=1	tr|G5BFX7|G5BFX7_HETGA	OSGIN1	51 kDa	99% (1)
Translation initiation proteins:					
1	tr|F1LN59|F1LN59_RAT Eukaryotic translation initiation factor 4, gamma 2 OS=Rattus norvegicus OX=10116 GN=Eif4g2 PE=1 SV=2	tr|F1LN59|F1LN59_RAT	Eif4g2	102 kDa	100% (2)
2	sp|Q62818|EI2BB_RAT Translation initiation factor eIF-2B subunit beta OS=Rattus norvegicus OX=10116 GN=Eif2b2 PE=2 SV=1	sp|Q62818|EI2BB_RAT	Eif2b2	39 kDa	99% (1)
3	sp|Q64270|EI2BA_RAT Translation initiation factor eIF-2B subunit alpha OS=Rattus norvegicus OX=10116 GN=Eif2b1 PE=2 SV=1	sp|Q64270|EI2BA_RAT (+3)	Eif2b1	34 kDa	99% (1)
4	tr|A0A091DM45|A0A091DM45_FUKDA Eukaryotic translation initiation factor 4 gamma 1 OS=Fukomys damarensis OX=885580 GN=H920_07067 PE=4 SV=1	tr|A0A091DM45|A0A091DM45_FUKDA	H920_07067	20 kDa	99% (1)
5	tr|A0A0P6J8P2|A0A0P6J8P2_HETGA Translation initiation factor eIF-2B subunit delta isoform 3 OS=Heterocephalus glaber OX=10181 GN=EIF2B4 PE=3 SV=1	tr|A0A0P6J8P2|A0A0P6J8P2_HETGA (+1)	EIF2B4	58 kDa	99% (1)
6	tr|D3ZUV3|D3ZUV3_RAT Eukaryotic translation initiation factor 2A OS=Rattus norvegicus OX=10116 GN=Eif2a PE=1 SV=3	tr|D3ZUV3|D3ZUV3_RAT	Eif2a	65 kDa	99% (1)
7	tr|G5BAU6|G5BAU6_HETGA Eukaryotic translation initiation factor 2 subunit 2 OS=Heterocephalus glaber OX=10181 GN=GW7_19087 PE=4 SV=1	tr|G5BAU6|G5BAU6_HETGA	GW7_19087	23 kDa	99% (1)
8	tr|G5C5F9|G5C5F9_HETGA Eukaryotic translation initiation factor 1A OS=Heterocephalus glaber OX=10181 GN=GW7_10528 PE=4 SV=1	tr|G5C5F9|G5C5F9_HETGA	GW7_10528	7 kDa	99% (1)
9	tr|G5C9S0|G5C9S0_HETGA Eukaryotic translation initiation factor 2 subunit 2 OS=Heterocephalus glaber OX=10181 GN=GW7_19390 PE=4 SV=1	tr|G5C9S0|G5C9S0_HETGA	GW7_19390	26 kDa	99% (1)
Calcium related proteins:					

1	sp|O70150-2|KCC1B_RAT Isoform 2 of Calcium/calmodulin-dependent protein kinase type 1B OS=Rattus norvegicus OX=10116 GN=Pnck	sp|O70150-2|KCC1B_RAT (+2)	Pnck	38 kDa	99% (1)
2	sp|O88751|CABP1_RAT Calcium-binding protein 1 OS=Rattus norvegicus OX=10116 GN=Cabp1 PE=1 SV=2	sp|O88751|CABP1_RAT	Cabp1	33 kDa	99% (1)
3	sp|O88831-2|KKCC2_RAT Isoform 2 of Calcium/calmodulin-dependent protein kinase kinase 2 OS=Rattus norvegicus OX=10116 GN=Camkk2	sp|O88831-2|KKCC2_RAT (+11)	Camkk2	60 kDa	99% (1)
4	sp|P11507-2|AT2A2_RAT Isoform 2 of Sarcoplasmic/endoplasmic reticulum calcium ATPase 2 OS=Rattus norvegicus OX=10116 GN=Atp2a2	sp|P11507-2|AT2A2_RAT (+1)	Atp2a2	110 kDa	99% (1)
5	sp|P70606|KCNN1_RAT Small conductance calcium-activated potassium channel protein 1 OS=Rattus norvegicus OX=10116 GN=Kcnn1 PE=1 SV=2	sp|P70606|KCNN1_RAT (+1)	Kcnn1	59 kDa	99% (1)
6	sp|Q66HC0|EFCB3_RAT EF-hand calcium-binding domain-containing protein 3 OS=Rattus norvegicus OX=10116 GN=Efcab3 PE=1 SV=1	sp|Q66HC0|EFCB3_RAT (+1)	Efcab3	50 kDa	99% (1)
7	sp|Q8R4C1|AT2C2_RAT Calcium-transporting ATPase type 2C member 2 OS=Rattus norvegicus OX=10116 GN=Atp2c2 PE=2 SV=1	sp|Q8R4C1|AT2C2_RAT (+2)	Atp2c2	103 kDa	99% (1)
8	tr|A0A091CWE7|A0A091CWE7_FUKDA Calcium-binding mitochondrial carrier protein Aralar1 OS=Fukomys damarensis OX=885580 GN=H920_16194 PE=3 SV=1	tr|A0A091CWE7|A0A091CWE7_FUKDA (+1)	H920_16194	75 kDa	99% (1)
9	tr|A0A091DQX2|A0A091DQX2_FUKDA Calcium/calmodulin-dependent protein kinase type 1D OS=Fukomys damarensis OX=885580 GN=H920_04046 PE=4 SV=1	tr|A0A091DQX2|A0A091DQX2_FUKDA	H920_04046	40 kDa	99% (1)
10	tr|A0A091E2H6|A0A091E2H6_FUKDA Voltage-dependent calcium channel subunit alpha-2/delta-1 (Fragment) OS=Fukomys damarensis OX=885580 GN=H920_01037 PE=4 SV=1	tr|A0A091E2H6|A0A091E2H6_FUKDA	H920_01037	106 kDa	99% (1)
11	tr|A0A091E627|A0A091E627_FUKDA EF-hand calcium-binding domain-containing protein 1 OS=Fukomys damarensis OX=885580 GN=H920_07944 PE=4 SV=1	tr|A0A091E627|A0A091E627_FUKDA	H920_07944	40 kDa	99% (1)
12	tr|A0A091EH55|A0A091EH55_FUKDA Voltage-dependent T-type calcium channel subunit alpha-1H OS=Fukomys damarensis OX=885580 GN=H920_03779 PE=4 SV=1	tr|A0A091EH55|A0A091EH55_FUKDA	H920_03779	250 kDa	99% (1)
13	tr|A0A1S3EPA1|A0A1S3EPA1_DIPOR EF-hand calcium-binding domain-containing protein 12 OS=Dipodomys ordii OX=10020 GN=Efcab12 PE=4 SV=1	tr|A0A1S3EPA1|A0A1S3EPA1_DIPOR	Efcab12	69 kDa	99% (1)
14	tr|A0A1S3EXH2|A0A1S3EXH2_DIPOR calcium/calmodulin-dependent protein kinase kinase 1 OS=Dipodomys ordii OX=10020 GN=Camkk1 PE=4 SV=1	tr|A0A1S3EXH2|A0A1S3EXH2_DIPOR	Camkk1	50 kDa	99% (1)
15	tr|A0A1S3GF99|A0A1S3GF99_DIPOR EF-hand calcium-binding domain-containing protein 3-like OS=Dipodomys ordii OX=10020 GN=LOC105997496 PE=4 SV=1	tr|A0A1S3GF99|A0A1S3GF99_DIPOR	LOC105997496	43 kDa	99% (1)
16	tr|A0A1S3GL91|A0A1S3GL91_DIPOR voltage-dependent P/Q-type calcium channel subunit alpha-1A OS=Dipodomys ordii OX=10020 GN=Cacna1a PE=3 SV=1	tr|A0A1S3GL91|A0A1S3GL91_DIPOR	Cacna1a	227 kDa	99% (1)
17	tr|D3ZD36|D3ZD36_RAT Ciliary-associated calcium-binding coiled-coil 1 OS=Rattus norvegicus OX=10116 GN=Cabcoco1 PE=4 SV=1	tr|D3ZD36|D3ZD36_RAT	Cabcoco1	35 kDa	99% (1)
18	tr|G5APS6|G5APS6_HETGA Two pore calcium channel protein 2 OS=Heterocephalus glaber OX=10181 GN=GW7_03273 PE=4 SV=1	tr|G5APS6|G5APS6_HETGA	GW7_03273	71 kDa	99% (1)

19	tr|G5BQM0|G5BQM0_HETGA Sodium/calcium exchanger 3 OS=Heterocephalus glaber OX=10181 GN=GW7_02730 PE=3 SV=1	tr|G5BQM0|G5BQM0_HETGA	GW7_02730	66 kDa	99% (1)
20	tr|G5BXU0|G5BXU0_HETGA Voltage-dependent T-type calcium channel subunit alpha-1H OS=Heterocephalus glaber OX=10181 GN=GW7_12957 PE=4 SV=1	tr|G5BXU0|G5BXU0_HETGA	GW7_12957	248 kDa	99% (1)

Table S4.2 Proteins bound to Ago2 stress granules in PC12 cells stimulated with carbachol.

	Protein	Accession #	Alternate ID	M.W.	Spectrum count
mRNA related proteins:					
1	tr|A0A091EHJ4|A0A091EHJ4_FUKDA Insulin-like growth factor 2 mRNA-binding protein 1 OS=Fukomys damarensis OX=885580 GN=H920_03643 PE=4 SV=1	tr|A0A091EHJ4|A0A091EHJ4_FUKDA	H920_03643	18 kDa	99% (1)
2	tr|G5B5T6|G5B5T6_HETGA Pre-mRNA-splicing factor RBM22 (Fragment) OS=Heterocephalus glaber OX=10181 GN=GW7_21393 PE=4 SV=1	tr|G5B5T6|G5B5T6_HETGA	GW7_21393	27 kDa	99% (1)
Transcription factors:					
1	sp|P54844|MAF_RAT Transcription factor Maf OS=Rattus norvegicus OX=10116 GN=Maf PE=1 SV=1	sp|P54844|MAF_RAT (+2)	Maf	38 kDa	99% (1)
2	sp|Q03062|HES5_RAT Transcription factor HES-5 OS=Rattus norvegicus OX=10116 GN=Hes5 PE=2 SV=1	sp|Q03062|HES5_RAT	Hes5	18 kDa	99% (1)
3	sp|Q4V8D6|BRF2_RAT Transcription factor IIIB 50 kDa subunit OS=Rattus norvegicus OX=10116 GN=Brf2 PE=2 SV=1	sp|Q4V8D6|BRF2_RAT	Brf2	47 kDa	99% (1)
4	sp|Q64305|PTF1A_RAT Pancreas transcription factor 1 subunit alpha OS=Rattus norvegicus OX=10116 GN=Ptf1a PE=1 SV=1	sp|Q64305|PTF1A_RAT (+1)	Ptf1a	35 kDa	99% (1)
5	tr|A0A091CPJ8|A0A091CPJ8_FUKDA Activating transcription factor 7-interacting protein 2 OS=Fukomys damarensis OX=885580 GN=H920_17592 PE=4 SV=1	tr|A0A091CPJ8|A0A091CPJ8_FUKDA	H920_17592	66 kDa	99% (1)
6	tr|A0A091D1I2|A0A091D1I2_FUKDA T-box transcription factor TBX22 OS=Fukomys damarensis OX=885580 GN=H920_12638 PE=4 SV=1	tr|A0A091D1I2|A0A091D1I2_FUKDA	H920_12638	59 kDa	99% (1)
7	tr|A0A0G2K2A4|A0A0G2K2A4_RAT MYB proto-oncogene, transcription factor OS=Rattus norvegicus OX=10116 GN=Myb PE=1 SV=1	tr|A0A0G2K2A4|A0A0G2K2A4_RAT	Myb	83 kDa	99% (1)
8	tr|A0A0P6J2L2|A0A0P6J2L2_HETGA Cyclic AMP-dependent transcription factor ATF-6 beta isoform b OS=Heterocephalus glaber OX=10181 GN=ATF6B PE=4 SV=1	tr|A0A0P6J2L2|A0A0P6J2L2_HETGA (+1)	ATF6B	76 kDa	99% (1)
9	tr|A0A1S3FD15|A0A1S3FD15_DIPOR doublesex- and mab-3-related transcription factor 2 OS=Dipodomys ordii OX=10020 GN=Dmrt2 PE=4 SV=1	tr|A0A1S3FD15|A0A1S3FD15_DIPOR	Dmrt2	49 kDa	99% (1)
10	tr|A0A1S3GBE2|A0A1S3GBE2_DIPOR cyclic AMP-dependent transcription factor ATF-6 alpha isoform X2 OS=Dipodomys ordii OX=10020 GN=Atf6 PE=4 SV=1	tr|A0A1S3GBE2|A0A1S3GBE2_DIPOR (+1)	Atf6	73 kDa	99% (1)
11	tr|A0A1S3GCS6|A0A1S3GCS6_DIPOR myelin transcription factor 1	tr|A0A1S3GCS6|A0A1S3GCS6_DIPOR (+1)	Myt1	129 kDa	99% (1)

	OS=Dipodomys ordii OX=10020 GN=Myt1 PE=4 SV=1				
12	tr|A0A1S3GHX6|A0A1S3GHX6_DIPOR T-box transcription factor TBX18 OS=Dipodomys ordii OX=10020 GN=Tbx18 PE=4 SV=1	tr|A0A1S3GHX6|A0A1S3GHX6_DIPOR	Tbx18	66 kDa	99% (1)
13	tr|F1LMD5|F1LMD5_RAT Metal response element-binding transcription factor 2 OS=Rattus norvegicus OX=10116 GN=Mtf2 PE=4 SV=1	tr|F1LMD5|F1LMD5_RAT (+1)	Mtf2	67 kDa	99% (1)
14	tr|F1LWK1|F1LWK1_RAT Similar to Forkhead box protein L1 (Forkhead-related protein FKHL11) (Forkhead-related transcription factor 7) (FREAC-7) OS=Rattus norvegicus OX=10116 GN=LOC680273 PE=4 SV=2	tr|F1LWK1|F1LWK1_RAT	LOC680273	25 kDa	99% (1)
15	tr|G5C823|G5C823_HETGA ETS-related transcription factor Elf-3 OS=Heterocephalus glaber OX=10181 GN=GW7_12034 PE=3 SV=1	tr|G5C823|G5C823_HETGA	GW7_12034	22 kDa	99% (1)
16	tr|G5C844|G5C844_HETGA Transcription factor BTF3 OS=Heterocephalus glaber OX=10181 GN=GW7_19899 PE=3 SV=1	tr|G5C844|G5C844_HETGA	GW7_19899	12 kDa	99% (1)
17	tr|Q9Z2J8|Q9Z2J8_RAT Cbfa1/Osf2 transcription factor (Fragment) OS=Rattus norvegicus OX=10116 PE=2 SV=1	tr|Q9Z2J8|Q9Z2J8_RAT		11 kDa	99% (1)
tRNA related proteins:					
1	sp|Q3KRC5|DUS3L_RAT tRNA-dihydrouridine(47) synthase [NAD(P)(+)]-like OS=Rattus norvegicus OX=10116 GN=Dus3l PE=2 SV=1	sp|Q3KRC5|DUS3L_RAT (+1)	Dus3l	72 kDa	99% (1)
2	tr|A0A091DP02|A0A091DP02_FUKDA Methionyl-tRNA synthetase, cytoplasmic OS=Fukomys damarensis OX=885580 GN=H920_14022 PE=3 SV=1	tr|A0A091DP02|A0A091DP02_FUKDA (+2)	H920_14022	88 kDa	99% (1)
3	tr|A0A0P6JH70|A0A0P6JH70_HETGA Bifunctional glutamate/proline--tRNA ligase OS=Heterocephalus glaber OX=10181 GN=EPRS PE=3 SV=1	tr|A0A0P6JH70|A0A0P6JH70_HETGA	EPRS	169 kDa	99% (1)
4	tr|A0A1S3GPK5|A0A1S3GPK5_DIPOR glycine--tRNA ligase OS=Dipodomys ordii OX=10020 GN=Gars PE=4 SV=1	tr|A0A1S3GPK5|A0A1S3GPK5_DIPOR	Gars	77 kDa	99% (1)
5	tr|A0A1W2Q6K7|A0A1W2Q6K7_RAT Glutamyl-tRNA amidotransferase subunit B (Fragment) OS=Rattus norvegicus OX=10116 GN=Gatb PE=4 SV=1	tr|A0A1W2Q6K7|A0A1W2Q6K7_RAT	Gatb	15 kDa	99% (1)
6	tr|G5BMK6|G5BMK6_HETGA Asparaginyl-tRNA synthetase, cytoplasmic OS=Heterocephalus glaber OX=10181 GN=GW7_21599 PE=4 SV=1	tr|G5BMK6|G5BMK6_HETGA	GW7_21599	14 kDa	99% (1)
7	tr|G5C4S7|G5C4S7_HETGA tRNA (Guanine(10)-N2)-methyltransferase homolog OS=Heterocephalus glaber OX=10181 GN=TRMT11 PE=4 SV=1	tr|G5C4S7|G5C4S7_HETGA	TRMT11	53 kDa	99% (1)
RNA polymerases:					
1	tr|A0A091CPW9|A0A091CPW9_FUKDA TAF5-like RNA polymerase II p300/CBP-associated factor-associated factor 65 kDa subunit 5L OS=Fukomys damarensis OX=885580 GN=H920_19320 PE=4 SV=1	tr|A0A091CPW9|A0A091CPW9_FUKDA	H920_19320	60 kDa	99% (1)
2	tr|A0A091DTW8|A0A091DTW8_FUKDA TAF5-like RNA polymerase II p300/CBP-associated factor-associated factor 65 kDa subunit 5L OS=Fukomys damarensis OX=885580 GN=H920_02996 PE=4 SV=1	tr|A0A091DTW8|A0A091DTW8_FUKDA	H920_02996	19 kDa	99% (1)
3	tr|A0A1S3EXC1|A0A1S3EXC1_DIPOR probable RNA polymerase II nuclear localization protein SLC7A6OS OS=Dipodomys ordii OX=10020 GN=Slc7a6os PE=4 SV=1	tr|A0A1S3EXC1|A0A1S3EXC1_DIPOR	Slc7a6os	35 kDa	99% (1)
4	tr|A0A1S3EZW5|A0A1S3EZW5_DIPOR TATA box-binding protein-associated	tr|A0A1S3EZW5|A0A1S3EZW5_DIPOR	Taf1b	62 kDa	99% (1)

	factor RNA polymerase I subunit B OS=Dipodomys ordii OX=10020 GN=Taf1b PE=4 SV=1				
5	tr|A0A1S3F1X3|A0A1S3F1X3_DIPOR poly(A) RNA polymerase, mitochondrial isoform X2 OS=Dipodomys ordii OX=10020 GN=Mtpap PE=4 SV=1	tr|A0A1S3F1X3|A0A1S3F1X3_DIPOR (+1)	Mtpap	57 kDa	99% (1)
6	tr|A0A1S3GGJ3|A0A1S3GGJ3_DIPOR mediator of RNA polymerase II transcription subunit 12 OS=Dipodomys ordii OX=10020 GN=Med12 PE=4 SV=1	tr|A0A1S3GGJ3|A0A1S3GGJ3_DIPOR	Med12	244 kDa	99% (1)
Heat shock proteins:					
1	tr|A0A0G2K435|A0A0G2K435_RAT DnaJ heat shock protein family (Hsp40) member C7 OS=Rattus norvegicus OX=10116 GN=Dnajc7 PE=1 SV=1	tr|A0A0G2K435|A0A0G2K435_RAT	Dnajc7	66 kDa	99% (1)
2	tr|A0A0P6J3P1|A0A0P6J3P1_HETGA Activator of 90 kDa heat shock protein ATPase homolog 2 OS=Heterocephalus glaber OX=10181 GN=AHSA2 PE=4 SV=1	tr|A0A0P6J3P1|A0A0P6J3P1_HETGA	AHSA2	18 kDa	99% (1)
Translation initiation proteins:					
1	sp|Q3T1J1|IF5A1_RAT Eukaryotic translation initiation factor 5A-1 OS=Rattus norvegicus OX=10116 GN=Eif5a PE=1 SV=3	sp|Q3T1J1|IF5A1_RAT (+2)	Eif5a	17 kDa	99% (1)
2	sp|Q5PPG7|EIF2D_RAT Eukaryotic translation initiation factor 2D OS=Rattus norvegicus OX=10116 GN=Eif2d PE=1 SV=1	sp|Q5PPG7|EIF2D_RAT	Eif2d	63 kDa	99% (1)
3	sp|Q64350|EI2BE_RAT Translation initiation factor eIF-2B subunit epsilon OS=Rattus norvegicus OX=10116 GN=Eif2b5 PE=1 SV=2	sp|Q64350|EI2BE_RAT	Eif2b5	80 kDa	99% (1)
4	tr|A0A0G2K273|A0A0G2K273_RAT Eukaryotic translation initiation factor 3 subunit E OS=Rattus norvegicus OX=10116 GN=LOC100909481 PE=3 SV=1	tr|A0A0G2K273|A0A0G2K273_RAT	LOC100909481	52 kDa	99% (1)
5	sp|Q3B8Q2|IF4A3_RAT Eukaryotic initiation factor 4A-III OS=Rattus norvegicus OX=10116 GN=Eif4a3 PE=1 SV=1	sp|Q3B8Q2|IF4A3_RAT	Eif4a3	47 kDa	99% (1)
6	tr|A0A0P6K2W0|A0A0P6K2W0_HETGA Interferon-induced, double-stranded RNA-activated protein kinase isoform a OS=Heterocephalus glaber OX=10181 GN=EIF2AK2 PE=4 SV=1	tr|A0A0P6K2W0|A0A0P6K2W0_HETGA (+1)	EIF2AK2	61 kDa	99% (1)
Calcium related proteins:					
1	sp|A7VL23|KCMB3_RAT Calcium-activated potassium channel subunit beta-3 OS=Rattus norvegicus OX=10116 GN=Kcnmb3 PE=2 SV=1	sp|A7VL23|KCMB3_RAT	Kcnmb3	26 kDa	99% (1)
2	sp|P70549|NAC3_RAT Sodium/calcium exchanger 3 OS=Rattus norvegicus OX=10116 GN=Slc8a3 PE=1 SV=1	sp|P70549|NAC3_RAT (+1)	Slc8a3	103 kDa	99% (1)
3	sp|Q63421|PDE1C_RAT Calcium/calmodulin-dependent 3',5'-cyclic nucleotide phosphodiesterase 1C OS=Rattus norvegicus OX=10116 GN=Pde1c PE=1 SV=1	sp|Q63421|PDE1C_RAT (+5)	Pde1c	87 kDa	99% (1)
4	sp|Q7TNJ7|KCC1G_RAT Calcium/calmodulin-dependent protein kinase type 1G OS=Rattus norvegicus OX=10116 GN=Camk1g PE=2 SV=1	sp|Q7TNJ7|KCC1G_RAT	Camk1g	53 kDa	99% (1)
5	sp|Q9Z0Y8-2|CAC1I_RAT Isoform 2 of Voltage-dependent T-type calcium channel subunit alpha-1I OS=Rattus norvegicus OX=10116 GN=Cacna1i	sp|Q9Z0Y8-2|CAC1I_RAT (+1)	Cacna1i	205 kDa	99% (1)
6	tr|A0A091DKT8|A0A091DKT8_FUKDA Calcium-transporting ATPase OS=Fukomys damarensis OX=885580 GN=H920_05868 PE=3 SV=1	tr|A0A091DKT8|A0A091DKT8_FUKDA (+3)	H920_05868	107 kDa	99% (1)

7	tr|A0A091DPZ8|A0A091DPZ8_FUKDA Calcium homeostasis modulator protein 2 OS=Fukomys damarensis OX=885580 GN=H920_06282 PE=4 SV=1	tr|A0A091DPZ8|A0A091DPZ8_FUKDA	H920_06282	101 kDa	99% (1)
8	tr|A0A091DRM2|A0A091DRM2_FUKDA EF-hand calcium-binding domain-containing protein 2 OS=Fukomys damarensis OX=885580 GN=H920_13222 PE=4 SV=1	tr|A0A091DRM2|A0A091DRM2_FUKDA	H920_13222	15 kDa	99% (1)
9	tr|A0A091DS09|A0A091DS09_FUKDA Calcium-binding and coiled-coil domain-containing protein 2 OS=Fukomys damarensis OX=885580 GN=H920_03641 PE=3 SV=1	tr|A0A091DS09|A0A091DS09_FUKDA	H920_03641	100 kDa	99% (1)
10	tr|A0A091E3P3|A0A091E3P3_FUKDA Sodium/potassium/calcium exchanger 5 OS=Fukomys damarensis OX=885580 GN=H920_08826 PE=3 SV=1	tr|A0A091E3P3|A0A091E3P3_FUKDA	H920_08826	56 kDa	99% (1)
11	tr|A0A091ELJ3|A0A091ELJ3_FUKDA Extracellular calcium-sensing receptor OS=Fukomys damarensis OX=885580 GN=H920_02083 PE=4 SV=1	tr|A0A091ELJ3|A0A091ELJ3_FUKDA	H920_02083	75 kDa	99% (1)
12	tr|A0A1S3FU28|A0A1S3FU28_DIPOR calcium uptake protein 3, mitochondrial OS=Dipodomys ordii OX=10020 GN=Micu3 PE=4 SV=1	tr|A0A1S3FU28|A0A1S3FU28_DIPOR (+2)	Micu3	50 kDa	99% (1)
13	tr|A0A1S3GJ12|A0A1S3GJ12_DIPOR EF-hand calcium-binding domain-containing protein 13 OS=Dipodomys ordii OX=10020 GN=Efcab13 PE=4 SV=1	tr|A0A1S3GJ12|A0A1S3GJ12_DIPOR	Efcab13	243 kDa	99% (1)
14	tr|G5APP2|G5APP2_HETGA Tumor-associated calcium signal transducer 2 OS=Heterocephalus glaber OX=10181 GN=GW7_13500 PE=4 SV=1	tr|G5APP2|G5APP2_HETGA	GW7_13500	26 kDa	99% (1)
15	tr|G5AQP6|G5AQP6_HETGA Voltage-dependent calcium channel subunit alpha-2/delta-4 (Fragment) OS=Heterocephalus glaber OX=10181 GN=GW7_05647 PE=4 SV=1	tr|G5AQP6|G5AQP6_HETGA	GW7_05647	128 kDa	99% (1)
16	tr|G5BJB7|G5BJB7_HETGA Sodium/calcium exchanger 1 OS=Heterocephalus glaber OX=10181 GN=GW7_11585 PE=3 SV=1	tr|G5BJB7|G5BJB7_HETGA	GW7_11585	65 kDa	99% (1)
17	sp|P11505-1|AT2B1_RAT Isoform D of Plasma membrane calcium-transporting ATPase 1 OS=Rattus norvegicus OX=10116 GN=Atp2b1	sp|P11505-1|AT2B1_RAT	Atp2b1	139 kDa	100% (2)
18	tr|A0A1S3GEQ6|A0A1S3GEQ6_DIPOR calcium-binding mitochondrial carrier protein SCaMC-1-like OS=Dipodomys ordii OX=10020 GN=LOC105997461 PE=3 SV=1	tr|A0A1S3GEQ6|A0A1S3GEQ6_DIPOR	LOC105997461	54 kDa	100% (2)

Table S4.3 Proteins bound to Ago2 stress granules in PC12 cells exposed to heat shock.

	Protein	Accession #	Alternate ID	M.W.	Spectrum count
mRNA related proteins:					
1	tr|A0A091D5H0|A0A091D5H0_FUKDA Pre-mRNA-processing-splicing factor 8 OS=Fukomys damarensis OX=885580 GN=H920_13028 PE=4 SV=1	tr|A0A091D5H0|A0A091D5H0_FUKDA (+3)	H920_13028	274 kDa	99% (1)
2	tr|A0A091D738|A0A091D738_FUKDA Insulin-like growth factor 2 mRNA-binding protein 3 OS=Fukomys damarensis OX=885580 GN=H920_12544 PE=4 SV=1	tr|A0A091D738|A0A091D738_FUKDA	H920_12544	59 kDa	99% (1)
3	tr|A0A091DHN4|A0A091DHN4_FUKDA mRNA-decapping enzyme 1B	tr|A0A091DHN4|A0A091DHN4_FUKDA	H920_07975	65 kDa	99% (1)

	OS=Fukomys damarensis OX=885580 GN=H920_07975 PE=4 SV=1				
4	tr|A0A091DJM2|A0A091DJM2_FUKDA Pre-mRNA cleavage complex 2 protein Pcf11 OS=Fukomys damarensis OX=885580 GN=H920_08112 PE=4 SV=1	tr|A0A091DJM2|A0A091DJM2_FUKDA	H920_08112	188 kDa	99% (1)
5	tr|A0A1S3EVL7|A0A1S3EVL7_DIPOR cap-specific mRNA (Nucleoside-2'-O-)-methyltransferase 2 OS=Dipodomys ordii OX=10020 GN=Cmtr2 PE=4 SV=1	tr|A0A1S3EVL7|A0A1S3EVL7_DIPOR	Cmtr2	88 kDa	99% (1)
6	tr|A0A1S3EYP3|A0A1S3EYP3_DIPOR pre-mRNA cleavage complex 2 protein Pcf11 isoform X2 OS=Dipodomys ordii OX=10020 GN=Pcf11 PE=4 SV=1	tr|A0A1S3EYP3|A0A1S3EYP3_DIPOR (+2)	Pcf11	186 kDa	99% (1)
Transcription factors:					
1	sp|A2VD12|PBIP1_RAT Pre-B-cell leukemia transcription factor-interacting protein 1 OS=Rattus norvegicus OX=10116 GN=Pbxip1 PE=1 SV=1	sp|A2VD12|PBIP1_RAT (+1)	Pbxip1	80 kDa	99% (1)
2	sp|P56222|PO3F2_RAT POU domain, class 3, transcription factor 2 OS=Rattus norvegicus OX=10116 GN=Pou3f2 PE=1 SV=1	sp|P56222|PO3F2_RAT (+1)	Pou3f2	47 kDa	99% (1)
3	sp|P56225|PO5F2_RAT POU domain, class 5, transcription factor 2 OS=Rattus norvegicus OX=10116 GN=Pou5f2 PE=2 SV=2	sp|P56225|PO5F2_RAT	Pou5f2	37 kDa	99% (1)
4	sp|P70475|MYT1L_RAT Myelin transcription factor 1-like protein OS=Rattus norvegicus OX=10116 GN=Myt1l PE=1 SV=3	sp|P70475|MYT1L_RAT (+1)	Myt1l	133 kDa	99% (1)
5	tr|A0A091CPH2|A0A091CPH2_FUKDA Doublesex-and mab-3-related transcription factor B1 OS=Fukomys damarensis OX=885580 GN=H920_17737 PE=4 SV=1	tr|A0A091CPH2|A0A091CPH2_FUKDA	H920_17737	28 kDa	99% (1)
6	tr|A0A091CYW2|A0A091CYW2_FUKDA Transcription factor ETV6 OS=Fukomys damarensis OX=885580 GN=H920_13585 PE=3 SV=1	tr|A0A091CYW2|A0A091CYW2_FUKDA	H920_13585	63 kDa	99% (1)
7	tr|A0A091E720|A0A091E720_FUKDA Cyclic AMP-dependent transcription factor ATF-6 alpha OS=Fukomys damarensis OX=885580 GN=H920_00195 PE=4 SV=1	tr|A0A091E720|A0A091E720_FUKDA	H920_00195	62 kDa	99% (1)
8	tr|A0A0N8ET04|A0A0N8ET04_HETGA T-box transcription factor TBX19 OS=Heterocephalus glaber OX=10181 GN=TBX19 PE=4 SV=1	tr|A0A0N8ET04|A0A0N8ET04_HETGA (+1)	TBX19	48 kDa	99% (1)
9	tr|A0A1S3EJC7|A0A1S3EJC7_DIPOR RE1-silencing transcription factor isoform X2 OS=Dipodomys ordii OX=10020 GN=Rest PE=4 SV=1	tr|A0A1S3EJC7|A0A1S3EJC7_DIPOR (+1)	Rest	117 kDa	99% (1)
10	tr|A0A1S3ENU9|A0A1S3ENU9_DIPOR transcription factor 12 isoform X9 OS=Dipodomys ordii OX=10020 GN=Tcf12 PE=4 SV=1	tr|A0A1S3ENU9|A0A1S3ENU9_DIPOR	Tcf12	47 kDa	99% (1)
11	tr|A0A1S3FBE3|A0A1S3FBE3_DIPOR doublesex- and mab-3-related transcription factor 1 OS=Dipodomys ordii OX=10020 GN=Dmrt1 PE=4 SV=1	tr|A0A1S3FBE3|A0A1S3FBE3_DIPOR (+1)	Dmrt1	28 kDa	99% (1)
12	tr|A0A1S3FJB4|A0A1S3FJB4_DIPOR transcription factor CP2-like protein 1 OS=Dipodomys ordii OX=10020 GN=Tfcp2l1 PE=4 SV=1	tr|A0A1S3FJB4|A0A1S3FJB4_DIPOR (+1)	Tfcp2l1	55 kDa	99% (1)
13	tr|A0A1S3FX19|A0A1S3FX19_DIPOR LOW QUALITY PROTEIN: transcription factor SOX-10 OS=Dipodomys ordii OX=10020 GN=Sox10 PE=4 SV=1	tr|A0A1S3FX19|A0A1S3FX19_DIPOR	Sox10	50 kDa	99% (1)
14	tr|D3ZLV5|D3ZLV5_RAT AT-hook transcription factor OS=Rattus norvegicus OX=10116 GN=Akna PE=1 SV=1	tr|D3ZLV5|D3ZLV5_RAT	Akna	153 kDa	99% (1)

15	tr|D3ZZ13|D3ZZ13_RAT Transcription factor SOX OS=Rattus norvegicus OX=10116 GN=Sox12 PE=4 SV=1	tr|D3ZZ13|D3ZZ13_RAT	Sox12	34 kDa	99% (1)
16	tr|G5AM15|G5AM15_HETGA Runt-related transcription factor OS=Heterocephalus glaber OX=10181 GN=GW7_16276 PE=4 SV=1	tr|G5AM15|G5AM15_HETGA	GW7_16276	54 kDa	99% (1)
17	tr|G5C3D4|G5C3D4_HETGA Transcription factor 19 OS=Heterocephalus glaber OX=10181 GN=GW7_04764 PE=4 SV=1	tr|G5C3D4|G5C3D4_HETGA	GW7_04764	37 kDa	99% (1)
18	tr|Q4Z8P1|Q4Z8P1_RAT Fli-1 proto-oncogene, ETS transcription factor OS=Rattus norvegicus OX=10116 GN=Fli1 PE=1 SV=1	tr|Q4Z8P1|Q4Z8P1_RAT	Fli1	51 kDa	99% (1)
tRNA related proteins:					
1	sp|Q68FW7|SYTM_RAT Threonine--tRNA ligase, mitochondrial OS=Rattus norvegicus OX=10116 GN=Tars2 PE=2 SV=1	sp|Q68FW7|SYTM_RAT	Tars2	82 kDa	99% (1)
2	tr|A0A0N8EU10|A0A0N8EU10_HETGA tRNA wybutosine-synthesizing protein 3 homolog isoform 2 OS=Heterocephalus glaber OX=10181 GN=TYW3 PE=4 SV=1	tr|A0A0N8EU10|A0A0N8EU10_HETGA	TYW3	48 kDa	99% (1)
3	tr|A0A1S3GPK8|A0A1S3GPK8_DIPOR tRNA-dihydrouridine synthase OS=Dipodomys ordii OX=10020 GN=Dus4l PE=3 SV=1	tr|A0A1S3GPK8|A0A1S3GPK8_DIPOR	Dus4l	36 kDa	99% (1)
4	tr|G5BH39|G5BH39_HETGA Threonyl-tRNA synthetase, mitochondrial OS=Heterocephalus glaber OX=10181 GN=GW7_05802 PE=3 SV=1	tr|G5BH39|G5BH39_HETGA	GW7_05802	81 kDa	99% (1)
5	tr|G5BJ35|G5BJ35_HETGA Threonyl-tRNA synthetase, cytoplasmic OS=Heterocephalus glaber OX=10181 GN=GW7_21114 PE=3 SV=1	tr|G5BJ35|G5BJ35_HETGA	GW7_21114	92 kDa	99% (1)
6	tr|G5BMJ2|G5BMJ2_HETGA Glutamyl-tRNA(Gln) amidotransferase subunit B, mitochondrial OS=Heterocephalus glaber OX=10181 GN=GATB PE=3 SV=1	tr|G5BMJ2|G5BMJ2_HETGA	GATB	69 kDa	99% (1)
7	tr|G5C2Y2|G5C2Y2_HETGA Putative tRNA (Adenine(58)-N(1))-methyltransferase catalytic subunit TRMT61B OS=Heterocephalus glaber OX=10181 GN=TRMT61B PE=4 SV=1	tr|G5C2Y2|G5C2Y2_HETGA	TRMT61B	54 kDa	99% (1)
8	tr|G5C686|G5C686_HETGA tRNA-dihydrouridine synthase 2-like protein OS=Heterocephalus glaber OX=10181 GN=GW7_02382 PE=4 SV=1	tr|G5C686|G5C686_HETGA	GW7_02382	55 kDa	99% (1)
RNA polymerases:					
1	tr|A0A091D4E6|A0A091D4E6_FUKDA TATA box-binding protein-associated factor RNA polymerase I subunit A OS=Fukomys damarensis OX=885580 GN=H920_13144 PE=4 SV=1	tr|A0A091D4E6|A0A091D4E6_FUKDA (+2)	H920_13144	68 kDa	99% (1)
2	tr|A0A091DAU9|A0A091DAU9_FUKDA Mediator of RNA polymerase II transcription subunit 17 OS=Fukomys damarensis OX=885580 GN=MED17 PE=3 SV=1	tr|A0A091DAU9|A0A091DAU9_FUKDA (+1)	MED17	73 kDa	99% (1)
3	tr|A0A091EHB9|A0A091EHB9_FUKDA Mediator of RNA polymerase II transcription subunit 15 OS=Fukomys damarensis OX=885580 GN=MED15 PE=3 SV=1	tr|A0A091EHB9|A0A091EHB9_FUKDA (+2)	MED15	80 kDa	99% (1)
4	tr|A0A0G2JTZ3|A0A0G2JTZ3_RAT TATA box-binding protein-associated factor RNA polymerase I subunit A OS=Rattus norvegicus OX=10116 GN=Taf1a PE=4 SV=1	tr|A0A0G2JTZ3|A0A0G2JTZ3_RAT	Taf1a	53 kDa	99% (1)
5	tr|A0A0P6J8D2|A0A0P6J8D2_HETGA Mediator of RNA polymerase II transcription subunit 1	tr|A0A0P6J8D2|A0A0P6J8D2_HETGA	MED1	168 kDa	99% (1)

	OS=Heterocephalus glaber OX=10181 GN=MED1 PE=3 SV=1				
6	tr|A0A0P6K376|A0A0P6K376_HETGA RNA polymerase I-specific transcription initiation factor RRN3 OS=Heterocephalus glaber OX=10181 GN=RRN3 PE=4 SV=1	tr|A0A0P6K376|A0A0P6K376_HETGA (+1)	RRN3	75 kDa	99% (1)
7	tr|A0A1S3EPP9|A0A1S3EPP9_DIPOR RNA polymerase II-associated protein 1 OS=Dipodomys ordii OX=10020 GN=Rpap1 PE=4 SV=1	tr|A0A1S3EPP9|A0A1S3EPP9_DIPOR	Rpap1	134 kDa	99% (1)
8	tr|A0A1S3FAY6|A0A1S3FAY6_DIPOR DNA-directed RNA polymerase III subunit RPC7-like isoform X2 OS=Dipodomys ordii OX=10020 GN=Polr3gl PE=4 SV=1	tr|A0A1S3FAY6|A0A1S3FAY6_DIPOR	Polr3gl	18 kDa	99% (1)
Heat shock proteins:					
1	tr|G5BWG9|G5BWG9_HETGA Heat shock 70 kDa protein 6 OS=Heterocephalus glaber OX=10181 GN=GW7_00490 PE=4 SV=1	tr|G5BWG9|G5BWG9_HETGA	GW7_00490	26 kDa	99% (1)
Stress proteins:					
1	tr|A0A1S3GXP3|A0A1S3GXP3_DIPOR Stress-associated endoplasmic reticulum protein OS=Dipodomys ordii OX=10020 GN=Serp2 PE=3 SV=1	tr|A0A1S3GXP3|A0A1S3GXP3_DIPOR (+2)	Serp2	7 kDa	99% (1)
Translation initiation proteins:					
1	sp|P70541|EI2BG_RAT Translation initiation factor eIF-2B subunit gamma OS=Rattus norvegicus OX=10116 GN=Eif2b3 PE=2 SV=2	sp|P70541|EI2BG_RAT	Eif2b3	50 kDa	99% (1)
2	sp|Q5XI72|IF4H_RAT Eukaryotic translation initiation factor 4H OS=Rattus norvegicus OX=10116 GN=Eif4h PE=1 SV=1	sp|Q5XI72|IF4H_RAT (+6)	Eif4h	27 kDa	99% (1)
3	tr|A0A1L1WKF3|A0A1L1WKF3_NINCN Eukaryotic translation initiation factor 2B (Fragment) OS=Niviventer confucianus OX=248811 PE=2 SV=1	tr|A0A1L1WKF3|A0A1L1WKF3_NINCN		22 kDa	99% (1)
4	tr|G5BP48|G5BP48_HETGA Eukaryotic translation initiation factor 1A, X-chromosomal OS=Heterocephalus glaber OX=10181 GN=GW7_09468 PE=4 SV=1	tr|G5BP48|G5BP48_HETGA	GW7_09468	12 kDa	99% (1)
Calcium related proteins:					
1	tr|A0A0P6K3B4|A0A0P6K3B4_HETGA 85 kDa calcium-independent phospholipase A2 isoform b OS=Heterocephalus glaber OX=10181 GN=PLA2G6 PE=4 SV=1	tr|A0A0P6K3B4|A0A0P6K3B4_HETGA (+1)	PLA2G6	84 kDa	100% (2)
2	sp|P11506-10|AT2B2_RAT Isoform XC of Plasma membrane calcium-transporting ATPase 2 OS=Rattus norvegicus OX=10116 GN=Atp2b2	sp|P11506-10|AT2B2_RAT (+16)	Atp2b2	130 kDa	99% (1)
3	sp|Q8VHW7-2|CCG6_RAT Isoform Short of Voltage-dependent calcium channel gamma-6 subunit OS=Rattus norvegicus OX=10116 GN=Cacng6	sp|Q8VHW7-2|CCG6_RAT (+1)	Cacng6	24 kDa	99% (1)
4	sp|Q91XJ0|CREST_RAT Calcium-responsive transcription coactivator OS=Rattus norvegicus OX=10116 GN=Ss18l1 PE=1 SV=1	sp|Q91XJ0|CREST_RAT	Ss18l1	44 kDa	99% (1)
5	tr|A0A091DAS0|A0A091DAS0_FUKDA Two pore calcium channel protein 2 OS=Fukomys damarensis OX=885580 GN=H920_11257 PE=4 SV=1	tr|A0A091DAS0|A0A091DAS0_FUKDA	H920_11257	103 kDa	99% (1)
6	tr|A0A091E0V8|A0A091E0V8_FUKDA Calcium uptake protein 1, mitochondrial OS=Fukomys damarensis OX=885580 GN=H920_01629 PE=4 SV=1	tr|A0A091E0V8|A0A091E0V8_FUKDA	H920_01629	54 kDa	99% (1)
7	tr|A0A091EN06|A0A091EN06_FUKDA Calcium-activated potassium channel subunit alpha-1 OS=Fukomys damarensis OX=885580 GN=H920_01668 PE=3 SV=1	tr|A0A091EN06|A0A091EN06_FUKDA	H920_01668	131 kDa	99% (1)
8	tr|A0A1L1WKE8|A0A1L1WKE8_RAT Calcium modulating ligand (Fragment)	tr|A0A1L1WKE8|A0A1L1WKE8_RAT (+1)		24 kDa	99% (1)

	OS=Rattus norvegicus OX=10116 PE=2 SV=1				
9	tr|A0A1S3EPI6|A0A1S3EPI6_DIPOR C2 calcium-dependent domain-containing protein 4A OS=Dipodomys ordii OX=10020 GN=C2cd4a PE=4 SV=1	tr|A0A1S3EPI6|A0A1S3EPI6_DIPOR	C2cd4a	74 kDa	99% (1)
10	tr|A0A1S3FBW2|A0A1S3FBW2_DIPOR sodium/calcium exchanger 1 isoform X2 OS=Dipodomys ordii OX=10020 GN=Slc8a1 PE=3 SV=1	tr|A0A1S3FBW2|A0A1S3FBW2_DIPOR	Slc8a1	104 kDa	99% (1)
11	tr|A0A1S3FPF3|A0A1S3FPF3_DIPOR C2 calcium-dependent domain-containing protein 4C OS=Dipodomys ordii OX=10020 GN=C2cd4c PE=4 SV=1	tr|A0A1S3FPF3|A0A1S3FPF3_DIPOR	C2cd4c	45 kDa	99% (1)
12	tr|A0A1S3FTJ2|A0A1S3FTJ2_DIPOR EF-hand calcium-binding domain-containing protein 4B OS=Dipodomys ordii OX=10020 GN=Cracr2a PE=4 SV=1	tr|A0A1S3FTJ2|A0A1S3FTJ2_DIPOR	Cracr2a	46 kDa	99% (1)
13	tr|A0A1S3GMY9|A0A1S3GMY9_DIPOR EF-hand calcium-binding domain-containing protein 10-like OS=Dipodomys ordii OX=10020 GN=LOC105999654 PE=4 SV=1	tr|A0A1S3GMY9|A0A1S3GMY9_DIPOR	LOC105999654	17 kDa	99% (1)
14	tr|G5BAF4|G5BAF4_HETGA Sarcoplasmic reticulum histidine-rich calcium-binding protein OS=Heterocephalus glaber OX=10181 GN=GW7_13612 PE=4 SV=1	tr|G5BAF4|G5BAF4_HETGA	GW7_13612	67 kDa	99% (1)
15	tr|G5BDD6|G5BDD6_HETGA Small conductance calcium-activated potassium channel protein 3 OS=Heterocephalus glaber OX=10181 GN=GW7_05186 PE=4 SV=1	tr|G5BDD6|G5BDD6_HETGA	GW7_05186	82 kDa	99% (1)

Table S4.4 Proteins bound to Ago2 stress granules in PC12 cells exposed to hypo-osmotic stress.

	Protein	**Accession #**	**Alternate ID**	**M.W.**	**Spectrum count**
mRNA related proteins:					
1	sp|Q80ZG5|SLU7_RAT Pre-mRNA-splicing factor SLU7 OS=Rattus norvegicus OX=10116 GN=Slu7 PE=1 SV=2	sp|Q80ZG5|SLU7_RAT (+1)	Slu7	68 kDa	99% (1)
2	tr|A0A091CSJ7|A0A091CSJ7_FUKDA Putative pre-mRNA-splicing factor ATP-dependent RNA helicase DHX15 OS=Fukomys damarensis OX=885580 GN=H920_17774 PE=4 SV=1	tr|A0A091CSJ7|A0A091CSJ7_FUKDA (+2)	H920_17774	91 kDa	99% (1)
3	tr|A0A0U1RRY8|A0A0U1RRY8_RAT UPF2, regulator of nonsense mediated mRNA decay (Fragment) OS=Rattus norvegicus OX=10116 GN=Upf2 PE=1 SV=1	tr|A0A0U1RRY8|A0A0U1RRY8_RAT (+1)	Upf2	58 kDa	99% (1)
4	tr|G5AZF4|G5AZF4_HETGA Pre-mRNA-splicing regulator WTAP OS=Heterocephalus glaber OX=10181 GN=GW7_06519 PE=4 SV=1	tr|G5AZF4|G5AZF4_HETGA	GW7_06519	35 kDa	99% (1)
5	tr|G5B7R6|G5B7R6_HETGA Pre-mRNA-processing factor 40-like protein A OS=Heterocephalus glaber OX=10181 GN=GW7_17978 PE=4 SV=1	tr|G5B7R6|G5B7R6_HETGA	GW7_17978	76 kDa	99% (1)
6	tr|Q9QWQ2|Q9QWQ2_RAT Rat (wistar) alpha-2u globulin mRNA (Fragment) OS=Rattus norvegicus OX=10116 PE=3 SV=1	tr|Q9QWQ2|Q9QWQ2_RAT		17 kDa	99% (1)
Transcription factors:					
1	sp|Q01750|T2FB_RAT General transcription factor IIF subunit 2	sp|Q01750|T2FB_RAT (+4)	Gtf2f2	28 kDa	99% (1)

	OS=Rattus norvegicus OX=10116 GN=Gtf2f2 PE=1 SV=1				
2	tr|A0A091CV02|A0A091CV02_FUKDA Transcription factor YY2 OS=Fukomys damarensis OX=885580 GN=H920_16257 PE=4 SV=1	tr|A0A091CV02|A0A091CV02_FUKDA	H920_16257	69 kDa	99% (1)
3	tr|A0A091CXQ7|A0A091CXQ7_FUKDA Transcription factor E3 OS=Fukomys damarensis OX=885580 GN=H920_15943 PE=4 SV=1	tr|A0A091CXQ7|A0A091CXQ7_FUKDA (+3)	H920_15943	62 kDa	99% (1)
4	tr|A0A091D4T4|A0A091D4T4_FUKDA Transcription factor 12 OS=Fukomys damarensis OX=885580 GN=H920_12613 PE=4 SV=1	tr|A0A091D4T4|A0A091D4T4_FUKDA (+6)	H920_12613	52 kDa	99% (1)
5	tr|A0A091DBZ6|A0A091DBZ6_FUKDA ETS-related transcription factor Elf-2 OS=Fukomys damarensis OX=885580 GN=H920_10879 PE=4 SV=1	tr|A0A091DBZ6|A0A091DBZ6_FUKDA	H920_10879	13 kDa	99% (1)
6	tr|A0A091DH54|A0A091DH54_FUKDA T-box transcription factor TBX18 OS=Fukomys damarensis OX=885580 GN=H920_08237 PE=4 SV=1	tr|A0A091DH54|A0A091DH54_FUKDA (+1)	H920_08237	49 kDa	99% (1)
7	tr|A0A091DPX1|A0A091DPX1_FUKDA Transcription factor LBX1 OS=Fukomys damarensis OX=885580 GN=H920_06247 PE=4 SV=1	tr|A0A091DPX1|A0A091DPX1_FUKDA (+1)	H920_06247	19 kDa	99% (1)
8	tr|A0A091E2P8|A0A091E2P8_FUKDA Thyroid transcription factor 1-associated protein 26 OS=Fukomys damarensis OX=885580 GN=H920_01771 PE=4 SV=1	tr|A0A091E2P8|A0A091E2P8_FUKDA	H920_01771	28 kDa	99% (1)
9	tr|A0A091E2Y0|A0A091E2Y0_FUKDA Transcription factor IIIB 50 kDa subunit OS=Fukomys damarensis OX=885580 GN=H920_01539 PE=4 SV=1	tr|A0A091E2Y0|A0A091E2Y0_FUKDA	H920_01539	47 kDa	99% (1)
10	tr|A0A1S3F625|A0A1S3F625_DIPOR transcription factor TFIIIB component B'' homolog OS=Dipodomys ordii OX=10020 GN=Bdp1 PE=4 SV=1	tr|A0A1S3F625|A0A1S3F625_DIPOR	Bdp1	228 kDa	99% (1)
11	tr|A0A1S3G2E8|A0A1S3G2E8_DIPOR Runt-related transcription factor OS=Dipodomys ordii OX=10020 GN=Runx1 PE=4 SV=1	tr|A0A1S3G2E8|A0A1S3G2E8_DIPOR (+1)	Runx1	50 kDa	99% (1)
12	tr|A0A1S3G5A1|A0A1S3G5A1_DIPOR HMG box transcription factor BBX isoform X1 OS=Dipodomys ordii OX=10020 GN=Bbx PE=4 SV=1	tr|A0A1S3G5A1|A0A1S3G5A1_DIPOR (+2)	Bbx	108 kDa	99% (1)
13	tr|A0A1S3GC22|A0A1S3GC22_DIPOR AT-hook-containing transcription factor OS=Dipodomys ordii OX=10020 GN=Akna PE=4 SV=1	tr|A0A1S3GC22|A0A1S3GC22_DIPOR	Akna	146 kDa	99% (1)
14	tr|G5AT36|G5AT36_HETGA General transcription factor 3C polypeptide 5 OS=Heterocephalus glaber OX=10181 GN=GW7_03375 PE=4 SV=1	tr|G5AT36|G5AT36_HETGA	GW7_03375	62 kDa	99% (1)
15	tr|G5AVV2|G5AVV2_HETGA Transcription factor Dp-1 (Fragment) OS=Heterocephalus glaber OX=10181 GN=GW7_08579 PE=3 SV=1	tr|G5AVV2|G5AVV2_HETGA	GW7_08579	44 kDa	99% (1)
16	tr|G5C6B2|G5C6B2_HETGA General transcription factor II-I repeat domain-containing protein 2B OS=Heterocephalus glaber OX=10181 GN=GW7_12170 PE=4 SV=1	tr|G5C6B2|G5C6B2_HETGA	GW7_12170	106 kDa	99% (1)
tRNA related proteins:					
1	sp|Q3KRD0|SYDM_RAT Aspartate--tRNA ligase, mitochondrial OS=Rattus norvegicus OX=10116 GN=Dars2 PE=1 SV=1	sp|Q3KRD0|SYDM_RAT	Dars2	74 kDa	99% (1)
2	tr|A0A091CUK8|A0A091CUK8_FUKDA tRNA (adenine(58)-N(1))-methyltransferase non-catalytic subunit TRM6 OS=Fukomys damarensis OX=885580 GN=H920_16421 PE=3 SV=1	tr|A0A091CUK8|A0A091CUK8_FUKDA (+4)	H920_16421	56 kDa	99% (1)

3	tr|A0A091DEA6|A0A091DEA6_FUKDA tRNA-dihydrouridine(47) synthase [NAD(P)(+)] OS=Fukomys damarensis OX=885580 GN=H920_09750 PE=3 SV=1	tr|A0A091DEA6|A0A091DEA6_FUKDA	H920_09750	61 kDa	99% (1)
4	tr|A0A091DUF5|A0A091DUF5_FUKDA tRNA-dihydrouridine synthase 1-like OS=Fukomys damarensis OX=885580 GN=H920_02958 PE=4 SV=1	tr|A0A091DUF5|A0A091DUF5_FUKDA (+2)	H920_02958	54 kDa	99% (1)
5	tr|A0A091E906|A0A091E906_FUKDA Glutamyl-tRNA(Gln) amidotransferase subunit B, mitochondrial OS=Fukomys damarensis OX=885580 GN=GATB PE=3 SV=1	tr|A0A091E906|A0A091E906_FUKDA	GATB	62 kDa	99% (1)
6	tr|A0A091E9L2|A0A091E9L2_FUKDA Putative tRNA pseudouridine synthase 2 OS=Fukomys damarensis OX=885580 GN=H920_06647 PE=4 SV=1	tr|A0A091E9L2|A0A091E9L2_FUKDA	H920_06647	37 kDa	99% (1)
7	tr|A0A0P6J3Q6|A0A0P6J3Q6_HETGA tRNA (Cytosine(34)-C(5))-methyltransferase isoform 2 OS=Heterocephalus glaber OX=10181 GN=NSUN2 PE=3 SV=1	tr|A0A0P6J3Q6|A0A0P6J3Q6_HETGA (+1)	NSUN2	86 kDa	99% (1)
8	tr|A0A1S3EUN6|A0A1S3EUN6_DIPOR tRNA-dihydrouridine(20) synthase [NAD(P)+]-like OS=Dipodomys ordii OX=10020 GN=Dus2 PE=4 SV=1	tr|A0A1S3EUN6|A0A1S3EUN6_DIPOR	Dus2	43 kDa	99% (1)
9	tr|A0A1S3GID6|A0A1S3GID6_DIPOR S-adenosyl-L-methionine-dependent tRNA 4-demethylwyosine synthase-like OS=Dipodomys ordii OX=10020 GN=LOC105998465 PE=4 SV=1	tr|A0A1S3GID6|A0A1S3GID6_DIPOR	LOC105998465	80 kDa	99% (1)
10	tr|F1M8A9|F1M8A9_RAT Peptidyl-tRNA hydrolase 1 homolog OS=Rattus norvegicus OX=10116 GN=Ptrh1 PE=4 SV=1	tr|F1M8A9|F1M8A9_RAT	Ptrh1	22 kDa	99% (1)
11	tr|G5AJX3|G5AJX3_HETGA Lysine--tRNA ligase OS=Heterocephalus glaber OX=10181 GN=GW7_15127 PE=3 SV=1	tr|G5AJX3|G5AJX3_HETGA	GW7_15127	63 kDa	99% (1)
12	tr|O35880|O35880_RAT Isoleucyl tRNA synthetase OS=Rattus norvegicus OX=10116 PE=2 SV=1	tr|O35880|O35880_RAT		6 kDa	99% (1)
RNA polymerases:					
1	tr|A0A091E2E8|A0A091E2E8_FUKDA RNA polymerase I-specific transcription initiation factor RRN3 OS=Fukomys damarensis OX=885580 GN=H920_01707 PE=4 SV=1	tr|A0A091E2E8|A0A091E2E8_FUKDA	H920_01707	79 kDa	99% (1)
2	tr|A0A1S3FGA8|A0A1S3FGA8_DIPOR DNA-directed RNA polymerase subunit beta OS=Dipodomys ordii OX=10020 GN=Polr1b PE=3 SV=1	tr|A0A1S3FGA8|A0A1S3FGA8_DIPOR	Polr1b	128 kDa	99% (1)
3	tr|A0A1S3G4R2|A0A1S3G4R2_DIPOR mediator of RNA polymerase II transcription subunit 26 isoform X1 OS=Dipodomys ordii OX=10020 GN=Med26 PE=4 SV=1	tr|A0A1S3G4R2|A0A1S3G4R2_DIPOR (+1)	Med26	63 kDa	99% (1)
4	tr|A0A1S3GI13|A0A1S3GI13_DIPOR DNA-directed DNA/RNA polymerase mu OS=Dipodomys ordii OX=10020 GN=Polm PE=3 SV=1	tr|A0A1S3GI13|A0A1S3GI13_DIPOR	Polm	55 kDa	99% (1)
5	tr|A0A1S3GIR3|A0A1S3GIR3_DIPOR DNA-directed RNA polymerase III subunit RPC9 OS=Dipodomys ordii OX=10020 GN=Crcp PE=4 SV=1	tr|A0A1S3GIR3|A0A1S3GIR3_DIPOR	Crcp	17 kDa	99% (1)
6	tr|G5C0Z7|G5C0Z7_HETGA Mediator of RNA polymerase II transcription subunit 12-like protein OS=Heterocephalus glaber OX=10181 GN=GW7_20769 PE=4 SV=1	tr|G5C0Z7|G5C0Z7_HETGA	GW7_20769	98 kDa	99% (1)
7	tr|G5C9B1|G5C9B1_HETGA TAF5-like RNA polymerase II p300/CBP-associated factor-associated factor 65 kDa subunit 5L OS=Heterocephalus glaber OX=10181 GN=GW7_06489 PE=4 SV=1	tr|G5C9B1|G5C9B1_HETGA	GW7_06489	40 kDa	99% (1)

Heat shock proteins:					
1	sp|Q9QZ58|HSPB3_RAT Heat shock protein beta-3 OS=Rattus norvegicus OX=10116 GN=Hspb3 PE=2 SV=1	sp|Q9QZ58|HSPB3_RAT	Hspb3	17 kDa	99% (1)
2	tr|A0A0G2JVE2|A0A0G2JVE2_RAT DnaJ heat shock protein family (Hsp40) member C15 OS=Rattus norvegicus OX=10116 GN=Dnajc15 PE=1 SV=1	tr|A0A0G2JVE2|A0A0G2JVE2_RAT (+1)	Dnajc15	15 kDa	99% (1)
3	tr|A0A1S3EUY4|A0A1S3EUY4_DIPOR heat shock factor protein 4 isoform X3 OS=Dipodomys ordii OX=10020 GN=Hsf4 PE=3 SV=1	tr|A0A1S3EUY4|A0A1S3EUY4_DIPOR (+4)	Hsf4	49 kDa	99% (1)
4	tr|A0A1S3GEJ4|A0A1S3GEJ4_DIPOR heat shock 70 kDa protein 4 OS=Dipodomys ordii OX=10020 GN=Hspa4 PE=3 SV=1	tr|A0A1S3GEJ4|A0A1S3GEJ4_DIPOR	Hspa4	60 kDa	99% (1)
5	tr|A0A1S3GP00|A0A1S3GP00_DIPOR heat shock 70 kDa protein 1B OS=Dipodomys ordii OX=10020 GN=LOC105999841 PE=3 SV=1	tr|A0A1S3GP00|A0A1S3GP00_DIPOR	LOC105999841	70 kDa	99% (1)
6	tr|G5ARG8|G5ARG8_HETGA Heat shock 70 kDa protein 12A OS=Heterocephalus glaber OX=10181 GN=GW7_21295 PE=4 SV=1	tr|G5ARG8|G5ARG8_HETGA	GW7_21295	77 kDa	99% (1)
Translation initiation proteins:					
1	tr|A0A1S3FWP2|A0A1S3FWP2_DIPOR Eukaryotic translation initiation factor 3 subunit L OS=Dipodomys ordii OX=10020 GN=Eif3l PE=3 SV=1	tr|A0A1S3FWP2|A0A1S3FWP2_DIPOR	Eif3l	61 kDa	99% (1)
2	tr|A0A1S3GRE5|A0A1S3GRE5_DIPOR LOW QUALITY PROTEIN: eukaryotic translation initiation factor 4E transporter-like OS=Dipodomys ordii OX=10020 GN=LOC105999910 PE=4 SV=1	tr|A0A1S3GRE5|A0A1S3GRE5_DIPOR	LOC105999910	104 kDa	99% (1)
3	tr|G5C4X2|G5C4X2_HETGA Eukaryotic translation initiation factor 4 gamma 3 OS=Heterocephalus glaber OX=10181 GN=GW7_01849 PE=4 SV=1	tr|G5C4X2|G5C4X2_HETGA	GW7_01849	177 kDa	99% (1)
Calcium related proteins:					
1	tr|A0A1S3EP39|A0A1S3EP39_DIPOR EF-hand calcium-binding domain-containing protein 8 OS=Dipodomys ordii OX=10020 GN=Efcab8 PE=4 SV=1	tr|A0A1S3EP39|A0A1S3EP39_DIPOR	Efcab8	118 kDa	99% (2)
2	sp|P27732-10|CAC1D_RAT Isoform 10 of Voltage-dependent L-type calcium channel subunit alpha-1D OS=Rattus norvegicus OX=10116 GN=Cacna1d	sp|P27732-10|CAC1D_RAT (+19)	Cacna1d	245 kDa	99% (2)
3	sp|Q66H96|CABP7_RAT Calcium-binding protein 7 OS=Rattus norvegicus OX=10116 GN=Cabp7 PE=1 SV=1	sp|Q66H96|CABP7_RAT (+2)	Cabp7	24 kDa	99% (1)
4	sp|Q68FX6|CABS1_RAT Calcium-binding and spermatid-specific protein 1 OS=Rattus norvegicus OX=10116 GN=Cabs1 PE=1 SV=1	sp|Q68FX6|CABS1_RAT	Cabs1	42 kDa	99% (1)
5	sp|Q9WTN5|TPC1_RAT Two pore calcium channel protein 1 OS=Rattus norvegicus OX=10116 GN=Tpcn1 PE=1 SV=2	sp|Q9WTN5|TPC1_RAT	Tpcn1	94 kDa	99% (1)
6	tr|A0A091DDJ5|A0A091DDJ5_FUKDA Calcium-binding protein 2 OS=Fukomys damarensis OX=885580 GN=H920_10191 PE=4 SV=1	tr|A0A091DDJ5|A0A091DDJ5_FUKDA (+1)	H920_10191	28 kDa	99% (1)
7	tr|A0A091DKA1|A0A091DKA1_FUKDA EF-hand calcium-binding domain-containing protein 7 OS=Fukomys damarensis OX=885580 GN=H920_15351 PE=4 SV=1	tr|A0A091DKA1|A0A091DKA1_FUKDA	H920_15351	74 kDa	99% (1)
8	tr|A0A091E0N8|A0A091E0N8_FUKDA Calcium-dependent secretion activator 2 OS=Fukomys damarensis OX=885580 GN=H920_09976 PE=4 SV=1	tr|A0A091E0N8|A0A091E0N8_FUKDA	H920_09976	24 kDa	99% (1)
9	tr|A0A1S3ENV9|A0A1S3ENV9_DIPOR sodium/potassium/calcium exchanger 5	tr|A0A1S3ENV9|A0A1S3ENV9_DIPOR	Slc24a5	55 kDa	99% (1)

	OS=Dipodomys ordii OX=10020 GN=Slc24a5 PE=3 SV=1				
10	tr|A0A1S3ESA2|A0A1S3ESA2_DIPOR calcium-regulated heat stable protein 1 OS=Dipodomys ordii OX=10020 GN=Carhsp1 PE=4 SV=1	tr|A0A1S3ESA2|A0A1S3ESA2_DIPOR	Carhsp1	16 kDa	99% (1)
11	tr|A0A1S3F932|A0A1S3F932_DIPOR calcium homeostasis modulator protein 3 OS=Dipodomys ordii OX=10020 GN=Calhm3 PE=4 SV=1	tr|A0A1S3F932|A0A1S3F932_DIPOR	Calhm3	39 kDa	99% (1)
12	tr|A0A1S3FSE8|A0A1S3FSE8_DIPOR calcium-independent phospholipase A2-gamma isoform X1 OS=Dipodomys ordii OX=10020 GN=Pnpla8 PE=4 SV=1	tr|A0A1S3FSE8|A0A1S3FSE8_DIPOR (+2)	Pnpla8	88 kDa	99% (1)
13	tr|A0A1S3FTA4|A0A1S3FTA4_DIPOR voltage-dependent calcium channel subunit alpha-2/delta-4 OS=Dipodomys ordii OX=10020 GN=Cacna2d4 PE=4 SV=1	tr|A0A1S3FTA4|A0A1S3FTA4_DIPOR	Cacna2d4	119 kDa	99% (1)
14	tr|A0A1S3GWA7|A0A1S3GWA7_DIPOR calcium and integrin-binding protein 1 OS=Dipodomys ordii OX=10020 GN=Cib1 PE=4 SV=1	tr|A0A1S3GWA7|A0A1S3GWA7_DIPOR	Cib1	23 kDa	99% (1)

Table S4.5 Top 100 mRNA's bound to Ago2 in cells stimulated with carbachol.

	Chromosome	-log10(P-value)	Log2 Fold Change	Gene	Ensembl ID	Feature	Size
1	chr3	400	7.315979903	Chgb	ENSRNOG00000021269	CDS	6
2	chr3	400	7.293964101	Chgb	ENSRNOG00000021269	CDS	20
3	chr3	400	7.273717867	Chgb	ENSRNOG00000021269	CDS	6
4	chr3	400	7.090682783	Chgb	ENSRNOG00000021269	CDS	10
5	chr3	400	7.08000105	Chgb	ENSRNOG00000021269	CDS	4
6	chr3	400	7.010683461	Chgb	ENSRNOG00000021269	CDS	6
7	chr6	318.4022956	8.777086442	Chga	ENSRNOG00000052549	CDS	11
8	chr7	311.1491389	9.73302165	Atp5f1b	ENSRNOG00000002840	CDS	17
9	chr7	310.3494301	8.741307529	Atp5f1b	ENSRNOG00000002840	CDS	20
10	chr6	298.4888748	8.686248511	Chga	ENSRNOG00000052549	CDS	18
11	chr6	293.8682104	8.663622756	Chga	ENSRNOG00000052549	CDS	29
12	chr7	290.2766379	8.646078072	Atp5f1b	ENSRNOG00000002840	CDS	15
13	chr7	283.0452603	8.611031125	Atp5f1b	ENSRNOG00000002840	CDS	13
14	chr6	281.5995358	8.602659564	Chga	ENSRNOG00000052549	CDS	25
15	chr7	281.4760203	9.590716074	Atp5f1b	ENSRNOG00000002840	CDS	18
16	chr3	276.2037601	7.598455496	Chgb	ENSRNOG00000021269	CDS	21
17	chr6	273.3652518	8.560777652	Chga	ENSRNOG00000052549	CDS	7
18	chr3	264.6138449	7.538274783	Chgb	ENSRNOG00000021269	CDS	24
19	chr3	262.4969533	7.526521601	Chgb	ENSRNOG00000021269	CDS	4
20	chr3	244.4937602	9.388870555	Chgb	ENSRNOG00000021269	CDS	45
21	chr3	240.898144	9.367618006	Chgb	ENSRNOG00000021269	CDS	13
22	chr3	239.6296228	9.360187801	Chgb	ENSRNOG00000021269	CDS	14
23	chr3	238.9017312	7.395347312	Chgb	ENSRNOG00000021269	CDS	4
24	chr3	237.3955251	7.387246813	Chgb	ENSRNOG00000021269	CDS	3
25	chr3	234.9654518	9.331767628	Chgb	ENSRNOG00000021269	CDS	15
26	chr3	233.0722694	9.320751401	Chgb	ENSRNOG00000021269	CDS	6
27	chr7	229.4113409	8.313075205	Atp5f1b	ENSRNOG00000002840	CDS	4
28	chr7	225.6635385	9.274947711	Atp5f1b	ENSRNOG00000002840	CDS	14
29	chr3	223.7701201	9.262601835	Chgb	ENSRNOG00000021269	CDS	4
30	chr3	221.2261907	9.246571725	Chgb	ENSRNOG00000021269	CDS	4
31	chr3	221.1514713	8.261715931	Chgb	ENSRNOG00000021269	CDS	36
32	chr3	211.7197028	9.183417996	Chgb	ENSRNOG00000021269	CDS	5
33	chr3	206.3950491	9.148378718	Chgb	ENSRNOG00000021269	CDS	23

34	chr3	205.1132045	9.139725406	Chgb	ENSRNOG00000021269	CDS	3
35	chr3	203.4326928	8.143577732	Chgb	ENSRNOG00000021269	CDS	7
36	chr3	203.3436704	7.572017936	Chgb	ENSRNOG00000021269	CDS	6
37	chr3	202.0782953	7.563416217	Chgb	ENSRNOG00000021269	CDS	11
38	chr7	194.5750207	8.08067098	Atp5f1b	ENSRNOG00000002840	CDS	27
39	chr3	193.5217424	9.05635532	Chgb	ENSRNOG00000021269	CDS	6
40	chr6	192.4478478	8.065521786	Chga	ENSRNOG00000052549	CDS	14
41	chr3	189.8477609	7.476492489	Chgb	ENSRNOG00000021269	CDS	11
42	chr7	189.6491409	7.474454783	Plec	ENSRNOG00000023781	CDS	27
43	chr7	187.6260089	9.011737678	Atp5f1b	ENSRNOG00000002840	CDS	45
44	chr6	187.4144896	8.027459174	Chga	ENSRNOG00000052549	CDS	36
45	chr3	184.6774342	8.006458875	Chgb	ENSRNOG00000021269	CDS	42
46	chr3	181.0925624	7.978693347	Chgb	ENSRNOG00000021269	CDS	11
47	chr3	180.8667492	7.977614697	Chgb	ENSRNOG00000021269	CDS	11
48	chr7	180.670628	7.975454973	Plec	ENSRNOG00000023781	CDS	6
49	chr3	180.0174697	7.971125802	Chgb	ENSRNOG00000021269	CDS	4
50	chr7	179.7325643	7.400185869	Plec	ENSRNOG00000023781	CDS	10
51	chr3	178.9605974	8.943770128	Chgb	ENSRNOG00000021269	CDS	33
52	chr3	178.7695059	7.960245698	Chgb	ENSRNOG00000021269	CDS	6
53	chr3	176.853693	8.927104232	Chgb	ENSRNOG00000021269	CDS	10
54	chr3	175.1651382	8.913631495	Chgb	ENSRNOG00000021269	CDS	10
55	chr3	174.0626517	7.354382179	Chgb	ENSRNOG00000021269	CDS	10
56	chr3	173.2840448	7.917011493	Chgb	ENSRNOG00000021269	CDS	9
57	chr3	172.4369923	7.91024356	Chgb	ENSRNOG00000021269	CDS	7
58	chr3	171.1647195	7.900031756	Chgb	ENSRNOG00000021269	CDS	6
59	chr3	170.7401694	7.896611695	Chgb	ENSRNOG00000021269	CDS	4
60	chr3	167.3860087	7.867791419	Chgb	ENSRNOG00000021269	CDS	5
61	chr3	166.6749433	8.844313357	Chgb	ENSRNOG00000021269	CDS	12
62	chr3	165.8900686	7.856100147	Chgb	ENSRNOG00000021269	CDS	11
63	chr3	164.6423655	7.844313357	Chgb	ENSRNOG00000021269	CDS	6
64	chr3	162.9588344	7.830040907	Chgb	ENSRNOG00000021269	CDS	4
65	chr3	156.5796676	8.753962829	Chgb	ENSRNOG00000021269	CDS	46
66	chr6	155.7883227	7.766508083	Chga	ENSRNOG00000052549	CDS	3
67	chr7	154.7064236	7.190262799	Plec	ENSRNOG00000023781	CDS	17
68	chr3	154.527017	7.755222275	Chgb	ENSRNOG00000021269	CDS	13
69	chr7	153.8658175	7.182794128	Plec	ENSRNOG00000023781	CDS	5
70	chr3	151.9283448	8.711772019	Chgb	ENSRNOG00000021269	CDS	13
71	chr3	151.504301	8.707874597	Chgb	ENSRNOG00000021269	CDS	30
72	chr3	148.1042487	8.676310274	Chgb	ENSRNOG00000021269	CDS	3
73	chr3	146.7134564	7.116392903	Chgb	ENSRNOG00000021269	CDS	18
74	chr3	145.6765969	7.67231573	Chgb	ENSRNOG00000021269	CDS	25
75	chr3	143.9115503	8.634490098	Chgb	ENSRNOG00000021269	CDS	8
76	chr3	143.7705355	7.653526878	Chgb	ENSRNOG00000021269	CDS	26
77	chr3	143.4884746	8.6303779	Chgb	ENSRNOG00000021269	CDS	5
78	chr3	138.421812	8.578672883	Chgb	ENSRNOG00000021269	CDS	38
79	chr3	138.0883574	7.597051413	Chgb	ENSRNOG00000021269	CDS	29
80	chr3	138.0007089	8.574398228	Chgb	ENSRNOG00000021269	CDS	3
81	chr3	135.1016094	7.568678914	Chgb	ENSRNOG00000021269	CDS	8
82	chr7	133.8654242	6.99086202	Plec	ENSRNOG00000023781	CDS	31
83	chr3	130.7357251	6.956235677	Chgb	ENSRNOG00000021269	CDS	10
84	chr3	128.5033482	8.473944907	Chgb	ENSRNOG00000021269	CDS	14
85	chr7	120.2706998	8.379100574	Plec	ENSRNOG00000023781	CDS	43
86	chr7	119.5495292	7.396961968	Atp5f1b	ENSRNOG00000002840	CDS	5
87	chr3	118.3048601	7.380733506	Chgb	ENSRNOG00000021269	CDS	15
88	chr3	116.4262295	8.335982341	Chgb	ENSRNOG00000021269	CDS	11
89	chr3	114.5569956	8.312219767	Chgb	ENSRNOG00000021269	CDS	13
90	chr7	111.3650272	7.29673452	Atp5f1b	ENSRNOG00000002840	CDS	3
91	chr3	106.7239446	8.213050772	Chgb	ENSRNOG00000021269	CDS	6
92	chr6	105.7182669	8.196457291	Chga	ENSRNOG00000052549	CDS	39
93	chr3	105.2980583	8.190883447	Chgb	ENSRNOG00000021269	CDS	5
94	chr3	99.81928361	8.116392903	Chgb	ENSRNOG00000021269	CDS	38
95	chr3	99.58347532	7.141652855	Chgb	ENSRNOG00000021269	CDS	7

96	chr7	98.41947713	6.566289159	Atp5f1b	ENSRNOG00000002840	CDS	51
97	chr3	97.92444683	8.088685973	Chgb	ENSRNOG00000021269	CDS	2
98	chr12	94.74781129	7.07261121	Trrap	ENSRNOG00000025244	Proximal intron (ncRNA)	32
99	chr3	93.91862676	8.029542489	Chgb	ENSRNOG00000021269	CDS	3
100	chr11	93.02769448	8.019095701	App	ENSRNOG00000006997	CDS	14

Table S4.6 Top 100 mRNA's bound to Ago2 in cells exposed to heat shock.

	Chromosome	-log10(P-value)	Log2 Fold Change	Gene	Ensembl ID	Feature	Size
1	chr12	400	4.068446687	Actb	ENSRNOG00000034254	CDS	72
2	chr12	400	4.047667459	Actb	ENSRNOG00000034254	CDS	41
3	chr20	400	4.421478252	Zwint	ENSRNOG00000048682	3' UTR	143
4	chr7	400	4.705271218	RF00221|AC 127784.1	ENSRNOG00000052611|| ENSRNOG00000059190	Proximal intron	34
5	chr7	400	4.705271218	AC127784.1| RF00221	ENSRNOG00000052611|| ENSRNOG00000059190	Noncoding exon	28
6	chrM	400	4.304729443	COX2	ENSRNOG00000030371	CDS	183
7	chrM	400	4.158519398	COX2	ENSRNOG00000030371	CDS	29
8	chrM	400	6.176040806	AY172581.18	ENSRNOG00000032609	Noncoding exon	28
9	chrM	400	4.952820914	chrM.trna4-GlnTTG	chrM.trna4-GlnTTG	tRNA	6
10	chrM	400	4.704893401	chrM.trna4-GlnTTG	chrM.trna4-GlnTTG	tRNA	27
11	chr9	255.7574996	10.32597433	rno-mir-375	MI0006140	miRNA	11
12	chr9	255.7574996	10.32597433	rno-mir-375	MI0006140	miRNA	9
13	chr9	245.5614482	10.26777945	rno-mir-375	MI0006140	miRNA	2
14	chr17	181.6484802	7.881562231	rno-mir-27b	MI0000859	miRNA	8
15	chr17	181.6484802	7.881562231	rno-mir-27b	MI0000859	miRNA	7
16	chr17	181.6484802	7.881562231	rno-mir-27b	MI0000859	miRNA	7
17	chr19	145.4657355	9.520295988	rno-mir-27a	MI0000860	miRNA	8
18	chr19	145.4657355	9.520295988	rno-mir-27a	MI0000860	miRNA	7
19	chr19	145.4657355	9.520295988	rno-mir-27a	MI0000860	miRNA	7
20	chr2	79.0504246	4.321006067	Fdps	ENSRNOG00000043377	CDS	49
21	chr17	76.05749589	5.970098906	Cmahp	ENSRNOG00000003094	3' UTR	144
22	chr8	74.26085504	4.758353728	Cadm1	ENSRNOG00000018778	3' UTR	49
23	chr8	68.42428116	5.162743984	Cadm1	ENSRNOG00000018778	3' UTR	58
24	chr17	67.84578546	7.472599246	rno-mir-23b	MI0000853	miRNA	13
25	chr17	66.36077676	6.887636745	rno-mir-23b	MI0000853	miRNA	11
26	chr20	66.16995194	6.49664472	Nudt3	ENSRNOG00000061176	Distal intron	164
27	chr20	61.99046412	3.445677947	Zwint	ENSRNOG00000048682	3' UTR	105
28	chr20	61.78099212	3.259605523	Zwint	ENSRNOG00000048682	3' UTR	106
29	chr2	59.16032088	4.037213101	Fdps	ENSRNOG00000043377	CDS	51
30	chr2	58.86626953	3.191890329	Fdps	ENSRNOG00000043377	CDS	64
31	chr16	53.4097716	6.592731824	Ifi30	ENSRNOG00000019387	3' UTR	119
32	chr2	53.10797779	3.6932587	Fdps	ENSRNOG00000043377	CDS	40
33	chr3	47.07778333	4.577781483	Ctsa	ENSRNOG00000015857	CDS	99
34	chr11	46.70843137	4.369194861	RF01299	ENSRNOG00000053621	Proximal intron	44
35	chr11	46.07719153	4.353075196	RF01299	ENSRNOG00000053621	Noncoding exon	6
36	chr1	43.5559552	4.286732701	RF00186	ENSRNOG00000057952	Proximal intron	38
37	chr1	42.77448396	4.179817497	RF00186	ENSRNOG00000057952	Noncoding exon	27
38	chr7	42.61305538	3.724622871	Tuba1a	ENSRNOG00000060728	CDS	137
39	chr1	41.52196768	4.145465992	RF00186	ENSRNOG00000057952	Noncoding exon	6
40	chr11	41.52196768	4.145465992	RF01299	ENSRNOG00000053621	Noncoding exon	15
41	chr17	41.49396632	7.747706484	rno-let-7d	MI0000601	miRNA	11
42	chr16	40.5095868	5.844568023	Ifi30	ENSRNOG00000019387	3' UTR	62

43	chr17	40.04922758	6.747706484	rno-let-7d	MI0000601	miRNA	12
44	chr9	38.87208182	6.7070645	Rrp36	ENSRNOG00000017836	CDS	232
45	chr3	37.334057	7.600149296	Grin1	ENSRNOG00000011726	5' splice site	36
46	chr2	35.55267805	7.531977793	rno-mir-16	MI0000844	miRNA	15
47	chr2	35.55267805	7.531977793	rno-mir-16	MI0000844	miRNA	11
48	chr3	33.58656125	5.600149296	Grin1	ENSRNOG00000011726	CDS	47
49	chr14	32.40624887	4.50851882	Rtn4	ENSRNOG00000004621	CDS	22
50	chr2	31.239074	6.410671497	Rhobtb3	ENSRNOG00000012414	CDS	133
51	chrM	31.19741782	3.445677947	AY172581.2	ENSRNOG00000029145	Noncoding exon	20
52	chrM	31.19741782	3.445677947	AY172581.2	ENSRNOG00000029145	Noncoding exon	10
53	chr19	30.21485425	7.305701937	rno-mir-23a	MI0000852	miRNA	13
54	chr19	30.21485425	7.305701937	rno-mir-23a	MI0000852	miRNA	10
55	chr1	30.00703138	3.405600507	Ftl1	ENSRNOG00000020843	CDS	6
56	chr12	29.23674426	4.385136405	Ppp1cc	ENSRNOG00000001269	CDS	108
57	chr1	28.97819072	4.720739437	Cln3	ENSRNOG00000019103	CDS	99
58	chr3	28.93479387	4.113834383	Ctsa	ENSRNOG00000015857	CDS	51
59	chr1	27.91578131	4.899709578	Patl1	ENSRNOG00000021052	CDS	132
60	chr2	27.78012744	3.555061406	Hmgcr	ENSRNOG00000016122	3' UTR	151
61	chr2	27.68526927	4.06320831	Anxa5	ENSRNOG00000014453	3' UTR	143
62	chr11	27.27417001	4.870563232	App	ENSRNOG00000006997	3' UTR	62
63	chr8	27.07171171	3.352221782	Cadm1	ENSRNOG00000018778	3' UTR	91
64	chr20	26.48157819	3.329853969	Zwint	ENSRNOG00000048682	3' UTR	53
65	chr14	26.0807545	4.250206825	Rtn4	ENSRNOG00000004621	CDS	48
66	chr14	25.93979338	4.108296199	Rtn4	ENSRNOG00000004621	CDS	48
67	chr7	25.78773247	4.577781483	Reep6	ENSRNOG00000033262	CDS	63
68	chr14	25.60844743	4.385136405	Psme4	ENSRNOG00000060340	CDS	118
69	chr20	25.39604574	6.132370334	Sik1	ENSRNOG00000001189	CDS	58
70	chr8	24.81353697	6.101343439	Ilf3	ENSRNOG00000022741	Distal intron	78
71	chr10	24.51478981	4.516380938	Pank3	ENSRNOG00000007419	CDS	76
72	chr6	24.44608616	5.192491327	Dock4	ENSRNOG00000004823	CDS	46
73	chr2	23.86305759	3.790775206	Hmgcr	ENSRNOG00000016122	CDS	101
74	chr1	23.58169871	3.072546175	Zfp180	ENSRNOG00000029336	5' UTR	129
75	chr1	23.11749015	6.935333487	rno-mir-125a	MI0000895	miRNA	16
76	chr1	23.11749015	6.935333487	rno-mir-125a	MI0000895	miRNA	8
77	chr10	23.08172321	4.262279657	Cltc	ENSRNOG00000004291	CDS	44
78	chr1	23.06549145	3.498347015	Ftl1	ENSRNOG00000020843	CDS	20
79	chr19	22.72172667	3.840815889	Mvd	ENSRNOG00000013376	CDS	90
80	chr10	22.60961252	4.419083737	rno-mir-3064	MI0030357	miRNA proximal	50
81	chr19	22.48747596	5.970098906	rno-mir-328a	MI0000602	miRNA	23
82	chr9	22.18367642	5.069634579	Khsrp	ENSRNOG00000047628	Proximal intron	90
83	chr16	22.15473448	4.613405393	Ghitm	ENSRNOG00000013961	CDS	44
84	chr7	21.93756205	6.863183702	rno-let-7i	MI0000835	miRNA	16
85	chr7	21.93756205	6.863183702	rno-let-7i	MI0000835	miRNA	8
86	chr5	21.06943299	4.004046237	Atp6v1g1	ENSRNOG00000008163	3' UTR	228
87	chr9	20.87801362	3.747706484	Khsrp	ENSRNOG00000047628	Proximal intron	98
88	chr20	20.86267976	5.350370987	Sik1	ENSRNOG00000001189	CDS	35
89	chr6	20.86267976	5.350370987	Dock4	ENSRNOG00000004823	CDS	48
90	chr8	20.7587066	6.787234848	Coro2b	ENSRNOG00000015257	Distal intron	38
91	chr8	20.7587066	6.787234848	Coro2b	ENSRNOG00000015257	Distal intron	32
92	chr8	20.7587066	6.787234848	Coro2b	ENSRNOG00000015257	Distal intron	22
93	chr7	20.6784637	3.385136405	Plec	ENSRNOG00000023781	CDS	52
94	chr1	20.24299896	4.503780901	Zfand5	ENSRNOG00000018107	CDS	104
95	chrX	20.16868896	5.825708996	Usp9x	ENSRNOG00000003261	CDS	45
96	chr3	20.06497163	3.221637673	Snrpb	ENSRNOG00000006961	CDS	95
97	chr10	19.94100491	4.092354656	rno-mir-3064	MI0030357	Proximal intron	53
98	chr10	19.60702181	4.465306754	Cltc	ENSRNOG00000004291	CDS	13
99	chr8	19.59029879	5.787234848	Ilf3	ENSRNOG00000022741	Distal intron	14
100	chr18	19.58103799	6.7070645	Rnf125	ENSRNOG00000057832	CDS	42